Involvement of CRISP2 in the organization of dense protein structures in porcine sperm Min Zhang 2023

Involvement of CRISP2 in the organization of dense protein structures in porcine sperm

Min Zhang

Involvement of CRISP2 in the organization of dense protein structures in porcine sperm

Min Zhang

2023

ISBN: 978-94-6458-830-9

DOI: 10.33540/1617

Thesis layout and cover design: Min Zhang and Juli Yang

Print by: Ridderprint, www.ridderprint.nl

Involvement of CRISP2 in the organization of dense protein structures in porcine sperm

De rol van CRISP2 in de organisatie van compacte eiwitstructuren in varkenssperma
(met een samenvatting in het Nederlands)

Proefschrift

ter verkrijging van de graad van doctor aan de
Universiteit Utrecht
op gezag van de
rector magnificus, prof.dr. H.R.B.M. Kummeling,
ingevolge het besluit van het college voor promoties
in het openbaar te verdedigen op

dinsdag 17 januari 2023 des middags te 2.15 uur

door

Min Zhang

geboren op 16 mei 1990
te Zaozhuang, China

Promotoren:

Dr. B.M. Gadella
Prof. dr. J.B. Helms

Dit proefschrift werd (mede) mogelijk gemaakt met financiële steun van China Scholarship Council.

Contents

Chapter 1

General introduction

1 The basic design of mammalian spermatozoa

1.1 Spermatogenesis

Spermatozoa are unique, highly polarized cells. Spermatogenesis, the process in which spermatozoa are produced, begins with mitotic proliferation of a spermatogonium (A1) which undergo 5 cell divisions to form B spermatogonia. All the B spermatogonia then divide to form resting primary spermatocytes. First meiotic division begins from one primary spermatocyte into two secondary spermatocytes followed by a second meiotic division to give rise to four haploid spermatids [1-3]. Thus, one A1 spermatogonium forms 256 spermatids. These spermatids enter the stage of spermiogenesis in which round spermatids transform into spermatozoa [4]. Spermiogenesis is a complex process, generally comprised of four phases, namely the Golgi phase, the cap phase, the elongation phase and the compaction and sperm cell releasing phase. Spermiogenesis is completed with the formation and release of spermatozoa with a head containing a haploid nucleus and acrosome, and a flagellum (Figure 1). Sperm cell formation is a highly efficient and continuous process. Boars used for artificial insemination (AI) in the Netherlands typically produce around 5000 sperm cells per second, which is approximately ten times more than man.

1.2 The main features of the sperm head

The core of the mammalian sperm head is the flattened sperm nucleus. Condensation of chromatin is a hallmark during spermiogenesis and is achieved by a range of histone modifications and histone variants incorporation, which are required for replacement with transition nuclear proteins (TNPs) and nearly complete removal of histones [5-7]. Later during spermatid elongation, TNPs are in turn replaced with protamines that bind to the phosphate neckbone of DNA using the arginine-rich domain as an anchor at the major groove of the alfa-helix of DNA. Then through intra-protamine disulfide bonding (by the oxidization of their cysteine residues), the protaminated DNA is ultra-compacted into DNA toroids which is

genetically inactive until unwrapping in the cytosol of the fertilized oocyte [8, 9]. The sperm nucleus is surrounded by the nuclear envelop (NE), a double membrane that encloses chromatin. The other organelle is the acrosome, a membranous organelle located over the anterior part of the sperm head. The acrosome is a Golgi derived structure enriched in hydrolytic and proteolytic acrosomal enzymes [9-11]. The acrosome contents are enclosed between the outer acrosomal membrane (OAM) which is located just beneath the plasma membrane (PM) and the inner acrosomal membrane (IAM) lying over the outer membrane of the NE. In the middle of the sperm head underlying the PM, a narrow part of the acrosome is called the equatorial segment (EqS) [12].

In eutherian mammals, the sperm NE (at the cytosolic side), except in the region of tail implantation, is enveloped in a condensed protein layer called the perinuclear theca (PT) [13]. The PT is structurally divided into two regions, the sub-acrosomal layer (SAL-PT) apically residing between the inner acrosomal membrane and the NE as well as the post-acrosomal sheath (PAS-PT) caudally filling between the PM and the NE [13-15] (Figure 1). The assembly of the SAL-PT is accompanied with the formation of the acrosome during the early stage of spermiogenesis [15]. While the PAS-PT proteins are translated in the cytoplasmic lobe, stored and transported by the manchette [15]. The assembly of the PAS-PT is concomitant with the descent of the microtubular manchette during the elongation phase of spermiogenesis [16]. The assembly route and the protein resources, propose SAL-PT functions related to secretory vesicle activities, nuclear docking and acrosomal capping. The PAS-PT is assembled independent on the formation of the SAL-PT [17] and has been proposed housing sperm-born oocyte activating factors [18].

1.3 Structures of the sperm tail and sperm motility

The sperm flagellum is a specialized motile cilium that powers the sperm to swim through the

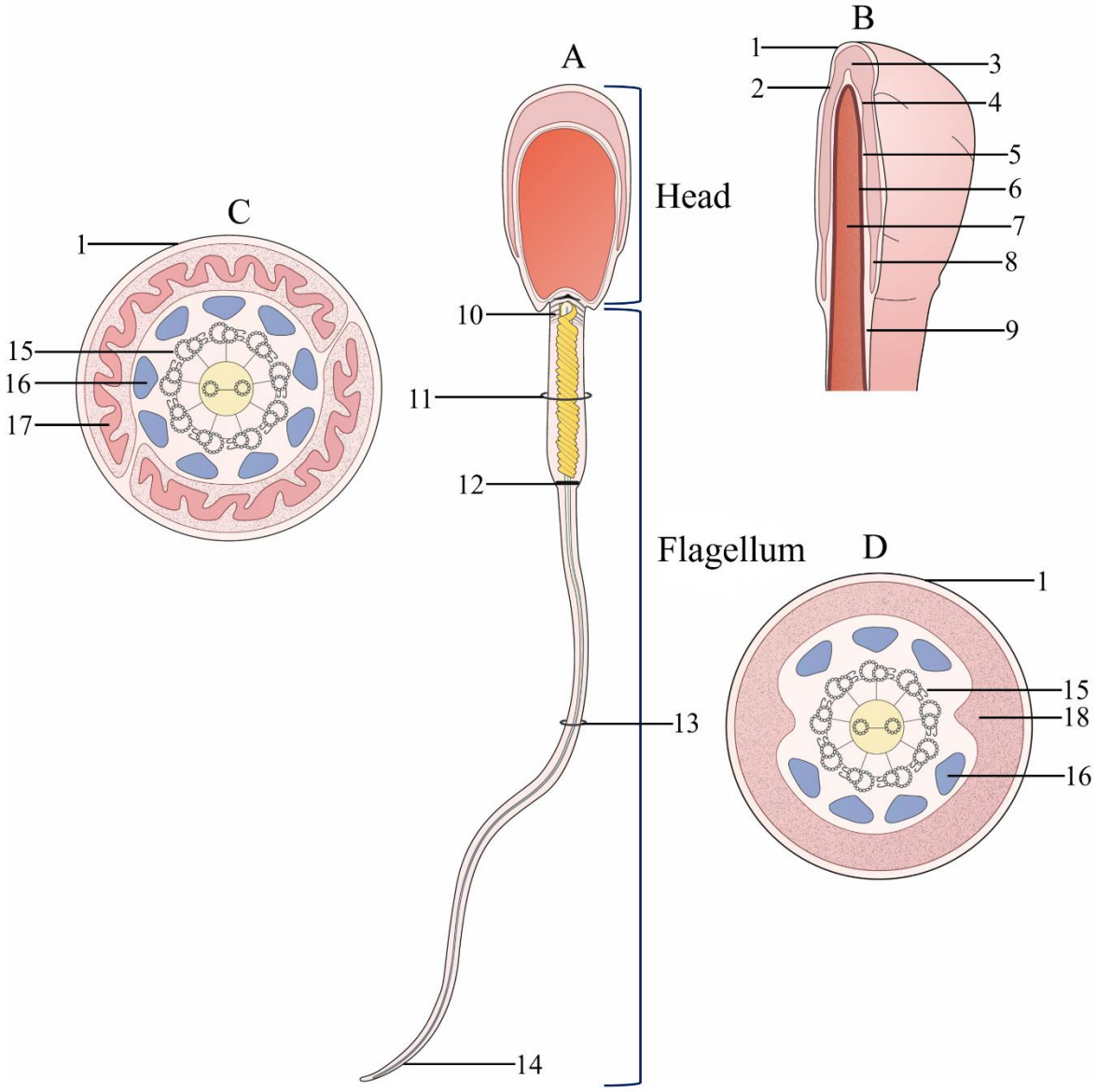

Figure 1. Diagrammatic representation of the boar sperm cell. (A) An overview of the sperm cell composed of a head and a flagellum. (B) A mid-sagittal section through the sperm head. (C) A cross section of the mid piece. (D) A cross section of the principal piece. 1, plasma membrane; 2, outer acrosomal membrane; 3, acrosome; 4, inner acrosomal membrane; 5, sub-acrosomal layer (SAL); 6, nuclear envelop; 7, nucleus; 8, equatorial segment; 9, post acrosomal sheath (PAS). The SAL and PAS make up the perinuclear theca (PT). 10, connecting piece; 11, mid piece; 12, annulus ring; 13, principal piece; 14, end piece; 15, axoneme (9+2); 16, outer dense fiber; 17, mitochondria sheath; 18, fiber sheath.

female reproductive tract, to find and to fuse with the egg. The mammalian sperm flagellum is highly conversed and can be divided into four major parts, the connecting piece, the mid piece, the principal piece and the end piece [19] (Figure 1). The connecting piece is the conjunction

tightening the sperm head and tail. Moreover, it has been proposed to contribute to sperm motility [20]. The pair of centrioles are important for connecting piece formation as well as axoneme assembly during elongation phase. The axoneme is the core of the sperm tail and contains a structure of nine outer doublet microtubules and a central pair of microtubules (9 + 2) associated with radial spokes and dynein arms [19]. The axoneme is surrounded by other accessory structures including the outer dense fibers (ODFs), the fiber sheath (FS) and mitochondrial sheath (MS, with approximately 100 coiled mitochondria). In the mid piece, the axoneme is surrounded by the ODFs and the MS. In the principal piece, the axoneme is surrounded by 7 ODFs and the MS is replaced with the FS, two longitudinal columns attaching to two microtubule doublets (3 and 8) of the ODFs. The MS and FS are separated by an electron-dense ring structure called the annulus [21]. In the end piece, only the axoneme is retained. All the accessory components are necessary for normal tail structures and correct sperm motility. Specifically, the MS carries all sperm's mitochondria and possesses functions similar to those of somatic mitochondria which are indispensable for oxidative phosphorylation to produce ATP for energy supply [22]. The ODFs elongate from the connecting piece and provides the rigidity to the sperm tail. Defects in ODFs lead to abnormal tail structure, altered wave and/or poor motility, thus male infertility [23-25]. The FS includes important metabolic pathways for energy production. For example, the FS utilizes glycolysis for sperm motility [26].

2 The journey of testicular sperm to the oviduct and oocyte fertilization

2.1 Sperm maturation in the epididymis

Although released testicular spermatozoa are morphologically complete, they are non-motile and incapable of fertilizing an egg [27, 28]. Spermatozoa experience biochemical and morphological changes as they pass through the epididymis, collectively called epididymal maturation [29]. Spermatozoa transit from caput to cauda regions of this organ and caudal spermatozoa are motile and have acquired the potential to fertilize an egg (Figure 2).

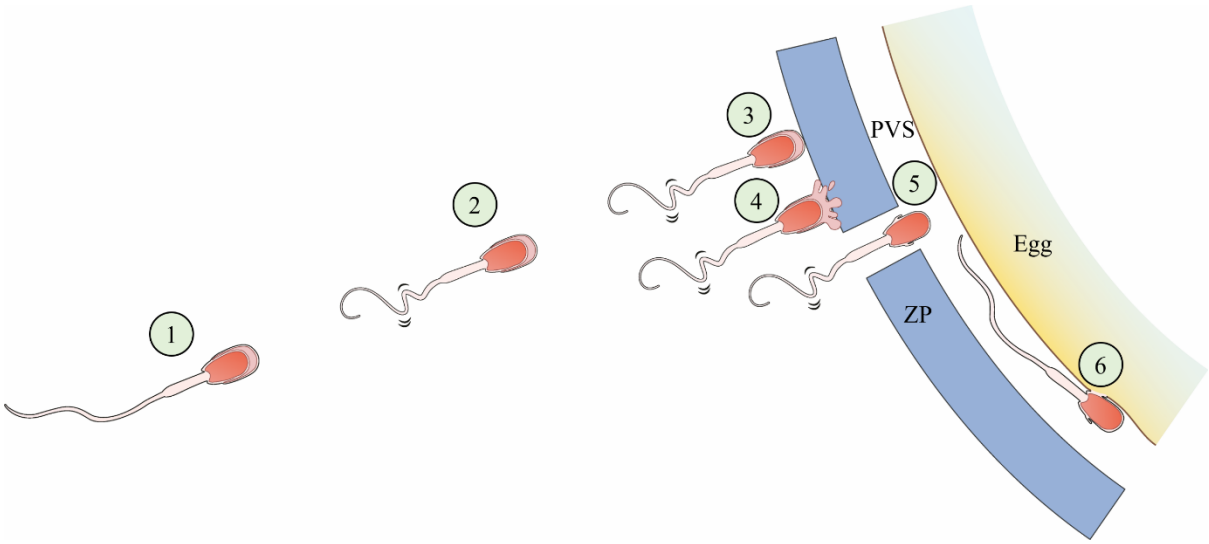

Figure 2. Steps of epididymal or ejaculated spermatozoa to fuse with the egg during mammalian fertilization. ① Epididymal or ejaculated spermatozoa with basic movement ability. ② Spermatozoa undergoing capacitation including cholesterol efflux, increased membrane fluidity, PKA activation and protein tyrosine phosphorylation and development of hyperactivated motility. ③ Sperm-ZP binding. ④ ZP-induced acrosomal exocytosis. ⑤ Sperm penetration through the ZP and reaching the perivitelline space (PVS). ⑥ Sperm-egg fusion via the EqS.

The most obvious morphological change of testicular sperm when passing through the epididymal tract is the removal of the cytoplasmic droplet (CD) which first is retracted from the sperm connecting piece towards the end piece of sperm and then is shed off from the sperm cell. This CD removal is a sign of sperm maturation [30, 31]. Strikingly, during epididymal passage, spermatozoa also undergo removal and adsorption of peripheral proteins [32, 33]. Given that testicular spermatozoa are translationally silent, the newly coated proteins are secreted by the epithelial cells lining of the epididymis and the removed proteins are resorbed by the same epithelium [34]. Both removal and renewal of sperm coating are implicated to be functional for later sperm-egg interactions [35, 36]. In addition, sugar- and lipid- composition and distribution on the sperm surface are altered during epididymal transit as well [29, 37, 38]. The sperm tail also undergoes extensive changes during epididymal sperm maturation and these changes include the increase in disulfide bond formation between proteins in the ODFs and rise in intracellular cAMP content [39, 40]. These changes yield a more rigid and powerful

flagellum with potential beat and forward motion capacity. It is still not clear that how caudal spermatozoa acquire progressive movement, while testicular and caput epididymal spermatozoa do not. However, the acquirement of progressive sperm motility is a hallmark for successful epididymal sperm maturation.

2.2 Ejaculation

During ejaculation, stored cauda epididymal spermatozoa are first pre-dispositioned in the vas deferens and through contractions of the musculature of the male genital tract mixed with fluids secreted by the accessory sex glands, especially the prostate and seminal vesicle [41]. The resulting ejaculate contains a fluid called seminal plasma with the mature and motile spermatozoa. Ejaculated spermatozoa and seminal plasma together are called semen. Seminal plasma is not necessary for effective sperm function, as caudal spermatozoa can already fertilize oocytes *in vitro* [42, 43]. However, *in vivo*, seminal plasma is important for stabilizing spermatozoa and allow them to pass through the cervix and uterus towards the oviduct where they will meet the oocyte post ovulation. In addition to serve as a carrier medium, seminal plasma also provides nutritional substrates, stabilizing factors such as buffering capacity to counteract the acid pH in the female tract and containing reducing agents to protect spermatozoa against potential oxidation being exposure to atmospheric oxygen [44].

2.3 Capacitation

Once spermatozoa reach the tip of the uterine horn, they must prepare for meeting and fertilizing the oocyte, which occurs in the oviduct. The protective factors of seminal plasma must first be removed and the sperm cells need to be activated. This process takes place in the so-called sperm reservoir which is created at the uterine tubule junction (where the uterus connects to the oviduct). Spermatozoa must bind and reside there for a period (2-6 hours in most mammals) to acquire fertilization capacity. This process was initially and independently reported by Chang [45] and Austin [46], and is since then collectively called sperm capacitation. The milestone

that capacitation could be achieved *in vitro* by incubating epididymal or ejaculated spermatozoa in a defined medium [47, 48] helps to uncover the mechanisms underlying sperm capacitation. In fact, these attempts have led to formulate incubation protocols to achieve *in vitro* fertilization (IVF) for many mammalian species (including human, mouse, cow, sow, goat, ram and rabbit). Protocols developed for *in vitro* capacitation on several different mammalian species have demonstrated three critical constitutes, HCO_3^-, Ca^{2+} and a cholesterol acceptor, usually fatty acid free (FAF) serum albumin [49-51].

2.3.1 Cholesterol efflux from the sperm plasma membrane

Cholesterol is vital to stabilize the PM of spermatozoa and inhibits conformation dynamics of membrane proteins [52, 53]. A substantial amount of sperm surface cholesterol (in boar sperm about 40 % [54]) must be removed before sperm become capacitated. Therefore, cholesterol is considered a decapacitation factor that must be removed in order to achieve a capacitated state [55]. For this reason, FAF albumin, an effective cholesterol acceptor, is a key component in the IVF or capacitation medium [56]. However, high-density lipoproteins (HDLs) are preferred candidates for accepting cholesterol *in vivo*, because high concentrations of HDLs are found in the oviduct and other fluids of the genital tract [57, 58]. Moreover, evidence shows that HDLs alone are efficient to elicit cholesterol efflux in ram spermatozoa [59]. Cholesterol efflux from the sperm PM results in alterations in lipid ordering and increases membrane fluidity and permeability, the later contributing to other events involved in sperm capacitation [60, 61]. Cholesterol efflux also alters lipid microdomains and induces protein aggregations on the anterior head plasma membrane, which is considered the specific site where a capacitated sperm cell can bind to the oocyte after having penetrated the zona pellucida [62, 63].

2.3.2 Tyrosine phosphorylation

Tyrosine phosphorylation is a characteristic of capacitation in mammalian spermatozoa and has been demonstrated in many species including bovine [64], hamster [65], porcine [66], rat [67],

human [68], mouse [69], equine [70]. The flagellum is the major component of the sperm gaining increased tyrosine phosphorylation during capacitation [71] as shown by immunocytochemistry in most of the species except boars [72]. The classical signaling pathway triggering tyrosine phosphorylation cascades during capacitation is that HCO_3^- enters sperm cells via a Na^+/HCO_3^- cotransporter and stimulates the enzyme soluble adenylyl cyclase (sAC) to elevate cyclic adenosine monophosphate (cAMP) levels, finally leading to the activation of protein kinase A (PKA) [73]. Additionally, evidence shows that other tyrosine kinases might also be involved in sperm capacitation. The mitogen-activated protein kinases (MAPKs), also known as extracellular signal-regulated kinases (ERKs), are involved in signal transduction during sperm capacitation [74]. It has been proposed that crosstalk between those pathways may regulate tyrosine phosphorylation during capacitation [75], but this has not been established yet.

Tyrosine phosphorylation during capacitation is also affected by other factors. It has been shown that cholesterol efflux from the sperm plasma membrane increases protein tyrosine phosphorylation mainly via the cAMP/PKA pathway [56]. In addition, increased membrane permeability after cholesterol efflux also accelerates transportation of HCO_3^- and ions such as Ca^{2+} into sperm cells and affects downstream signaling molecules [49, 76]. It has been proposed that mild reactive oxygen species (ROS) production during sperm capacitation can activate both PKA and ERK pathways [61, 77], while more massive ROS production is detrimental for sperm.

2.3.3 Hyperactivation

Sperm hyperactivation is a beating pattern of the sperm tail, characterized by high-amplitude and asymmetrical thrashing and is required for *in vivo* fertilization [61, 78, 79]. Sperm hyperactivation occurs just before fertilization once the sperm cells are released from the sperm reservoir at the utero tubal junction (or after a period of incubation in the IVF or capacitation

medium). The typical high vigorous pattern of movement is thought to provide propulsive forces for sperm to swim through the oviductal mucus and penetrate the zona pellucida (ZP) of the oocyte [80-82]. The physiological factors triggering sperm hyperactivation *in vivo* are only poorly understood. This contrasts with *in vitro* studies, where it has been shown that Ca^{2+} plays important roles in triggering hyperactivated motility. Sperm treated with Ca^{2+} ionophore A23187 or that were permeabilized using detergents, both artificially increase cytoplasmic Ca^{2+} levels, thus inducing flagellum sperm hyperactivation [82, 83]. Extracellular Ca^{2+} is entering the sperm normally through Ca^{2+} channels [79]. Specifically, CatSper channel, a sperm-specific, low voltage-dependent Ca^{2+} channel is localized in the principal piece of the sperm tail [84, 85]. Numerous studies have shown that CatSper null mice are infertile and sperm from CatSper null mice fail to penetrate the ZP [79]. In addition to extracellular Ca^{2+}, local Ca^{2+} stored in an organelle in the base of the sperm tail, namely the redundant nuclear envelope (RNE), also contributes to cytoplasmic Ca^{2+} level [79]. Hyperactivated sperm must undergo acrosome exocytosis as a concerted requirement to penetrate through the ZP. However, these two events are not coupled, for instance, bull spermatozoa incubated in certain media can undergo acrosomal exocytosis without being hyperactivated in motility [86].

2.4 Sperm-egg recognition and binding

A released sperm cell from the utero tubal junction will have hyperactive motility and enters the oviduct where it finally will meet in the ampulla part the just ovulated oocyte. The processes involved are extremely difficult to follow *in situ* but with the development of reliable IVF protocols, powerful methods are now available to study the mystery of fertilization process outside the mother. Since the first “test tube” baby was successfully born in 1978 [87], IVF is nowadays a routine technique to aid fertility of subfertile human couples.

Mammalian oocytes are coated with dense glycoproteins that together comprise the ZP, which

is involved in mechanical protection, spermatozoa recognition and binding, induction of the acrosome exocytosis and defense against polyspermy [88]. There are four mammalian ZP glycoproteins, commonly named ZP1, ZP2, ZP3 and ZP4. Mammalian ZP is normally composed of three to four ZP proteins depending on the presence of ZP1 or ZP4, or both [89, 90]. For example, human ZP is comprised of four ZP proteins [91], mouse ZP lacks ZP4 [92], pig and cow ZP is formed of ZP2, ZP3 and ZP4 [93, 94]. Moreover, the composition of ZP proteins as well as the glycosylation sites of individual ZP protein are different among species [90]. Therefore, it has been accepted that mammalian sperm-egg binding is a carbohydrate dependent, species-specific recognition process [90, 95].

From the side of sperm, the primary sperm-ZP binding occurs in the apical ridge area of the sperm head plasma membrane [96]. Secondary zona binding is accomplished by intra-acrosomal proteins after the ZP-induced acrosome reaction. The apical ridge of the sperm head plasma membrane is modulated during capacitation and shows increased ZP-binding affinity. Many proteins showing ZP-binding affinity have been identified, such as spermadhesins, milk fat globule-EGF factor 8 protein (MFGE8), zonadhesin (ZAN), proacrosin/acrosin (ACR), acrosin binding protein (ACRBP), zona pellucida binding protein 1 (ZPBP1) [97-100]. Additionally, there is evidence that seminolipid from the sperm lipid rafts as well as chaperones are involved in remodeling/formation of sperm-ZP binding sites [98, 101]. Nonetheless, the specific mechanism of the sperm-ZP interaction is still relatively unclear. It is believed that the sperm-ZP binding relies on coordinated multiple concomitant and synergistic binding events organized on the sperm head surface [90, 102].

2.5 Acrosomal exocytosis and sperm-egg penetration

Acrosomal exocytosis, also called acrosome reaction (AR), involves membrane fusion and release of acrosomal contents. It plays a vital role in the fertilization process [103, 104], which

is induced by the ZP (in pig [105] and bovine [106]) or earlier when sperm cells interact with the intercellular matrix of the cumulus mass (in rodents [107, 108]). The PM fuses with the OAM at multiple sites and they are shed as hybrid vesicles [109]. Soluble *N*-ethylmaleimide-sensitive factor attachment protein receptor (SNARE) proteins and Rab proteins have been reported to regulate the membrane fusion process [110, 111]. In addition to the ZP, progesterone is also a physiologically relevant inducer for AR [112, 113]. Ca^{2+} influx is a characteristic of AR and plays an important role in this process [114, 115]. Both ZP and progesterone can induce Ca^{2+} influx into sperm cells to undergo AR [116]. In addition, chemical stimuli such as calcium ionophore A23187, which induces a rapid Ca^{2+} influx, are widely used to study AR *in vitro* [117, 118].

For many years, it was believed that AR exposure of acrosomal lysins such as acrosin, a trypsin-like protease, are responsible for dissolving the ZP and allowing sperm penetration through the ZP [114, 119-121]. However, spermatozoa from acrosin deficient mouse can penetrate the ZP [122]. A recent study demonstrates that acrosin is indeed indispensable for hamster spermatozoa penetration through the ZP [123]. Studies show that specific proteasomal inhibitors effectively prevent sperm-ZP penetration, raising the possibility that the ubiquitin-proteasome system is involved in sperm-ZP interaction [124-126].

2.6 Sperm-egg fusion

After the AR, the sperm will penetrate through the ZP and reach the perivitelline space where its EqS will be oriented in parallel with the oolemma (PM of the oocyte). The sperm-egg fusion is mediated by protein-protein interactions between a variety of molecules from both gametes membrane surfaces [127]. The PM of the EqS of the sperm head remains intact after AR and is believed the initial site where the sperm bind and fuse with the oolemma and thus the specific area involved in fertilization of the oocyte [128]. To date, IZUMO1 (present in sperm)-JUNO

(present in oolemma) is the only known interacting protein essential for mammalian sperm-egg interaction. IZUMO1 is an immunoglobulin (Ig)-like type I membrane protein and JUNO is a glycosylphosphatidylinositol (GPI)-anchored protein. The ligand-receptor interaction of IZUMO1-JUNO exists in mice and human [129, 130]. However, IZUMO1-JUNO is not sufficient to initiate sperm-egg interaction [131]. In addition to IZUMO1, there are other sperm proteins involved in this process. Those include sperm acrosome membrane-associated protein 6 (SPACA6), sperm-oocyte fusion required 1 (SOF1), transmembrane protein 95 (TMEM95), fertilization influencing membrane protein (FIMP), DC-STAMP domain containing 1 (DCST1) and DCST2 [132]. Apart from JUNO, CD9, another egg protein, also participates in sperm-egg fusion [133, 134]. Gamete fusion is a complex process and many research questions remain unaddressed. For instance, despite the crucial importance of fertilization in metazoan life, it is still enigmatic which proteins are inducing the intercellular membrane fusion. The current proteins known to be involved, do not contain a predicted membrane fusion domain.

3 The presence of CRISPs in mammalian sperm and their putative roles in mammalian reproduction

Cysteine-rich secretory proteins (CRISPs) are a branch of CRISPs, Antigen-5 and Pathogenesis Related-1 (PR-1) proteins that together define the CAP super family. CRISPs are characterized by presence of 16 cysteine residues forming intra disulfide bonds [135]. CRISPs are expressed mainly in the mammalian male reproductive tract as well as in the venom secretory ducts of reptiles such as snakes and lizards [136, 137].

3.1 The structure of CRISPs

CRISPs inherited a conserved CAP domain that is characterized for all CAP family membranes and a CRISP domain, comprising of a characteristic ion channel regulatory (ICR) domain and a hinge connecting the CAP and ICR domain [138] (Figure 3). The CAP domain is approximately 20 kDa in size and 150 amino acids in length. The CAP domain has four highly

conserved motifs (CAP1-4) and forms a unique structural α-β-α sandwich fold [139]. These conserved motifs may contribute to the common amyloidogenic property of CAP proteins [140]. The CAP domain is characterized by conserved histidines, coupled with glutamic acid residues and stabilized by hydrogen boding between those residues. The CAP domain contains a large groove along which the histidine and glutamic acid residues are oriented and can directly bind divalent cations, such as Zn^{2+}, Mg^{2+} and Hg^{2+} [139]. 10 out of 16 cysteine residues are clustered in the CRISP domain. The hinge domain contains 20 amino acids and two crossed disulfide bonds to ensure the rigidity of the ridge as well as to prevent interactions between the CAP and ICR domain [139, 141]. The ICR domain comprises of approximately 40 amino acids and contains a hydrophobic core, stabilized by three disulfide bonds [139].

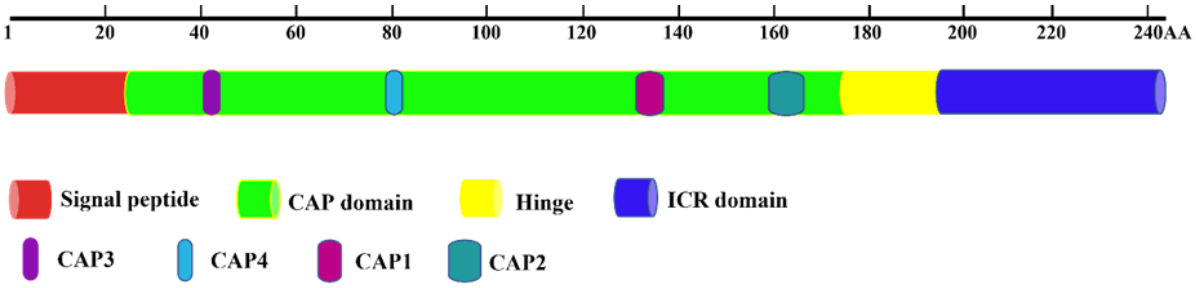

Figure 3. Schematic representation of mammalian CRISPs showing the structural characteristics including a signal peptide (red), a CAP domain (green) with four conserved CAP motifs (CAP1-4), a hinge (yellow) and an ion channel regulatory (ICR) domain (blue). AA, amino acid.

3.2 The expression and localization of mammalian CRISPs

There are three CRISPs (CRISP1, CRISP2 and CRISP3) expressed in mammals (Figure 4). In some rodents, an additional CRISP (CRISP4) exists. Phylogenetic analysis shows that CRISP4 and CRISP1 are derived from the same gene [139] (Figure 4). CRISP1 and rodent CRISP4 are highly enriched in epididymal fluid and bind to the sperm surface during epididymal maturation (Figure 5). Human and mouse CRISP1 are found highly expressed in the caudal epididymal region [142, 143]. Recently, CRISP1 has been shown also to be expressed in the female tract of mouse [144]. CRISP4 in mouse and rat is enriched in the caput region of the epididymis [145,

146]. CRISP3 has a wide expression pattern, not only restricted to male reproductive tract, but also in other regions such as salivary gland. In the male genital tract CRISP3 is secreted during ejaculation by seminal vesicle and the prostate and is present in the seminal plasma [147] (Figure 5). In agreement with this, CRISP3 is enriched in seminal plasma especially in horses [148, 149]. CRISP3 is one of the most highly upregulated proteins in prostate cancer patients and the expression levels of CRISP3 are correlated with the tumor stage [150, 151]. Recent studies showed that CRISP3 facilitates prostate cancer invasion and progression and thus is a potential maker and target for diagnosis or therapy of prostate cancer [152]. CRISP1,3 and 4 are secretory proteins that can be added to the sperm surface during epididymal maturation (CRISP1/4) or during ejaculation (CRISP3).

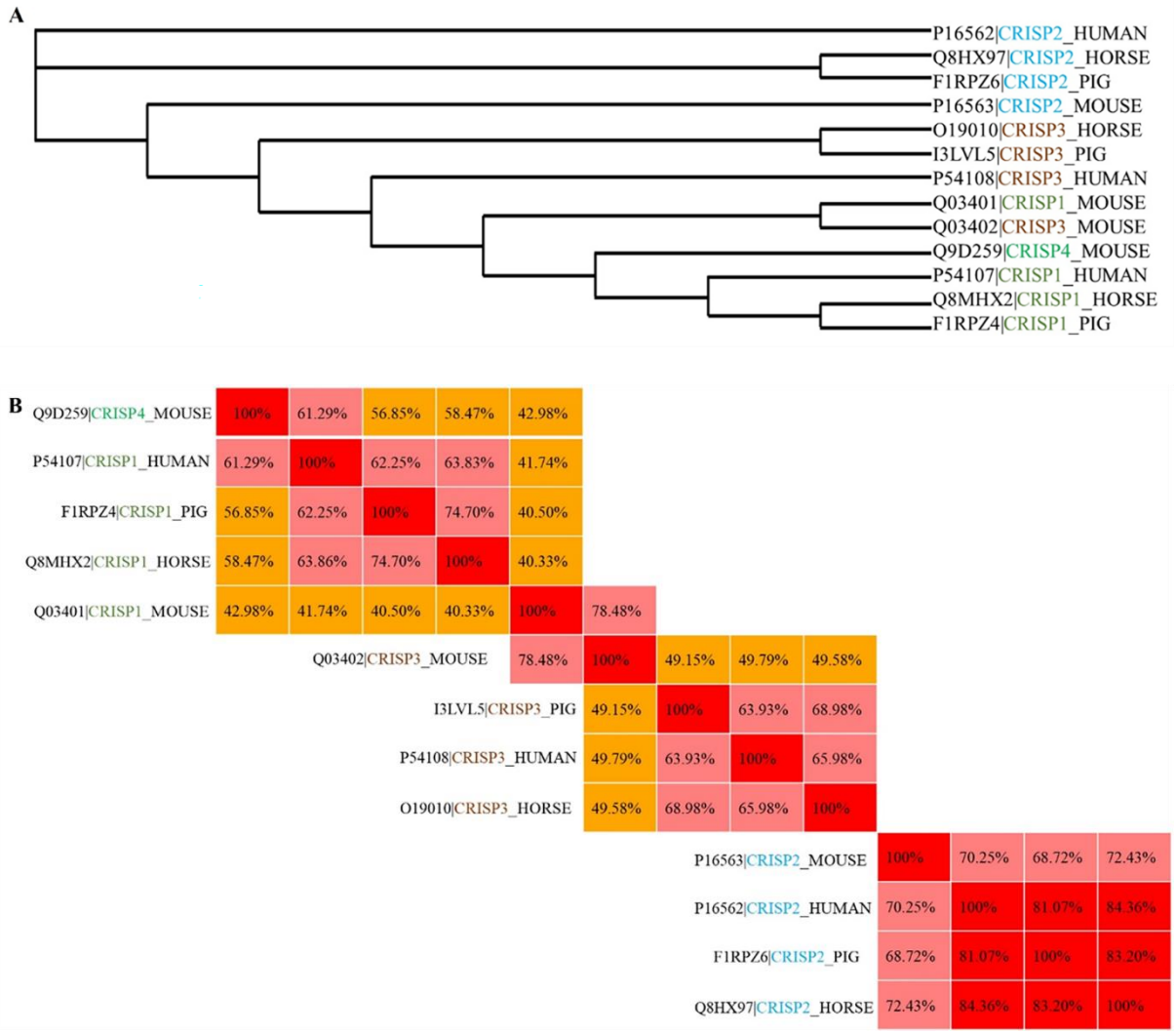

Figure 4. Phylogenetic tree (A) and percent identity matrix (B) based on UniProt alignment (https://www.uniprot.org/) showing the sequence similarity of CRISPs from human, horse, pig and mouse. Amongst CRISPs, CRISP2 is the most conversed subfamily cross species. Mouse CRISP4 is clustered in the CRISP1 subfamily from human, horse and pig. Mouse CRISPs show the most variability among those species. Colors correspond to the following percent identity: dark red, 80–100%; light red, 60–79%; orange, 40–59%.

In contrast to the CRISPs described above, CRISP2 is the sole one expressed in mammalian testis (Figure 5). It is also the only CRISP that is present inside the sperm cell. CRISP2 was initially characterized as a major component of guinea pig acrosome and thus was called acrosomal autoantigen 1 [153]. Later, it was identified as a testis specific gene expressed in mouse and rat, named TPX-1 [154, 155]. CRISP2 is synthesized by developing spermatids and is incorporated into the dense structures of the sperm head and tail [156, 157]. CRISP2 has been particularly investigated in guinea pig, rat, human and mouse. CRISP2 shows a conserved location in the sperm acrosome, the connecting piece and the ODFs of the sperm tail [154, 156, 158].

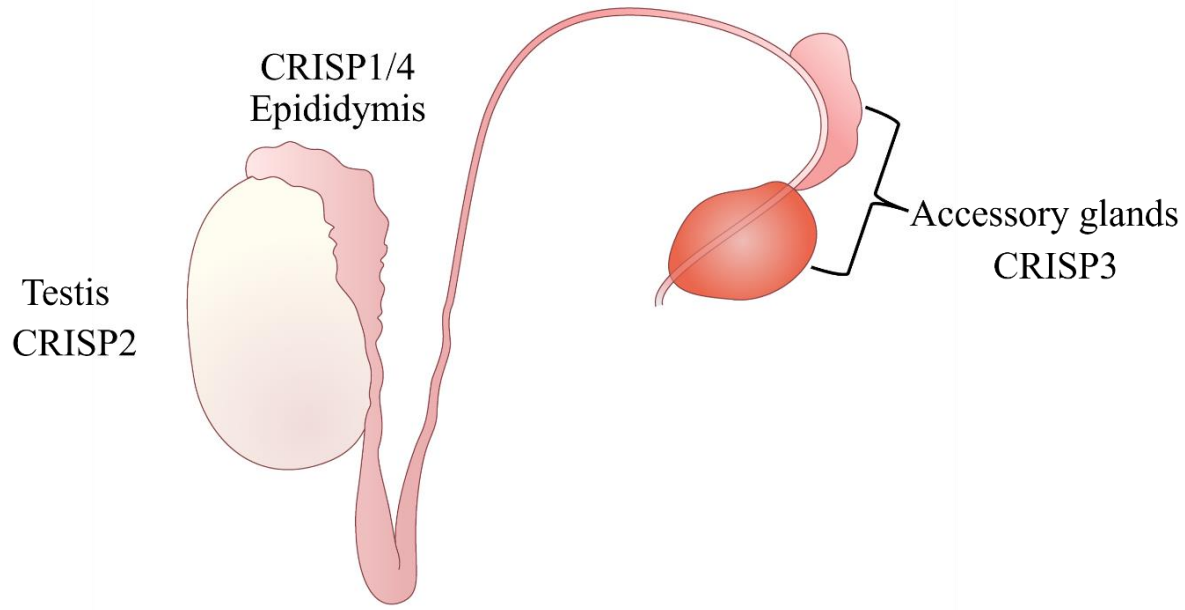

Figure 5. Expression patterns of mammalian CRISPs in the male reproductive tract. CRISP1/4 are expressed in the epididymis, secreted from the epithelia of the epididymal duct and absorbed to the

sperm surface during epididymal transit. CRISP2 is the only CRISP expressed in the mammalian testis and is localized intracellularly in sperm cells. CRISP3 is expressed in the accessory secretory male sex glands (mainly the seminal vesicle and prostate) and mixed in the seminal plasma during ejaculation.

3.3 The role of CRISP2 in sperm function and male fertility

3.3.1 Non-genetic studies

CRISP2 has gained intensive attention among CRISPs, since it is the only CRISP localized intracellularly in the sperm. CRISP2 has been described to be of acrosomal origin and to reassociate to the EqS after the AR and thus to be implied in the gamete fusion process. As will be shown in **chapter 2**, however, we have evidence from pig sperm that CRISP2 is not present in the acrosomal lumen but abundant in the post acrosomal sheath region. The surface exposure of CRISP2 at the EqS as documented in **chapter 4** is in line with what was originally explained as reassociation of the protein [159]. There is a significant decrease in the percentage of fertilized eggs in presence of anti-CRISP2 [160, 161]. Although recombinant mouse CRISP2 can bind to the surface of zona-free egg, this event is reduced by epididymal CRISPs which after being associated to the sperm head surface may act as complementary binding sites to the egg surface [160]. The ion channel regulatory capacity as well as the conserved sperm location in the connecting piece and the ODFs of the sperm tail suggests a role for CRISP2 in regulating sperm motility. *In vitro* studies showed that the ICR domain of CRISP2 can regulate Ca^{2+} flow through ryanodine receptor channels (RyR 1 and 2) [162]. Indeed RyRs are localized in the connecting piece of human spermatozoa [163]. Moreover, a yeast two-hybrid screen of an adult mouse testis shows that CatSper 1 is a potential partner binding to CRISP2 [164]. The expression of CRISP2 is lower in human patients with asthenozoospermia [165, 166]. Aberrant CRISP2 expression is correlated with lower progressive sperm motility and abnormal sperm morphology [165].

3.3.2 Knockout animal models

CRISP2 knock out mice males are not infertile [167, 168] and Crisp2$^{-/-}$ males have morphologically normal testes and epididymal sperm [167]. Nevertheless, Crisp2$^{-/-}$ males show fertilization defects when subjected to unilateral vasectomy or mated with hormone-treated females [167]. Later studies with CRISP2 and CRISP4 double knockout mice males showed that there is still no infertility phenotype. However, under more demanding conditions such as when mated with super-ovulated females, significant fertilization defects are observed in Crisp2$^{-/-}$/Crisp4$^{-/-}$ males compared to controls or even single CRISP2 knockout males [169]. Triple and quadruple Crisp gene knockout mice by CRISPR/Cas9 have a dramatic disruption of male fertility, including a severe reduction in average litter size (less than one) and high numbers of completely infertile male mice [169]. Sperm migration in the female tract, fertilization rates and embryo development are all inhibited [169]. These studies provide strong evidence for functional redundancy between CRISPs and indicate that CRISPs are indispensable for male fertility.

In addition, the physiology of sperm from CRISP knock out males has been investigated in order to understand the underlying molecular mechanisms. Sperm from Crisp2$^{-/-}$ males exhibit a significant defect in fertilization rates when using ZP-free eggs and a more pronounced decrease when using cumulus or ZP-surround eggs [167]. In addition, Crisp2$^{-/-}$ sperm have lower hyperactivated motility, impaired ability to undergo progesterone-induced acrosome reaction after *in vitro* capacitation [164, 167], and exhibit a clear dysregulation of Ca^{2+} homeostasis [167]. Morphologically, sperm lacking CRISP2 have a stiffness in the midpiece [164]. Sperm from Crisp2$^{-/-}$/Crisp4$^{-/-}$ males show severe fertilization defects compared to single knock out mice likely due to a combination of the impaired abilities described above [169]. Interestingly, sperm from triple and quadruple CRISP knockout mice that include Crisp2$^{-/-}$ show defects in gamete fusion which is not observed in Crisp1$^{-/-}$/Crisp3$^{-/-}$ mutant

mice [169]. Comparation of those knock out animal models indicate that CRISP2 holds an independent function for flagellar rigidity, which is critical for hyperactivated motility during sperm migration in the oviduct and sperm-egg interaction [170].

4 Outline of this thesis

The goal of the present work was to characterize and address the biochemical structural and physiological features and the fate of testicular CRISP2 in mammalian fertilization using a pig model, which was less studied when compared to other mammalian species. The relevance and feasibility of using pig as a model to study human fertilization process and assisted reproductive therapy has been reviewed [171].

In **chapter 2**, the localization of CRISP2 was studied in ejaculated boar spermatozoa using confocal immunofluorescent imaging as well as immunogold labeling on ultrathin cryo-coupes using transmission electron microscopy (TEM). Our data revealed that CRISP2 was localized in the PAS-PT of the sperm head, the connecting piece as well as the FS and ODFs of the sperm tail. No visible CRISP2 signal was observed in the acrosome lumen. By isolating and purifying sperm head and tail fractions, we studied the biochemical properties of CRISP2 from the head and tail. The results showed that CRISP2 was present in high molecular weight complexes in the sperm head fractions and was sensitive to β-mercapto-ethanol treatment. However, CRISP2 was present as SDS and β-mercapto-ethanol resistant multimers in the sperm tail fractions. Interestingly, 8 M urea effectively caused disassociation of CRISP2 from the protein complexes in the form of CRISP2 monomers. CRISP2 oligomers in the sperm head and tail are assembled in different ways.

In **chapter 3**, we observed the behavior of CRISP2 during *in vitro* capacitation, ionophore A23781 induced acrosome reaction, and the fate of CRISP2 during *in vitro* fertilization (6-8 h

post insemination). Exposure of CRISP2 on the apical ridge and the EqS was observed after *in vitro* capacitation and this exposure was associated with elevated protein tyrosine phosphorylation. Rapid dispersal of CRISP2 from the PAS-PT was observed within the oocyte cytoplasm, while the sperm nucleus was still condensed. CRISP2 was undetectable in the two pronuclear stage while the sperm mitochondria were still linearly arranged. These data indicate that reduction of disulfide bridges within CRISP2 oligomers may be instrumental for PT dispersal and PT elimination.

In **chapter 4**, taking the advantages of the adapted protocol to isolate PT proteins from sperm heads as described in chapter 2 in order to find enriched proteins of the PT proteins, we identified PT proteome of boar spermatozoa using a high-resolution proteomic approach. By diverse functional analyses, we provide comprehensive insights into PT residing proteins. We also discuss the function of the PT proteins, as identified by proteomics, after fertilization i.e., when the PT rapidly disperses as described in chapter 3.

Intrigued by the findings that CRISP2 was involved in protein complexes in the PT as well as in the ODF and FS under native conditions as described in chapter 2, in **chapter 5**, we identified the CRISP2 interacting proteome. We used two independent techniques to isolate CRISP2 interacting proteins namely: (i) after co-immunoprecipitation with CRISP2; and (ii) after loading native sperm proteins on gel followed by electrophoresis and cutting the CRISP2 containing protein complex. Both CRISP2 containing protein aggregates were used for native digestion. The interacting proteins were identified with a quantitative, label free liquid chromatography mass spectrometry (LC-MS/MS) approach. Despite the absence of CRISP2 in the lumen of the acrosome as described in chapter 2, it showed interactions with acrosin and ACRBP and thus may be coupled to these proteins through the acrosomal membranes. With

proximity ligation assays, changes in CRISP2 interactions with ACRBP and acrosin have been observed and are discussed in this chapter with respect to the functional implications in mammalian fertilization.

Finally, in the last chapter, **chapter 6**, the findings described in chapter 2-5 and future perspectives are discussed.

References

1. de Kretser DM, Loveland KL, Meinhardt A, Simorangkir D, Wreford N. Spermatogenesis. Hum Reprod 1998; 13 Suppl 1:1-8.
2. Roosen-Runge EC, Holstein AF. The human rete testis. Cell Tissue Res 1978; 189:409-433.
3. Griswold MD. Spermatogenesis: The Commitment to Meiosis. Physiol Rev 2016; 96:1-17.
4. Hess RA, de Franca LR. Spermatogenesis and Cycle of the Seminiferous Epithelium. In: Cheng CY (ed.) Molecular Mechanisms in Spermatogenesis. New York, NY: Springer New York; 2008: 1-15.
5. Boskovic A, Torres-Padilla ME. How mammals pack their sperm: a variant matter. Genes Dev 2013; 27:1635-1639.
6. McCarrey JR, Geyer CB, Yoshioka H. Epigenetic regulation of testis-specific gene expression. Ann N Y Acad Sci 2005; 1061:226-242.
7. Meistrich ML, Mohapatra B, Shirley CR, Zhao M. Roles of transition nuclear proteins in spermiogenesis. Chromosoma 2003; 111:483-488.
8. Domenjoud L, Kremling H, Burfeind P, Maier W-M, Engel W. On the expression of protamine genes in the testis of man and other mammals. Andrologia 1991; 23:333-337.
9. Balhorn R, Cosman M, Thornton K, Krishnan V, Corzett M, Bench G, Kramer C, Lee J, Hud N, Allen M. The male gamete: from basic knowledge to clinical applications. In: Cache River Press, Vienna, IL; 1999.
10. Thomas CA, Garner DL, DeJarnette JM, Marshall CE. Fluorometric assessments of acrosomal integrity and viability in cryopreserved bovine spermatozoa. Biol Reprod 1997; 56:991-998.
11. Kashiwabara S, Arai Y, Kodaira K, Baba T. Acrosin biosynthesis in meiotic and postmeiotic spermatogenic cells. Biochem Biophys Res Commun 1990; 173:240-245.
12. Bedford JM, Moore HD, Franklin LE. Significance of the equatorial segment of the acrosome of the spermatozoon in eutherian mammals. Exp Cell Res 1979; 119:119-126.
13. Longo FJ, Cook S. Formation of the perinuclear theca in spermatozoa of diverse mammalian species: relationship of the manchette and multiple band polypeptides. Mol Reprod Dev 1991; 28:380-393.
14. Oko RJ. Developmental expression and possible role of perinuclear theca proteins in mammalian spermatozoa. Reproduction, Fertility and Development 1995; 7:777-797.
15. Oko R, Sutovsky P. Biogenesis of sperm perinuclear theca and its role in sperm functional competence and fertilization. Journal of Reproductive Immunology 2009; 83:2-7.
16. Tovich PR, Sutovsky P, Oko RJ. Novel aspect of perinuclear theca assembly revealed by immunolocalization of non-nuclear somatic histones during bovine spermiogenesis. Biology of reproduction 2004; 71:1182-1194.
17. Wu AT, Sutovsky P, Xu W, van der Spoel AC, Platt FM, Oko R. The postacrosomal assembly of sperm head protein, PAWP, is independent of acrosome formation and dependent on microtubular manchette transport. Developmental biology 2007; 312:471-483.
18. Sutovsky P, Manandhar G, Wu A, Oko R. Interactions of sperm perinuclear theca with the oocyte: Implications for oocyte activation, anti-polyspermy defense, and assisted reproduction. Microscopy Research and Technique 2003; 61:362-378.
19. Lehti MS, Sironen A. Formation and function of sperm tail structures in association with sperm motility defects†. Biology of Reproduction 2017; 97:522-536.
20. Lindemann CB, Lesich KA. Functional anatomy of the mammalian sperm flagellum. Cytoskeleton 2016; 73:652-669.
21. Toure A, Rode B, Hunnicutt GR, Escalier D, Gacon G. Septins at the annulus of mammalian sperm. 2011; 392:799-803.

22. Melser S, Lavie J, Bénard G. Mitochondrial degradation and energy metabolism. Biochimica et Biophysica Acta (BBA) - Molecular Cell Research 2015; 1853:2812-2821.
23. Yang K, Meinhardt A, Zhang B, Grzmil P, Adham IM, Hoyer-Fender S. The small heat shock protein ODF1/HSPB10 is essential for tight linkage of sperm head to tail and male fertility in mice. Mol Cell Biol 2012; 32:216-225.
24. Hetherington L, Schneider EK, Scott C, DeKretser D, Muller CH, Hondermarck H, Velkov T, Baker MA. Deficiency in Outer Dense Fiber 1 Is a Marker and Potential Driver of Idiopathic Male Infertility. Mol Cell Proteomics 2016; 15:3685-3693.
25. Zhao W, Li Z, Ping P, Wang G, Yuan X, Sun F. Outer dense fibers stabilize the axoneme to maintain sperm motility. J Cell Mol Med 2018; 22:1755-1768.
26. Miki K, Willis WD, Brown PR, Goulding EH, Fulcher KD, Eddy EM. Targeted Disruption of the Akap4 Gene Causes Defects in Sperm Flagellum and Motility. Developmental Biology 2002; 248:331-342.
27. Dacheux JL, Castella S, Gatti JL, Dacheux F. Epididymal cell secretory activities and the role of proteins in boar sperm maturation. Theriogenology 2005; 63:319-341.
28. Burkin HR, Miller DJ. Zona pellucida protein binding ability of porcine sperm during epididymal maturation and the acrosome reaction. Developmental Biology 2000; 222:99-109.
29. Gervasi MG, Visconti PE. Molecular changes and signaling events occurring in spermatozoa during epididymal maturation. Andrology 2017; 5:204-218.
30. Rengan AK, Agarwal A, van der Linde M, du Plessis SS. An investigation of excess residual cytoplasm in human spermatozoa and its distinction from the cytoplasmic droplet. Reproductive Biology and Endocrinology 2012; 10:92.
31. Cooper TG. The epididymis, cytoplasmic droplets and male fertility. Asian journal of andrology 2011; 13:130.
32. Dacheux J-L, Castella S, Gatti JL, Dacheux F. Epididymal cell secretory activities and the role of proteins in boar sperm maturation. Theriogenology 2005; 63:319-341.
33. Guyonnet B, Dacheux F, Dacheux JL, Gatti JL. The epididymal transcriptome and proteome provide some insights into new epididymal regulations. J Androl 2011; 32:651-664.
34. Hinton BT, Robaire B. The Epididymis: From Molecules to Clinical Practice; a Comprehensive Survey of the Efferent Ducts, the Epidiymus, and the Vas Deferens. Kluwer Academic/Plenum Publishers; 2002.
35. Kuo YW, Li SH, Maeda K, Gadella BM, Tsai PS. Roles of the reproductive tract in modifications of the sperm membrane surface. J Reprod Dev 2016; 62:337-343.
36. van Gestel RA, Brewis IA, Ashton PR, Brouwers JF, Gadella BM. Multiple proteins present in purified porcine sperm apical plasma membranes interact with the zona pellucida of the oocyte. Mol Hum Reprod 2007; 13:445-454.
37. Saez F, Ouvrier A, Drevet J. Epididymis cholesterol homeostasis and sperm fertilizing ability. Asian Journal of Andrology 2011; 13:11-17.
38. Rejraji H, Sion B, Prensier G, Carreras M, Motta C, Frenoux JM, Vericel E, Grizard G, Vernet P, Drevet JR. Lipid remodeling of murine epididymosomes and spermatozoa during epididymal maturation. Biol Reprod 2006; 74:1104-1113.
39. Calvin HI, Bedford JM. Formation of disulphide bonds in the nucleus and accessory structures of mammalian spermatozoa during maturation in the epididymis. J Reprod Fertil Suppl 1971; 13:Suppl 13:65-75.
40. Vadnais ML, Aghajanian HK, Lin A, Gerton GL. Signaling in Sperm: Toward a Molecular Understanding of the Acquisition of Sperm Motility in the Mouse Epididymis1. Biology of Reproduction 2013; 89.
41. Maxwell W, De Graaf S, Ghaoui RE-H, Evans G. Seminal plasma effects on sperm handling and female fertility. Society of Reproduction and Fertility supplement 2007; 64:13.

42. Martins C, Rumpf R, Pereira D, Dode M. Cryopreservation of epididymal bovine spermatozoa from dead animals and its uses in vitro embryo production. Animal reproduction science 2007; 101:326-331.
43. Chaveiro A, Cerqueira C, Silva J, Franco J, da Silva FM. Evaluation of frozen thawed cauda epididymal sperms and in vitro fertilizing potential of bovine sperm collected from the cauda epididymal. Iranian Journal of Veterinary Research 2015; 16:188.
44. Druart X, Rickard JP, Tsikis G, de Graaf SP. Seminal plasma proteins as markers of sperm fertility. Theriogenology 2019; 137:30-35.
45. Chang MC. Fertilizing capacity of spermatozoa deposited into the fallopian tubes. Nature 1951; 168:697-698.
46. Austin C. Observations on the penetration of the sperm into the mammalian egg. Australian journal of biological sciences 1951; 4:581-596.
47. Edwards RG, Bavister BD, Steptoe PC. Early stages of fertilization in vitro of human oocytes matured in vitro. Nature 1969; 221:632-635.
48. Bavister B. Capacitation of golden hamster spermatozoa during incubation in culture medium. Reproduction 1973; 35:161-163.
49. Boatman DE, Robbins RS. Bicarbonate: carbon-dioxide regulation of sperm capacitation, hyperactivated motility, and acrosome reactions. Biol Reprod 1991; 44:806-813.
50. Langlais J, Kan F, Granger L, Raymond L, Bleau G, Roberts K. Identification of sterol acceptors that stimulate cholesterol efflux from human spermatozoa during in vitro capacitation. Gamete research 1988; 20:185-201.
51. Ruknudin A, Silver I. Ca2+ uptake during capacitation of mouse spermatozoa and the effect of an anion transport inhibitor on Ca2+ uptake. Molecular reproduction and development 1990; 26:63-68.
52. Davis BK. Interaction of lipids with the plasma membrane of sperm cells. I. The antifertilization action of cholesterol. Arch Androl 1980; 5:249-254.
53. Hamilton DW, Jones AL, Fawcett DW. Cholesterol biosynthesis in the mouse epididymis and ductus deferens: a biochemical and morphological study. Biol Reprod 1969; 1:167-184.
54. Flesch FM, Brouwers JF, Nievelstein PF, Verkleij AJ, van Golde LM, Colenbrander B, Gadella BM. Bicarbonate stimulated phospholipid scrambling induces cholesterol redistribution and enables cholesterol depletion in the sperm plasma membrane. J Cell Sci 2001; 114:3543-3555.
55. Cross NL. Role of Cholesterol in Sperm Capacitation1. Biology of Reproduction 1998; 59:7-11.
56. Visconti PE, Ning X, Fornés MW, Alvarez JG, Stein P, Connors SA, Kopf GS. Cholesterol efflux-mediated signal transduction in mammalian sperm: cholesterol release signals an increase in protein tyrosine phosphorylation during mouse sperm capacitation. Dev Biol 1999; 214:429-443.
57. Langlais J, Kan FW, Granger L, Raymond L, Bleau G, Roberts KD. Identification of sterol acceptors that stimulate cholesterol efflux from human spermatozoa during in vitro capacitation. Gamete Res 1988; 20:185-201.
58. Ehrenwald E, Foote RH, Parks JE. Bovine oviductal fluid components and their potential role in sperm cholesterol efflux. Mol Reprod Dev 1990; 25:195-204.
59. Bernecic NC, de Graaf SP, Leahy T, Gadella BM. HDL mediates reverse cholesterol transport from ram spermatozoa and induces hyperactivated motility. Biol Reprod 2021; 104:1271-1281.
60. Leahy T, Gadella BM. New insights into the regulation of cholesterol efflux from the sperm membrane. Asian journal of andrology 2015; 17:561-567.
61. Aitken RJ, Nixon B. Sperm capacitation: a distant landscape glimpsed but unexplored. Molecular Human Reproduction 2013; 19:785-793.

62. Shadan S, James PS, Howes EA, Jones R. Cholesterol Efflux Alters Lipid Raft Stability and Distribution During Capacitation of Boar Spermatozoa1. Biology of Reproduction 2004; 71:253-265.
63. van Gestel RA, Brewis IA, Ashton PR, Helms JB, Brouwers JF, Gadella BM. Capacitation-dependent concentration of lipid rafts in the apical ridge head area of porcine sperm cells. Mol Hum Reprod 2005; 11:583-590.
64. Galantino-Homer HL, Visconti PE, Kopf GS. Regulation of protein tyrosine phosphorylation during bovine sperm capacitation by a cyclic adenosine 3'5'-monophosphate-dependent pathway. Biol Reprod 1997; 56:707-719.
65. Visconti PE, Stewart-Savage J, Blasco A, Battaglia L, Miranda P, Kopf GS, Tezón JG. Roles of bicarbonate, cAMP, and protein tyrosine phosphorylation on capacitation and the spontaneous acrosome reaction of hamster sperm. Biol Reprod 1999; 61:76-84.
66. Flesch FM, Colenbrander B, van Golde LM, Gadella BM. Capacitation induces tyrosine phosphorylation of proteins in the boar sperm plasma membrane. Biochem Biophys Res Commun 1999; 262:787-792.
67. Lewis B, Aitken RJ. A redox-regulated tyrosine phosphorylation cascade in rat spermatozoa. J Androl 2001; 22:611-622.
68. Aitken RJ, Buckingham DW, Harkiss D, Paterson M, Fisher H, Irvine DS. The extragenomic action of progesterone on human spermatozoa is influenced by redox regulated changes in tyrosine phosphorylation during capacitation. Mol Cell Endocrinol 1996; 117:83-93.
69. Visconti PE, Moore GD, Bailey JL, Leclerc P, Connors SA, Pan D, Olds-Clarke P, Kopf GS. Capacitation of mouse spermatozoa. II. Protein tyrosine phosphorylation and capacitation are regulated by a cAMP-dependent pathway. Development 1995; 121:1139-1150.
70. Pommer AC, Rutllant J, Meyers SA. Phosphorylation of protein tyrosine residues in fresh and cryopreserved stallion spermatozoa under capacitating conditions. Biol Reprod 2003; 68:1208-1214.
71. Urner F, Leppens-Luisier G, Sakkas D. Protein tyrosine phosphorylation in sperm during gamete interaction in the mouse: the influence of glucose. Biol Reprod 2001; 64:1350-1357.
72. Petrunkina AM, Friedrich J, Drommer W, Bicker G, Waberski D, Töpfer-Petersen E. Kinetic characterization of the changes in protein tyrosine phosphorylation of membranes, cytosolic Ca2+ concentration and viability in boar sperm populations selected by binding to oviductal epithelial cells. Reproduction 2001; 122:469-480.
73. Visconti PE. Understanding the molecular basis of sperm capacitation through kinase design. Proceedings of the National Academy of Sciences 2009; 106:667-668.
74. Luconi M, Barni T, Vannelli GB, Krausz C, Marra F, Benedetti PA, Evangelista V, Francavilla S, Properzi G, Forti G, Baldi E. Extracellular signal-regulated kinases modulate capacitation of human spermatozoa. Biol Reprod 1998; 58:1476-1489.
75. Luna C, Colás C, Pérez-Pé R, Cebrián-Pérez JA, Muiño-Blanco T. A novel epidermal growth factor-dependent extracellular signal-regulated MAP kinase cascade involved in sperm functionality in sheep. Biol Reprod 2012; 87:93.
76. DasGupta S, Mills CL, Fraser LR. Ca(2+)-related changes in the capacitation state of human spermatozoa assessed by a chlortetracycline fluorescence assay. J Reprod Fertil 1993; 99:135-143.
77. Naz RK, Rajesh PB. Role of tyrosine phosphorylation in sperm capacitation / acrosome reaction. Reproductive biology and endocrinology : RB&E 2004; 2:75-75.
78. Yanagimachi R. The movement of golden hamster spermatozoa before and after capacitation. J Reprod Fertil 1970; 23:193-196.
79. Suarez SS. Control of hyperactivation in sperm. Hum Reprod Update 2008; 14:647-657.

80. Quill TA, Sugden SA, Rossi KL, Doolittle LK, Hammer RE, Garbers DL. Hyperactivated sperm motility driven by CatSper2 is required for fertilization. Proc Natl Acad Sci U S A 2003; 100:14869-14874.
81. Stauss CR, Votta TJ, Suarez SS. Sperm motility hyperactivation facilitates penetration of the hamster zona pellucida. Biol Reprod 1995; 53:1280-1285.
82. Suarez SS, Dai XB, DeMott RP, Redfern K, Mirando MA. Movement characteristics of boar sperm obtained from the oviduct or hyperactivated in vitro. J Androl 1992; 13:75-80.
83. Ho HC, Granish KA, Suarez SS. Hyperactivated motility of bull sperm is triggered at the axoneme by Ca2+ and not cAMP. Dev Biol 2002; 250:208-217.
84. Carlson AE, Quill TA, Westenbroek RE, Schuh SM, Hille B, Babcock DF. Identical phenotypes of CatSper1 and CatSper2 null sperm. J Biol Chem 2005; 280:32238-32244.
85. Jin J, Jin N, Zheng H, Ro S, Tafolla D, Sanders KM, Yan W. Catsper3 and Catsper4 are essential for sperm hyperactivated motility and male fertility in the mouse. Biol Reprod 2007; 77:37-44.
86. Marquez B, Suarez SS. Different signaling pathways in bovine sperm regulate capacitation and hyperactivation. Biol Reprod 2004; 70:1626-1633.
87. Steptoe PC, Edwards RG. Birth after the reimplantation of a human embryo. The Lancet 1978; 312:366.
88. Moros-Nicolás C, Chevret P, Jiménez-Movilla M, Algarra B, Cots-Rodríguez P, González-Brusi L, Avilés M, Izquierdo-Rico MJ. New Insights into the Mammalian Egg Zona Pellucida. International Journal of Molecular Sciences 2021; 22:3276.
89. Izquierdo-Rico MJ, Moros-Nicolás C, Pérez-Crespo M, Laguna-Barraza R, Gutiérrez-Adán A, Veyrunes F, Ballesta J, Laudet V, Chevret P, Avilés M. ZP4 Is Present in Murine Zona Pellucida and Is Not Responsible for the Specific Gamete Interaction. Frontiers in Cell and Developmental Biology 2021; 8.
90. Tumova L, Zigo M, Sutovsky P, Sedmikova M, Postlerova P. Ligands and Receptors Involved in the Sperm-Zona Pellucida Interactions in Mammals. Cells 2021; 10:133.
91. Lefièvre L, Conner SJ, Salpekar A, Olufowobi O, Ashton P, Pavlovic B, Lenton W, Afnan M, Brewis IA, Monk M, Hughes DC, Barratt CL. Four zona pellucida glycoproteins are expressed in the human. Hum Reprod 2004; 19:1580-1586.
92. Bleil JD, Wassarman PM. Structure and function of the zona pellucida: Identification and characterization of the proteins of the mouse oocyte's zona pellucida. Developmental Biology 1980; 76:185-202.
93. Hedrick JL, Wardrip NJ. On the macromolecular composition of the zona pellucida from porcine oocytes. Dev Biol 1987; 121:478-488.
94. Noguchi S, Yonezawa N, Katsumata T, Hashizume K, Kuwayama M, Hamano S, Watanabe S, Nakano M. Characterization of the zona pellucida glycoproteins from bovine ovarian and fertilized eggs. Biochim Biophys Acta 1994; 1201:7-14.
95. Clark GF. A role for carbohydrate recognition in mammalian sperm-egg binding. Biochemical and Biophysical Research Communications 2014; 450:1195-1203.
96. Boerke A, Tsai P, Garcia-Gil N, Brewis I, Gadella B. Capacitation-dependent reorganization of microdomains in the apical sperm head plasma membrane: functional relationship with zona binding and the zona-induced acrosome reaction. Theriogenology 2008; 70:1188-1196.
97. Jones R, Brown C, Lancaster R. Carbohydrate-binding properties of boar sperm proacrosin and assessment of its role in sperm-egg recognition and adhesion during fertilization. Development 1988; 102:781-792.
98. Kongmanas K, Kruevaisayawan H, Saewu A, Sugeng C, Fernandes J, Souda P, Angel JB, Faull KF, Aitken RJ, Whitelegge J. Proteomic characterization of pig sperm anterior head

plasma membrane reveals roles of acrosomal proteins in ZP3 binding. Journal of cellular physiology 2015; 230:449-463.
99. Hardy DM, Garbers DL. A Sperm Membrane Protein That Binds in a Species-specific Manner to the Egg Extracellular Matrix Is Homologous to von Willebrand Factor (∗). Journal of Biological Chemistry 1995; 270:26025-26028.
100. Ensslin M, Vogel T, Calvete JJ, Thole HH, Schmidtke J, Matsuda T, Töpfer-Petersen E. Molecular Cloning and Characterization of P47, a Novel Boar Sperm-Associated Zona Pellucida-Binding Protein Homologous to a Family of Mammalian Secretory Proteins1. Biology of Reproduction 1998; 58:1057-1064.
101. Khalil MB, Chakrabandhu K, Xu H, Weerachatyanukul W, Buhr M, Berger T, Carmona E, Vuong N, Kumarathasan P, Wong PTT, Carrier D, Tanphaichitr N. Sperm capacitation induces an increase in lipid rafts having zona pellucida binding ability and containing sulfogalactosylglycerolipid. Developmental Biology 2006; 290:220-235.
102. Gupta SK. Unraveling the intricacies of mammalian fertilization. Asian journal of andrology 2014; 16:801-802.
103. Tomes CN. Molecular mechanisms of membrane fusion during acrosomal exocytosis. Soc Reprod Fertil Suppl 2007; 65:275-291.
104. Mayorga LS, Tomes CN, Belmonte SA. Acrosomal exocytosis, a special type of regulated secretion. IUBMB Life 2007; 59:286-292.
105. Berger T, Turner KO, Meizel S, Hedrick JL. Zona pellucida-induced acrosome reaction in boar sperm. Biol Reprod 1989; 40:525-530.
106. Hyttel P, Greve T, Callesen H. Ultrastructural aspects of oocyte maturation and fertilization in cattle. J Reprod Fertil Suppl 1989; 38:35-47.
107. Jin M, Fujiwara E, Kakiuchi Y, Okabe M, Satouh Y, Baba SA, Chiba K, Hirohashi N. Most fertilizing mouse spermatozoa begin their acrosome reaction before contact with the zona pellucida during in vitro fertilization. Proceedings of the National Academy of Sciences 2011; 108:4892-4896.
108. Huang T, Fleming A, Yanagimachi R. Only acrosome‐reacted spermatozoa can bind to and penetrate zona pellucida: A study using the guinea pig. Journal of Experimental Zoology 1981; 217:287-290.
109. Tsai PS, Garcia-Gil N, van Haeften T, Gadella BM. How pig sperm prepares to fertilize: stable acrosome docking to the plasma membrane. PLoS One 2010; 5:e11204.
110. Tsai PS, Brewis IA, van Maaren J, Gadella BM. Involvement of complexin 2 in docking, locking and unlocking of different SNARE complexes during sperm capacitation and induced acrosomal exocytosis. PLoS One 2012; 7:e32603.
111. Michaut M, Tomes CN, De Blas G, Yunes R, Mayorga LS. Calcium-triggered acrosomal exocytosis in human spermatozoa requires the coordinated activation of Rab3A and N-ethylmaleimide-sensitive factor. Proc Natl Acad Sci U S A 2000; 97:9996-10001.
112. Osman RA, Andria ML, Jones AD, Meizel S. Steroid induced exocytosis: the human sperm acrosome reaction. Biochemical and biophysical research communications 1989; 160:828-833.
113. Meizel S, Turner KO. Progesterone acts at the plasma membrane of human sperm. Molecular and Cellular Endocrinology 1991; 77:R1-R5.
114. Yanagimachi R. Mammalian fertilization. The physiology of reproduction 1994.
115. Breitbart H. Role and regulation of intracellular calcium in acrosomal exocytosis. Journal of reproductive immunology 2002; 53:151-159.
116. Kirkman-Brown JC, Punt EL, Barratt CL, Publicover SJ. Zona pellucida and progesterone-induced Ca2+ signaling and acrosome reaction in human spermatozoa. J Androl 2002; 23:306-315.

117. Liu DY, Baker HW. Calcium ionophore-induced acrosome reaction correlates with fertilization rates in vitro in patients with teratozoospermic semen. Human Reproduction 1998; 13:905-910.
118. Jamil K, White IG. Induction of acrosomal reaction in sperm with ionophore A23187 and calcium. Arch Androl 1981; 7:283-292.
119. Honda A, Siruntawineti J, Baba T. Role of acrosomal matrix proteases in sperm–zona pellucida interactions. Human Reproduction Update 2002; 8:405-412.
120. Urch UA, Wardrip NJ, Hedrick JL. Limited and specific proteolysis of the zona pellucida by acrosin. Journal of Experimental Zoology 1985; 233:479-483.
121. Mao HT, Yang WX. Modes of acrosin functioning during fertilization. Gene 2013; 526:75-79.
122. Baba T, Azuma S, Kashiwabara S-i, Toyoda Y. Sperm from mice carrying a targeted mutation of the acrosin gene can penetrate the oocyte zona pellucida and effect fertilization. Journal of Biological Chemistry 1994; 269:31845-31849.
123. Hirose M, Honda A, Fulka H, Tamura-Nakano M, Matoba S, Tomishima T, Mochida K, Hasegawa A, Nagashima K, Inoue K, Ohtsuka M, Baba T, et al. Acrosin is essential for sperm penetration through the zona pellucida in hamsters. Proceedings of the National Academy of Sciences 2020; 117:2513-2518.
124. Wang H, Song C, Duan C, Shi W, Li C, Chen D, Wang Y. Effects of ubiquitin-proteasome pathway on mouse sperm capacitation, acrosome reaction and in vitro fertilization. Chinese Science Bulletin 2002; 47:127-132.
125. Sun QY, Fuchimoto D, Nagai T. Regulatory roles of ubiquitin–proteasome pathway in pig oocyte meiotic maturation and fertilization. Theriogenology 2004; 62:245-255.
126. Sutovsky P, Manandhar G, McCauley TC, Caamaño JN, Sutovsky M, Thompson WE, Day BN. Proteasomal Interference Prevents Zona Pellucida Penetration and Fertilization in Mammals1. Biology of Reproduction 2004; 71:1625-1637.
127. Primakoff P, Myles DG. Cell–cell membrane fusion during mammalian fertilization. FEBS Letters 2007; 581:2174-2180.
128. Bedford J, Moore H, Franklin L. Significance of the equatorial segment of the acrosome of the spermatozoon in eutherian mammals. Experimental cell research 1979; 119:119-126.
129. Jean C, Haghighirad F, Zhu Y, Chalbi M, Ziyyat A, Rubinstein E, Gourier C, Yip P, Wolf JP, Lee JE, Boucheix C, Barraud-Lange V. JUNO, the receptor of sperm IZUMO1, is expressed by the human oocyte and is essential for human fertilisation. Hum Reprod 2019; 34:118-126.
130. Bianchi E, Doe B, Goulding D, Wright GJ. Juno is the egg Izumo receptor and is essential for mammalian fertilization. Nature 2014; 508:483-487.
131. Inoue N, Hagihara Y, Wright D, Suzuki T, Wada I. Oocyte-triggered dimerization of sperm IZUMO1 promotes sperm–egg fusion in mice. Nature communications 2015; 6:1-12.
132. Deneke VE, Pauli A. The Fertilization Enigma: How Sperm and Egg Fuse. Annual Review of Cell and Developmental Biology 2021; 37:391-414.
133. Kaji K, Oda S, Shikano T, Ohnuki T, Uematsu Y, Sakagami J, Tada N, Miyazaki S, Kudo A. The gamete fusion process is defective in eggs of Cd9-deficient mice. Nature genetics 2000; 24:279-282.
134. Miyado K, Yamada G, Yamada S, Hasuwa H, Nakamura Y, Ryu F, Suzuki K, Kosai K, Inoue K, Ogura A. Requirement of CD9 on the egg plasma membrane for fertilization. Science 2000; 287:321-324.
135. Koppers AJ, Reddy T, O'Bryan MK. The role of cysteine-rich secretory proteins in male fertility. Asian J Androl 2011; 13:111-117.
136. Gibbs GM, O'Bryan MK. Cysteine rich secretory proteins in reproduction and venom. Society of Reproduction and Fertility supplement 2007; 65:261-267.

137. Yamazaki Y, Morita T. Structure and function of snake venom cysteine-rich secretory proteins. Toxicon 2004; 44:227-231.
138. Gibbs GM, Roelants K, O'Bryan MK. The CAP Superfamily: Cysteine-Rich Secretory Proteins, Antigen 5, and Pathogenesis-Related 1 Proteins—Roles in Reproduction, Cancer, and Immune Defense. Endocrine Reviews 2008; 29:865-897.
139. Gaikwad AS, Hu J, Chapple DG, O'Bryan MK. The functions of CAP superfamily proteins in mammalian fertility and disease. Hum Reprod Update 2020; 26:689-723.
140. Sheng J, Olrichs NK, Gadella BM, Kaloyanova DV, Helms JB. Regulation of Functional Protein Aggregation by Multiple Factors: Implications for the Amyloidogenic Behavior of the CAP Superfamily Proteins. Int J Mol Sci 2020; 21.
141. Sheng J, Gadella BM, Olrichs NK, Kaloyanova DV, Helms JB. The less conserved metal-binding site in human CRISP1 remains sensitive to zinc ions to permit protein oligomerization. Scientific Reports 2021; 11:5498.
142. Gibbs GM, Orta G, Reddy T, Koppers AJ, Martínez-López P, de la Vega-Beltràn JL, Lo JC, Veldhuis N, Jamsai D, McIntyre P. Cysteine-rich secretory protein 4 is an inhibitor of transient receptor potential M8 with a role in establishing sperm function. Proceedings of the National Academy of Sciences 2011; 108:7034-7039.
143. Hu J, Merriner DJ, O'Connor AE, Houston BJ, Furic L, Hedger MP, O'Bryan MK. Epididymal cysteine-rich secretory proteins are required for epididymal sperm maturation and optimal sperm function. MHR: Basic science of reproductive medicine 2018; 24:111-122.
144. Ernesto JI, Weigel Muñoz M, Battistone MA, Vasen G, Martínez-López P, Orta G, Figueiras-Fierro D, De la Vega-Beltran JL, Moreno IA, Guidobaldi HA, Giojalas L, Darszon A, et al. CRISP1 as a novel CatSper regulator that modulates sperm motility and orientation during fertilization. The Journal of cell biology 2015; 210:1213-1224.
145. Jalkanen J, Huhtaniemi I, Poutanen M. Mouse cysteine-rich secretory protein 4 (CRISP4): a member of the Crisp family exclusively expressed in the epididymis in an androgen-dependent manner. Biology of Reproduction 2005; 72:1268-1274.
146. Nolan MA, Wu L, Bang HJ, Jelinsky SA, Roberts KP, Turner TT, Kopf GS, Johnston DS. Identification of rat cysteine-rich secretory protein 4 (Crisp4) as the ortholog to human CRISP1 and mouse Crisp4. Biology of reproduction 2006; 74:984-991.
147. Reddy T, Gibbs GM, Merriner DJ, Kerr JB, O'Bryan MK. Cysteine-rich secretory proteins are not exclusively expressed in the male reproductive tract. Developmental dynamics: an official publication of the American Association of Anatomists 2008; 237:3313-3323.
148. Guasti PN, Souza FF, Scott C, Papa PM, Camargo LS, Schmith RA, Monteiro GA, Hartwig FP, Papa FO. Equine seminal plasma and sperm membrane: Functional proteomic assessment. Theriogenology 2020; 156:70-81.
149. Novak S, Smith TA, Paradis F, Burwash L, Dyck MK, Foxcroft GR, Dixon WT. Biomarkers of in vivo fertility in sperm and seminal plasma of fertile stallions. Theriogenology 2010; 74:956-967.
150. Noh B, Sung J, Kim Y, Chang S, Park Y. Prognostic value of ERG, PTEN, CRISP3 and SPINK1 in predicting biochemical recurrence in prostate cancer. Oncology Letters 2016; 11:3621-3630.
151. Bjartell A, Johansson R, Bjork T, Gadaleanu V, Lundwall A, Lilja H, Kjeldsen L, Udby L. Immunohistochemical detection of cysteine-rich secretory protein 3 in tissue and in serum from men with cancer or benign enlargement of the prostate gland. Prostate 2006; 66:591-603.

152. Volpert M, Furic L, Hu J, O'Connor AE, Rebello RJ, Keerthikumar S, Evans J, Merriner DJ, Pedersen J, Risbridger GP. CRISP3 expression drives prostate cancer invasion and progression. Endocrine-Related Cancer 2020; 27:415-430.
153. Hardy DM, Huang TT, Jr., Driscoll WJ, Tung KK, Wild GC. Purification and characterization of the primary acrosomal autoantigen of guinea pig epididymal spermatozoa. Biol Reprod 1988; 38:423-437.
154. Kasahara M, Gutknecht J, Brew K, Spurr N, Goodfellow PN. Cloning and mapping of a testis-specific gene with sequence similarity to a sperm-coating glycoprotein gene. Genomics 1989; 5:527-534.
155. Foster JA, Gerton GL. Autoantigen 1 of the guinea pig sperm acrosome is the homologue of mouse Tpx-1 and human TPX1 and is a member of the cysteine-rich secretory protein (CRISP) family. Molecular Reproduction and Development 1996; 44:221-229.
156. O'Bryan MK, Sebire K, Meinhardt A, Edgar K, Keah HH, Hearn MT, De Kretser DM. Tpx-1 is a component of the outer dense fibers and acrosome of rat spermatozoa. Mol Reprod Dev 2001; 58:116-125.
157. Maeda T, Nishida J, Nakanishi Y. Expression pattern, subcellular localization and structure--function relationship of rat Tpx-1, a spermatogenic cell adhesion molecule responsible for association with Sertoli cells. Dev Growth Differ 1999; 41:715-722.
158. Busso D, Cohen DJ, Hayashi M, Kasahara M, Cuasnicú PS. Human testicular protein TPX1/CRISP-2: localization in spermatozoa, fate after capacitation and relevance for gamete interaction. Mol Hum Reprod 2005; 11:299-305.
159. Nimlamool W, Bean BS, Lowe-Krentz LJ. Human sperm CRISP2 is released from the acrosome during the acrosome reaction and re-associates at the equatorial segment. Mol Reprod Dev 2013; 80:488-502.
160. Busso D, Goldweic NM, Hayashi M, Kasahara M, Cuasnicú PS. Evidence for the involvement of testicular protein CRISP2 in mouse sperm-egg fusion. Biol Reprod 2007; 76:701-708.
161. Muñoz MW, Ernesto JI, Bluguermann C, Busso D, Battistone MA, Cohen DJ, Cuasnicú PS. Evaluation of Testicular Sperm CRISP2 as a Potential Target for Contraception. Journal of Andrology 2012; 33:1360-1370.
162. Gibbs GM, Scanlon MJ, Swarbrick J, Curtis S, Gallant E, Dulhunty AF, O'Bryan MK. The cysteine-rich secretory protein domain of Tpx-1 is related to ion channel toxins and regulates ryanodine receptor Ca2+ signaling. Journal of Biological Chemistry 2006; 281:4156-4163.
163. Harper CV, Barratt CL, Publicover SJ. Stimulation of human spermatozoa with progesterone gradients to simulate approach to the oocyte. Induction of [Ca(2+)](i) oscillations and cyclical transitions in flagellar beating. J Biol Chem 2004; 279:46315-46325.
164. Lim S, Kierzek M, O'Connor AE, Brenker C, Merriner DJ, Okuda H, Volpert M, Gaikwad A, Bianco D, Potter D, Prabhakar R, Strünker T, et al. CRISP2 Is a Regulator of Multiple Aspects of Sperm Function and Male Fertility. Endocrinology 2019; 160:915-924.
165. Zhou J-H, Zhou Q-Z, Lyu X-M, Zhu T, Chen Z-J, Chen M-K, Xia H, Wang C-Y, Qi T, Li X, Liu C-D. The Expression of Cysteine-Rich Secretory Protein 2 (CRISP2) and Its Specific Regulator miR-27b in the Spermatozoa of Patients with Asthenozoospermia1. Biology of Reproduction 2015; 92.
166. Jing XW, Xing RW, Zhou QZ, Yu QF, Guo WB, Chen SM, Chu QJ, Feng CQ, Mao XM. [Expressions of cysteine-rich secretory protein 2 in asthenospermia]. Zhonghua Nan Ke Xue 2011; 17:203-207.

167. Brukman NG, Miyata H, Torres P, Lombardo D, Caramelo JJ, Ikawa M, Da Ros VG, Cuasnicú PS. Fertilization defects in sperm from Cysteine-rich secretory protein 2 (Crisp2) knockout mice: implications for fertility disorders. Mol Hum Reprod 2016; 22:240-251.
168. Lim S, Kierzek M, O'Connor AE, Brenker C, Merriner DJ, Okuda H, Volpert M, Gaikwad A, Bianco D, Potter D, Prabhakar R, Strünker T, et al. CRISP2 Is a Regulator of Multiple Aspects of Sperm Function and Male Fertility. Endocrinology 2019; 160:915-924.
169. Curci L, Brukman NG, Weigel Muñoz M, Rojo D, Carvajal G, Sulzyk V, Gonzalez SN, Rubinstein M, Da Ros VG, Cuasnicú PS. Functional redundancy and compensation: Deletion of multiple murine Crisp genes reveals their essential role for male fertility. Faseb j 2020; 34:15718-15733.
170. Gonzalez SN, Sulzyk V, Weigel Muñoz M, Cuasnicu PS. Cysteine-Rich Secretory Proteins (CRISP) are Key Players in Mammalian Fertilization and Fertility. Front Cell Dev Biol 2021; 9:800351.
171. Zigo M, Maňásková-Postlerová P, Zuidema D, Kerns K, Jonáková V, Tůmová L, Bubeníčková F, Sutovsky P. Porcine model for the study of sperm capacitation, fertilization and male fertility. Cell Tissue Res 2020; 380:237-262.

Chapter 2

Characterization of different oligomeric forms of CRISP2 in the perinuclear theca versus the fibrous tail structures of boar spermatozoa

M. Zhang[1], E.G. Bromfield[1,2], T. Veenendaal[3], J. Klumperman[3], J.B. Helms[1], B.M. Gadella[1,4*]

[1]Department of Biomolecular Health Sciences, Faculty of Veterinary Medicine, Utrecht University, the Netherlands;

[2]Priority Research Centre for Reproductive Science, University of Newcastle, New South Wales, Australia;

[3]Section Cell Biology, Center for Molecular Medicine, University Medical Center Utrecht, Utrecht University, the Netherlands;

[4]Department of Farm Animal Health, Faculty of Veterinary Medicine, Utrecht University, Utrecht, the Netherlands.

Published as:
Zhang M, Bromfield EG, Veenendaal T, Klumperman J, Helms JB, Gadella BM. Characterization of different oligomeric forms of CRISP2 in the perinuclear theca versus the fibrous tail structures of boar spermatozoa. Biol Reprod. 2021 Nov 15;105(5):1160-1170.

Abstract

Mammalian sperm carry a variety of highly condensed insoluble protein structures such as the perinuclear theca, the fibrous sheath and the outer dense fibers, which are essential to sperm function. We studied the role of cysteine rich secretory protein 2 (CRISP2), a known inducer of non-pathological protein amyloids, in pig sperm with a variety of techniques. CRISP2, which is synthesized during spermatogenesis, was localized by confocal immunofluorescent imaging in the tail and in the post-acrosomal region of the sperm head. High resolution localization by immunogold labeling electron microscopy (EM) of ultrathin cryosections revealed that CRISP2 was present in the perinuclear theca and neck region of the sperm head, as well as in the outer dense fibers and the fibrous sheath of the sperm tail. Interestingly, we found that under native, non-reducing conditions CRISP2 formed oligomers both in the tail and the head but with different molecular weights and different biochemical properties. The tail oligomers were insensitive to reducing conditions but completely dissociated into monomers under 8 M urea treatment, while the head 250 kDa CRISP2 positive oligomer completely dissociated into CRISP2 monomers under reducing conditions. The head specific dissociation of CRISP2 oligomer is likely a result of the reduction of various sulfhydryl groups in the cysteine rich domain of this protein. The sperm head CRISP2 shared typical solubilization characteristics with other perinuclear theca proteins as was shown with sequential detergent and salt treatments. Thus, CRISP2 is likely to participate in the formation of functional protein complexes in both the sperm tail and sperm head, but with differing oligomeric organization and biochemical properties. Future studies will be devoted to the understand the role of CRISP2 in sperm protein complexes formation and how this contributes to the fertilization processes.

Keywords: CRISP-2; fibrous sheath; outer dense fibers; perinuclear theca; pig sperm; protein oligomers.

Introduction

Cysteine-rich secretory proteins (CRISPs) are members of the CAP (CRISPs, Antigen 5 and Pathogenesis related protein 1) superfamily that are expressed in all eukaryotes. The CAP family proteins have been widely implicated in many physiological and pathological processes including immunity, venom toxicity, reproduction and cancer biology [1-3]. Evolutionary studies have revealed that the CRISP subfamily is only found in amniotes [4,5]. In reptiles, CRISPs are found in venoms and many snake venom CRISPs have been characterized in the last decades [4, 5]. In mammals, three paralogues of four CRISP members have been described: CRISP1, CRISP2, CRISP3 and CRISP4, with CRISP4 only found in some rodent species [6]. These proteins are 20-30 kDa in size and share an N-terminal CAP domain containing four conserved motifs and a C-terminal cysteine-rich domain connected with a hinge [1, 7]. Mammalian CRISPs are highly expressed in male reproductive tract tissues where CRISP1 and CRISP4 are secreted by epithelial cells lining the ductus epididymis, while CRISP2 expression is initiated during spermatogenesis in the testis [8]. CRISP3 is known to be secreted into seminal plasma by epithelial cells from accessory gland such as the prostate and the seminal vesicle [9]. Importantly, double knock out (DKO) Crisp1/Crisp4 mice demonstrate a male subfertility phenotype [10], while a similar DKO model indicated a decreased sperm motility phenotype without a loss of fertility [11]. Numerous studies have shown that CRISP3 expression is significantly increased in prostate cancer cells and is a valuable maker for prostate cancer prognosis [12-15].

Gene manipulation studies of CRISP2 have recently revealed that CRISP2 is important for sperm motility, sperm-egg fusion and male fertility. Crisp2 knockout mice showed a significant fertility dysfunction phenotype [16] as the sperm they produce have lower acrosome reaction rates in response to progesterone and show an altered flagellum beating

pattern [17]. In line with this, low expression levels of CRISP2 are observed in sperm from asthenoteratozoospermia patients and is proposed as a causal factor of male infertility [18-20]. One rationale for why CRISP2 defects may affect male fertility lies in observation that CRISP2 is the sole CRISP that is expressed during the early stages of spermiogenesis where CRISP2 mRNA undergoes a significant translational delay before CRISP2 protein is incorporated in to the developing sperm head and tail [17, 21]. Unlike other mammalian CRISPs, CRISP2 gene expression is not dependent on androgen regulation, nor is the protein post-translationally modified by glycosylation [22]. CRISP2 shows a conserved localization pattern in the sperm acrosome, connecting piece and the outer dense fibers of the sperm tail among human, mouse and guinea pig spermatozoa [21, 23, 24]. Notably, in human sperm, CRISP2 is released from the acrosome and reoriented at the equatorial segment after the acrosome reaction, suggesting a possible involvement in the orchestration of sperm-egg fusion [23]. Human sperm CRISP2 protein is detected as a 25 kDa band on immunoblots and it is stably associated with sperm pellet in acidic medium, but is known to be completely soluble when held in a medium at pH 11 [23]. Two forms of CRISP2: 25 kDa and 27 kDa are present in the rat sperm acrosome and outer dense fibers [21].

Mammalian sperm carry a variety of highly condensed insoluble protein structures such as the perinuclear theca (PT). This cytoskeletal structure flanks the nucleus of mammalian mature sperm. It can be divided into two structurally continuous but functionally distinct regions: the sub-acrosomal layer (SAL) and the post-acrosomal sheath (PAS) [25, 26]. Proteins of the SAL reside between the inner acrosomal membrane and the nuclear envelope at the equatorial segment region of the sperm head, while posterior from the acrosome, proteins reside between the plasmalemma and the nuclear envelope making up the PAS [26]. Dozens of proteins have been identified as constituents of the PT of mammalian sperm over the last decades, however

the function of the PT during and following fertilization is largely unknown. Besides the PT, also insoluble protein aggregates have been observed in the acrosome [27-29]. Moreover two other insoluble protein aggregates are observed in the sperm tail, where the axoneme is surrounded by 9 outer dense fiber structures and in the principal piece of the sperm tail the axoneme and these outer dense fibers (ODF) are also surrounded by the fibrous sheath (FS) [30]. These two structures serve the longitudinal and radial properties of the sperm flagellum for effective and efficient motility required to fertilize the egg. From previous studies, it is known that all the above mentioned highly condensed non-soluble sperm protein structures contain CRISP2 [21]. Of specific interest in this context is the property of CAP proteins such as CRISP2 (and other CRISP proteins) to form protein oligomers [31]. While little is known regarding this oligomer formation, the CAP domain of CRISP proteins may enable this [32], and the cysteine rich region of the protein may also be involved in protein aggregate formation in a redox sensitive manner [33-35]. Despite these intriguing leads, the involvement of CRISP2 in the diverse insoluble condensed protein structures in spermatozoa has not been addressed biochemically. Therefore, we have investigated the localization and organization of CRISP2 in boar sperm by (i) using immunolabeling techniques combined with both confocal and transmission electron microscopy, (ii) isolating the diverse protein dense structures and to determine the oligomeric organization of CRISP2 under reducing and non-reducing conditions and (iii) investigating the dissociation of CRISP2 under high urea conditions.

Materials and Methods

Reagents and antibodies

All chemicals were obtained from Sigma (St. Louis, MO, USA) unless otherwise stated. The goat polyclonal antibody against CRISP2 (aa77-89) (Cat#: MBS422304) and paired CRISP2 blocking peptide (Cat#: MBS427212) were obtained from MyBiosource (San Diego, CA, USA). The rabbit polyclonal antibody against CRISP2 (Cat#: 19066-1-A) was obtained from

Proteintech (Chicago, IL, USA) and the mouse anti α-tubulin monoclonal antibody was purchased from Sigma (Cat#: T5168).

Boar sperm preparation

Semen was collected over gauze to remove gelatinous materials and debris. The collected semen from highly fertile boars was diluted to 20 million sperm/mL in a commercial diluter and packed in insemination tubes of 80 mL and transported at 17 °C to our lab by a courier from a commercial breeder (Cooperative Center for Artificial Insemination in Pigs, Veghel, the Netherlands) and stored in a cool box (17 °C) until use. Sperm quality was established by evaluating motility, viability, concentration, and morphological parameters. Sperm cells were washed through a discontinuous Percoll® (GE Healthcare, Piscataway, NJ, USA) gradients consisting of 4 mL 35% v/v and 2 mL 70% v/v Percoll in HEPES-buffered saline (HBS: 20 mM HEPES, 137 mM NaCl, 10 mM glucose, 2.5 mM KCl, 0.1% kanamycin, pH 7.6) at 750 × *g* for 15 min at room temperature (RT) using MIKRO 200 (Hettich, Tuttlingen, Germany). The top and interface layers were removed and sperm pellets were further washed in phosphate buffered saline (PBS), (137 mM NaCl, 8.0 mM Na2HPO4·2H2O, 1.5mM KH2PO4, 2.7 mM KCl, pH 7.4) at 750 × *g* for 10 min, at RT. All solutions were iso-osmotic (290-300 mOsm/kg) and at RT before use.

Isolation of sperm heads and tails

Percoll® washed sperm cells ($1x10^8$) were resuspended in 1.5 mL PBS and 1 mM Phenylmethylsulfonyl fluoride (PMSF) was added to protect against protein degradation. Sperm in solution were sonicated on ice at nine microns using an MSE (East Sussex, UK) Ltd Soniprep 150 sonicator at 15-s bursts with 45-s interval, 3 cycles until >99% of all sperm heads and tails were dissociated. Sonicated sperm heads and tails were separated through a 62% (w/v) sucrose gradient in 10 mM Tris-HCl (pH 7.4) at 50,000 rpm and a temperature of 4 °C for 90 min using a SW 60Ti swinging-bucket rotor (Beckman, Mississauga, Canada). This

ultracentrifugation step resulted in the pelleting of the heads, which are denser than the sucrose, at the centrifugal bottom of the tube and the tails can then be collected from the interface between the solution and the sucrose. The sperm heads and tails were collected and placed in separate tubes, washed twice with PBS at 14,000 x *g*, at 4 °C for 20 min using MIKRO 200R (Hettich, Tuttlingen, Germany), and then used directly or frozen at -80°C for later use.

Isolation of PT proteins from the sonicated boar sperm head

Perinuclear theca proteins from the boar sperm head were isolated as previously described [36, 37]. Purified sperm heads were first extracted in 0.2% (v/v) Triton X-100 for 1 h at RT with agitation. Following the incubations, the solution was then subjected to centrifugation at 2500 x *g* for 10 min at RT and the resulting supernatants were recovered. The pellets were then extracted in 1M KCl as the first step extraction. After washing, the pellets were then extracted in 0.1 M NaOH overnight at 4 °C with agitation. PT proteins were then retrieved from the alkaline extraction supernatants. The resulting pellets were washed twice with PBS before the next extraction and/or before being solubilized in sodium dodecyl sulfate (SDS) sample buffer/fixed in 4% paraformaldehyde (PFA) for immunostaining.

Detergent fractionation of sperm heads and tails

Purified, sonicated sperm heads were subjected to serial extractions to investigate CRISP2 extractability as previously reported [37]. Briefly, sonicated sperm heads were first extracted in 1% (v/v) NP-40 at RT with agitation for 2 h. Following the incubations, the solution was subjected to centrifugation at 2500 x *g*, at RT for 10 min and the resulting supernatants were recovered. The pellets were then extracted in 1% (w/v) SDS for 2 h, at RT, with agitation. The resulting pellets were washed twice with PBS before the next extraction and/or before being solubilized in SDS sample buffer.

Purified sperm tails were incubated in 1% (v/v) Triton X-100 (50 mM HEPES, 150 mM NaCl,

pH 7.2, 1%Triton X-100) on ice or SDS-EDTA buffer (1% SDS, 75 mM NaCl, 24 mM EDTA, pH 6.0) for 30 min at RT and centrifuged at 14,000 x *g*, for 15 min. Soluble and insoluble fractions were collected, respectively. Insoluble pellets were further denatured in 2x SDS sample buffer (100 mM Tris, pH 6.8, 4% SDS, 0.04% bromophenol blue, 20% glycerol, 5% β-mercapto-ethanol) and boiled for 10 min. For an additional experiment, sperm tails were directly solubilized in 2x SDS sample buffer (for details see Immunoblotting), boiled for 10 min or solubilized in 8 M urea (in 2x SDS sample buffer), without heating.

Blue native PAGE and native blots

The sperm head and tail fractions were extracted in 1% (v/v) Triton X-100 (50 mM HEPES, 150 mM NaCl, pH 7.2, 1%Triton X-100) for 30 min on ice, followed by a 15 min centrifugation at 14,000g, 4°C. Supernatants were recovered and mixed with 4x Native Sample Buffer (400 mM Tris HCl, pH 8.6, 40% glycerol, 0.04% Brom-phenol-Blue) and 5% G-250 sample additive (Cat#: BN2004, Thermo Scientific) before loading onto a 4-20% Mini-PROTEAN® TGX™ Precast Gels (Cat#: 4561094, Bio-Rad). Native running buffer (25 mM Tris base, 192 mM glycine, pH 8.3) and native PAGE™ cathode buffer additive (20X) (Cat#: BN2002, Thermo Scientific) were used to make cathode running buffer following the manufacturer's instruction. Electrophoresis was carried out at 150 V, RT for 2~2.5 h. Gels were either stained with Coomassie R-250 or prepared for native blots.

Native blots were performed as normal Western blots with the exception that Tris-Glycine Transfer Buffer (12 mM Tris base, 96 mM glycine, pH 8.3) was used. Proteins were blotted onto polyvinylidene difluoride (PVDF) membrane (GE Healthcare) at 25 V, RT for 1 h. After transfer, blotting membranes were fixed in 8% (v/v) acetic acid for 15 min and rinsed with water, then air dried overnight, RT. Dried membranes were rewet in methanol to remove excessive bound dye. After rinsing with water, membranes continued as normal western blots

immunodetection (see Immunoblotting). NativeMark™ unstained protein standard (Thermo Scientific) was used to estimate protein size.

Immunoblotting

Before loading on to an SDS-PAGE gel (5% stacking gel, 12% running gel), protein extracts were denatured in 4x SDS sample buffer (200 mM Tris-HCl, pH 6.8, 10% β-mercapto-ethanol, 8% SDS, 0.08% bromophenol blue, 40% glycerol) and boiled for 10 min. Under non-reducing conditions, β-mercapto-ethanol was omitted. Proteins were wet blotted onto 0.45 µm nitrocellulose membranes (GE Healthcare, Piscataway, NJ, USA) at 100V for 1 h. After blocking for 3 h at RT in 5% (w/v) BSA in PBS with 0.05% (v/v) Tween-20 (PBST), membranes were incubated with primary antibodies (diluted in PBST with 1% BSA) overnight at 4°C. Immunizing peptide solution was made with five times concentrated blocking peptide to antibody weight with agitation at RT for 1 h before incubating with membranes. After three washes in PBST for 15 min, membranes were incubated with horse radish peroxidase (HRP) conjugated secondary antibodies (mouse anti-goat HRP IgG, Cat#: 2354, Santa Cruz, CA, USA; goat anti-rabbit and mouse HRP IgG, Cat#: P0448, Agilent) for 1 h at RT. After rinsing four times in PBST for 20 min, membranes were developed using chemiluminescence (ECL-detection kit; Supersignal West Pico, Pierce, Rockford IL, USA). Migration levels of proteins were visualized using PageRuler™ Plus pre-stained protein ladder, 10 to 250 kDa (Thermo Scientific).

Indirect immunofluorescence staining

Sperm cells were fixed in 4% PFA for 15 min at RT, then 20 µL of the sperm suspension was deposited on Superfrost slides (Thermo Scientific) and covered with coverslips, then dried at RT for 20 min. Coverslips were floated with PBS and removed. For permeabilization, sperm cells were permeabilized using 0.5% (v/v) Triton X-100 for 15 min, at RT. After rinsing with PBS, slides were blocked with 1% (w/v) BSA in PBS for 1h at RT, incubated overnight at 4°C

with a CRISP2 antibody (1:250 in 1% BSA). Slides were washed again before incubation for 1 h at RT with either Alexa Fluor 568-conjugated donkey anti-goat IgG [H+L] (Cat#: A-11057, Thermo Scientific) or donkey anti-rabbit IgG [H+L] (Cat#: A-10042, Thermo Scientific) and counterstaining with Hoechst 33342 (1ug/mL, Sigma) for 10 min, at RT. After extensive washing with PBS, slides were mounted with FluorSave™ reagent (Cat#: 345789, Merck Millipore) and covered with coverslips. For negative controls, the primary antibody was either pre-incubated with CRISP2 blocking peptide or the primary antibody was omitted. Observations were performed on a Leica SPE-II confocal microscope using a 63x objective (NA 1.3, HCX PLANAPO oil) and images were analyzed by evaluating the fluorescence intensity for CRISP2 and DNA (Hoechst33342) in each channel using Image J software (bundled with 64-bit Java 1.8.0_172, National Institutes of Health, Bethesda, MD, USA).

Immunogold labelling

Percoll® washed sperm cells ($10x10^6$) were resuspended in 0.5 mL PBS, mixed with equal volume of 4% paraformaldehyde (PFA) (Electron Microscopy Sciences) and fixed for 5 min at RT. The fixative was removed by centrifugation at 750 x *g*, for 5 min at RT. Fresh 4% PFA was added and cells were fixed overnight. 4% PFA was then replaced with 1% PFA and cells were stored at 4°C. Further processing of samples for ultrathin cryosectioning and immuno-labeling according to the protein A-gold method was performed as described previously [38]. In brief, fixed cells were washed with 0.05 M glycine in PBS, resuspended and pelleted in 12% gelatin in PBS at 37°C. The cell pellet was solidified on ice and cut into small blocks. For cryoprotection, blocks were infiltrated overnight with 2.3 M sucrose at 4°C, then mounted on aluminum pins and frozen in liquid nitrogen. A 1:1 mixture of 2.3 M sucrose and 1.8% methylcellulose was used to pick up the ultrathin cryosections (60 nm). CRISP2 was detected by using the rabbit polyclonal antibody against CRISP2 (Cat#: 19066-1-A, Proteintech, Chicago, IL, USA) detected by 10 nm Protein A coupled gold particles (Cell Microscopy Core,

UMC Utrecht, the Netherlands). Stained with 2% uranyl acetate oxalate and 0.4% uranyl acetate in methylcellulose to increase contrast. EM imaging was done using a JEOL 1011 microscope.

Results

Characterization of CRISP2 in boar sperm heads and tails

Immunoblotting of extracts from whole sperm cells under reducing conditions showed CRISP2 detected across multiple protein bands besides the expected monomeric molecular weight of ~25 kDa (Figure 1A). The specificity of the primary antibody was validated by both pre-blocking using the epitope peptide or by primary antibody omission, and in both cases no positive signal was observed on Western blots (Figure 1A). Interestingly, further immunoblotting on purified sperm heads and tails revealed that the three higher molecular weight (MW) CRISP2 bands (~100 kDa, ~50 kDa, ~35 kDa) were exclusively and consistently present in the sperm tail fractions, while the ~25 kDa monomer only resided in sperm heads (Figure 1A). When non-reducing conditions were used, the ~25 kDa was not visible while a high MW CRISP2 band (> ~250 kDa) was observed in the sperm head fraction. Under the same non-reducing conditions, the ~35 kDa and ~100 kDa bands in the whole sperm cell and tail fraction were no longer detected, however, the ~50 kDa remained (Figiure 1B). It is likely that the 35 kDa and 100 kDa bands, only visible under reducing conditions, were originally present in the higher molecular weight complexes shown in Figure 1B and C. The reduction of disulfide bridges (CRISP2 is highly enriched in cysteine residues) may be the driving force to allow this dissociation of CRISP2 from CRISP2-containing higher MW protein complexes. The 50 kDa form appears to be β-mercapto-ethanol insensitive which may indicate that another type of covalent interaction of CRISP2 is involved which is independent of disulfide bridge reduction. Note that CRISP2 is a CAP family member and has been reported to have amyloid forming properties [31]. In parallel to the Western blots of Figure 1 complimentary SDS-PAGE gels were stained with Coomassie blue to show the total protein loading for whole sperm and the

tail and head subfractions (Supplementary Figure S1). Here we observed that under non-reducing conditions the signal at the top of the gel was increased (>250 kDa), as well as two bands at ~50 kDa and ~45kDa (Supplementary Figure S1 A). Under native conditions, CRISP2 migrated to ~300-1,000 kDa protein complexes in the whole sperm and in the sperm head; while CRISP2 was involved in two complexes, ~150 kDa and ~200 kDa, in the tail fraction. The latter band was also present in low amounts in the whole sperm lane as well as in the sperm head fraction (Figure 1C). Again, specificity of the primary antibody was validated by pre-incubating with specific blocking peptide (data not shown). The purity of the sperm heads (>99%) versus tail fractions (>95%) from sonicated sperm samples were scored by phase-contrast microscopy (Supplementary Figure S2).

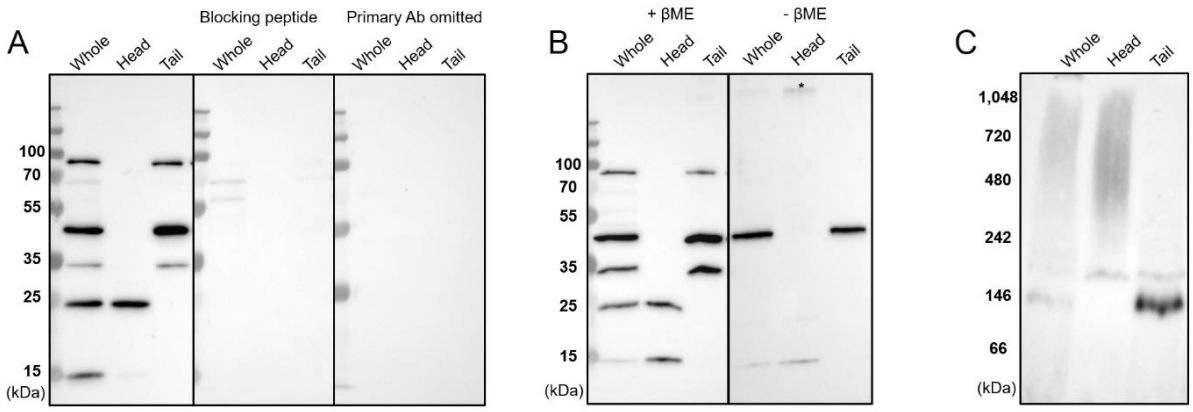

Figure 1. CRISP2 is present as multimers in boar sperm. (A) Western blots of CRISP2 on the extracts from whole sperm cells, sperm heads and sperm tails. (B) Western blots of CRISP2 on the extracts from sperm heads and sperm tails with or without β-mercapto-ethanol (βME). There was a positive band (> ~250 kDa, asterisk) observed in the head fraction in the absence of βME. (C) Native blots showing that CRISP2 was participating in a ~200 kDa protein complex in the sperm head and was involved in two complexes: ~150 kDa and ~200 kDa in the tail fraction. The immunoreactivity of all the detected bands were absent when the CRISP2 primary Ab (goat polyclonal) was pre-incubated with blocking peptide or omitted. Migration of molecular mass standards are sized in kDa.

Localization of CRISP2 in boar sperm

Previous studies have reported that CRISP2 was localized in the sperm acrosome, connecting piece and the outer dense fibers of the sperm tail in human, mouse and rat [21, 23, 24]. In our study, CRISP2 was localized in boar sperm by indirect immunofluorescent staining of either non-permeabilized or permeabilized sperm samples. Only boundary labelling between the post-acrosomal region and the equatorial segment was observed in non-permeabilized sperm cells**.** However, strong CRISP2 labelling was acquired after permeabilization in both the post-acrosomal region and the connecting piece indicating that CRISP2 is predominantly localized intracellular in the sperm (Figure 2).

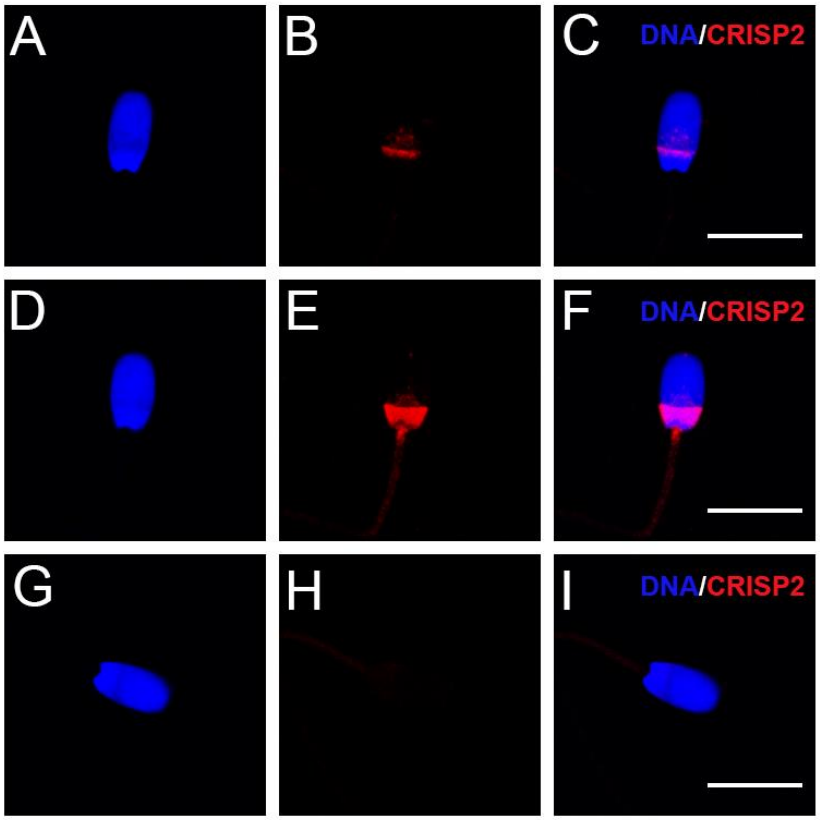

Figure 2. Immunofluorescent staining of CRISP2 in boar sperm. Percoll® washed sperm cells were fixed in 4% paraformaldehyde (PFA). (A-C) No permeabilization after fixation. (D-I) Permeabilized after fixation with 0.5% Triton X-100. (A, D) Hoechst 33342 staining, (B, E) CRISP2 immune labelling and (C, F) merge of both fluorescence. (G) Hoechst 33342 staining. (H) CRISP2 immune labelling after pre-incubation of the CRISP2 antibody with a blocking peptide. (I) merge of G and H fluorescence. Distance bar = 10 μm.

CRISP2 in the perinuclear theca of the sperm head

We focused first on the localization of CRISP2 in the post acrosomal region of sperm head. The solubility of CRISP2 was determined in the sperm head fraction that was subjected to a successive series of detergent fractionations. A small portion of ~25 kDa CRISP2 was able to be solubilized with 1% NP-40 detergent and an additional portion of CRISP2 became solubilized after 1% SDS extraction. However, the majority of CRISP2 remained in the insoluble pellets after these successive extractions (Figure 3A). The fact that CRISP2 predominantly remained in the insoluble pellet after 1% NP-40 extraction suggests that CRISP2 might reside in the perinuclear theca (PT) structure of the sperm head. To confirm this, a standard procedure to isolate the proteins of the PT was performed in accordance with [36, 37]. The CRISP2 containing sperm head fraction was first subjected to 0.2% Triton X-100 and only a small portion of CRISP2 was solubilized (Figure 3B) the subsequent treatment with 1 M KCl did not lead to any solubilization of CRISP2 while the 0.1 M NaOH treatment almost completely solubilized CRISP2 such that CRISP2 was barely detectable in the cell pellet but abundant in the supernatant (Figure 3B). This is in line to the solubilization behavior of PT proteins as reported previously [39]. Coomassie blue staining of SDS-PAGE gels were performed to show protein extractability in different detergents (Supplementary Figure S3A, B). It was noted that a ~15 kDa was consistently present on the immunoblots of whole sperm cells (Figure 1A) and sperm head fractions (Figure 1B and Figure 3). The ~15 kDa band labeling was able to be blocked by the blocking peptide (Figure 1A) indicating that it is a specific product from CRISP2. Moreover, it seems that this ~15 kDa was specifically from the head fraction and not the tail (Figure 1A and B). The ~15 kDa is the size of CAP domain of CRISP2. This may indicate that the hinge connecting the CAP and c-terminal cysteine-rich domain is insensitive to PMSF. Immunostaining on isolated sperm heads confirmed the predominant localization of CRISP2 in the post-acrosomal region and its PT specific solubilization behavior (Figure 3C). Note that that 0.2% Triton X-100 revealed some additional staining of CRISP2 possibly from

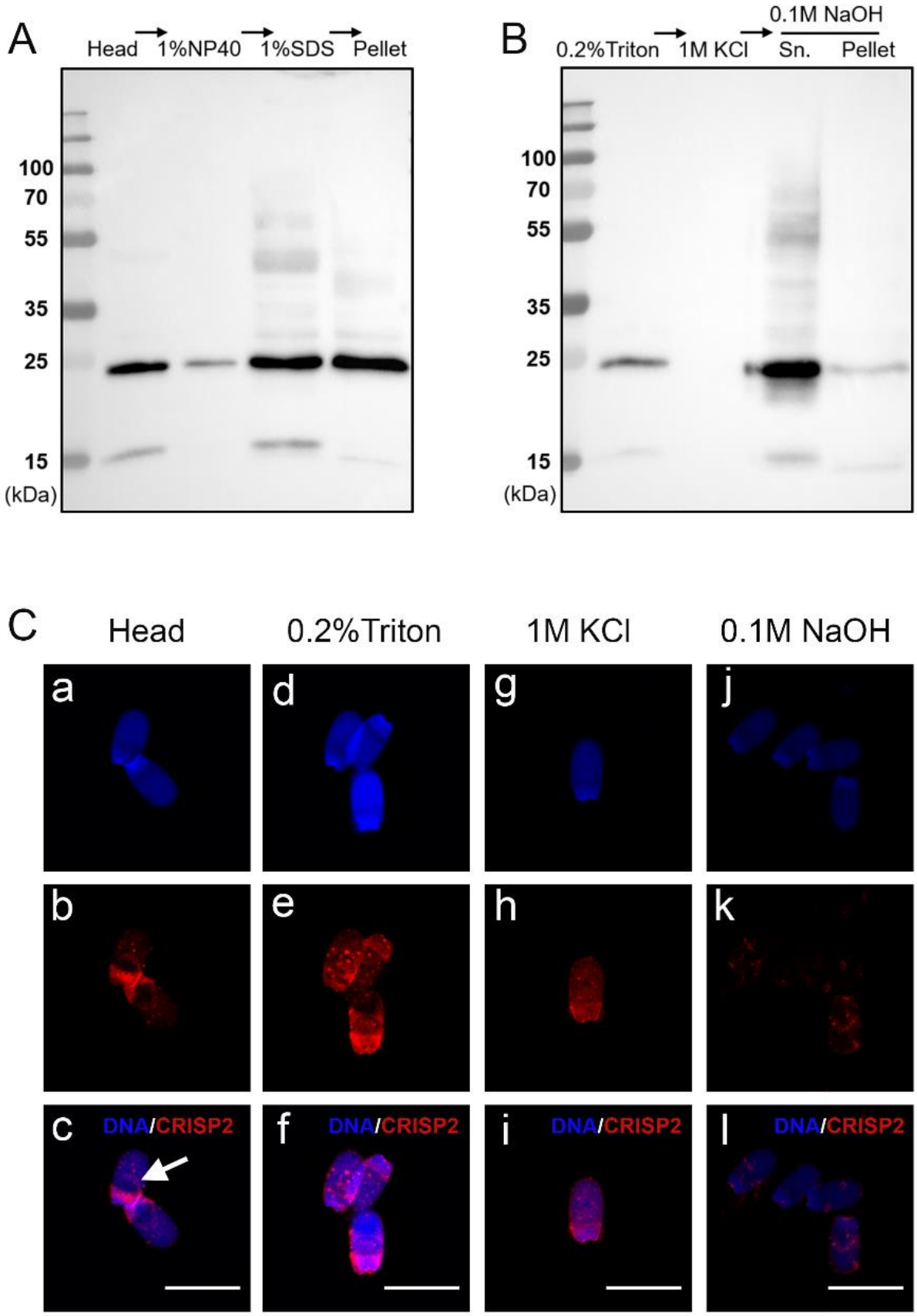

Figure 3. Biochemical characterization of CRISP2 from boar sperm head. (A) Detergent fractionation of sperm heads. Western blots of CRISP2 on the extracts of 1% NP-40, 1% SDS and the

resulting pellet. The head lane was loaded as control to shows the presence of ~25 kDa CRISP2 in the sperm head. (B) Extraction of perinuclear theca (PT) proteins from sperm heads. Western blots of CRISP2 on the extracts of 0.2% Triton X-100, 1M KCl, 0.1 M NaOH and the resulting pellet. (C) Immunofluorescent staining of CRISP2 on the sperm head and the resulting pellets from 0.2% Triton X-100, 1M KCl, 0.1 M NaOH. Extra labelling of CRISP2 was observed at the equatorial segments (arrow) of the head after sonication. (a, d, g and j) Hoechst 33342 staining. (b, e, h and k) CRISP2 imune labelling. (c, f, i and l) merged signals. The distance bar = 10 μm.

an intra-acrosomal origin (Figure 3C, arrowed). To complement these findings, immunogold labelling of CRISP2 was performed to show the intracellular ultra-localization of CRISP2 using transmission EM on ultrathin cryo-coupes of boar sperm. The best working antibody against CRISP2 for this technique was a Rabbit polyclonal. Immunofluorescent staining of permeabilized boar sperm confirmed that this rabbit anti-CRISP2 antibody also labelled the post acrosomal region and connecting piece of the sperm cells (Supplementary Figure S4 A). Furthermore, immunofluorescent staining of ultrathin sperm sections revealed the same staining pattern (Supplementary Figure S4 B). Indirect immunogold labelling using anti-CRISP2 antibody together with colloidal gold conjugated protein G revealed that the gold particles were specifically localized to the perinuclear theca between the plasma membrane and the nuclear envelop (Figure 4).

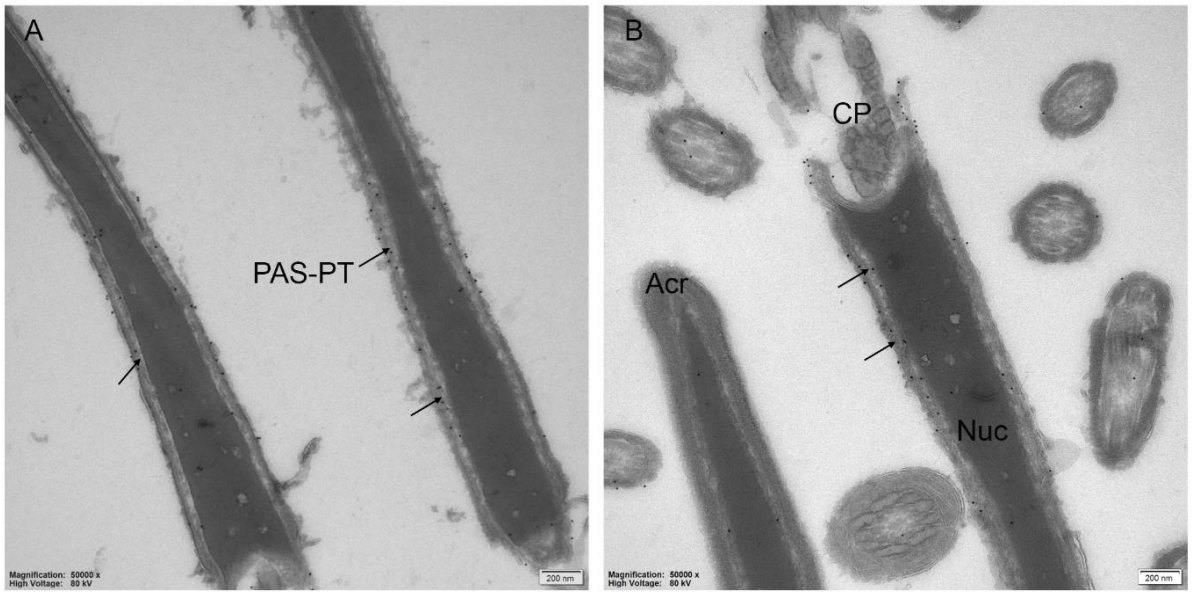

Figure 4. Ultrastructural localization of CRISP2 in boar spermatozoa. (A, B) Immunogold labelling of CRISP2 on sagittal sections through a whole sperm head showing that CRISP2 localized to the PAS-PT (arrow). (B) CRISP2 was not present in the Acrosome (cr) neither the Nucleus (Nuc). CP, connecting piece.

CRISP2 is present in both the outer dense fibers and fibrous sheath of the sperm tail

As described above, beyond its presence in the sperm head, CRISP2 was also present in the sperm tail in three high MW multimers that were not observed in the sperm head. To gain more information about subcellular localization and biochemical features of CRISP2, membrane fractionations of the tail were carried out. 1% Triton X-100 was used to solubilize membranes and the extrinsic and intrinsic membrane proteins that were not linked to cytoskeletal or extracellular matrix protein networks. SDS-EDTA effectively solubilizes the axoneme and plasma membrane, while it does not solubilize the connecting piece, the mitochondrial sheath, the outer dense fibers (ODF) and the fibrous sheath (FS) [40]. Immunoblotting of Triton X-100 extracted, as well as SDS-PAGE extracted, sperm tail fractions revealed that the three higher MW CRISP2 bands could be solubilized under these conditions (Figure 5A). However, in both cases multiple CRISP2 positive protein bands were detected in the insoluble pellet fractions with two prominent protein bands at ~75 kDa and ~55 kDa (Figure 5A). The protein α-tubulin was found in the Triton X-100 insoluble fraction, in contrast to its presence in the soluble fraction after SDS-EDTA treatment (Figure 5A). This profile of α-tubulin detergent solubility in sperm tail fractions is in line with that reported in the literature [41, 42]. We noted that there was an additional protein band of ~27 kDa (clearly different in molecular weight from the ~25 kDa band that appeared after urea treatment). The~27 kDa CRISP2 band was only observed in detergent extracts with SDS-EDTA, but not with Triton X-100 (Figure 5A). We, therefore, believe that the ~27 kDa was associated to insoluble tail material (in Figure 1 and 3) while it became solubilized specifically from the tail by SDS-EDTA treatment.

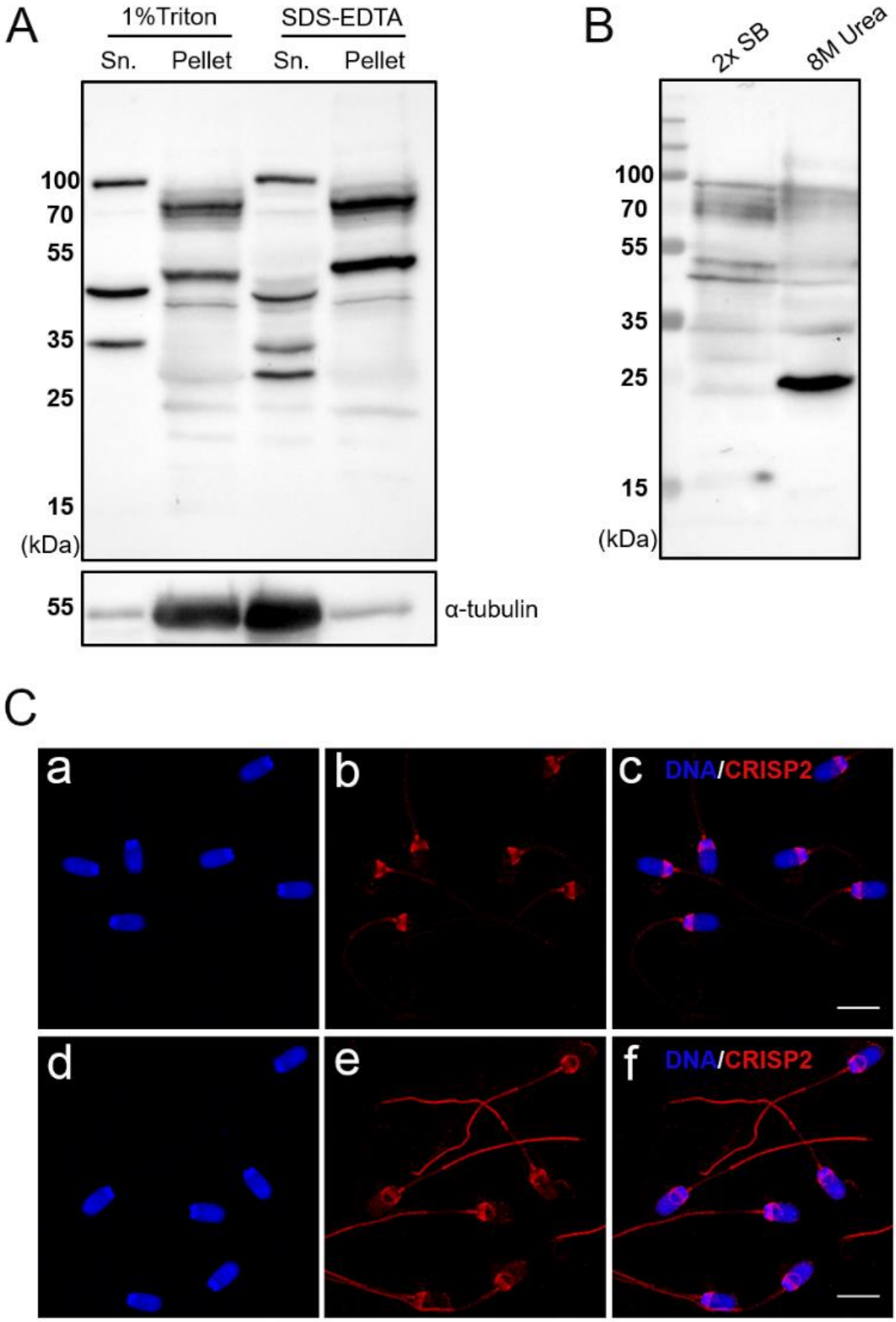
A
1%Triton
SDS-EDTA
Sn.
Pellet
Sn.
Pellet
100
70
55
35
25
15
(kDa)
55
α-tubulin
B
2x SB
8M Urea
100
70
55
35
25
15
(kDa)
C
a
b
c
DNA/CRISP2
d
e
f
DNA/CRISP2

Figure 5. CRISP2 is present in different βME resistant protein bands in sperm tails. (A) Western blots of CRISP2 on 1% Triton and SDS-EDTA treated soluble and insoluble fractions. α-tubulin was used to indicate the different solubility of sperm tails in these two detergents. (B) 8 M urea treatment in sperm tails resulted in the dissociation of higher MW bands into the 25 kDa monomeric form. (C) (a-c) Percoll® washed sperm cells were fixed in 4% PFA and permeabilized in 0.01% (w/v) Saponin for 15 min, at RT. 0.01% (w/v) Saponin was used all along the following steps. (a) Hoechst 33342 staining. (b) CRISP2 immune labeling. (c) Merge of a and b. (d-f) Percoll® washed sperm cells were first permeabilized in 0.01% (w/v) saponin for 15 min, at RT, then fixed in 4% PFA. (d) Hoechst 33342 staining, (e) CRISP2 immune labelling. (f) Merge d and e. The distance bar = 10 μm.

When sperm tail fractions were directly denatured in 2x SDS sample buffer, all CRISP2 protein bands described above were present (Figure 5B). However, treatment with 8 M urea, resulted in a high -but not complete- dissociation of all higher MW bands into the 25 kDa monomeric form with the exception of the ~35 kDa protein band (Figure 5B). Using PNGase F to digest the tail lysate did not result in the truncation of the ~35 kDa band. This may suggest that the porcine 35 kDa band is a splice variant expressed by the same gene as the 25 kDa band. However, this remains to be confirmed. It is also important to note that a 35 kDa positive band for CRISP2 has been previously detected in transfected HEK293 cells transiently expressing human CRISP2 Coomassie blue stained gels run in parallel to immunoblots revealed protein band molecular weights shifted in the 2x SB and 8M urea conditions and that both lanes contained the same protein load (Supplementary Figure S5). CRISP2 immunostaining of sperm that were first fixed and then permeabilized exhibited no labeling of the sperm tail while the sperm head and neck were labelled (Figure 5Cb). In contrast, sperm that were permeabilized with a low concentration of saponin prior to fixation revealed additional clear labeling in the principal piece of the tail and some labeling of the central part of the mid-piece (Figure 5Ce). Pre-fixation permeabilization has previously been used to improve specificity labelling of cytoskeleton structures [43]. It is likely that low concentrations of saponin permeabilization before fixation allows the antibody to recognize its epitope on the CRISP2 protein in the

principal piece. Immunogold labeling of ultrathin cryosections of boar sperm tail cross sections further confirmed that CRISP2 labeling was found in the ODF, but not at the plasma membrane or mitochondria of the mid-piece (Figure 6A and B). This agrees with the central staining of CRISP2 in the mid-piece (Figure 5Ce). Beyond the ODF, CRISP2 labeling was also observed in the FS of the principal piece (Figure 6C). Longitudinal sections confirmed CRISP2 labelling in the FS and ODF, as well as the absence of labeling in other structures (Figure 6D).

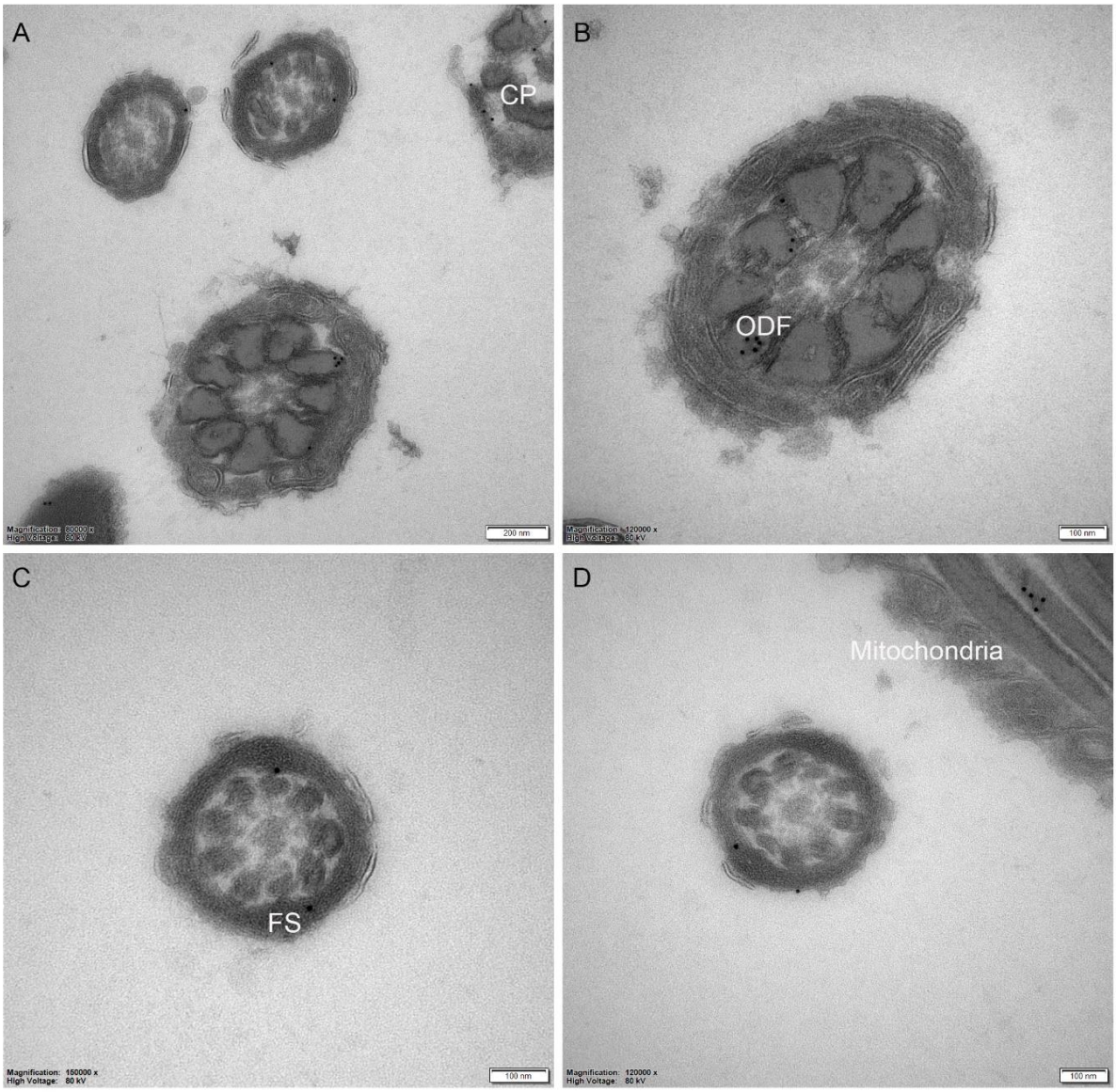

Figure 6. Ultrastructural localization of CRISP2 in boar sperm tail. (A) Immunogold labelling of CRISP2 on cross sections of the sperm tail showing that CRISP2 localized to the CP, ODF and FS. (B) A cross section of the mid piece. (C) A cross section of the principal piece. (D) A longitudinal section showing that CRISP2 localized in the ODF but absent in the mitochondria or the plasma membrane of the sperm tail.

Discussion

Cysteine-rich secretory proteins (CRISPs) have attracted much attention in the field of reproduction due to their roles in male fertility. However, a biochemical understanding of CRISP protein structures and functions is still lacking. Evolutionary analysis on CRISPs from mammals as well as reptile venoms revealed that they have a highly conserved scaffold structure, but with diverse biological functions that were influenced by selective pressure among sites and lineages [5, 43, 44]. The gene expression of CRISPs in the pig has been well studied and the expression of CRISP2 in the testis is confirmed, as described for other mammals [45, 46]. Porcine CRISP2 (UniProt ID: F1RPZ6) protein has a high sequence similarity to CRISP2 of other mammalian species: 80.7% to human (UniProt ID: P16562), 78.3% to guinea pig (UniProt ID: Q60477) and 68.9% to mouse (UniProt ID: P16563) based on UniProt alignment (http://www.uniprot.org).

The perinuclear theca and CRISP2

In our study, biochemical analysis and ultralocalization studies of boar spermatozoa revealed that CRISP2 is localized in the post acrosomal sheath region of mature boar sperm head and more specifically those that reside in the perinuclear theca (PT). The PT is a unique cytoskeletal scaffold structure that is resistant to sonication and non-ionic detergent extraction; where even disulfide bond-reducing agents fail to solubilize proteins from the PT [26, 47]. The PT has been reported to play a vital role in spermiogenesis but may also play a role in processes that occur post fertilization. In support of this theory, the PT has been reported to harbor molecules essential for oocyte activation and early embryo development [47-49]. The PT is assembled during the elongation phase of spermatid development, shortly after abundant CRISP2 protein expression can be detected in round spermatids [8, 26, 50]. Early studies have reported that a 25 kDa protein is one of the dominant PT protein bands on gel electrophoresis [39, 51] and later CRISP2 was identified in the perforatorium which is part of the PT in rat spermatozoa [21, 52].

It is known that CRISPs possess ten out of sixteen cysteine residues clustered in the C-terminal domain and these cysteine residues are involved in disulfide bond formation [53]. Interestingly, CRISP2 was present in boar sperm heads as part of a 250 kDa protein complex under non-reducing conditions while it was dissociated into 25 kDa monomers under reducing conditions. The use of β-mercapto-ethanol as a reducing agent results in the reduction of disulfide bridges between cysteine residues that are highly enriched in the cysteine rich domain of CRISP2. In theory, these reduced cysteine groups can both form intra- as well as inter- protein disulfide bridges. Thus, we propose that CRISP2 in the PT is organized into a ~250 kDa complex that is formed via covalent disulfide bridges between the participating proteins.

CRISP2 in the sperm tail

In the tail both the fibrous sheath (FS) and the outer dense fibers (ODF) are two condensed and highly insoluble protein structures which are unique to the mammalian sperm flagellum [40]. The protein composition of the FS and the ODF differ between different mammalian species, with three abundant proteins identified in isolated rat sperm FS and up to seven major proteins reported in rat sperm ODF [54-56]. Seven major protein bands have been revealed in human sperm FS [57] and two protein bands have been detected in human sperm ODF [58]. These FS protein bands are now known to consist of A-kinase anchoring proteins (AKAPs) AKAP3 and AKAP4 while ODF1 is the main and sole sperm-specific protein of the ODF [59-62]. Importantly, Akap4 knock out male mice are infertile and Odf2 gene deletion resulted in abnormal sperm tails in the mouse [63, 64]. In a case study on an infertile man it was found that AKAP4 was absent in the FS [65]. It is becoming clear that the FS and the ODF are not only simply structures regulating flagellum beating but are also more dynamically involved in sperm physiology, for example, in cell signaling and metabolism [40, 66]. Interestingly, in the sperm tail CRISP2 was present in ~150 kDa and ~200 kDa protein complexes under native conditions. These CRISP2 containing protein complexes dissociated into three different β-mercapto-

ethanol insoluble oligomeric forms. The three CRISP2 oligomers could be solubilized using more stringent detergent conditions (either 1% Triton X-100 or SDS-EDTA), in the presence of β-mercapto-ethanol; however, two oligomeric forms still remained insoluble (Figure 5A). Under reducing conditions, the sperm tail fraction contained all five oligomeric bands, while an 8 M urea treatment caused a degree of dissociation of higher MW bands into 25 kDa monomers. A combination of SDS sample buffer and 8 M urea was used for efficient protein solubilization [67]. This behavior demonstrates that the oligomers in the sperm tail may interact in absence of covalent linkages, which is in contrast to CRISP2 oligomer bonding in the sperm head. Consistent with our study is the observation that *in vitro* recombinant mouse CRISP2 protein is involved in amyloid formation in the presence of Zn^{2+} [31]. It is possible that a Zn^{2+} interaction within CRISP2 and between CRISP2 or other proteins, is involved in the formation of reduction insensitive CRISP2 oligomers in the sperm tail. Moreover, we have demonstrated with other CAP family proteins that Zn^{2+} can result in the formation of amyloid oligomeric structures *in vitro* that depend on the CAP domain [31, 32]. The involvement of Zn^{2+} in establishing specific features of the sperm tail during epididymal sperm maturation has been reported previously [68, 69]. Moreover, most of sperm's Zn^{2+} has indeed been reported to reside in the ODF [70]. We propose here that the ODF and FS oligomeric formation of CRISP2 molecules may occur in the sperm tail in a similar way. Immunogold labeling confirmed that CRISP2 was localized in the FS, the ODF and the connecting piece. This is consistent with previous studies observing the same localization [21, 24]. No signals were observed in the mitochondria or at the plasma membrane, nor in the nucleus of the sperm.

In conclusion, this study reports for the first time the precise localization and biochemical features of CRISP2 in boar spermatozoa. We demonstrate that CRISP2 is present as a 300-1,000- kDa oligomers in the sperm head perinuclear theca structure and that this oligomer is

stabilized covalently by reduction sensitive disulfide bridges. In contrast in the sperm tail FS and ODF, five smaller oligomers of CRISP2 were detected that are largely reduction insensitive and likely dependent on the CAP domain.

We are currently working on unraveling the CRISP2 interactome in the sperm tail (in the ODF and FS) versus sperm head (in the PT). In part there are expected to be differences in CRISP2-interacting proteins in the PT compared to the ODF and FS due to the specific protein composition and architecture of these regions. It is also possible that the oligomerization conditions in these structures also differ. For instance, local differences in redox balance (PT, in the head) or in Zn^{2+} levels (ODF, FS in the tail) may contribute to the differences noted in CRISP2 oligomers in the sperm head versus tail. In CRISP2 loss of function models in mouse alterations in stiffness of the mid-piece and aberrant motility have been detected in sperm and consequently a subfertile phenotype was observed [17]. The fact that CRISP2 multimers are not sensitive to reducing agents may indicate that in the tail the Zn^{2+} dependent oligomerization into more amyloid like CRISP2 structures took place. In fact, Zn^{2+} levels have been described to change under capacitating conditions and this may well relate to altered motility properties of sperm [71]. It is yet unknown whether such Zn^{2+} changes will cause altered CRISP2 interactions in the ODF and FS and thus affect the elastic properties of these structures.

Additionally, our study shows that CRISP2 oligomers in the PT are very reduction sensitive. This aligns with previous reports for the mouse that demonstrate that the post acrosomal sheath (part of the PT) is rapidly broken down post-fertilization by glutathione-S-transferase omega 2 [72]. Given that this enzyme is also present in boar spermatozoa (identification after proteomic analysis of the PT; Chapter 4), it may be involved in reducing the disulfide bridges of CRISP2 in the PT and alter CRISP2 containing high MW protein complexes [72]. The PT emerges as a

well-formed and condensed structure during the elongation phase of spermatids and is supposed to be functional in protecting the pore free part of the nuclear envelope. Likely the oxidation of free sulfhydryl groups in CRISP2 are involved in the condensation of the PT during late spermatid development until epididymal maturation [73] and this process has also been described for the formation flagellar structures that are involved in sperm motility [74]. Future studies will be devoted to the role of CRISP2 (a known inducer of non-pathological protein amyloids) in sperm protein complex formation, the identity of any additional proteins in CRISP2 containing complexes, and the function of the different oligomeric CRISP2 organizations in the sperm head versus sperm tail in fertilization and post-fertilization processes.

Acknowledgments

MZ is financed by the China Scholarship Council (CSC)(No.201606170117). EGB is recipient of an NHMRC CJ Martin Early Career Fellowship (APP1138701). The electron microscopy lab of JK is part of the National Roadmap for Large-Scale Research Infrastructure 2017–2018, project number 184.034.014, (partly) financed by the Dutch Research Council (NWO).

References

1. Gibbs GM, Roelants K, O'Bryan MK. The CAP superfamily: cysteine-rich secretory proteins, antigen 5, and pathogenesis-related 1 proteins--roles in reproduction, cancer, and immune defense. Endocr Rev 2008; 29:865-897.
2. Gibbs GM, Lo JC, Nixon B, Jamsai D, O'Connor AE, Rijal S, Sanchez-Partida LG, Hearn MT, Bianco DM, O'Bryan MK. Glioma pathogenesis-related 1-like 1 is testis enriched, dynamically modified, and redistributed during male germ cell maturation and has a potential role in sperm-oocyte binding. Endocrinology 2010; 151:2331-2342.
3. Gaikwad AS, Hu J, Chapple DG, O'Bryan MK. The functions of CAP superfamily proteins in mammalian fertility and disease. Hum Reprod Update 2020.
4. Fry BG, Casewell NR, Wüster W, Vidal N, Young B, Jackson TNW. The structural and functional diversification of the Toxicofera reptile venom system. Toxicon 2012; 60:434-448.
5. Tadokoro T, Modahl CM, Maenaka K, Aoki-Shioi N. Cysteine-Rich Secretory Proteins (CRISPs) From Venomous Snakes: An Overview of the Functional Diversity in A Large and Underappreciated Superfamily. Toxins (Basel) 2020; 12.
6. Jalkanen J, Huhtaniemi I, Poutanen M. Mouse cysteine-rich secretory protein 4 (CRISP4): a member of the Crisp family exclusively expressed in the epididymis in an androgen-dependent manner. Biol Reprod 2005; 72:1268-1274.

7. Vicens A, Trevino CL. Positive Selection in the Evolution of Mammalian CRISPs. J Mol Evol 2018; 86:635-645.
8. Koppers AJ, Reddy T, O'Bryan MK. The role of cysteine-rich secretory proteins in male fertility. Asian J Androl 2011; 13:111-117.
9. Udby L, Bjartell A, Malm J, Egesten A, Lundwall A, Cowland JB, Borregaard N, Kjeldsen L. Characterization and localization of cysteine-rich secretory protein 3 (CRISP-3) in the human male reproductive tract. J Androl 2005; 26:333-342.
10. Carvajal G, Brukman NG, Weigel Muñoz M, Battistone MA, Guazzone VA, Ikawa M, Haruhiko M, Lustig L, Breton S, Cuasnicu PS. Impaired male fertility and abnormal epididymal epithelium differentiation in mice lacking CRISP1 and CRISP4. Scientific reports 2018; 8:17531-17531.
11. Hu J, Merriner DJ, O'Connor AE, Houston BJ, Furic L, Hedger MP, O'Bryan MK. Epididymal cysteine-rich secretory proteins are required for epididymal sperm maturation and optimal sperm function. Mol Hum Reprod 2018; 24:111-122.
12. Pathak BR, Breed AA, Deshmukh P, Mahale SD. Androgen receptor mediated epigenetic regulation of CRISP3 promoter in prostate cancer cells. J Steroid Biochem Mol Biol 2018; 181:20-27.
13. Asmann YW, Kosari F, Wang K, Cheville JC, Vasmatzis G. Identification of differentially expressed genes in normal and malignant prostate by electronic profiling of expressed sequence tags. Cancer Res 2002; 62:3308-3314.
14. Noh BJ, Sung JY, Kim YW, Chang SG, Park YK. Prognostic value of ERG, PTEN, CRISP3 and SPINK1 in predicting biochemical recurrence in prostate cancer. Oncol Lett 2016; 11:3621-3630.
15. Volpert M, Furic L, Hu J, O'Connor AE, Rebello RJ, Keerthikumar S, Evans J, Merriner DJ, Pedersen J, Risbridger GP, McIntyre P, O'Bryan MK. CRISP3 expression drives prostate cancer invasion and progression. Endocr Relat Cancer 2020; 27:415-430.
16. Brukman NG, Miyata H, Torres P, Lombardo D, Caramelo JJ, Ikawa M, Da Ros VG, Cuasnicu PS. Fertilization defects in sperm from Cysteine-rich secretory protein 2 (Crisp2) knockout mice: implications for fertility disorders. Mol Hum Reprod 2016; 22:240-251.
17. Lim S, Kierzek M, O'Connor AE, Brenker C, Merriner DJ, Okuda H, Volpert M, Gaikwad A, Bianco D, Potter D, Prabhakar R, Strünker T, et al. CRISP2 Is a Regulator of Multiple Aspects of Sperm Function and Male Fertility. Endocrinology 2019; 160:915-924.
18. Heidary Z, Zaki-Dizaji M, Saliminejad K, Khorramkhorshid HR. Expression Analysis of the CRISP2, CATSPER1, PATE1 and SEMG1 in the Sperm of Men with Idiopathic Asthenozoospermia. J Reprod Infertil 2019; 20:70-75.
19. Gholami D, Salman Yazdi R, Jami MS, Ghasemi S, Sadighi Gilani MA, Sadeghinia S, Teimori H. The expression of Cysteine-Rich Secretory Protein 2 (CRISP2) and miR-582-5p in seminal plasma fluid and spermatozoa of infertile men. Gene 2020; 730:144261.
20. Wang H, Zhou Z, Xu M, Li J, Xiao J, Xu ZY, Sha J. A spermatogenesis-related gene expression profile in human spermatozoa and its potential clinical applications. J Mol Med (Berl) 2004; 82:317-324.
21. O'Bryan MK, Sebire K, Meinhardt A, Edgar K, Keah HH, Hearn MT, De Kretser DM. Tpx-1 is a component of the outer dense fibers and acrosome of rat spermatozoa. Mol Reprod Dev 2001; 58:116-125.
22. Haendler B, Habenicht UF, Schwidetzky U, Schuttke I, Schleuning WD. Differential androgen regulation of the murine genes for cysteine-rich secretory proteins (CRISP). Eur J Biochem 1997; 250:440-446.
23. Busso D, Cohen DJ, Hayashi M, Kasahara M, Cuasnicú PS. Human testicular protein TPX1/CRISP-2: localization in spermatozoa, fate after capacitation and relevance for gamete interaction. Mol Hum Reprod 2005; 11:299-305.

24. Hardy DM, Huang TT, Jr., Driscoll WJ, Tung KK, Wild GC. Purification and characterization of the primary acrosomal autoantigen of guinea pig epididymal spermatozoa. Biol Reprod 1988; 38:423-437.
25. Oko RJ. Developmental expression and possible role of perinuclear theca proteins in mammalian spermatozoa. Reprod Fertil Dev 1995; 7:777-797.
26. Oko R, Sutovsky P. Biogenesis of sperm perinuclear theca and its role in sperm functional competence and fertilization. J Reprod Immunol 2009; 83:2-7.
27. Foster JA, Gerton GL. The Acrosomal Matrix. Adv Anat Embryol Cell Biol 2016; 220:15-33.
28. Guyonnet B, Egge N, Cornwall GA. Functional amyloids in the mouse sperm acrosome. Mol Cell Biol 2014; 34:2624-2634.
29. Oko R. Occurrence and formation of cytoskeletal proteins in mammalian spermatozoa. Andrologia 1998; 30:193-206.
30. Lehti MS, Sironen A. Formation and function of sperm tail structures in association with sperm motility defects. Biol Reprod 2017; 97:522-536.
31. Sheng J, Olrichs NK, Geerts WJ, Li X, Rehman AU, Gadella BM, Kaloyanova DV, Helms JB. Zinc binding regulates amyloid-like aggregation of GAPR-1. Biosci Rep 2019; 39.
32. Sheng J, Olrichs NK, Gadella BM, Kaloyanova DV, Helms JB. Regulation of Functional Protein Aggregation by Multiple Factors: Implications for the Amyloidogenic Behavior of the CAP Superfamily Proteins. Int J Mol Sci 2020; 21.
33. Cabrillana ME, Monclus MA, Sáez Lancellotti TE, Boarelli PV, Clementi MA, Vincenti AE, Yunes RFM, Fornés MW. Characterization of flagellar cysteine-rich sperm proteins involved in motility, by the combination of cellular fractionation, fluorescence detection, and mass spectrometry analysis. 2011; 68:491-500.
34. Moghadam M, Ganji A, Varasteh A, Falak R, Sankian M. Refolding process of cysteine-rich proteins:Chitinase as a model. Rep Biochem Mol Biol 2015; 4:19-24.
35. Sheng J, Olrichs NK, Geerts WJ, Kaloyanova DV, Helms JB. Metal ions and redox balance regulate distinct amyloid-like aggregation pathways of GAPR-1. Sci Rep 2019; 9:15048.
36. Oko R, Aarabi M, Mao J, Balakier H, Sutovsky P. Sperm-Specific WW-Domain-Binding Proteins. In: De Jonge CJ, Barratt CLR (eds.), The Sperm Cell: Production, Maturation, Fertilization, Regeneration, 2 ed. Cambridge: Cambridge University Press; 2017: 157-176.
37. Hamilton LE, Acteau G, Xu W, Sutovsky P, Oko R. The developmental origin and compartmentalization of glutathione-s-transferase omega 2 isoforms in the perinuclear theca of eutherian spermatozoa. Biol Reprod 2017; 97:612-621.
38. Slot JW, Geuze HJ. Cryosectioning and immunolabeling. Nat Protoc 2007; 2:2480-2491.
39. Oko R, Maravei D. Protein composition of the perinuclear theca of bull spermatozoa. Biol Reprod 1994; 50:1000-1014.
40. Cao WL, Gerton GL, Moss SB. Proteomic profiling of accessory structures from the mouse sperm flagellum. Molecular & Cellular Proteomics 2006; 5:801-810.
41. Zhou J, Yang F, Leu NA, Wang PJ. MNS1 is essential for spermiogenesis and motile ciliary functions in mice. PLoS Genet 2012; 8:e1002516-e1002516.
42. Kwon JT, Ham S, Jeon S, Kim Y, Oh S, Cho C. Expression of uncharacterized male germ cell-specific genes and discovery of novel sperm-tail proteins in mice. PloS one published 2017; PMID: PMID.
43. Arevalo L, Brukman NG, Cuasnicu PS, Roldan ERS. Evolutionary analysis of genes coding for Cysteine-RIch Secretory Proteins (CRISPs) in mammals. BMC Evol Biol 2020; 20:67.
44. Sunagar K, Johnson WE, O'Brien SJ, Vasconcelos V, Antunes A. Evolution of CRISPs associated with toxicoferan-reptilian venom and mammalian reproduction. Mol Biol Evol 2012; 29:1807-1822.

45. Song CY, Gao B, Wu H, Wang XY, Zhou HY, Wang SZ, Li BC, Chen GH, Mao JD. Spatial and temporal gene expression of Fn-type II and cysteine-rich secretory proteins in the reproductive tracts and ejaculated sperm of Chinese Meishan pigs. Reprod Domest Anim 2011; 46:848-853.
46. Vadnais ML, Foster DN, Roberts KP. Molecular cloning and expression of the CRISP family of proteins in the boar. Biol Reprod 2008; 79:1129-1134.
47. Sutovsky P, Oko R, Hewitson L, Schatten G. The Removal of the Sperm Perinuclear Theca and Its Association with the Bovine Oocyte Surface during Fertilization. Dev Biol 1997; 188:75-84.
48. Sutovsky P, Manandhar G, Wu A, Oko R. Interactions of sperm perinuclear theca with the oocyte: implications for oocyte activation, anti-polyspermy defense, and assisted reproduction. Microsc Res Tech 2003; 61:362-378.
49. Hamilton LE, Suzuki J, Acteau G, Shi M, Xu W, Meinsohn MC, Sutovsky P, Oko R. WBP2 shares a common location in mouse spermatozoa with WBP2NL/PAWP and like its descendent is a candidate mouse oocyte-activating factor. Biol Reprod 2018; 99:1171-1183.
50. Foster JA, Gerton GL. Autoantigen 1 of the guinea pig sperm acrosome is the homologue of mouse Tpx-1 and human TPX1 and is a member of the cysteine-rich secretory protein (CRISP) family. Mol Reprod Dev 1996; 44:221-229.
51. Korley R, Pouresmaeili F, Oko R. Analysis of the Protein Composition of the Mouse Sperm Perinuclear Theca and Characterization of its Major Protein Constituent1. Biol Reprod 1997; 57:1426-1432.
52. Oko R, Clermont Y. Isolation, structure and protein composition of the perforatorium of rat spermatozoa. Biol Reprod 1988; 39:673-687.
53. Gibbs GM, Scanlon MJ, Swarbrick J, Curtis S, Gallant E, Dulhunty AF, O'Bryan MK. The Cysteine-rich Secretory Protein Domain of Tpx-1 Is Related to Ion Channel Toxins and Regulates Ryanodine Receptor Ca2+ Signaling. 2006; 281:4156-4163.
54. Oko R. Comparative Analysis of Proteins from the Fibrous Sheath and Outer Dense Fibers of Rat Spermatozoa1. Biol Reprod 1988; 39:169-182.
55. Olson GE, Sammons DW. Structural Chemistry of Outer Dense Fibers of Rat Sperm1. Biol Reprod 1980; 22:319-332.
56. Vera JC, Brito M, Zuvic T, Burzio LO. Polypeptide composition of rat sperm outer dense fibers. A simple procedure to isolate the fibrillar complex. J Biol Chem 1984; 259:5970-5977.
57. Jassim A, Gillott DJ, Al-Zuhdi Y, Gray A, Foxon R, Bottazzo GF. Isolation and biochemical characterization of the human sperm tail fibrous sheath. Human Reproduction 1992; 7:86-94.
58. Henkel R, Stalf T, Mertens N, Miska W, Schill WB. Outer dense fibres of human spermatozoa: partial characterization and possible physiological functions. Int J Androl 1994; 17:68-73.
59. Brown PR, Miki K, Harper DB, Eddy EM. A-Kinase Anchoring Protein 4 Binding Proteins in the Fibrous Sheath of the Sperm Flagellum. Biol Reprod 2003; 68:2241-2248.
60. Eddy EM, Toshimori K, O'Brien DA. Fibrous sheath of mammalian spermatozoa. Microsc Res Tech 2003; 61:103-115.
61. Hetherington L, Schneider EK, Scott C, DeKretser D, Muller CH, Hondermarck H, Velkov T, Baker MA. Deficiency in Outer Dense Fiber 1 Is a Marker and Potential Driver of Idiopathic Male Infertility. 2016; 15:3685-3693.
62. Lehti MS, Sironen A. Formation and function of sperm tail structures in association with sperm motility defects†. Biology of Reproduction 2017; 97:522-536.
63. Fang X, Huang L-L, Xu J, Ma C-Q, Chen Z-H, Zhang Z, Liao C-H, Zheng S-X, Huang P, Xu W-M, Li N, Sun L. Proteomics and single-cell RNA analysis of Akap4-knockout mice

model confirm indispensable role of Akap4 in spermatogenesis. Dev Biol 2019; 454:118-127.
64. Tarnasky H, Cheng M, Ou Y, Thundathil JC, Oko R, van der Hoorn FA. Gene trap mutation of murine Outer dense fiber protein-2 gene can result in sperm tail abnormalities in mice with high percentage chimaerism. BMC Dev Biol 2010; 10:67.
65. Baccetti B, Collodel G, Estenoz M, Manca D, Moretti E, Piomboni P. Gene deletions in an infertile man with sperm fibrous sheath dysplasia. Human Reproduction 2005; 20:2790-2794.
66. Amaral A, Castillo J, Estanyol JM, Ballescà JL, Ramalho-Santos J, Oliva R. Human Sperm Tail Proteome Suggests New Endogenous Metabolic Pathways. 2013; 12:330-342.
67. Peach M, Marsh N, Miskiewicz EI, MacPhee DJ. Solubilization of proteins: the importance of lysis buffer choice. Methods Mol Biol 2015; 1312:49-60.
68. Baccetti B, Pallini V, Burrini AG. The accessory fibers of the sperm tail. II. Their role in binding zinc in mammals and cephalopods. J Ultrastruct Res 1976; 54:261-275.
69. Henkel R, Baldauf C, Bittner J, Weidner W, Miska W. Elimination of zinc from the flagella of spermatozoa during epididymal transit is important for motility. Reproductive Technology 2001; 10:280-285.
70. Bertelsmann H, Sieme H, Behne D, Kyriakopoulos A. Is the distribution of selenium and zinc in the sublocations of spermatozoa regulated? Ann N Y Acad Sci 2007; 1095:204-208.
71. Kerns K, Zigo M, Drobnis EZ, Sutovsky M, Sutovsky P. Zinc ion flux during mammalian sperm capacitation. Nat Commun 2018; 9:2061.
72. Hamilton LE, Suzuki J, Aguila L, Meinsohn MC, Smith OE, Protopapas N, Xu W, Sutovsky P, Oko R. Sperm-borne glutathione-S-transferase omega 2 accelerates the nuclear decondensation of spermatozoa during fertilization in mice†. Biol Reprod 2019; 101:368-376.
73. Fujii J, Tsunoda S. Redox regulation of fertilisation and the spermatogenic process. Asian J Androl 2011; 13:420-423.
74. Cabrillana ME, Monclus MA, Sáez Lancellotti TE, Boarelli PV, Clementi MA, Vincenti AE, Yunes RF, Fornés MW. Characterization of flagellar cysteine-rich sperm proteins involved in motility, by the combination of cellular fractionation, fluorescence detection, and mass spectrometry analysis. Cytoskeleton (Hoboken) 2011; 68:491-500.

Supplementary Figures

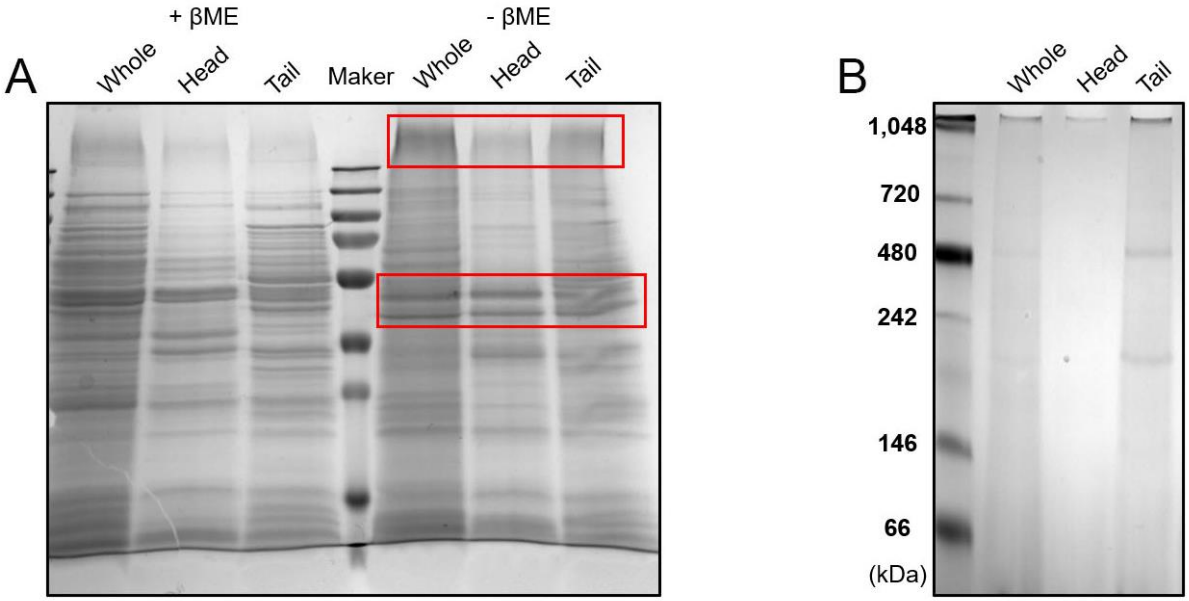

Supplementary Figure S1. Coomassie blue staining and native blue staining. Same amount whole sperm cells/heads/tails were lysed in the same volume buffer and the same amount lysates were loaded on SDS-PAGE gels. (A) Reduced and non-reduced conditions were analyzed by SDS-PAGE and coomassie blue staining. (B) Native conditions were viewed by native blue staining.

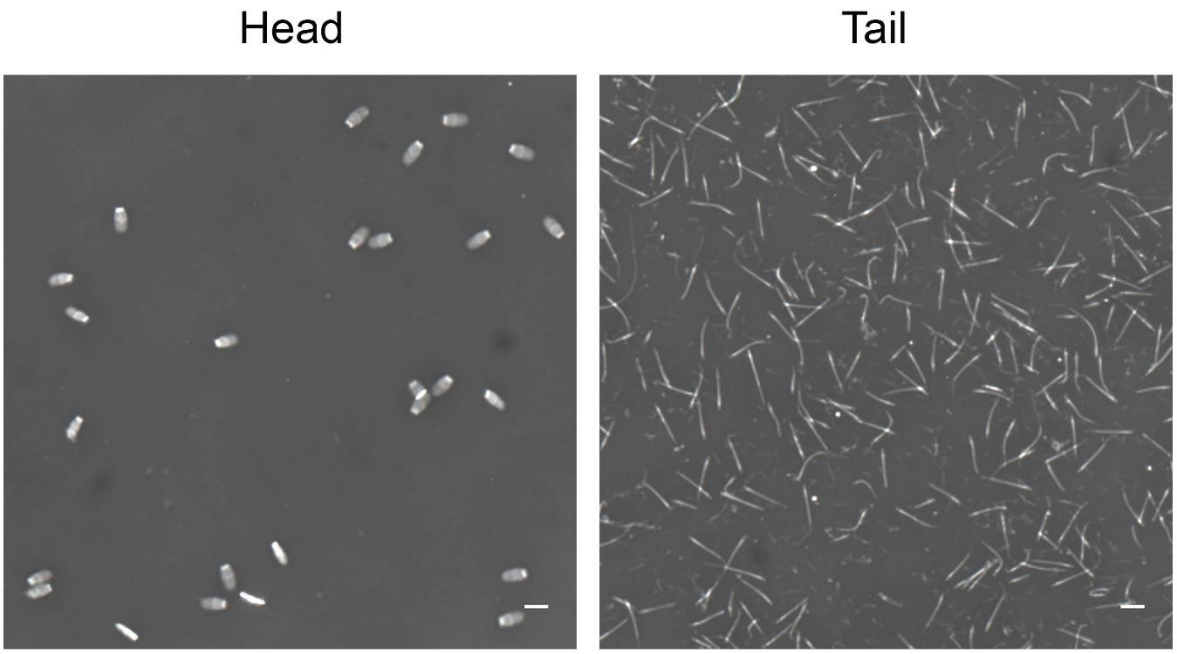

Supplementary Figure S2. Phase contrast microscopy of separated sperm heads and tails. Separated heads and tails were fixed in 4% PFA for 15 min, RT. 20 µL of the suspension was deposited on Super frost slides (Thermo Scientific) and covered with coverslips, then dried at RT for 20 min. Images were collected using a 1.6x/20x objective OLYMPUS BX41 phase contrast microscopy. Distance bar = 10 µm.

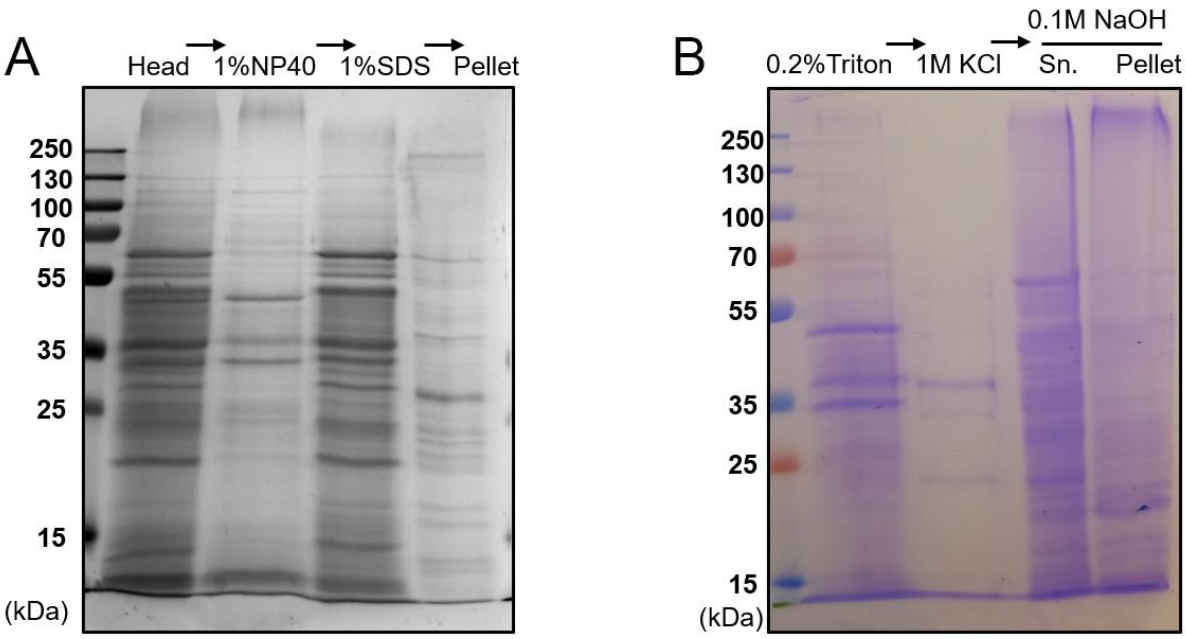

Supplementary Figure S3. Protein extractability in different detergents. (A) Extracts of 1% NP-40, 1% SDS and the resulting pellet were analyzed by SDS-PAGE and coomassie blue staining. (B) SDS-PAGE and coomassie blue staining on the extracts of 0.2% Triton X-100, 1M KCl, 0.1 M NaOH and the resulting pellet.

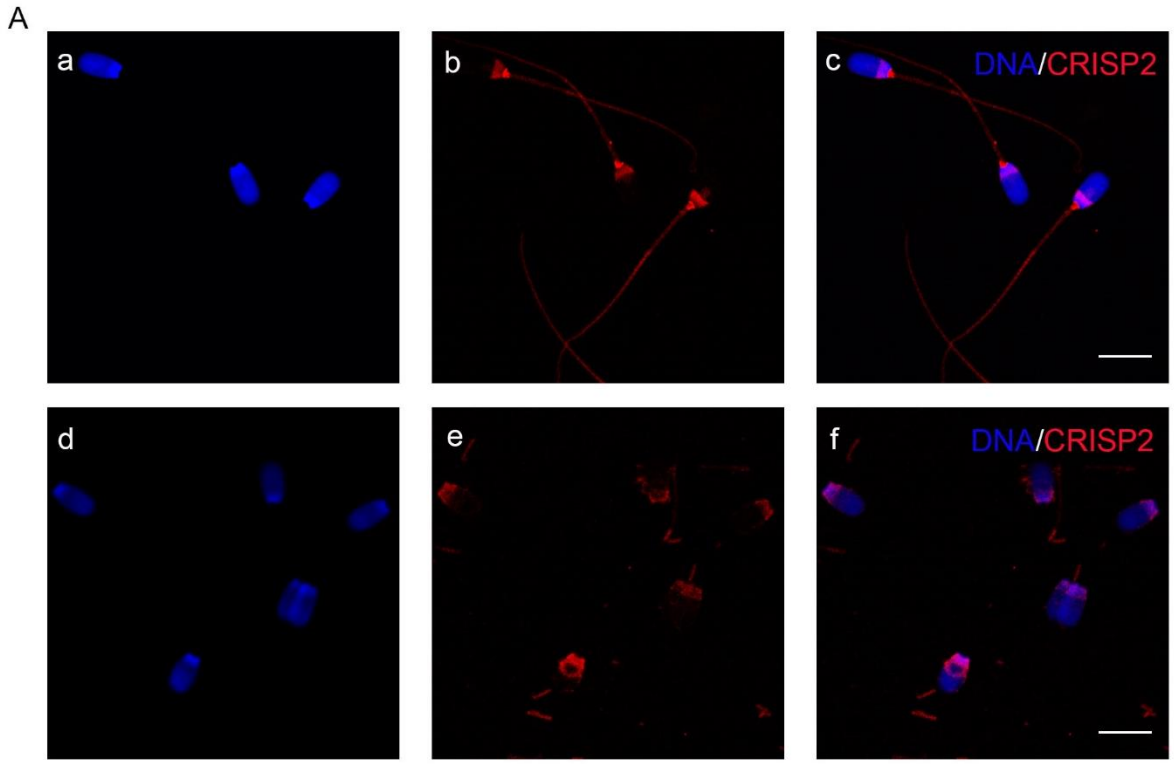

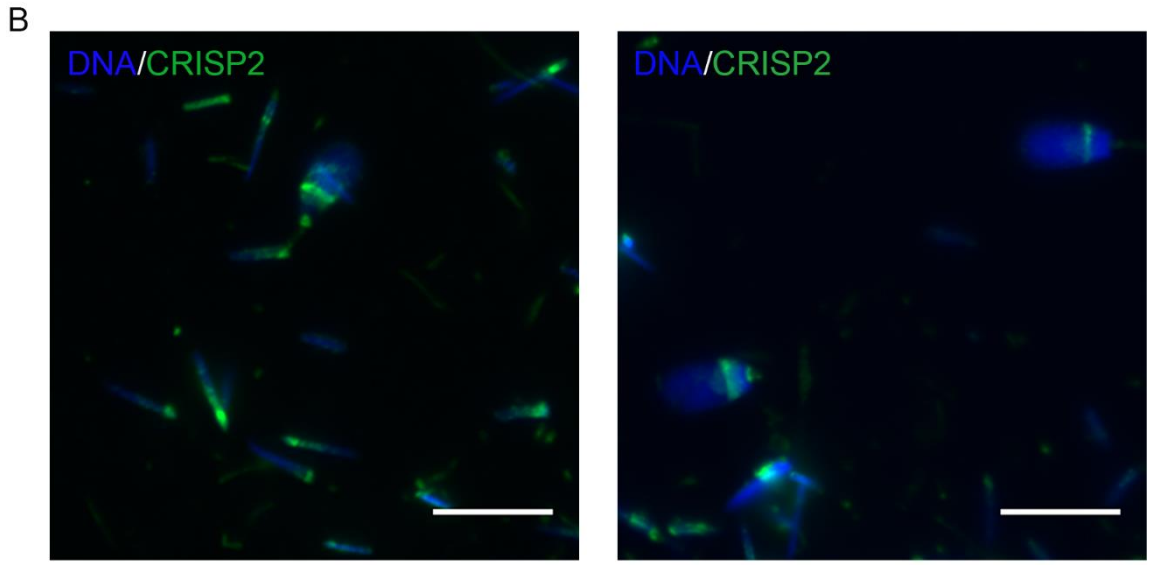

Supplementary Figure S4. The rabbit anti-CRISP2 antibody also labelled the post acrosomal region and connecting piece of the sperm cells. (A) (a-c) Immunofluorescent staining of CRISP2 in 4% PFA fixed and 0.5% Triton X-100 permeabilized sperm cells. (a) Hoechst 33342 staining, (b) CRISP2 immune labelling (c) Merge of a and b. (d-f) CRISP2 signals retained in the post acrosomal region after sonication. (d) Hoechst 33342 staining, (e) CRISP2 immune labeling, (f) Merge of d and e. (B) Immunofluorescent staining of CRISP2 on ultra-thin sperm sections to show (i) CRISP2 labelled the same regions as detected in intact permeabilized sperm cells, (ii) CRISP2 staining pattern was identical to the immunogold labelling. Distance bar = 10 μm.

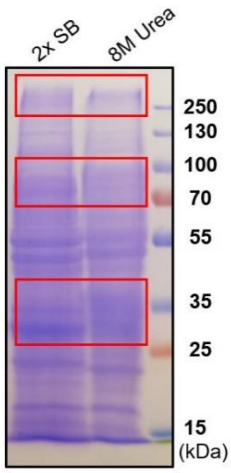

Supplementary Figure S5. SDS-PAGE and coomassie blue staining of tail lysates from 2X SB and 8M urea. Visible changes after 8M urea treatment were marked by red tangles.

Chapter 3

The fate of porcine sperm CRISP2 from the perinuclear theca before and after in vitro fertilization

M. Zhang[1,3], E.G. Bromfield[1,2], J.B. Helms[1], B.M. Gadella[1,3*]

[1]Department of Biomolecular Health Sciences, Faculty of Veterinary Medicine, Utrecht University, the Netherlands

[2]Priority Research Centre for Reproductive Science, The University of Newcastle, New South Wales, Australia

[3]Department of Farm Animal Health, Faculty of Veterinary Medicine, Utrecht University, Utrecht, the Netherlands.

Published as:
Zhang M, Bromfield EG, Helms JB, Gadella BM. The fate of porcine sperm CRISP2 from the perinuclear theca before and after in vitro fertilization. Biol Reprod. 2022 Nov 14;107(5):1242-1253.

Abstract

In a previous study we reported that porcine sperm cysteine rich secretory protein 2 (CRISP2) is localized in the post-acrosomal sheath (PAS)-perinuclear theca (PT) as reduction-sensitive oligomers. In the current study, the decondensation and removal of CRISP2 was investigated during in vitro sperm capacitation, both after induction of the acrosome reaction and after in vitro fertilization. Confocal immunofluorescent imaging revealed that additional CRISP2 fluorescence appeared on the apical ridge and on the equatorial segment (EqS) of the sperm head following capacitation, likely due to cholesterol removal. After an ionophore A23187 induced acrosome reaction, CRISP2 immunofluorescence disappeared from the apical ridge and the EqS area partly due to the removal of the acrosomal shroud vesicles but also partly due to its presence in a subdomain of EqS (EqSS). The fate of sperm head CRISP2 was further examined post-fertilization. In vitro matured porcine oocytes were co-incubated with boar sperm cells for 6-8 h and the zygotes were processed for CRISP2 immunofluorescent staining. Notably, decondensation of CRISP2, and thus of the sperm PT, occurred while the sperm nucleus was still fully condensed. CRISP2 was no longer detectable in fertilized oocytes in which sperm nuclear decondensation and paternal pronucleus formation were apparent. This rapid dispersal of CRISP2 in the PT is likely regulated by redox reactions for which its cysteine rich domain is sensitive. Reduction of disulfide bridges within CRISP2 oligomers may be instrumental for PT dispersal and PT elimination.

Keywords: CRISP2; porcine; sperm; perinuclear theca; decondensation; fertilization; oocyte.

Introduction

To achieve the capacity to fertilize an egg, mammalian spermatozoa must undergo a series of biochemical and physiological changes, defined as capacitation, in the female reproductive tract [1], or in a defined medium in vitro [2], to become competent to fertilize a mature oocyte. Sperm capacitation involves multiple signaling events including cholesterol efflux and protein tyrosine phosphorylation [3]. Eventually, these changes result in a sperm surface reordering that primes sperm to bind to the oocyte zona pellucida (ZP) and induces the subsequent zona-induced acrosomal exocytosis. Both are required for the sperm to penetrate the ZP and to enable fusion with the oolemma [4]. Redistribution of lipids and proteins have been observed on the sperm surface during capacitation [5, 6]. The sperm anterior head plasma membrane is remodeled during capacitation [7, 8] and this area is considered the primary site where sperm bind to the ZP. Following capacitation, a controlled exocytotic event termed the acrosome reaction takes place, releasing acrosomal granules which likely contain enzymes believed to aid in penetrating the ZP [9]. In acrosome reacted sperm, intra-acrosomal components become exposed at the surface of the equatorial segment (EqS) of the sperm head, which is commonly considered the first site where sperm fuse with the oolemma [10]. Numerous sperm proteins have been reported to appear at the EqS after the acrosome reaction and are essential for sperm-egg fusion, for example, IZUMO-1 [11, 12], CD9 [13], cysteine rich secretory protein 2 (CRISP2) [14-16].

After sperm-egg fusion, the post-acrosomal sheath (PAS)-perinuclear theca (PT) of the sperm head is exposed to the ooplasm. The PT is a highly condensed protein structure housed in the minimal cytosolic space between the nuclear envelope and plasma membrane in the mature mammalian sperm cell. In most of the eutherian species, the PT consists of two structurally continuous regions named the sub-acrosomal layer (SAL) and PAS [17]. The PAS-PT has

gained attention over the past decades as it is held that the PAS-PT houses the sperm borne, oocyte-activating factor (SOAF) responsible for oocyte activation and zygotic development [17-20]. The two favored SOAF candidates are phospholipase C zeta (PLCζ) and post-acrosomal WW domain-binding protein (PAWP). Both PLCζ and PAWP have been shown to be responsible for triggering $Ca2^{+}$ oscillations within the oocyte [18-22]. Crucially, the PAS-PT is the first internal structure solubilized in the ooplasm and the sperm born cytosolic molecules are released into the oocyte cytoplasm at fertilization [17, 23]. Disulfide bond reduction has been considered as the main driving force leading to sperm head solubilization [24, 25]. This is supported by the presence of glutathione-S-transferase omega 2 (GSTO2) as an oxidative-reductive enzyme in the PAS-PT region [26]. This enzyme plays an active role in facilitating sperm nuclear decondensation likely through the reduction of disulfide bonds within sperm chromatin [27]. On the one hand, the sperm head structures including the PT must first be disassembled in the oocyte cytoplasm before sperm nuclear decondensation can take place. Before dissociation, the PT is a rigid condensed structure that protects the sperm nucleus and does not permit surrounding enzymes to initiate decondensation of the highly protamine-packed DNA. On the other hand, the proteins that are dissociating from the PT can be recruited to de- or re- stabilize sperm chromatin until male pronucleus formation [28].

The latest phylogenetic analysis shows that mammalian CRISPs have three distinct lineages, CRISP1, CRISP2 and CRISP3 [29]. CRISP4, found in some rodents, is derived from the same gene as CRISP1 [29]. CRISP1 and CRISP4 are characterized as epididymal proteins that adhere to the sperm surface during sperm epididymal maturation [30, 31]. Unlike other CRISPs, CRISP3 expression is not restricted to the reproductive tract and shows a greater diversity among species [29, 32]. Related to sperm, CRISP3 is present on ejaculated human spermatozoa, similar to human CRISP1 [33]. Interestingly, CRISP3 is found enriched in equine seminal

plasma and is a valuable factor for sperm quality [34, 35]. Downregulation of CRISP2 expression has been observed in human patients with asthenozoospermia and has been linked with male infertility [36-38]. CRISP2 has gained attention as it is the sole CRISP endogenously produced during spermatogenesis [39] and thus is the only intracellular CRISP while CRISP1, 3 and 4 are soluble proteins secreted by either the accessory sex glands or the epididymis and adsorb to the sperm surface outside the testis in the male genital tract [30, 34, 40]. Human CRISP2 reassociates with the EqS only after acrosome reaction [14] and a similar result is observed for mouse spermatozoa [16]. However, the underlying mechanisms supporting CRISP2 cellular redistribution and/or exposure is still unclear. Studies on human and rodent CRISP2 show that CRISP2 is involved in fertilization events especially at the site of sperm-egg fusion [15, 16, 41]. Despite a morphologically normal acrosome, Crisp2$^{-/-}$ sperm have a defect in their ability to undergo an acrosome reaction when provoked by progesterone [42]. Additionally, Crisp2$^{-/-}$ sperm exhibit greatly lower motility due to stiffening of the midpiece of the sperm tail [42]. Thus, CRISP2 knockout males are subfertile [42, 43]. Interestingly, our previous study on porcine spermatozoa demonstrated that CRISP2 resides in the PAS-PT and that CRISP2 in the sperm head forms reduction-sensitive oligomers [44]. The domestic pig is genetically very close to human and has often been used as a biomedical model [45]. Importantly, porcine gamete development is partly similar to human gamete development. Examples include centrosome paternal inheritance as well as timely zygotic development [10]. In this study, we have followed the fate of CRISP2 as a reporter component of the PT (i) during in vitro porcine sperm capacitation, (ii) after the calcium ionophore induced acrosome reaction and (iii) during in vitro fertilization until male pronucleus formation (in the time period of 6-8 hours post co-incubation of mature porcine oocytes with porcine sperm). The dynamics of CRISP2 dispersal and degradation in the peri-fertilization period, and thus of the PT, are

discussed in view of the implications for sperm chromatin decondensation and male pronucleus formation.

Materials and methods

Reagents and antibodies

All chemicals were obtained from Sigma (St. Louis, MO, USA) unless otherwise stated. Goat polyclonal antibody against CRISP2 (aa77-89) (MBS422304) was obtained from MyBiosource (San Diego, CA, USA). Mouse monoclonal antibody against phosphotyrosine (pTyr) (clone 4G10) was purchased from Sigma. Rabbit polyclonal to alpha tubulin (ab15246) was obtained from Abcam. Mouse monoclonal antibody against GAPDH was purchased from Santa Cruz Biotechnology (Santa Cruz, CA, USA).

Boar spermatozoa preparation

Ethical review and approval were not required for the animal study because semen samples are delivered from a commercial breeder. Written informed consent was obtained from the owners for the participation of their animals in this study. Freshly ejaculated sperm cells from highly fertile boars were obtained from a commercial breeder (Cooperative Center for Artificial Insemination in Pigs, Veghel, the Netherlands). The collected semen was diluted to 20 million sperm/ml in a commercial diluter, shipped in 80 ml sealed insemination tubes in a cool box (17 °C) until use. Diluted sperm from 2~3 different ejaculates were pooled and washed through a discontinuous Percoll (GE Healthcare) gradient (35% v/v and 70% v/v) in HEPES-buffered saline (HBS; 20 mM HEPES, 137 mM NaCl, 10 mM glucose, 2.5 mM KCl, 0.1% kanamycin, pH 7.6) for 750 x g for 15 min, room temperature (RT). Top and interface layers were removed, sperm pellets were further washed in HBS at 750 x g for 10 min at RT. All solutions were iso-osmotic (290-300 mOsm/kg) and at RT before use.

In vitro capacitation and calcium ionophore A23187 induced acrosome reaction

The capacitating medium (CM) used in this study is a modified Tyrode's medium containing 90 mM NaCl, 10.0 mM HEPES, 3.0 mM KCl, 0.4 mM $MgCl_2$, 2.0 mM $CaCl_2 \cdot 2H_2O$, 0.3 mM Na_2HPO_4, 25 mM $NaHCO_3$, 2.0 mM Na-pyruvate, 5.0 mM D-glucose, 21.6 mM sodium DL-lactate, 3.0 mg/ml bovine serum albumin (BSA) (fatty acid free), 290-300 mOsm/kg, pH 7.4. Medium supplied with neither $CaCl_2$, $NaHCO_3$ nor BSA (300 mOsm/kg was achieved by compensatory NaCl addition) was defined as non-capacitating medium (NCM). Na-pyruvate and BSA were added into the medium on the same day prior to use. Complete CM and NCM were brought to equilibrium in an incubator (38.5°C, 5% CO_2) with loose lids or in the water bath (38.5°C) with lid on for at least 2 h respectively before adding to sperm. Percoll washed sperm were suspended in CM (1 ml, 20×10^6 sperm/ml) in open vials for 2.5 h at 38.5°C in the incubator with 5% CO_2 or incubated in NCM (1 ml, 20×10^6 sperm/ml) in air-tight vials for 2.5 h at 38.5°C in pre-warmed water bath.

Sperm cells were exposed to 5 µM calcium ionophore A23187 during the last 30 min of capacitation to induce an acrosome reaction. All sperm incubations were carried out in 5 ml polystyrene round bottom tubes (Falcon, 352054; Life Sciences, Corning, NY, USA). After incubation, sperm cells were spun down and washed twice with phosphate buffered saline (PBS) (137 mM NaCl, 8.0 mM Na_2HPO_4, 1.5 mM KH_2PO_4, 2.7 mM KCl, pH 7.4) at 750 x g for 10 min at RT. Cells were either processed for immunofluorescence or stored at -80°C for later use.

Immunofluorescence staining of sperm

Non-capacitated (NC), capacitated (CAP), and acrosome reacted (AR) sperm cells were stained using a LIVE/DEAD fixable blue kit (L23105, Thermo Scientific) to examine cell viability following the manufacturer's instructions. Briefly, washed sperm cells (20×10^6) were resuspended in 1 ml PBS and 2 µl fluorescent reactive LIVE/DEAD dye was added. After mixing, cells were incubated in the dark with the dye for 30 min at RT. Then the cells were

washed twice with PBS at 750 x g for 10 min to remove excessive dye and fixed in 4% paraformaldehyde (PFA) for 15 min at RT. A suspension of 100 µl sperm (10^5 sperm/ml) was deposited in the chamber built by imaging spacers (GBL654008, Merck) on Superfrost slides (Thermo Scientific). Sperm cells were settled down for 30 min at RT. Sperm cells were further permeabilized using 0.5% (v/v) Triton X-100 for 15 min at RT. After rising with PBS, cells were blocked using 1% (w/v) BSA in PBS for 1 h at RT, incubated overnight at 4°C with goat anti-CRISP2 or/and mouse anti-pTyr. Wells were then washed three times for 30 min in PBS before incubation for 1 h at RT with Alexa Fluor 568-conjugated donkey anti-goat IgG [H+L] or/and Alexa Fluor 488-conjugated goat anti-mouse (Thermo Scientific) and counterstaining with Alexa Fluor 488-conjugated peanut agglutinin lectin (PNA) (Thermo Scientific) or/and Hoechst 33342 (1µg/ml, Sigma) at RT for 20 min. After extensive washing with PBS, slides were mounted with FluorSave reagent (Merck Millipore) and covered with coverslips. For negative controls, primary antibodies were omitted. Observations were performed on a Leica SPE-II confocal microscope using a 63x objective (NA 1.3, HCX PLANAPO oil). Scale bar was added by Image J software (bundled with 64-bit Java 1.8.0_172, National Institutes of Health, Bethesda, MD, USA).

Porcine oocyte collection and in vitro maturation

Ovaries were collected from gilts from a local slaughterhouse within 2 h after slaughter. Cumulus-oocyte complexes (COCs) were obtained by aspirating medium sized follicles (3-6 mm diameter) with an 18 g needle fixed to a vacuum pump via 50 ml conical tube and matured as previously described [46]. Briefly, COCs were recovered and washed in a modified Tyrode's lactate-HEPES medium (TL-HEPES, 114.0 mM NaCl, 3.2 mM KCl, 2.0 mM $NaHCO_3$, 0.25 mM Na-pyruvate, 0.4 mM NaH_2PO_4, 10.0 mM HEPES, 0.1% (w/v) polyvinylpyrrolidone (PVP), 10.0 mM Na-lactate, 0.5 mM $MgCl_2 \cdot 6H_2O$, 2.0 mM $CaCl_2 \cdot 2H_2O$). COCs were further washed twice in pre-warmed Medium 199 (Gibco) supplemented with 2.2 mg/ml $NaHCO_3$

(Medium C incomplete) and washed once in pre-equilibrated Medium C incomplete supplemented with 10% porcine serum, 1 mM Na-pyruvate and 0.6 mM cysteine (oocyte maturation medium; OMM). COCs were transferred in groups of 40-50 per well in to a 4-well dish containing 500 µl equilibrated OMM-I (OMM supplemented with 0.2 mM cysteamine, 0.05 IU/ml recombinant human follicle-stimulating hormone (rhFSH, Organon, Oss, The Netherlands), 100 units/ml penicillin and 100 ug/ml streptomycin (Gibco)) and incubated at 38.5°C with 5% CO_2 for 22 h. After 22 h, COCs were then washed twice in OMM-II (OMM-I without rhFSH), and then placed in 500 µl OMM-II for an additional 20 h to reach the metaphase II stage.

In vitro fertilization

The expanded cumulus cells were removed by using a micropipette set at 150 µl and pipetting the contents of the dish in and out 30 times. Denuded oocytes were then washed twice in equilibrated IVF medium (113.1 mM NaCl, 3.0 mM KCl, 20.0 mM Tris, 11.0 mM glucose, 1.0 mM caffeine, 7.5 mM $CaCl_2 \cdot 2H_2O$, 0.1% BSA (fatty acid free), 5 mM Na-pyruvate (add on the day of fertilization), 100 units/ml penicillin and 100 µg/ml streptomycin, 275-290 mOsm/kg, equilibrated overnight in the incubator at 38.5°C in 5% CO_2) and transferred in groups of 40-50 oocytes into a 4-well dish containing 500 µl IVF medium and cultured at 38.5°C with 5% CO_2 until adding sperm. Freshly ejaculated sperm cells (from 3 different boars) were mixed and washed twice in IVF medium at 700 x g for 4 min at RT. Sperm pellets were resuspended in 3 ml of IVF medium and pre-stained with 0.5 µM MitoTracker Red (Thermo Scientific) in 37°C water bath for 15 min. After twice washing with IVF medium, sperm suspensions were added into oocytes at a final concentration of 2.5×10^5 sperm/ml and co-incubated at 38.5°C with 5% CO_2 for 6-8 h or 24 h. At 24 h post-IVF, the presumptive zygotes were removed from the IVF wells, washed twice in pre-equilibrated synthetic oviductal fluid (SOF) medium [47] and placed in groups of 40-50 per 500 µl SOF medium for further development at 38.5°C with 5% CO_2

and 7% O_2. The cleavage rate (⩾2-cell) and blastocyst formation of embryos were assessed 48 h and 7 days after IVF, respectively (Table 1).

Table 1. The cleavage (≥2-cell) and blastocyst formation.

No. of examined oocytes		⩾ 2-Cell (at 48 h)	Blastocysts (at day 7)
Group	45	27	3
	47	19	3
	50	41	3
	50	40	7
	46	25	7
	39	27	2
		⩾ 2-Cell rate (%)	Blastocysts relative to total oocytes (%)
Total	277	64.3 ± 16.0%	8.9 ± 4.5%

Six groups from three independent experiments. The cleavage (≥2-cell) and blastocyst formation of embryos were assessed 48 h and 7 days after IVF, respectively. The number of 2 cell and blastocyst stages were observed per group. The percentages for cleavage (≥ 2-Cell) rate and blastocyst rate are expressed as the mean ± SD.

Immunostaining of oocytes/zygotes

Immunostaining analysis of oocytes was carried out as previously described [20] with minor modifications. Before fixation, the zona pellucida was removed by briefly incubating with 0.5% (w/v) protease in TL-HEPES. The zona-free zygotes were fixed in 4% PFA for 15 min at RT and stored in 0.1 M phosphate buffer (PB)-0.01% (w/v) PVP at 4°C if not used immediately (no longer than 5 days). Oocytes were permeabilized in 0.1 M PB-0.01% (w/v) PVP with 0.1% Triton X-100 for 1 h at RT, then blocked in 0.1M PB-0.01% PVP (w/v) with 1% (w/v) BSA for 45 min at RT. After this, zygotes were incubated with a CRISP2 antibody (1:100) diluted in 0.1M PB-0.01% PVP (w/v) with 1% (w/v) BSA at 4°C, overnight. After three times washing

in 0.1M PB-0.01% PVP (w/v), oocytes were incubated with Alexa Fluor 488-conjugated or Alexa Fluor 568-conjugated donkey anti-goat IgG [H+L] (Thermo Scientific) for 1 h at RT in the dark. After extensive washing, oocytes were counterstained with 20 ug/ml Hoechst 33342 for 10 min at RT. Oocytes were mounted in imaging spacers (GBL654008, Merck) on Superfrost slides (Thermo Scientific) with FluorSave reagent (Merck Millipore) and covered with coverslips. Observations were performed on a Leica SPE-II confocal microscope using a 63x objective (NA 1.3, HCX PLANAPO oil).

Sodium dodecyl sulfate-polyacrylamide gel electrophoresis (SDS-PAGE) and immunoblotting

An equal number of sperm cells were lysed in the same volume of RIPA lysis buffer (Thermo Scientific) with freshly added protease inhibitors containing aprotinin, leupeptin, pepstatin and phenylmethylsulfonyl fluoride (PMSF) (Thermo Scientific) on ice for 30 min with mixing. Cell debris was removed by centrifugation at 14,000 x g for 15 min, at 4°C. Supernatants were transferred to new tubes and denatured in 4 x SDS sample buffer (200 mM Tris-HCl, pH 6.8, 10% β-mercapto-ethanol, 8% SDS, 0.08% bromophenol blue, 40% glycerol) and boiled for 10 min. The same amount of each lysate was loaded on to an SDS-PAGE gel (5% stacking gel, 12% resolving gel) and were blotted onto 0.2 μm nitrocellulose membranes (GE Healthcare, Piscataway, NJ, USA) at 100V for 1 h. After blocking for 3 h at RT in 5% (w/v) BSA in PBS with 0.05% (v/v) Tween-20 (PBST), membranes were incubated with primary antibodies (diluted in PBST with 1% BSA) overnight at 4°C. After three washes in PBST for 15 min, membranes were incubated with horse radish peroxidase (HRP) conjugated secondary antibodies (mouse anti-goat HRP IgG, sz-2354, Santa Cruz, CA, USA; goat anti-rabbit and mouse HRP IgG, P0448, Agilent) for 1 h at RT. After rinsing four times in PBST for 20 min, membranes were developed using chemiluminescence (ECL-detection kit; Supersignal West

Pico, Pierce, Rockford IL, USA). Protein band size was determined using a PageRuler Plus pre-stained protein ladder, 10 to 250 kDa (Thermo Scientific).

Results

Exposure of CRISP2 on the apical ridge and the equatorial segment of the sperm head during capacitation

We have characterized the biochemical properties of CRISP2 in ejaculated boar spermatozoa in earlier work [44]. Here we explored the fate of CRISP2 during in vitro capacitation and during the calcium ionophore induced acrosome reaction. To perform this study, we first focused on immunostaining of CRISP2 in non-capacitated (NC), capacitated (CAP) and acrosome reacted (AR) porcine sperm. This was performed in the presence of peanut agglutinin lectin (PNA) to assess the acrosome status. The results demonstrated that the fluorescent signals of CRISP2 in NC sperm were bright in the post-acrosomal region and the connecting piece, with weak signals in the sperm tail, as previously reported [44] (Figure 1, Supplementary figure S1A). Interestingly, after incubation in capacitating medium (CM), a population (34.2 ± 3.8%; Table 2) of sperm with intact acrosomes showed strong CRISP2 labelling at the equatorial segment (EqS) region and the apical ridge of the sperm head (labeling type 2), while the majority possessed a staining pattern (labeling type1) that was consistent with NC sperm (Figure 1, Supplementary figure S1B). To eliminate the possibility that staining pattern in type 2 was associated with cell death, a live/dead blue staining was used to assess sperm viability. This revealed that the dead cells were not type 2 stained (Figure 1). After the calcium ionophore induced acrosome reaction, CRISP2 signals at the EqS and the apical ridge were not visible, but CRISP2 labeling was detected at the subdomain of EqS (EqSS) (Figure 1, Supplementary figure S1A). To address the point that additional CRISP2 staining of capacitated sperm was likely an exposure, fresh spermatozoa was incubated with 0.01% Saponin. Interestingly, the staining pattern of CRISP2 at the apical ridge and the EqS of the sperm head was mimicked.

CRISP2 signal in the apical ridge was observed when spermatozoa possessed a PNA positive and swollen acrosome (Figure 2A). Further, immunoblotting analysis of CRISP2 showed that Saponin treatment did not cause visible loss of CRISP2 from sperm cells (Figure 2B).

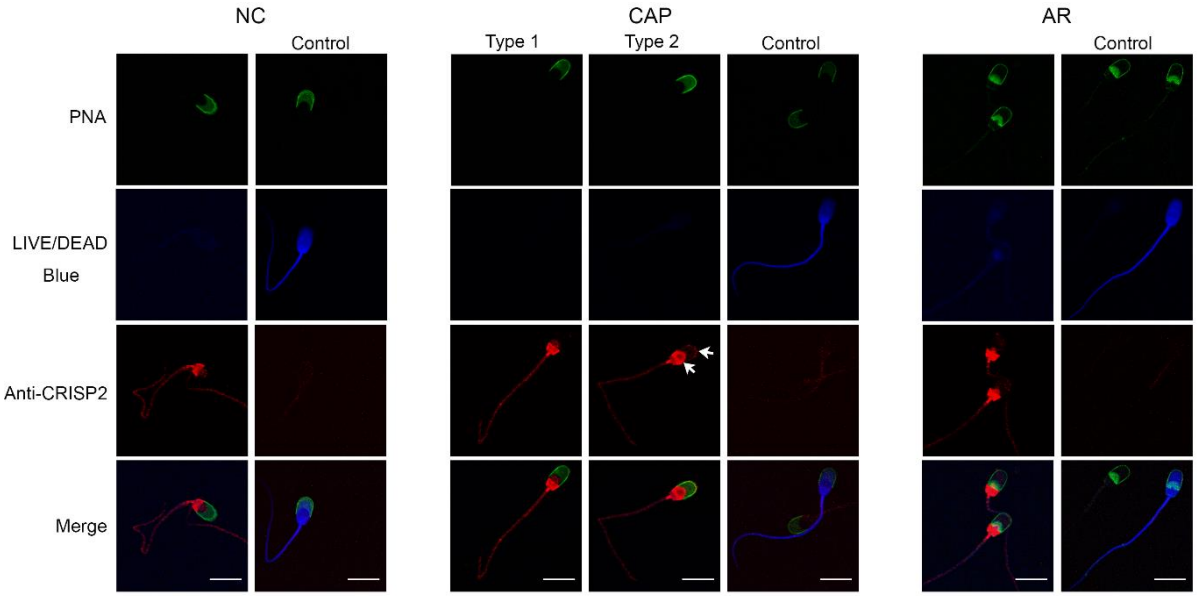

Figure 1. The distribution of porcine sperm CRISP2 during in vitro capacitation and the acrosome reaction. After incubation, non-capacitated (NC), capacitated (CAP), and acrosome reacted (AR) sperm cells were washed and labelled with a live/dead blue dye before fixation and permeabilization. Sperm cells were then labelled with anti-CRISP2 and Alexa Fluor 568-conjugated secondary antibodies (red) followed by Alexa Fluor 488-conjugated peanut agglutinin lectin (PNA) (green). The CRISP2 primary antibody was omitted and representative dead cells with bright blue signals were shown in control. Additional signals were observed on the apical ridge of sperm head and the equatorial segment (EqS) (arrows). Three ejaculates from different boars were mixed as one biological replicate and this experiment was replicated three times. Scale bar = 10 μm.

Table 2. Type 2 labeling of CRISP2 in pig sperm after in vitro capacitation.

	No. of examined sperm	Sperm showing Type 2 labeling
Group	206	77
	230	81
	217	65
		(%) Sperm showing Type 2 labeling
Total	653	34.2 ± 3.8%

In the case of in vitro capacitated sperm, the exposure of CRISP2 on the apical ridge and the EqS (labeling type2) was recorded. This experiment was replicated three times and the number of sperm examined as well as the number of those sperm with type 2 labeling for CRISP2 were expressed for each group. The percentage of sperm with type 2 labeling is expressed as the mean ± SD.

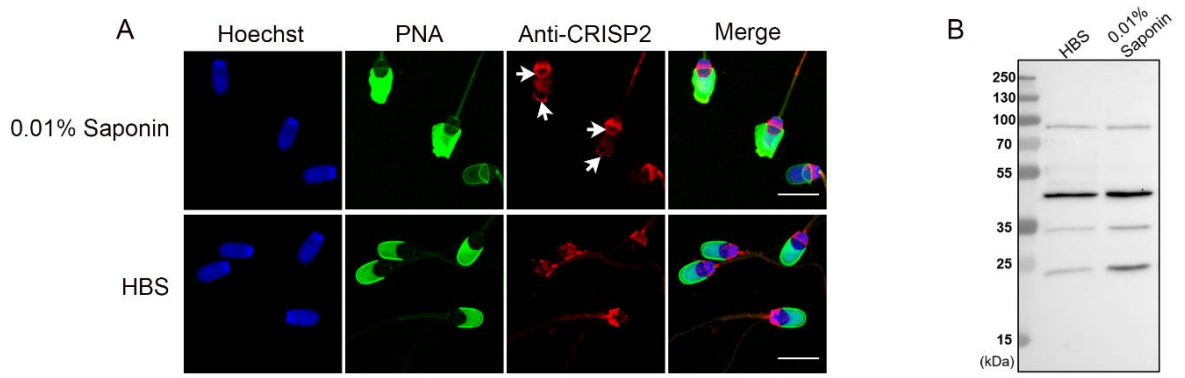

Figure 2. Saponin incubation with ejaculated spermatozoa mimics the exposure of CRISP2 at the apical ridge and the EqS of capacitated sperm. Percoll washed sperm cells were incubated in 0.01% Saponin supplied in HBS for 10 min at 37.5°C. After incubation, sperm cells were washed and sampled for immunostaining and immunoblotting analysis. (A) Sperm cells were fixed and permeabilized, probed with anti-CRISP2 followed by Alexa Fluor 568-conjugated (red) secondary antibodies, counterstained with Alexa Fluor 488-conjugated PNA (green) and Hoechst 33342 (blue). Scale bar = 10 μm. (B) Immunoblotting analysis of CRISP2 on the extracts from Saponin treated sperm probed with anti-CRISP2.

Additional appearance of CRISP2 is specific for capacitated sperm cells that show protein tyrosine phosphorylation

To confirm that the translocation of CRISP2 to the EqS and apical region was dependent on capacitation, protein tyrosine phosphorylation was analyzed to confirm the capacitation status of the cells. Coomassie brilliant blue staining analysis of lysates from NC, CAP and AR sperm was conducted to view total proteins loading and protein changes. As indicated in Figure 3A, the total protein amounts among the conditions were comparable, with three protein bands that changed depending on capacitation and acrosome reaction treatments: (i) A ~66 kDa protein band was absent in NC sperm and present in CAP and AR sperm. This likely corresponds to bovine serum albumin (BSA), which was not present in non-capacitating medium; (ii) A ~52

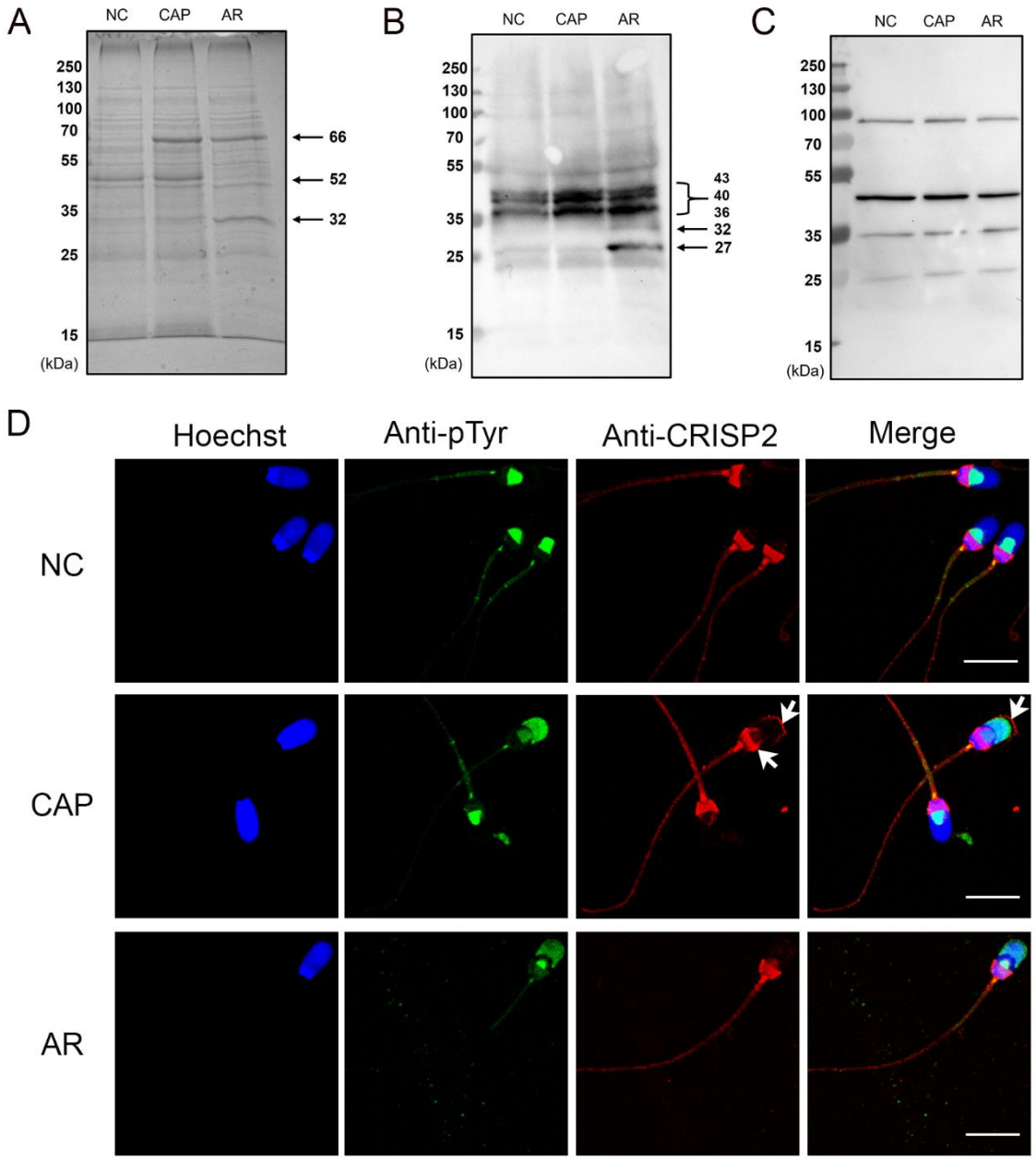

Figure 3. Exposure of CRISP2 at the apical ridge and the EqS of the sperm head during capacitation is an event associated with tyrosine phosphorylation. (A) Lysates from NC, CAP and AR sperm cells were analyzed by SDS-PAGE and Coomassie blue staining. Immunoblotting analysis of tyrosine phosphorylation and CRISP2 on the extracts from NC, CAP and AR sperm cells probed with anti-pTyr (B) and anti-CRISP2 (C) antibodies. (D) NC, CAP and AR sperm cells were co-incubated with anti-CRISP2 and anti-pTyr, labelled with Alexa Fluor 568-conjugated (red) and Alexa Fluor 488-conjugated second antibodies (green) and counterstained with Hoechst 33342 (blue). This experiment was replicated three times. Scale bar = 10 μm.

kDa protein band was present in NC and CAP sperm, but greatly decreased in AR sperm. This protein band likely represents proacrosin; and (iii) the ~32 kDa protein band associated with

AR sperm is in line with the corresponding increased tyrosine phosphorylated protein detected by immunoblots in Figure 3B. Immunoblotting analysis on lysates from NC, CAP and AR sperm showed that the intensity of ~43 kDa, ~40 kDa and ~36 kDa protein tyrosine-phosphorylation bands was increased when sperm were incubated in CM. Additional bands of ~32 kDa and ~27 kDa also appeared after calcium ionophore induced acrosomal exocytosis (Figure 3B). Previous studies have reported that protein tyrosine phosphorylation is enhanced at the acrosome in capacitated boar sperm, with consistently signals being present in the EqSS [48]. Similar results were observed in our study. In NC sperm, protein tyrosine phosphorylation was restricted to the EqSS (Figure 3D). After capacitation, a representative 25% sperm showed the tyrosine phosphorylation signal spreading over the acrosome. Among those, a representative 76% sperm showed additional CRISP2 labelling at the apical ridge and EqS (Figure 3D). After induction of the acrosome reaction, protein tyrosine phosphorylation labeling of the acrosome was observed with visible signals in the EqSS. Moreover, CRISP2 was colocalized with tyrosine phosphorylation fluorescence in the EqSS in AR sperm (Figure 3D). Immunoblot analysis of CRISP2 on lysates from NC, CAP and AR sperm cells was shown in Figure 3C.

Distribution of CRISP2 of sperm bound to zona pellucida

To further explore how CRISP2 is distributed post-fertilization, in vitro fertilization (IVF) was performed on matured porcine oocytes by coincubation with porcine sperm. Initial experiments focused on investigating the distribution of CRISP2 in the sperm that were bound to the oocyte zona pellucida (ZP). Immunostaining of CRISP2 revealed CRISP2 signal at the apical ridge, the EqS, the post-acrosomal region of the sperm head and in the sperm tail (Figure 4Aa). This distribution of CRISP2 was consistent with what we described above for CAP sperm that showed increased protein tyrosine phosphorylation. Sperm that were penetrating the ZP lost the signal on the apical ridge as well as on the EqS, but the immunofluorescence of CRISP2 in the post-acrosomal region was retained (Figure 4Aa). In Figure 4B, another capture of sperm

penetrating the ZP showed that CRISP2 stayed condensed in the post-acrosomal region. A recent study has shown that there is no CRISP2 mRNA expression in porcine ovary [49]. In our study, mature oocytes were collected and processed for immunoblotting analysis. Ejaculated sperm cells were used as a positive control. We have described in our earlier study that 8 M urea treatments cause high molecular CRISP2 complexes to disassociate into a monomer [44]. Here, denuded oocytes were also solubilized in 8 M urea to acquire an efficient denature of oocyte proteins. Our result revealed that no CRISP2 signal was detected on the immunoblot of the porcine oocytes lysates (Supplementary figure S2). Thus, the CRISP2 signal detected in Figure 4A/B was definitely coming from CRISP2 within boar spermatozoa.

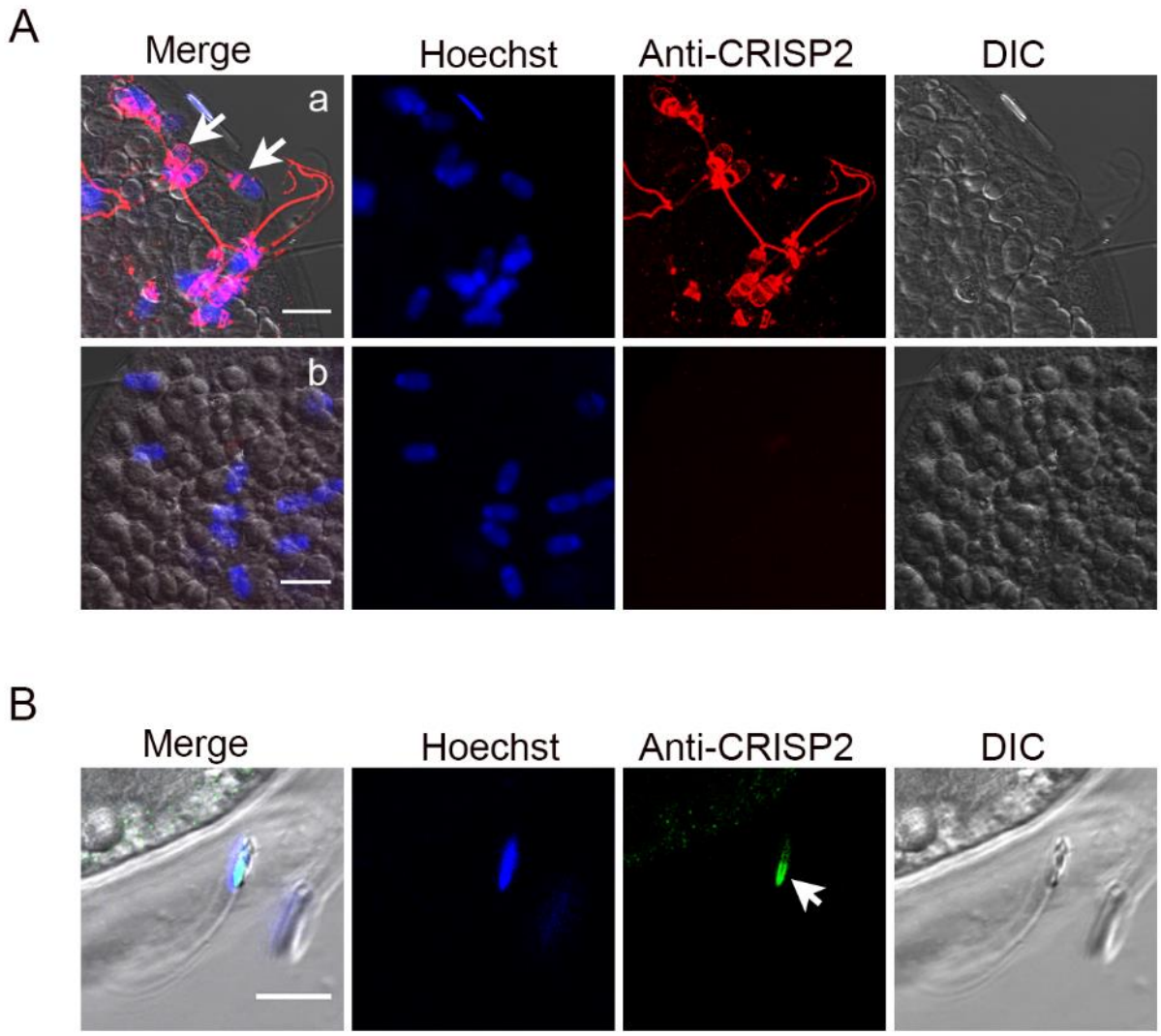

Figure 4. The distribution of sperm CRISP2 in zona bound and zona penetrated spermatozoa. Porcine oocytes and sperm were co-incubated for 6-8 h after insemination. Zygotes were fixed and

permeabilized for immunochemistry analysis. (A) Zygotes were labelled with anti-CRISP2 (a) followed by Alexa Fluor 568-conjugated (red) secondary antibodies and counterstained with Hoechst 33342 (blue). (b) The anti-CRISP2 was omitted. (B) Immunolocalization of CRISP2 of sperm penetrated in zona detected by Alexa Fluor 488-conjugated (green) secondary antibodies. Scale bar = 10 μm.

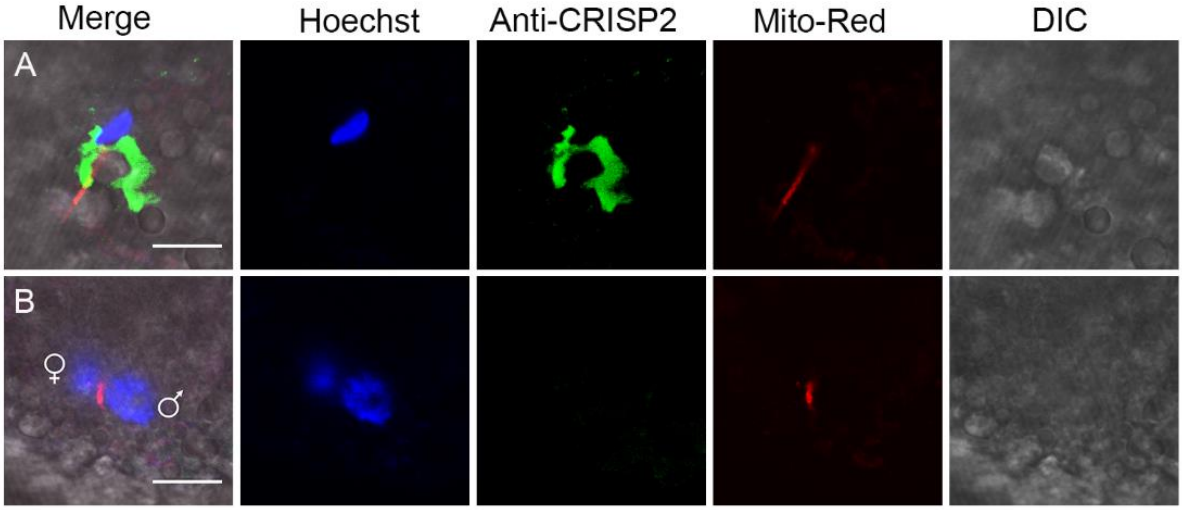

Figure 5. The fate of porcine sperm CRISP2 after incorporation with oocyte cytoplasm. Porcine oocytes and MitoTracker Red pre-stained sperm were co-incubated for 6-8 h after insemination. Zygotes were stripped of zona pellucida using 0.5% (w/v) protease prior to fixation and permeabilization, labelled with anti-CRISP2 detected by Alexa Fluor 488-conjugated (green) secondary antibodies and counterstained with Hoechst 33342 (blue). (A) Rapid dispersal of sperm CRISP2 was observed in the zygote after incorporation while the sperm nucleus was still condensed. Moreover, the mitochondria were compacted. (B) CRISP2 signals were beyond detection in the two-pronuclear stage. Scale bar = 10 μm.

Rapid dispersal of sperm CRISP2 prior to sperm nuclear decondensation

Intrigued by the findings that CRISP2 is a component of the post-acrosomal sheath (PAS)-perinuclear theca (PT) and the important roles of PAS-PT in early events of fertilization, we sought to investigate the fate of sperm CRISP2 in fertilized pig oocytes. Oocytes were co-incubated with fresh boar spermatozoa preloaded with fluorescent MitoTracker Red probe, cultured and sampled for CRISP2 detection. The dissociation of sperm CRISP2 from the PAS-PT was observed within the oolemma, while the sperm nucleus was still fully condensed and

the entire mitochondrial sheath was still intact (Figure 5A). Remarkably, sperm CRISP2 was undetectable in zygotes that were in the two-pronuclear stage, while sperm mitochondria were still linear arranged (Figure 5B, Supplementary figure S3B). Multilayer scanning (z-stack, step size 1 μm) was recorded to show the CRISP2 and sperm mitochondrial sheath originating from the fertilizing sperm cell (Supplementary file 1 and 2). Another fertilizing sperm was imaged and showed CRISP2 dispersal as well as a decreased intensity of CRISP2 immunofluorescence, while the sperm nucleus was still condensed (Supplementary figure S3A). This indicate that the PT dissociation (as imaged with CRISP2 immunolabeling) and degradation events occur earlier than sperm chromatin decondensation and degradation of the sperm mitochondria.

Discussion

In the past few decades, cysteine-rich secretory proteins (CRISPs) have been extensively investigated due to their proposed functions in reproductive events. Crucially, triple and quadruple CRISP knockout models have been described to have severely subfertile phenotypes and generate a higher number of sterile males [50] indicating that the CRISP family are indispensable for male fertility. The outcome that single and double knockout mice males are still fertile under various laboratory conditions is explained by compensatory mechanisms within homologous family proteins [42, 50-53]. However, the intracellular sperm CRISP2 cannot be compensated by other CRISPs that are associated to the sperm surface. CRISP2 is crucial for flexible sperm midpiece development suggesting that CRISP2 holds independent functions contributing to fertility process [42, 50].

In the present study, we investigated the fate and organization of boar sperm CRISP2 during in vitro capacitation, calcium ionophore induced acrosome reaction and throughout the first 6-8 h of IVF of porcine oocytes. Our data demonstrated that following capacitation, additional CRISP2 immunofluorescence was detected on the apical ridge as well as the equatorial segment

(EqS) of the sperm head. Interestingly, this staining pattern is similar to that we have obtained after incubating ejaculated porcine sperm with 0.01% Saponin. Saponin is a mild detergent and can be used at very low concentrations to selectively permeabilize the plasma membrane but not other interior membrane compartments [54]. Saponin removes cholesterol from membranes with little disintegration of the membranes themselves [54]. Physiologically, cholesterol removal is also observed in capacitating sperm cells [8, 55, 56]. Moreover, we showed previously that additional CRISP2 labeling of the EqS on ejaculated spermatozoa is observed only after sonication, not in untreated, intact sperm [44]. A similar phenomenon has been reported for equatorin, a sperm head equatorial protein, which is exposed at the EqS after sonication and protease inhibitors are unable to prevent the exposure [57]. A proteolytic reaction is not likely involved during the exposure of CRISP2 after sonication as the sonication medium was enriched with phenylmethylsulfonyl fluoride (PMSF) in order to inhibit proteases. Physiologically, the exposure of CRISP2 on the apical ridge and the EqS was only associated with capacitated sperm, as indicated by positive tyrosine phosphorylation labeling over the acrosome [48]. Protein tyrosine phosphorylation is a capacitation marker with the process thought to occur simultaneously with cholesterol depletion [8]. Sperm membrane cholesterol efflux is part of a signal transduction pathway involving elevated cAMP levels and protein kinase A (PKA) activity leading to protein tyrosine phosphorylation [3, 58]. Evidence demonstrates that cholesterol restricts the freedom of membrane proteins to undergo conformational changes [59]. The fact that human CRISP2 binds sterols in vitro may suggest a sterol binding function of CRISPs in sperm maturation and fertilization process [60]. Additionally, studies show that cholesterol removal disassociates the interaction between the proteins and caveolin, leading to the activation of caveolin-interacting proteins [61, 62]. Thus, we conclude that the exposure of CRISP2 on the apical ridge and the EqS is a capacitation associated phenomena likely driven by cholesterol efflux. Given that the capacitation status of

sperm is positively correlated to sperm-zona binding and acrosome reaction [63] as well as that the apical ridge of sperm head membrane has high affinity for sperm-zona binding after capacitation [64-66], our data suggest that CRISP2 on the apical ridge and the EqS of capacitated cells may be indicative of those cells that can bind to the ZP. This idea was supported by the immunofluorescent staining of CRISP2 of zona bound sperm that CRISP2 had a location on the apical ridge, the EqS, the post acrosomal region and the sperm tail.

It has been reported that the EqS still holds intact membranes even after the acrosome reaction [67]. Unexpectedly, our results revealed that the CRISP2 signal on the EqS disappeared after the acrosome reaction, while CRISP2 immunofluorescence was detected in a subdomain of EqS (EqSS). Initially, the EqSS was characterized as an unusual semicircular substructure within the EqS by atomic force microscopy in Artiodactyla spermatozoa [68]. The EqSS develops during sperm epididymal maturation [68] and is enriched in tyrosine phosphorylated proteins such as sperm acrosome-associated protein 1 and heat-shock protein 70 [69, 70]. The presence of CRISP2 in the EqSS was confirmed in our previous study when sonicated sperm heads are extracted in 0.2% Triton X-100 and this signal disappears after 0.1M NaOH extraction as the PAS-PT residing CRISP2 [44]. It indicates that EqSS as a substructure underlying the PT shares a similar biochemical extractability with the PT as shown by CRISP2. Topographical changes in the EqSS have been observed when sperm are introduced to calcium ionophore A23187 and thus this area has been speculated to initiate sperm-egg fusion within Artiodactyla [68]. However, no prominent structural changes or modifications of PT following the acrosome reaction have been reported yet. The loss of CRISP2 immunofluorescence from the EqS after ionophore A23187 induced acrosome reaction suggests that CRISP2 is not directly involved in sperm-egg fusion at this site.

Our key findings of this manuscript suggest that the PAS-PT residing CRISP2 in boar spermatozoa [44] is dispersed rapidly in the oocyte cytoplasm and this may be needed for subsequent nuclear decondensation and male pronucleus formation. In an attempt to quantify CRISP2 decondensation and its subsequent degradation, we have recorded 28 fertilized pig oocytes 6-8 h post-fertilization. Four of them showed the two pronuclear stage in which CRISP2 labeling was not visible (as shown in Figure 5B and Supplementary figure S3B). The other 24 of them showed a still condensed sperm nucleus and clear MitoTracker Red staining. However, only 5 out of these 24 fertilized oocytes showed CRISP2 dispersal while the other 19 had already degraded their CRISP2. This indicates that CRISP2 dispersal and degradation occur rapidly at fertilization and much earlier than sperm chromatin decondensation. The rapid dispersal of CRISP2 is likely due to the disassembly of disulfide bonds facilitated by GSTO2 [24, 27]. In the sperm head, CRISP2 resides in the condensed PT structure and is involved in formation of reduction-sensitive oligomers at its cysteine-rich domain, which fits with the conversed amyloidogenic behavior of CAP proteins [44, 71]. Removal of PAS-PT from sperm head is indispensable for sperm chromatin decondensation and the released molecules from PAS-PT are essential for oocyte activation [17]. The compacted organization of CRISP2 in the PAS-PT and its rapid disassociation from the sperm nuclear envelope post-fertilization (more or less immediately when the PAS-PT is exposed to oocyte cytoplasm) fits the model proposed by Sutovsky and Oko [17]. Notably, CRISP2 dispersal is complete prior to any signs of male nuclear decondensation, raising the possibility that disulfide bond reduction is the way to initiate PAS-PT solubilization. The oxidation of free thiol groups in proteins is reversibly regulated by redox reactions and is crucial in many cellular functions [71, 72]. Sperm cells carry physiological levels of reactive oxygen species (ROS) which play an important role in sperm maturation, capacitation, acrosome reaction and sperm-egg fusion [73]. We speculate that CRISP2 is modified concomitantly with PT condensation in the elongating phase of spermatids,

thus serving as a scaffold stabilizing the rigidity of PT as well as hampering the activity of certain proteins. Soon after sperm-egg incorporation, reduction of disulfide bridges within CRISP2 as a transduction signal leads to the solubilization of PT contents into the oocyte cytoplasm and subsequently the sperm nuclear decondensation. Once inside the oocyte, the decondensing PT will liberate other PT components into the oocyte's cytosol that may be relevant for post-fertilization changes in the oocyte. Of specific interest are the CRISP2 interacting PT proteins: post-acrosomal WW domain-binding protein (PAWP) and Ras-related protein Rab-2B (RAB2B) [74]. The release of RAB2B, can be important for locally regulating vesicle transport and membrane fusion [75]. Sperm that interacted with the oolemma showed condensed RAB2B staining (unpublished observations) supporting the idea that this PT component is introduced into the oocyte's cytosol at fertilization. A similar release of PAWP from the PT into the oocyte's cytosol may be involved in the induction of Ca^{2+} oscillations required for activating the oocyte [19, 20]. Finally, it is notable that CRISP2 is degraded soon after PT dispersal and is eliminated before a male pronucleus is formed. The PT structure is enriched in proteasome subunits (in fact it contains all subunits for re-assembly of a functional proteasome) [74]. The group of Sutovsky has designed a cell free system to follow dispersal and breakdown of sperm structures [76]. Such an approach in combination with redox titrations on sperm heads can be used to follow PT dispersion and break down in vitro. In this way it is possible to demonstrate that reassembly of these proteasome subunits into functional proteasomes will facilitate the destruction of the PT structure and other accessory sperm components as shown here for CRISP2.

Acknowledgments

MZ is financed by the China Scholarship Council (CSC) (No. 201606170117). EGB is recipient of an NHMRC CJ Martin early Career Fellowship (APP1138701). We thank Leni van Tol for an introduction of porcine in vitro fertilization and Richard Wubbolts and Esther van 't Veld

for their technical support at the Center of Cell Imaging in the Faculty of Veterinary Medicine at Utrecht University.

Conflict of interest

The authors have no conflict of interests.

Author contributions

MZ conducted the experiments, contributed to figure preparation, editing and wrote the draft of the manuscript. EB and JH provided critical appraisal of the data and reviewed the manuscript. BG conceived of the study and contributed to supervision, manuscript revision and editing.

Data availability

The data underlying this article will be shared on reasonable request to the corresponding author.

References

1. Austin CR, Bishop MW. Capacitation of mammalian spermatozoa. Nature 1958; 181:851.
2. Yanagimachi R, Chang MC. Fertilization of Hamster Eggs in vitro. Nature 1963; 200:281-282.
3. Visconti PE. Understanding the molecular basis of sperm capacitation through kinase design. Proc Natl Acad Sci U S A 2009; 106:667-668.
4. Gadella BM, Evans JP. Membrane fusions during mammalian fertilization. Adv Exp Med Biol 2011; 713:65-80.
5. Gadella BM, Lopes-Cardozo M, van Golde LM, Colenbrander B, Gadella TW, Jr. Glycolipid migration from the apical to the equatorial subdomains of the sperm head plasma membrane precedes the acrosome reaction. Evidence for a primary capacitation event in boar spermatozoa. J Cell Sci 1995; 108 (Pt 3):935-946.
6. Tsai PS, De Vries KJ, De Boer-Brouwer M, Garcia-Gil N, Van Gestel RA, Colenbrander B, Gadella BM, Van Haeften T. Syntaxin and VAMP association with lipid rafts depends on cholesterol depletion in capacitating sperm cells. Mol Membr Biol 2007; 24:313-324.
7. Gadella BM, Harrison RA. Capacitation induces cyclic adenosine 3',5'-monophosphate-dependent, but apoptosis-unrelated, exposure of aminophospholipids at the apical head plasma membrane of boar sperm cells. Biol Reprod 2002; 67:340-350.
8. Flesch FM, Brouwers JF, Nievelstein PF, Verkleij AJ, van Golde LM, Colenbrander B, Gadella BM. Bicarbonate stimulated phospholipid scrambling induces cholesterol redistribution and enables cholesterol depletion in the sperm plasma membrane. J Cell Sci 2001; 114:3543-3555.
9. Buffone MG, Hirohashi N, Gerton GL. Unresolved questions concerning mammalian sperm acrosomal exocytosis. Biol Reprod 2014; 90:112.
10. Zigo M, Maňásková-Postlerová P, Zuidema D, Kerns K, Jonáková V, Tůmová L, Bubeníčková F, Sutovsky P. Porcine model for the study of sperm capacitation, fertilization and male fertility. Cell Tissue Res 2020; 380:237-262.
11. Inoue N, Ikawa M, Isotani A, Okabe M. The immunoglobulin superfamily protein Izumo is required for sperm to fuse with eggs. Nature 2005; 434:234-238.

12. Ellerman DA, Pei J, Gupta S, Snell WJ, Myles D, Primakoff P. Izumo is part of a multiprotein family whose members form large complexes on mammalian sperm. Mol Reprod Dev 2009; 76:1188-1199.
13. Ito C, Yamatoya K, Yoshida K, Maekawa M, Miyado K, Toshimori K. Tetraspanin family protein CD9 in the mouse sperm: unique localization, appearance, behavior and fate during fertilization. Cell Tissue Res 2010; 340:583-594.
14. Nimlamool W, Bean BS, Lowe-Krentz LJ. Human sperm CRISP2 is released from the acrosome during the acrosome reaction and re-associates at the equatorial segment. Mol Reprod Dev 2013; 80:488-502.
15. Busso D, Cohen DJ, Hayashi M, Kasahara M, Cuasnicú PS. Human testicular protein TPX1/CRISP-2: localization in spermatozoa, fate after capacitation and relevance for gamete interaction. Mol Hum Reprod 2005; 11:299-305.
16. Busso D, Goldweic NM, Hayashi M, Kasahara M, Cuasnicú PS. Evidence for the involvement of testicular protein CRISP2 in mouse sperm-egg fusion. Biol Reprod 2007; 76:701-708.
17. Sutovsky P, Manandhar G, Wu A, Oko R. Interactions of sperm perinuclear theca with the oocyte: implications for oocyte activation, anti-polyspermy defense, and assisted reproduction. Microsc Res Tech 2003; 61:362-378.
18. Saunders CM, Larman MG, Parrington J, Cox LJ, Royse J, Blayney LM, Swann K, Lai FA. PLC zeta: a sperm-specific trigger of Ca(2+) oscillations in eggs and embryo development. Development 2002; 129:3533-3544.
19. Aarabi M, Balakier H, Bashar S, Moskovtsev SI, Sutovsky P, Librach CL, Oko R. Sperm-derived WW domain-binding protein, PAWP, elicits calcium oscillations and oocyte activation in humans and mice. Faseb j 2014; 28:4434-4440.
20. Wu AT, Sutovsky P, Manandhar G, Xu W, Katayama M, Day BN, Park KW, Yi YJ, Xi YW, Prather RS, Oko R. PAWP, a sperm-specific WW domain-binding protein, promotes meiotic resumption and pronuclear development during fertilization. J Biol Chem 2007; 282:12164-12175.
21. Kashir J, Jones C, Lee HC, Rietdorf K, Nikiforaki D, Durrans C, Ruas M, Tee ST, Heindryckx B, Galione A, De Sutter P, Fissore RA, et al. Loss of activity mutations in phospholipase C zeta (PLCζ) abolishes calcium oscillatory ability of human recombinant protein in mouse oocytes. Hum Reprod 2011; 26:3372-3387.
22. Nomikos M, Yu Y, Elgmati K, Theodoridou M, Campbell K, Vassilakopoulou V, Zikos C, Livaniou E, Amso N, Nounesis G, Swann K, Lai FA. Phospholipase Cζ rescues failed oocyte activation in a prototype of male factor infertility. Fertil Steril 2013; 99:76-85.
23. Sutovsky P, Oko R, Hewitson L, Schatten G. The removal of the sperm perinuclear theca and its association with the bovine oocyte surface during fertilization. Dev Biol 1997; 188:75-84.
24. Perreault SD, Wolff RA, Zirkin BR. The role of disulfide bond reduction during mammalian sperm nuclear decondensation in vivo. Dev Biol 1984; 101:160-167.
25. Sutovsky P, Schatten G. Depletion of glutathione during bovine oocyte maturation reversibly blocks the decondensation of the male pronucleus and pronuclear apposition during fertilization. Biol Reprod 1997; 56:1503-1512.
26. Hamilton LE, Acteau G, Xu W, Sutovsky P, Oko R. The developmental origin and compartmentalization of glutathione-s-transferase omega 2 isoforms in the perinuclear theca of eutherian spermatozoa. Biol Reprod 2017; 97:612-621.
27. Hamilton LE, Suzuki J, Aguila L, Meinsohn MC, Smith OE, Protopapas N, Xu W, Sutovsky P, Oko R. Sperm-borne glutathione-S-transferase omega 2 accelerates the nuclear decondensation of spermatozoa during fertilization in mice†. Biol Reprod 2019; 101:368-376.

28. Hamilton LE, Lion M, Aguila L, Suzuki J, Acteau G, Protopapas N, Xu W, Sutovsky P, Baker M, Oko R. Core Histones Are Constituents of the Perinuclear Theca of Murid Spermatozoa: An Assessment of Their Synthesis and Assembly during Spermiogenesis and Function after Gametic Fusion. Int J Mol Sci 2021; 22.
29. Gaikwad AS, Hu J, Chapple DG, O'Bryan MK. The functions of CAP superfamily proteins in mammalian fertility and disease. Hum Reprod Update 2020; 26:689-723.
30. Jalkanen J, Huhtaniemi I, Poutanen M. Mouse cysteine-rich secretory protein 4 (CRISP4): a member of the Crisp family exclusively expressed in the epididymis in an androgen-dependent manner. Biol Reprod 2005; 72:1268-1274.
31. Nolan MA, Wu L, Bang HJ, Jelinsky SA, Roberts KP, Turner TT, Kopf GS, Johnston DS. Identification of rat cysteine-rich secretory protein 4 (Crisp4) as the ortholog to human CRISP1 and mouse Crisp4. Biol Reprod 2006; 74:984-991.
32. Vadnais ML, Foster DN, Roberts KP. Molecular cloning and expression of the CRISP family of proteins in the boar. Biol Reprod 2008; 79:1129-1134.
33. Da Ros VG, Muñoz MW, Battistone MA, Brukman NG, Carvajal G, Curci L, Gómez-ElIas MD, Cohen DB, Cuasnicu PS. From the epididymis to the egg: participation of CRISP proteins in mammalian fertilization. Asian J Androl 2015; 17:711-715.
34. Guasti PN, Souza FF, Scott C, Papa PM, Camargo LS, Schmith RA, Monteiro GA, Hartwig FP, Papa FO. Equine seminal plasma and sperm membrane: Functional proteomic assessment. Theriogenology 2020; 156:70-81.
35. Restrepo G, Rojano B, Usuga A. Relationship of cysteine-rich secretory protein-3 gene and protein with semen quality in stallions. Reprod Domest Anim 2019; 54:39-45.
36. Jing XW, Xing RW, Zhou QZ, Yu QF, Guo WB, Chen SM, Chu QJ, Feng CQ, Mao XM. [Expressions of cysteine-rich secretory protein 2 in asthenospermia]. Zhonghua Nan Ke Xue 2011; 17:203-207.
37. Zhou JH, Zhou QZ, Lyu XM, Zhu T, Chen ZJ, Chen MK, Xia H, Wang CY, Qi T, Li X, Liu CD. The expression of cysteine-rich secretory protein 2 (CRISP2) and its specific regulator miR-27b in the spermatozoa of patients with asthenozoospermia. Biol Reprod 2015; 92:28.
38. Du Y, Huang X, Li J, Hu Y, Zhou Z, Sha J. Human testis specific protein 1 expression in human spermatogenesis and involvement in the pathogenesis of male infertility. Fertil Steril 2006; 85:1852-1854.
39. Foster JA, Gerton GL. Autoantigen 1 of the guinea pig sperm acrosome is the homologue of mouse Tpx-1 and human TPX1 and is a member of the cysteine-rich secretory protein (CRISP) family. Mol Reprod Dev 1996; 44:221-229.
40. Roberts KP, Ensrud-Bowlin KM, Piehl LB, Parent KR, Bernhardt ML, Hamilton DW. Association of the protein D and protein E forms of rat CRISP1 with epididymal sperm. Biol Reprod 2008; 79:1046-1053.
41. Muñoz MW, Ernesto JI, Bluguermann C, Busso D, Battistone MA, Cohen DJ, Cuasnicú PS. Evaluation of testicular sperm CRISP2 as a potential target for contraception. J Androl 2012; 33:1360-1370.
42. Lim S, Kierzek M, O'Connor AE, Brenker C, Merriner DJ, Okuda H, Volpert M, Gaikwad A, Bianco D, Potter D, Prabhakar R, Strünker T, et al. CRISP2 Is a Regulator of Multiple Aspects of Sperm Function and Male Fertility. Endocrinology 2019; 160:915-924.
43. Brukman NG, Miyata H, Torres P, Lombardo D, Caramelo JJ, Ikawa M, Da Ros VG, Cuasnicú PS. Fertilization defects in sperm from Cysteine-rich secretory protein 2 (Crisp2) knockout mice: implications for fertility disorders. Mol Hum Reprod 2016; 22:240-251.
44. Zhang M, Bromfield EG, Veenendaal T, Klumperman J, Helms JB, Gadella BM. Characterization of different oligomeric forms of CRISP2 in the perinuclear theca versus the fibrous tail structures of boar spermatozoa†. Biol Reprod 2021; 105:1160-1170.

45. Vodicka P, Smetana K, Jr., Dvoránková B, Emerick T, Xu YZ, Ourednik J, Ourednik V, Motlík J. The miniature pig as an animal model in biomedical research. Ann N Y Acad Sci 2005; 1049:161-171.
46. Schoevers EJ, Colenbrander B, Roelen BA. Developmental stage of the oocyte during antral follicle growth and cumulus investment determines in vitro embryo development of sow oocytes. Theriogenology 2007; 67:1108-1122.
47. Brinkhof B, van Tol HT, Groot Koerkamp MJ, Wubbolts RW, Haagsman HP, Roelen BA. Characterization of bovine embryos cultured under conditions appropriate for sustaining human naïve pluripotency. PLoS One 2017; 12:e0172920.
48. Luño V, López-Úbeda R, García-Vázquez FA, Gil L, Matás C. Boar sperm tyrosine phosphorylation patterns in the presence of oviductal epithelial cells: in vitro, ex vivo, and in vivo models. Reproduction 2013; 146:315-324.
49. Gao F, Wang P, Wang K, Fan Y, Chen Y, Chen Y, Ye C, Feng M, Li L, Zhang S, Wei H. Investigation Into the Relationship Between Sperm Cysteine-Rich Secretory Protein 2 (CRISP2) and Sperm Fertilizing Ability and Fertility of Boars. Front Vet Sci 2021; 8:653413.
50. Curci L, Brukman NG, Weigel Muñoz M, Rojo D, Carvajal G, Sulzyk V, Gonzalez SN, Rubinstein M, Da Ros VG, Cuasnicú PS. Functional redundancy and compensation: Deletion of multiple murine Crisp genes reveals their essential role for male fertility. Faseb j 2020; 34:15718-15733.
51. Weigel Muñoz M, Battistone MA, Carvajal G, Maldera JA, Curci L, Torres P, Lombardo D, Pignataro OP, Da Ros VG, Cuasnicú PS. Influence of the genetic background on the reproductive phenotype of mice lacking Cysteine-Rich Secretory Protein 1 (CRISP1). Biol Reprod 2018; 99:373-383.
52. Volpert M, Furic L, Hu J, O'Connor AE, Rebello RJ, Keerthikumar S, Evans J, Merriner DJ, Pedersen J, Risbridger GP, McIntyre P, O'Bryan MK. CRISP3 expression drives prostate cancer invasion and progression. Endocr Relat Cancer 2020; 27:415-430.
53. Carvajal G, Brukman NG, Weigel Muñoz M, Battistone MA, Guazzone VA, Ikawa M, Haruhiko M, Lustig L, Breton S, Cuasnicu PS. Impaired male fertility and abnormal epididymal epithelium differentiation in mice lacking CRISP1 and CRISP4. Sci Rep 2018; 8:17531.
54. Wassler M, Jonasson I, Persson R, Fries E. Differential permeabilization of membranes by saponin treatment of isolated rat hepatocytes. Release of secretory proteins. Biochem J 1987; 247:407-415.
55. Boerke A, Brouwers JF, Olkkonen VM, van de Lest CH, Sostaric E, Schoevers EJ, Helms JB, Gadella BM. Involvement of bicarbonate-induced radical signaling in oxysterol formation and sterol depletion of capacitating mammalian sperm during in vitro fertilization. Biol Reprod 2013; 88:21.
56. Bernecic NC, Zhang M, Gadella BM, Brouwers J, Jansen JWA, Arkesteijn GJA, de Graaf SP, Leahy T. BODIPY-cholesterol can be reliably used to monitor cholesterol efflux from capacitating mammalian spermatozoa. Sci Rep 2019; 9:9804.
57. Manandhar G, Toshimori K. Exposure of sperm head equatorin after acrosome reaction and its fate after fertilization in mice. Biol Reprod 2001; 65:1425-1436.
58. Travis AJ, Kopf GS. The role of cholesterol efflux in regulating the fertilization potential of mammalian spermatozoa. J Clin Invest 2002; 110:731-736.
59. Hamilton DW, Jones AL, Fawcett DW. Cholesterol biosynthesis in the mouse epididymis and ductus deferens: a biochemical and morphological study. Biol Reprod 1969; 1:167-184.
60. Choudhary V, Schneiter R. Pathogen-Related Yeast (PRY) proteins and members of the CAP superfamily are secreted sterol-binding proteins. Proc Natl Acad Sci U S A 2012; 109:16882-16887.

61. Okamoto T, Schlegel A, Scherer PE, Lisanti MP. Caveolins, a family of scaffolding proteins for organizing "preassembled signaling complexes" at the plasma membrane. J Biol Chem 1998; 273:5419-5422.
62. Baltiérrez-Hoyos R, Roa-Espitia AL, Hernández-González EO. The association between CDC42 and caveolin-1 is involved in the regulation of capacitation and acrosome reaction of guinea pig and mouse sperm. Reproduction 2012; 144:123-134.
63. Liu DY, Liu ML, Clarke GN, Baker HW. Hyperactivation of capacitated human sperm correlates with the zona pellucida-induced acrosome reaction of zona pellucida-bound sperm. Hum Reprod 2007; 22:2632-2638.
64. Flesch FM, Wijnand E, van de Lest CH, Colenbrander B, van Golde LM, Gadella BM. Capacitation dependent activation of tyrosine phosphorylation generates two sperm head plasma membrane proteins with high primary binding affinity for the zona pellucida. Mol Reprod Dev 2001; 60:107-115.
65. van Gestel RA, Brewis IA, Ashton PR, Brouwers JF, Gadella BM. Multiple proteins present in purified porcine sperm apical plasma membranes interact with the zona pellucida of the oocyte. Mol Hum Reprod 2007; 13:445-454.
66. Kongmanas K, Kruevaisayawan H, Saewu A, Sugeng C, Fernandes J, Souda P, Angel JB, Faull KF, Aitken RJ, Whitelegge J, Hardy D, Berger T, et al. Proteomic Characterization of Pig Sperm Anterior Head Plasma Membrane Reveals Roles of Acrosomal Proteins in ZP3 Binding. J Cell Physiol 2015; 230:449-463.
67. Nixon B, Cafe SL, Bromfield EG, De Iuliis GN, Dun MD. Capacitation and Acrosome Reaction: Histochemical Techniques to Determine Acrosome Reaction. In: Majzoub A, Agarwal A, Henkel R (eds.), Manual of Sperm Function Testing in Human Assisted Reproduction. Cambridge: Cambridge University Press; 2021: 81-92.
68. Ellis DJ, Shadan S, James PS, Henderson RM, Edwardson JM, Hutchings A, Jones R. Post-testicular development of a novel membrane substructure within the equatorial segment of ram, bull, boar, and goat spermatozoa as viewed by atomic force microscopy. J Struct Biol 2002; 138:187-198.
69. Jones R, James PS, Oxley D, Coadwell J, Suzuki-Toyota F, Howes EA. The equatorial subsegment in mammalian spermatozoa is enriched in tyrosine phosphorylated proteins. Biol Reprod 2008; 79:421-431.
70. Harayama H, Nishijima K, Murase T, Sakase M, Fukushima M. Relationship of protein tyrosine phosphorylation state with tolerance to frozen storage and the potential to undergo cyclic AMP-dependent hyperactivation in the spermatozoa of Japanese Black bulls. Mol Reprod Dev 2010; 77:910-921.
71. Sheng J, Olrichs NK, Gadella BM, Kaloyanova DV, Helms JB. Regulation of Functional Protein Aggregation by Multiple Factors: Implications for the Amyloidogenic Behavior of the CAP Superfamily Proteins. Int J Mol Sci 2020; 21.
72. Cai Z, Yan LJ. Protein Oxidative Modifications: Beneficial Roles in Disease and Health. J Biochem Pharmacol Res 2013; 1:15-26.
73. Du Plessis SS, Agarwal A, Halabi J, Tvrda E. Contemporary evidence on the physiological role of reactive oxygen species in human sperm function. J Assist Reprod Genet 2015; 32:509-520.
74. Zhang M, Chiozzi RZ, Skerrett-Byrne DA, Veenendaal T, Klumperman J, Heck AJR, Nixon B, Helms JB, Gadella BM, Bromfield EG. High Resolution Proteomic Analysis of Subcellular Fractionated Boar Spermatozoa Provides Comprehensive Insights Into Perinuclear Theca-Residing Proteins. Front Cell Dev Biol 2022; 10:836208.
75. Aizawa M, Fukuda M. Small GTPase Rab2B and Its Specific Binding Protein Golgi-associated Rab2B Interactor-like 4 (GARI-L4) Regulate Golgi Morphology. J Biol Chem 2015; 290:22250-22261.

76. Song WH, Sutovsky P. Porcine Cell-Free System to Study Mammalian Sperm Mitophagy. Methods Mol Biol 2019; 1854:197-207.

Supplementary materials

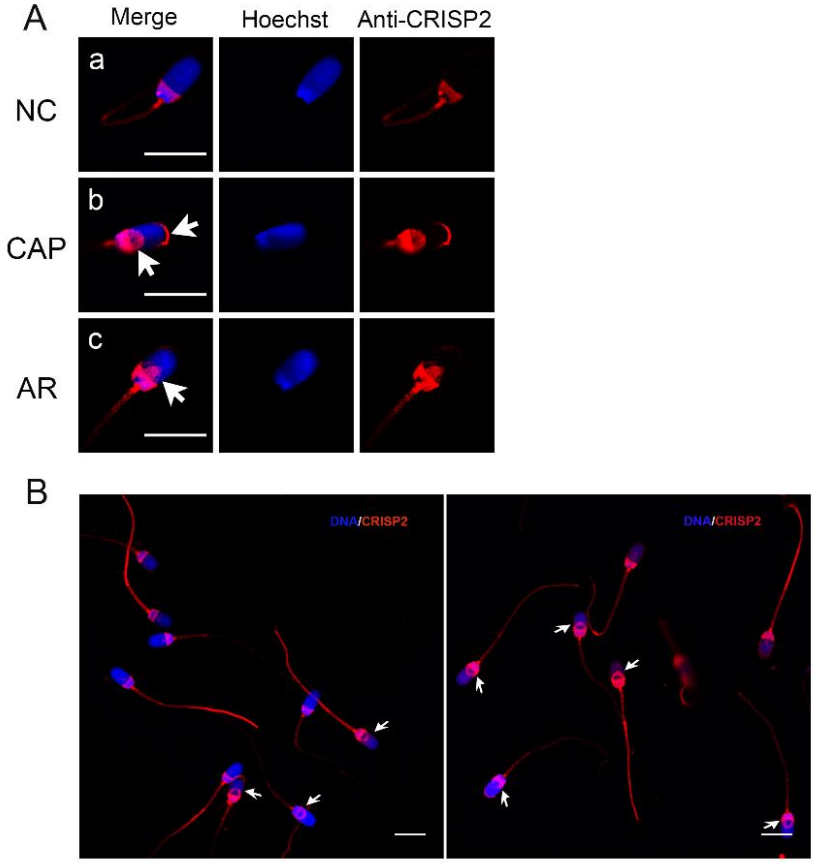

Supplementary figure S1. The distribution of CRISP2 following in vitro capacitation and acrosome reaction. (A) Representative single cell images showed the distribution of CRISP2 following capacitation and acrosome reaction. (a) CRISP2 was present in the post-acrosomal region, the connecting piece and faint signal in the sperm tail of NC sperm. (b) Additional signals of CRISP2 were detected on the apical ridge and the EqS of CAP sperm. (c) CRISP2 immunofluorescence was revealed in the subdomain of EqS (EqSS) of AR sperm. (B) In the case of capacitated sperm, overview on several cells were included to show the exposure of CRISP2 on the apical ridge and the EqS of the sperm head (arrowed). 2~3 ejaculates from different boars were mixed as one biological replicate and this experiment was replicated three times. Scale bar = 10 μm.

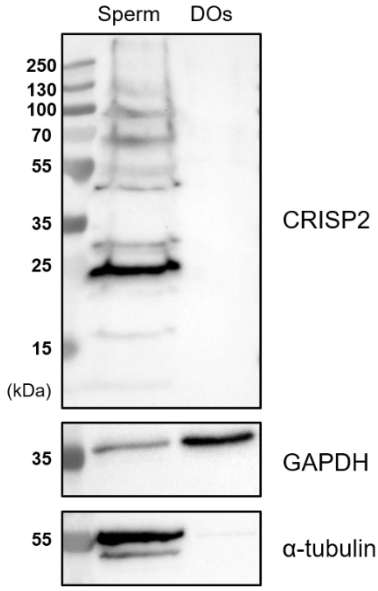

Supplementary figure S2. CRISP2 is not present in the porcine oocyte. After in vitro maturation, porcine oocytes were denuded by removing cumulus cells. Ejaculated sperm cells and denuded oocytes were lysed in 8 M urea as we described before [44]. 5 x10^5 sperm cells per lane, 20~30 oocytes per lane. Immunoblotting analysis of CRISP2 on the lysates from sperm and oocytes probed with anti-CRISP2. Membrane was stripped and re-probed with anti-GAPDH and α-tubulin.

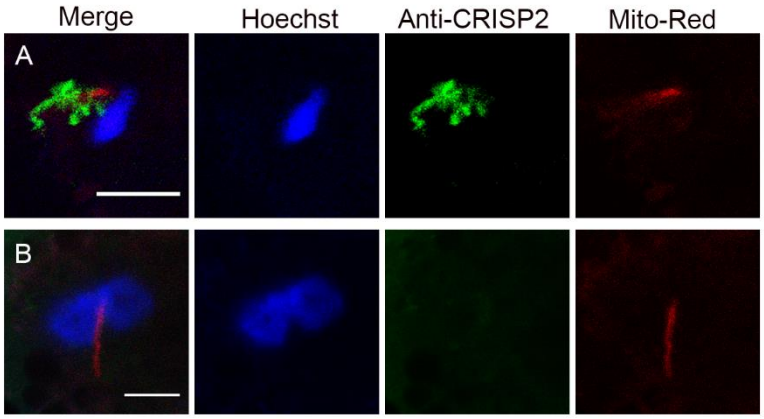

Supplementary figure S3. (A) Another fertilizing sperm was imaged and showed CRISP2 dispersal, while the sperm nucleus was still condensed. (B) An image of zygotes showed that sperm CRISP2 was undetectable in zygotes that were in the two-pronuclear stage, while sperm mitochondria were still linear arranged. Scale bar = 10 μm.

Supplementary file 1&2. Multilayer scanning (z-stack, step size 1 μm) of the zygotes in Figure 5A and 5B, respectively.

Accessible via https://doi.org/10.1093/biolre/ioac169.

Chapter 4

High resolution proteomic analysis of subcellular fractionated boar spermatozoa provides comprehensive insights into perinuclear theca-residing proteins

Min Zhang[1], Riccardo Zenezini Chiozzi[2,3], David A Skerrett-Byrne[4], Tineke Veenendaal[5], Judith Klumperman[5], Albert JR Heck[2,3], Brett Nixon[4], J Bernd Helms[1], Bart M Gadella[1]*, Elizabeth G Bromfield[1,4]

[1] Department of Biomolecular Health Sciences and Department of Farm and Animal Health, Faculty of Veterinary Medicine, Utrecht University, The Netherlands
[2] Biomolecular Mass Spectrometry and Proteomics, Bijvoet Centre for Biomolecular Research and Utrecht Institute for Pharmaceutical Sciences, Utrecht University, The Netherlands
[3] Netherlands Proteomics Centre, Utrecht, Netherlands[4] Structural Biochemistry, Bijvoet Centre for Biomolecular Research, Utrecht University, The Netherlands
[4] Priority Research Centre for Reproductive Science, School of Environmental and Life Sciences, Discipline of Biological Sciences, University of Newcastle, Callaghan, NSW, Australia
[5] Section Cell Biology, Center for Molecular Medicine, University Medical Center Utrecht, Utrecht University, The Netherlands

Published as:
Zhang M, Chiozzi RZ, Skerrett-Byrne DA, Veenendaal T, Klumperman J, Heck AJR, Nixon B, Helms JB, Gadella BM, Bromfield EG. High Resolution Proteomic Analysis of Subcellular Fractionated Boar Spermatozoa Provides Comprehensive Insights Into Perinuclear Theca-Residing Proteins. Front Cell Dev Biol. 2022 Feb 18;10:836208.

Abstract

The perinuclear theca (PT) is a highly condensed, largely insoluble protein structure that surrounds the nucleus of eutherian spermatozoa. Recent reports have indicated that the PT unexpectedly houses several somatic proteins, such as core histones, which may be important post-fertilization during re-modelling of the male pronucleus, yet little is known regarding the overall proteomic composition of the PT. Here, we report the first in depth, label-free proteomic characterization of the PT of boar spermatozoa following the implementation of a long-established subcellular fractionation protocol designed to increase the detection of low abundance proteins. A total of 1802 proteins were identified, a result that represents unparalleled depth of coverage for the boar sperm proteome and exceeds the entire annotated proteome of the *Sus scrofa* species so far. In the PT structure itself, we identified 813 proteins and confirmed the presence of previously characterized PT proteins including the core histones H2A, H2B, H3 and H4, as well as Ras-related protein Rab-2A (RAB2A) and Rab-2B (RAB2B) amongst other RAB proteins. In addition to these previously characterized PT proteins, our data revealed that the PT is replete in proteins critical for sperm-egg fusion and egg activation, including: Izumo family members 1-4 (IZUMO1-4) and phosphoinositide phospholipase C (PLCZ1). Through Ingenuity Pathway Analysis, we found surprising enrichment of endoplasmic reticulum (ER) proteins and the ER-stress response in the PT. This is particularly intriguing as it is currently held that the ER structure is lost during testicular sperm maturation. Using the String and Cytoscape tools to visualize protein-protein interactions revealed an intricate network of PT protein complexes, including numerous proteasome subunits. Collectively, these data suggest that the PT may be a unique site of cellular homeostasis that houses an abundance of protein degradation machinery. This fits with previous observations that the PT structure dissociates first within the oocyte post-fertilization. It remains to be explored whether proteasome subunits within the PT actively assist in the protein degradation

of paternal cell structures post-fertilization and how aberrations in PT protein content may delay embryonic development.

Keywords: fertilization; perinuclear theca; proteomics; sperm function; spermatozoa.

Introduction

The perinuclear theca (PT) is a unique, highly condensed, cytoskeletal structure that surrounds the nucleus of mature mammalian sperm cells. This structure is non-ionic detergent-resistant and, in most eutherian species, consists of three sub-domains termed the sub-acrosomal layer (SAL), the equatorial segment (ES) and post-acrosomal sheath (PAS) [1]. Originally the PT was thought to provide structural support to the nucleus during the long transit of sperm cells through the male and female reproductive tracts. More recently, the observations that the PAS-PT of the sperm cell is the first internal structure to become exposed in the ooplasm during fertilization has resulted in the PT receiving considerable attention for its potential roles in sperm-egg interaction [2, 3] and early events post-fertilization [4-6]. Crucially, in some species the PAS-PT has been proposed to harbor the sperm-oocyte activation factor(s) that are released post-fertilization in the ooplasm and are then responsible, at least in part, for triggering Ca^{2+} oscillations within the oocyte [2, 3].

While the identity of these egg activation factors has been long contested, current evidence appears to rest with the activity of two potential candidates; phospholipase C zeta (PLCζ) [7] and post-acrosomal WW domain-binding protein (PAWP, also known as WBP2NL) [4, 8]. Both PLCζ and PAWP have been found to reside within the PT in some species, generating the hypothesis that the PT may be enriched in proteins important for fertilization [1, 9]. Moreover, experiments conducted to determine the precise region of the sperm cell capable of activating the oocyte have revealed that when all membranes are removed using Triton X-100, leaving the PT, the sperm cell still retains the capacity for oocyte activation [10]. Finally, in the context of male infertility, patients with globozoospermia with an absence of the PAS-PT were infertile due to an inability to activate the oocyte [11]. This provides critical evidence for the importance of PT-resident proteins in ensuring successful fertilization.

Despite knowledge that the PT is essential for fertilization and that the proteins residing within this structure likely contribute to oocyte activation, a comprehensive proteomic investigation of the PT to understand its full contribution to these processes has yet to be performed. This is likely due to previous limitations in isolating PT proteins and the relatively slow uptake of proteomic technologies to investigate reproductive cells. However, even prior to the widespread use of mass spectrometry to characterize sperm proteins, pioneering work by Oko and Sutovsky and their respective colleagues revealed that the PT houses an unexpected array of proteins including somatic (core) histones [12] that appear to be de novo-synthesized during the round spermatid stage of development and are then assembled during spermatid elongation [13]. Remarkably, these histones then appear to play an important role post-fertilization as intra-cytoplasmic sperm injection (ICSI) of sperm cells depleted of PT-histones resulted in a delay in embryonic development [13]. Similarly, the PT-residing protein glutathione S-transferase omega 2 (GSTO2) has recently been shown to accelerate nuclear decondensation of sperm cells during fertilization [6], implying that multiple PT-enriched proteins may contribute to functions in the zygote.

Given the importance of the PT for fertilization, and our own recent characterization of the PT-residing protein cysteine rich secretory protein 2 (CRISP2) and its role in protein scaffolding in the sperm cell [14], we elected to conduct a comprehensive proteomic analysis of the isolated PT using a quantitative, label-free liquid chromatography mass spectrometry (LC-MS/MS) approach. This approach was able to be applied to PT proteins through the development of highly reproducible methods by the Sutovsky and Oko groups for isolating the PT and its proteins from the sperm head that have been published and used extensively [4, 12, 15, 16]. The

purpose of this mass spectrometry based-exploration of the PT was to provide a full inventory of PT-residing (proteins present in the PT but also present in other cell compartments) and PT-enriched (proteins with significantly higher abundance in the PT than other compartments) proteins in sperm cells that can be used as a resource for the sperm-egg activation and fusion fields to help shed light on the role of PT proteins during and post-fertilization. Moreover, given the extensive protein crosslinking by intra and inter protein disulfide bridge formation that takes place within the PT structure to ensure its condensed nature prior to egg interaction, we sought to construct a network of PT-enriched proteins that can be further probed to understand protein-protein interactions that take place within the PT. This work was conducted in boar spermatozoa due to the well-characterized nature of the PT in this species, our own work related to CRISP2 in the boar and due to the genetic and physiological relevance of pig reproductive processes to those of humans [17, 18].

Experimental procedures

Preparation of boar spermatozoa

Semen was collected from three mature and highly fertile boars. The collected semen was diluted to 20 million sperm/mL in a commercial diluent, packed in insemination tubes of 80 mL and transported at 17°C to Utrecht University by a courier from a commercial breeder (Cooperative Center for Artificial Insemination in Pigs, Veghel, the Netherlands). Semen samples were used within 12 h. Sperm cells were washed through discontinuous Percoll (GE Healthcare, Piscataway, NJ, USA) gradients as previously described [14].

Subcellular fractionation of boar sperm into head, tail and perinuclear theca components

To separate the sperm heads and tails, Percoll washed sperm cells ($1x10^8$) were resuspended in 1.5 mL PBS with 1 mM phenylmethylsulfonyl fluoride (PMSF) and sonicated on ice at nine microns using an MSE Ltd Soniprep 150 sonicator (East Sussex, UK) at 15-s bursts with 45-s interval for 3 cycles until >99% of all sperm heads were detached from tails. Sonicated sperm

cells were loaded on a 62% (w/v) sucrose gradient to isolate the sperm heads and tails as previously described [14]. Isolation of perinuclear theca (PT) proteins was performed via methods originally described by Oko and Maravei,1994 [19] and described in full in Zhang et al., 2021[14] (for schematic see Figure 1). Briefly, purified sperm heads underwent continuous extraction steps in 0.2% (v/v) Triton X-100 and 1 M KCl for 1 h at RT with agitation. Following this incubation, the resulting pellets were washed twice before the next extraction and/or fixed in 4% paraformaldehyde (PFA) for immunodetection. The PT proteins were obtained by incubating the resulting pellets in 0.1 M NaOH overnight at 4°C with agitation. The sperm heads, tails and PT fractions were used directly or frozen at -80°C for later analysis.

Sodium dodecyl sulfate–polyacrylamide gel electrophoresis (SDS-PAGE) and immunoblotting

PT fractions and the resulting pellets were denatured in 4 x SDS sample buffer (200 mM Tris-HCl, pH 6.8, 10% β-mercapto-ethanol, 8% SDS, 0.08% bromophenol blue, 40% glycerol) by boiling for 10 min. Samples were centrifuged at 14,000 x g for 2 min, at RT and loaded on to SDS-PAGE gels (5% stacking gel, 12% resolving gel) and were blotted onto 0.2 μm nitrocellulose membranes (GE Healthcare, Piscataway, NJ, USA) at 100V for 1 h. After blocking for 3 h at RT in 5% (w/v) BSA in PBS with 0.05% (v/v) Tween-20 (PBST), membranes were incubated with primary antibodies (Table S1) overnight at 4°C. After three washes in PBST for 15 min, membranes were incubated with horse radish peroxidase (HRP) conjugated secondary antibodies (Supplementary Table S1) for 1 h at RT. After rinsing four times in PBST for 20 min, membranes were developed using a chemiluminescence ECL-detection kit (Supersignal West Pico, Pierce, Rockford IL, USA). The molecular weight of proteins of interest were established using a PageRule Plus pre-stained protein ladder, 10 to 250 kDa (Thermo Scientific).

Immunofluorescence analysis

Whole sperm cells and sperm heads were fixed in 4% PFA for 15 min at RT and permeabilized using 0.5% (v/v) Triton X-100 for 15 min, at RT. For acrosin staining, sperm cells were fixed and permeabilized in -20°C methanol for 5 min, mixed with PBS and deposited on slides. After rinsing with PBS, slides were blocked with 1% (w/v) BSA in PBS for 1 h at RT, incubated overnight at 4°C with primary antibodies. Slides were washed again before incubation for 1 h at RT with secondary antibodies or 20 min with peanut agglutinin lectin (PNA) (Supplementary Table S1) and a Hoechst 33342 counterstain added for 10 min, at RT (1 µg/mL, Sigma). After extensive washing with PBS, slides were mounted with FluorSave reagent (Merck Millipore) and covered with coverslips. For all negative controls the primary antibody was omitted. Images were taken on a Leica SPE-II confocal microscope using a 63x objective (NA 1.3, HCX PLANAPO oil) and images were analyzed using Image J software (bundled with 64-bit Java 1.8.0_172, National Institutes of Health, Bethesda, MD, USA).

Immunogold labelling

Percoll washed whole sperm cells were resuspended in PBS, mixed with an equal volume of 4% PFA and fixed for 5 min at RT. The fixative was removed by centrifugation at 750 x g, for 5 min at RT. Fresh 4% PFA was added and cells were then fixed overnight. This 4% PFA was then replaced with 1% PFA and sperm cells were kept at 4°C. Further processing of samples for ultrathin cryo-sectioning and immunolabelling was performed according to the protein A-gold method as described previously [20]. Briefly, fixed cells were washed with 0.05 M glycine in PBS, resuspended and then pelleted in 12% gelatin in PBS at 37°C. The sperm pellet was solidified on ice and cut into small blocks. For cryoprotection, blocks were infiltrated overnight with 2.3 M sucrose at 4°C. The blocks were mounted on aluminum pins and frozen in liquid nitrogen. To pick up the ultrathin cryosections (60 nm), a 1:1 mixture of 2.3 M sucrose and 1.8% methylcellulose was used. RAB2B and PAWP were detected by 10 nm protein A coupled gold particles (Cell Microscopy Core, UMC Utrecht, the Netherlands) and stained with 2%

uranyl acetate oxalate and 0.4% uranyl acetate in methylcellulose to increase contrast. EM imaging was performed using a JEOL 1011 microscopy.

Sample preparation for mass spectrometry

Three biological replicates for sperm heads, tails and PT fractions were lysed following the protocol described by Leung et al., 2021 [21] for intact sperm cells. The lysis buffer contained 100 mM Tris-HCl pH 8.5, 7 M Urea, 1% Triton X-100, 5 mM tris-2(-carboxyethyl)-phosphine (TCEP), 30 mM chloroacetamide (CAA), 10 U/ml DNase I, 1 mM MgCl2, 1% benzonase (Merck Millipore, Darmstadt, Germany), 1 mM sodium orthovanadate, phosphoSTOP phosphatases inhibitors and Complete Mini EDTA-free protease inhibitors. Samples were sonicated on ice for 2 min using an ultrasonic processor (UP100H, Hielscher) at 80% amplitude. The proteins were then precipitated with chloroform/methanol and the dried protein pellet resuspended in digestion buffer (100 mM Tris-HCl pH 8.5, 1% sodium deoxycholate (Sigma-Aldrich), 5 mM TCEP, and 30 mM CAA). Trypsin and Lys-C proteases were added to a 1:25 and 1:100 ratio (w/w) respectively and protein digestion performed overnight at 37°C. The final peptide mixtures were desalted with solid-phase extraction C18 columns (Sep-Pak, Waters).

Liquid chromatography/mass spectrometry

1000 ng of peptides from each biological replicate were first injected onto an Agilent 1290 Infinity UHPLC system on a 50-cm analytical column packed with C18 beads (Agilent Poroshell EC-C18, 2.7 μm, 50 cm × 75 μm) coupled online to an Orbitrap HF (Thermo Fisher Scientific). The LC-MS settings were used as in the article of Hidalgo-Gutiérrez et al.,2021 [22] with minor modifications. After 5 min of loading with 100% buffer A (H_2O with 0.1% formic acid), peptides were eluted at 300 nL/min with a 95-min gradient from 10% to 40% of buffer B (80% acetonitrile and 20% H_2O with 0.1% formic acid). For MS acquisition, we used an MS1 Orbitrap scan at 120,000 resolution, automatic gain control (AGC) target of 3×10^6 ions and maximum inject time of 120 ms from 310 to 1600 m/z; the 15 most intense ions were submitted

to MS2 Orbitrap scan at 30,000 resolution, AGC target of 1×10^5 ions and maximum inject time of 54 ms (isolation window of 1.4 m/z, NCE at 28% and dynamic exclusion of 16 s). The proteomic approach undertaken in this manuscript is presented visually in Figure 1.

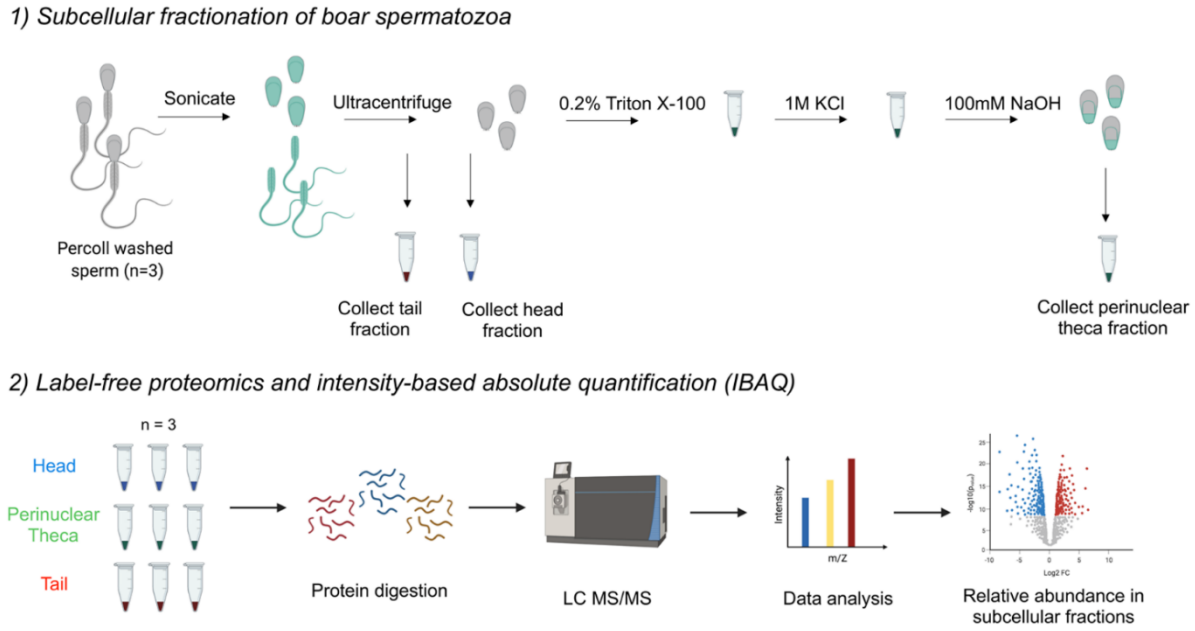

Figure 1. Workflow diagram for the isolation of the perinuclear theca (PT) and application of mass spectrometry-based proteomics to boar spermatozoa. (1) The separation of sperm heads and tails was performed first through sonication and second, through ultracentrifugation on a 62% sucrose gradient. To isolate the PT structures, boar sperm heads were then subjected to successive extraction steps using 0.2% Triton X100 and 1 M KCl for 1 h each with agitation. The resulting pellets were washed and then incubated in 0.1 M NaOH overnight. The 0.2% Triton X100 solubilizes proteins associated with the inner acrosomal membrane, 1 M KCl releases ionically attached PT proteins and the final 0.1 M NaOH extracts covalently bound PT proteins [23]. (2) Once three biological replicates of head, tail and PT material was collected, cell samples were lysed and proteins were digested. Peptides were injected onto an ultra-high-performance liquid chromatography (LC) system coupled to an Orbitrap HF mass spectrometer (MS). Data analysis was performed in MaxQuant to calculate intensity-based absolute quantification (iBAQ) values, and further analysis was conducted using the platforms: Perseus, Ingenuity Pathway Analysis (IPA), String and Cytoscape.

Proteomic data processing and analysis

The raw files were analyzed with MaxQuant (version 1.6.17) with all the default settings adding deamidation (NQ) as dynamic modification against the *Sus scrofa* reference proteome (UniProt

version of 08/2020 with 49,795 entries) adding common contaminants. MaxQuant was used with the standard parameters adding only the "iBAQ Quantification" and "Match between runs" with automatic values. The protein quantification generated from MaxQuant without "reverse" and "potential contaminants" were analyzed using Perseus (version 1.6.8.0) [24]. Only proteins with a quantitative value in all three replicates within at least one group, and ≥1 razor plus unique peptides were kept for further analysis. Log transformation and data normalization steps were performed using Perseus. Fold changes and significance calculations between the three sample groups 'head', 'tail', and 'perinuclear theca', were also generated in Perseus for the production of volcano plots, principal component analyses and heat maps. These data were exported from Perseus and plotted using GraphPad Prism (version 8.4.1). Using OmicsBox (version 1.3.11, BioBam Bioinformatics, Valencia, Spain), human homologues for each boar protein were mapped as described previously [25]. For the analysis of pathways enriched in each sample group, Ingenuity Pathway Analysis software (Qiagen) was applied to the refined human homolog proteomic lists, as described in Skerrett-Byrne et al., 2021 [26, 27]. Canonical pathway and disease and function analyses were generated and ranked by Z-score enrichment with a significance cut off of ≥ 2 for activation and ≤ -2 for inhibition. Enriched protein networks were generated using String version 11.5 [28] and modified in Cytoscape (version 3.8.2). These networks were prepared from refined protein lists for each sample group featuring all proteins significantly enriched in each subcellular fraction (p value ≤ 0.05; fold change ≥ 2) and those featuring uniquely in each subcellular fraction.

Results

Isolation of the sperm perinuclear theca and assessment of head and tail separation

To perform a definitive proteomic characterization of the perinuclear theca structure of the boar spermatozoa, an established method developed by Oko and Maravei was used to isolate the highly dense PT structures from sperm heads [19]. This method has been used extensively to

characterize individual proteins residing within the PT [14-16, 29, 30]. To simultaneously provide a proteomic characterization of the sperm head and tail for comparative purposes, the heads and tails of the cells were separated as described previously [14]. Although phase-contrast microscopy revealed populations of morphologically intact sperm heads and tails (see Chapter 2 for images of this separation), as this fractionation process features sonication steps, the membrane integrity of the isolated sperm heads was systematically assessed prior to their use for proteomics. This analysis was performed using peanut agglutinin lectin (PNA) and acrosin antibodies to investigate acrosomal status. PNA is a well characterized marker of the outer acrosomal membrane [31] and acrosin localizes to the acrosome matrix and inner acrosome membrane of boar sperm, respectively [32, 33]. Compared to whole spermatozoa (non-sonicated sperm cells; WS), there was a visible loss of PNA signal in the sonicated sperm heads, as well as a loss or disruption to the acrosin localization (Figure 2A and B). This indicated that there is likely to be a disruption to the outer acrosomal membrane and potentially to the acrosomal matrix due to the head isolation protocol. In summary, these data indicated some exterior membrane damage to the sperm heads and tails following the separation procedure. For this reason, the proteomic characterization of the head and tail fractions in this manuscript should be used primarily for comparative purposes to differentiate the proteins that are enriched in the PT structure. This is unlikely to be a physiological inventory of all proteins contained within the boar sperm head and tail as membrane protein detection may have been impeded by the requisite cell preparation method.

Proteomic characterization of boar sperm subcellular fractions

Proteomic characterization of the isolated head and tail components of boar spermatozoa revealed a total of 1,419, and 1,514 proteins identified in sperm heads and tails, respectively (Figure 3A). Notwithstanding any disruption to membrane proteins due to the cell separation methods, these data represent an unparalleled depth of coverage for the boar sperm proteome

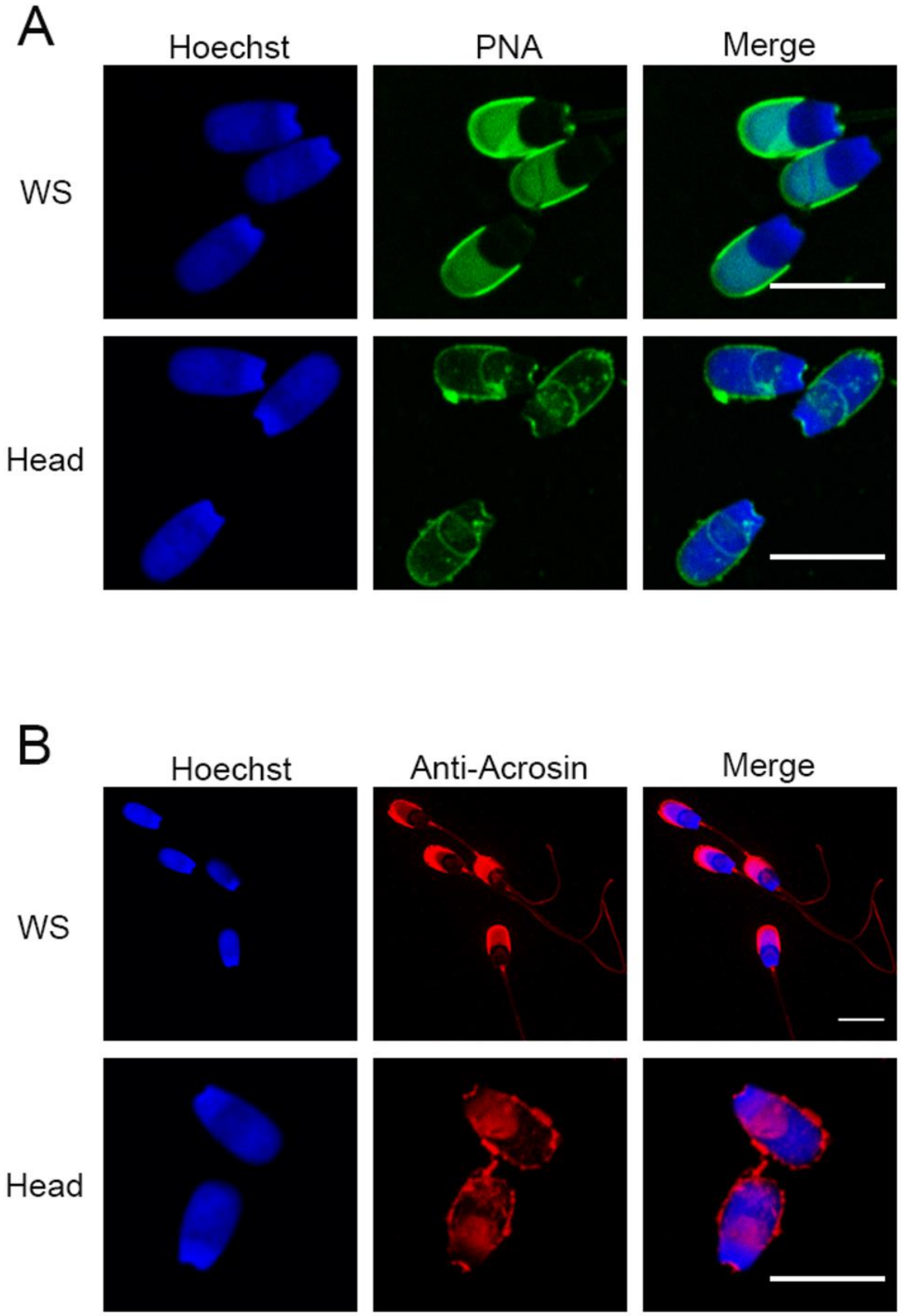

Figure 2. Assessment of sperm head and tail separation using immunofluorescence. (A) Immunofluorescence staining of peanut agglutinin lectin (PNA) in whole sperm cells (WS) and

fractionated sperm heads. (B) Immunofluorescence staining of acrosin in WS and fractionated sperm heads. Scale bar = 10 μm.

with an identification of 1,802 proteins in total (Supplementary File 1). Notably, the entire proteome of *Sus scrofa* currently consists of just 1,438 reviewed proteins. Within the minute structure of the PT itself we identified 813 proteins of which only 10% feature in the reference proteome for *Sus scrofa* and carry a reviewed protein status in UniProt (Figure 3A). This implies that many of the proteins contained within this cellular compartment may be cell-type specific and are not well characterized. Intriguingly, our analysis indicated that the PT structure encompasses 57% of all the proteins detected within the whole boar sperm head. This reveals the extent of protein compartmentalization that takes place within spermatozoa during the final phases of spermiogenesis in elongating spermatids when the PT structure is formed [34].

Despite the highly compartmentalized morphology of the sperm cell, our analysis revealed that a total of 1,150 proteins were shared between the head and tail, accounting for 81% of head proteins and 76% of tail proteins (Figure 3B). Thus, a total of 147 proteins were identified that were unique to the head and 336 proteins that were unique in the tail (Figure 3B, Supplementary File 1). While we expected that all PT proteins would also be accounted for in the sperm head fraction (as this fraction will contain the PT in situ), 47 proteins were identified in the PT that were not found to be present in all three replicates of the head samples. This may be due to the isolation protocol for the PT facilitating the identification of less abundant proteins that are often difficult to detect in whole sperm or in sperm heads. This phenomenon has been described previously during a subcellular proteomic study of isolated human sperm nuclei where more than half of the identified proteins had not been detected in any previous whole sperm cell proteomic analysis [31]. To assess the reproducibility of the replicates and the extent of differentiation between the subcellular compartments, a principal component analysis (PCA)

A

Sample	# Proteins		
	Total IDs	Unique IDs/ compartment	Reviewed/ unreviewed in UniProt
Head	1419	147	108/1311
Tail	1514	336	114/1400
Perinuclear theca	813	19	82/731

B

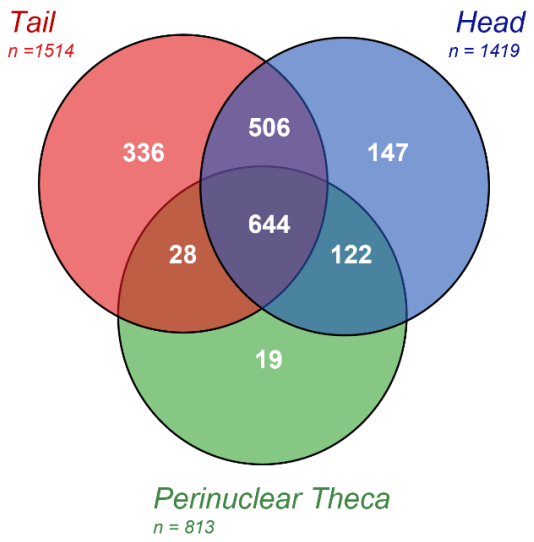

C

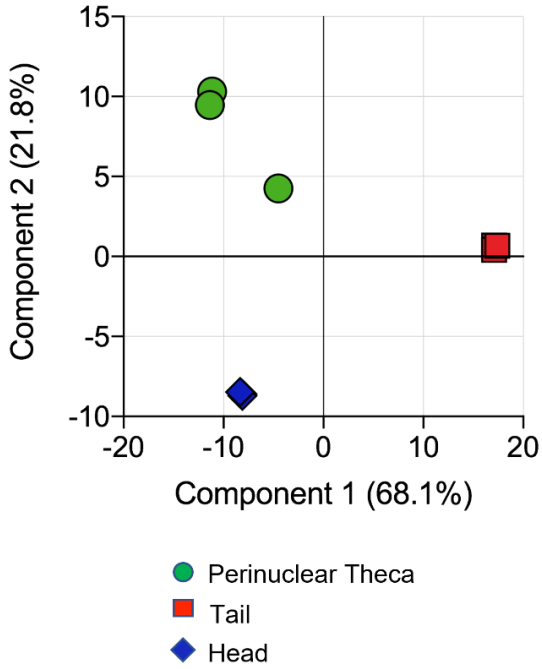

Figure 3. Characterization and comparison of boar sperm head, tail and PT protein compositions. (A) Following the restriction of each proteomic list based on the presence of each protein in all three replicates and strict quality control cutoffs, analysis of the head, tail and PT proteomes revealed 1419, 1514, and 813 proteins, respectively. Due to the limited annotation of the Sus scrofa proteome, a majority of the proteins featured in each sperm compartment held an 'unreviewed' status within the UniProt database. (B) Proteins detected in each cell compartment were compared using a Venn diagram and principal component analysis (C) revealing the close clustering of biological replicates.

was conducted (Figure 3C). Although one PT replicate was found to vary marginally from the other two, the PCA confirmed the high degree of similarity between the three biological replicates analyzed for each sample group. This analysis also demonstrated the clear disparity between the proteomic constituents of the head, tail and PT compartments. Fittingly, samples

from the head and PT were more closely associated than those of the head and tail or PT and tail, with component one accounting for 68.1% of the total variance between the samples.

Composition of the perinuclear theca proteome and validation

Within our PT proteome we identified well-known PT proteins that have been previously used to characterize this structure in other laboratories. These included: glutathione-S-transferase omega 2 (GSTO2); post-acrosomal sheath WW domain-binding protein (PAWP); several somatic histones including H2A, H2B, H3 and H4; as well as Ras-related protein Rab-2A and Ras-related protein Rab-2B (RAB2A; RAB2B). To further validate these data, we performed immunolocalization, immunoblotting and immuno-gold labelling experiments to confirm the presence of PAWP and RAB2B within the PT of boar spermatozoa. Immunolabelling of PAWP in whole sperm cells revealed a bright signal in the connecting piece with additional labelling in the post acrosomal region and sperm tail (Figure 4A). Immunolabelling in sperm heads after successive treatments with 0.2% Triton X-100, 1 M KCl and 0.1 M NaOH (as described in Figure 1) revealed that PAWP immunofluorescence was retained in the post acrosomal region and the equatorial segment of sperm heads after 0.2% Triton X-100 and 1 M KCl extraction. However, barely any PAWP signal was observed after 0.1 M NaOH treatment (Figure 4A). The additional foci of PAWP labeling on the equatorial segment of the sperm heads that was not present in the whole sperm cell staining is likely due to 0.2% Triton X-100 treatment before fixation exposing the epitope of this antigen. Immunoblotting analysis of PAWP under the same conditions revealed that PAWP was resistant to 0.2% Triton X-100 and 1 M KCl extraction. However, the majority of PAWP was recovered in 0.1 M NaOH extraction and a small residual amount of the protein was not solubilized and associated with the pellet; representing the sperm nuclear fraction (Figure 4B). Immunogold labeling of PAWP on ultrathin sections confirmed that PAWP was localized to the perinuclear theca between the plasma membrane and the nuclear envelope as well as in the connecting piece (Figure 5 A and B). Taken together, these

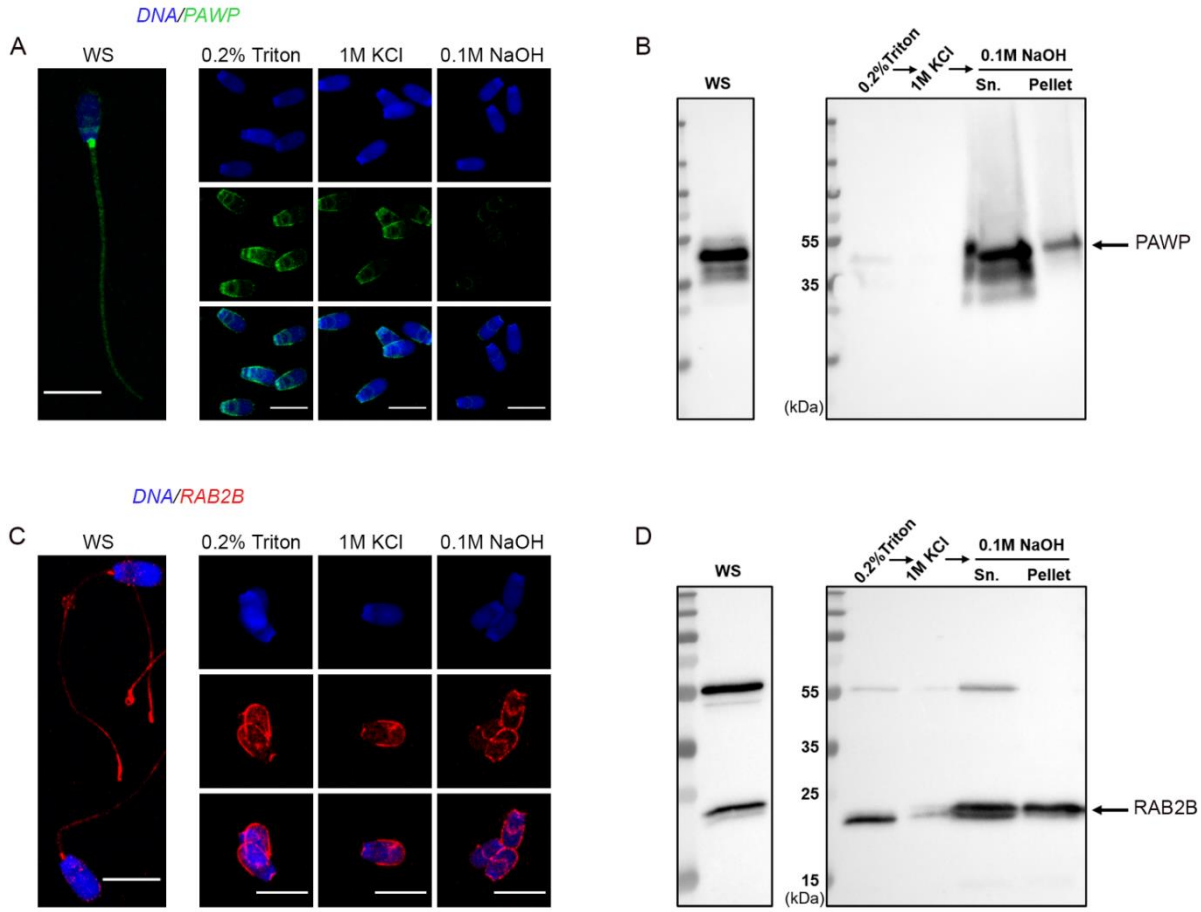

Figure 4. Validation of the presence of PAWP and RAB2B in the boar sperm PT. WS and sperm heads captured from each stage of the PT extraction protocol were examined through immunocytochemistry with antibodies to PAWP (A) and RAB2B (C). Scale bar = 10 µm. Immunoblotting analysis of PAWP and RAB2B after the successive extractions and the resulting pellets (pellet) probed with anti-PAWP (B) and anti-RAB2B (D) antibodies.

data confirm that PAWP is a specific PT residing protein in the boar. Immunostaining of RAB2B in whole sperm cells revealed a bright signal in the connecting piece and the tail of the sperm, but a weak signal in the sperm head (Figure 4C). However, immunostaining in sperm heads after successive treatments with 0.2% Triton X-100, 1 M KCl and 0.1 M NaOH revealed a stable and bright signal for RAB2B surrounding the sperm nucleus (Figure 4C). Additionally, immunoblotting analysis was used to evaluate the solubility of RAB2B from the sperm head. It was observed that besides the expected ~23 kDa protein, an additional ~55 kDa band was also

detected in the whole sperm cells (Figure 4D). Immunoblotting for the successive treatments revealed that RAB2B was partially solubilized by 0.2% Triton X-100 and very small amount was also detected through 1 M KCl extraction (Figure 4D). The 0.1 M NaOH treatment extracted a moderate amount of RAB2B with some still associated with the sperm nucleus(Figure 4D; pellet). It was observed that the relative ratio between the ~55 kDa and the ~23 kDa bands was altered between whole sperm cells to sperm heads indicating that the ~55 kDa was likely associated with the sperm tail (Figure 4D). This is fitting with the immunostaining of RAB2B in the whole sperm cells where strong RAB2B labeling was observed in the sperm tail (Figure 4C). Immunogold labelling of RAB2B on ultrathin cryo-coupes revealed that RAB2B was localized to and between the inner acrosomal membrane and the nuclear envelope indicating that RAB2B was residing in the sub-acrosomal layer of the perinuclear theca (Figure 5C). RAB2B also showed intensive labelling in the sperm nucleus as well as in the outer dense fibers (Figure 5C and D).

In addition to the previously characterized PT proteins validated above, our analysis revealed an extensive inventory of proteins known to be important for successful sperm-egg recognition and fertilization that reside within the PT structure (Supplementary File 1). Moreover, network analysis revealed that a subset of these fertilization-related proteins has the potential to interact within the PT (Figure 6A). This putative protein network included: Izumo sperm-egg fusion proteins 1-4 (IZUMO1-4), phosphoinositide phospholipase C (PLCZ1), cysteine-rich secretory protein 2 (CRISP2), testis-specific serine/threonine-protein kinase 6 (TSSK6) and several other related proteins (see Figure 6A). The detection of these fertilization-related proteins within the PT is congruous with the previously identified role for the PT structure in the process of sperm-egg interaction. Notably, we have recently confirmed that CRISP2 is indeed present within the

PT of boar spermatozoa and may play a role in protein scaffolding/ protein complex formation at this site [14].

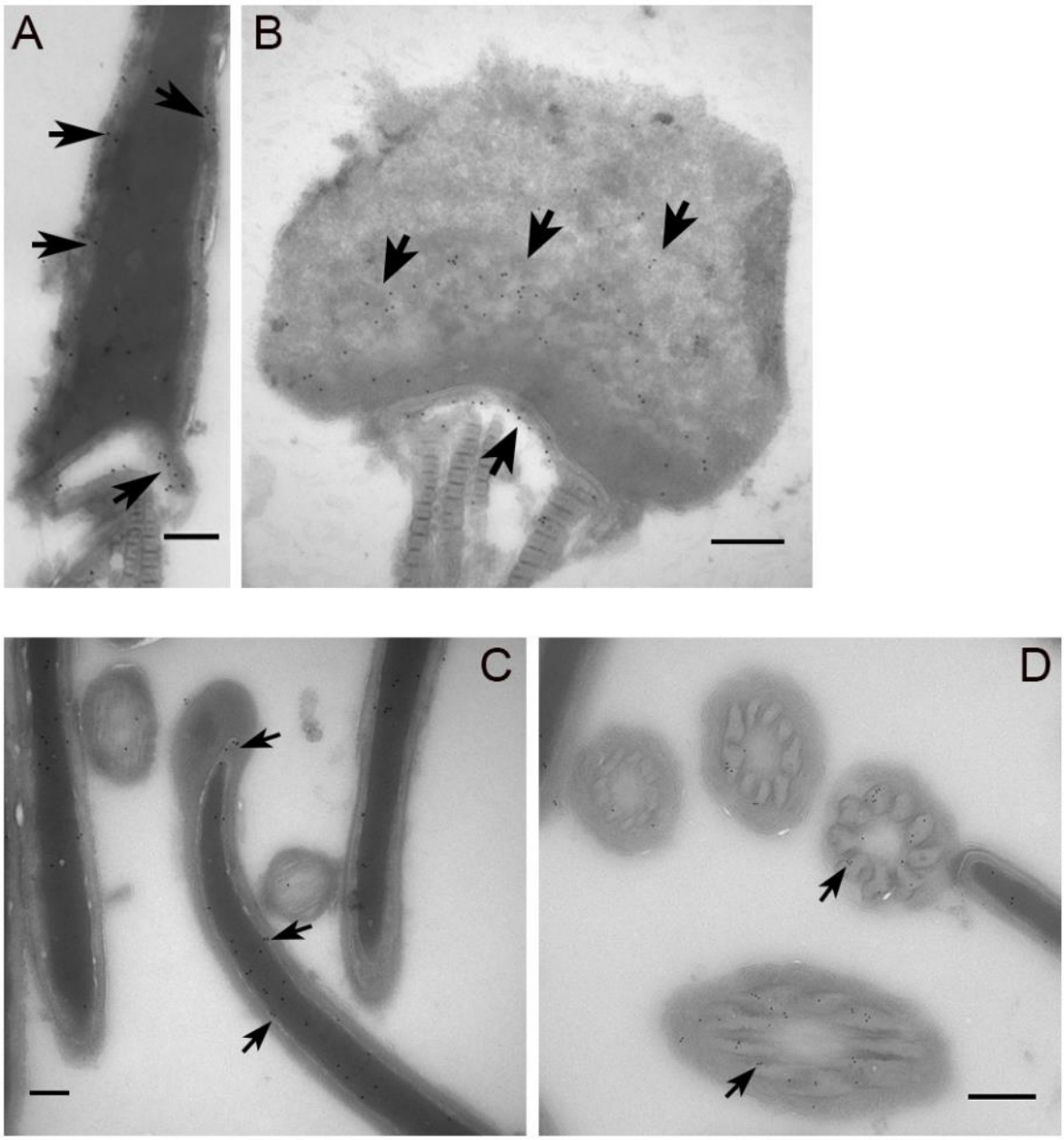

Figure 5. Ultrastructural localization of PAWP and RAB2B in boar spermatozoa. Immunogold labelling of PAWP on sagittal sections (A) and oblique sections through the post acrosomal sheath (PAS) region and (B) through a whole sperm head showing that PAWP localized to the PAS-PT and the connecting piece (arrow). (C) Immunogold labelling of RAB2B on sagittal section through a whole sperm head showing RAB2B localized to the sub-acrosomal layer and the sperm nucleus. (D) Immunogold labelling of RAB2B on cross sections of the sperm tail showing RAB2B localized to the outer dense fibers. Scale bar = 200 nm.

Additional characterization of the PT proteome using Ingenuity Pathway Analysis (IPA) software (Qiagen), revealed an increased enrichment for key fertilization-related functions in the PT compared to the sperm head proteome. These included the functions: 'binding of zona pellucida' and 'binding of sperm' (Figure 6B in which a -log10 *p*-value ≥ 1.3 indicates significance). Intriguingly, the PT proteome also supported several functions related to cellular homeostasis including 'metabolism and production of reactive oxygen species', 'autophagy', 'ion and potassium homeostasis', 'fatty acid metabolism', 'amyloidosis' and 'endoplasmic reticulum (ER) stress response in cells'. Moreover, several diseases linked to protein folding and ER stress were also found to be preferentially related to the PT proteome compared to that of the head. These diseases include 'Huntington disease' and 'Alzheimer disease' (Figure 6B) as well as related diseases such as chorea and cataract formation (data not shown) that are all underpinned by protein aggregation/misfolding and cellular stress. In keeping with this ER-like functional enrichment within the PT proteome, the well characterized ER-resident proteins calreticulin (CALR), calnexin (CANX), protein disulfide-isomerase A3 (PDIA3/ERp57) were all found to be present in the PT. For a full list of proteins detected within the isolated PT see Supplementary File 1.

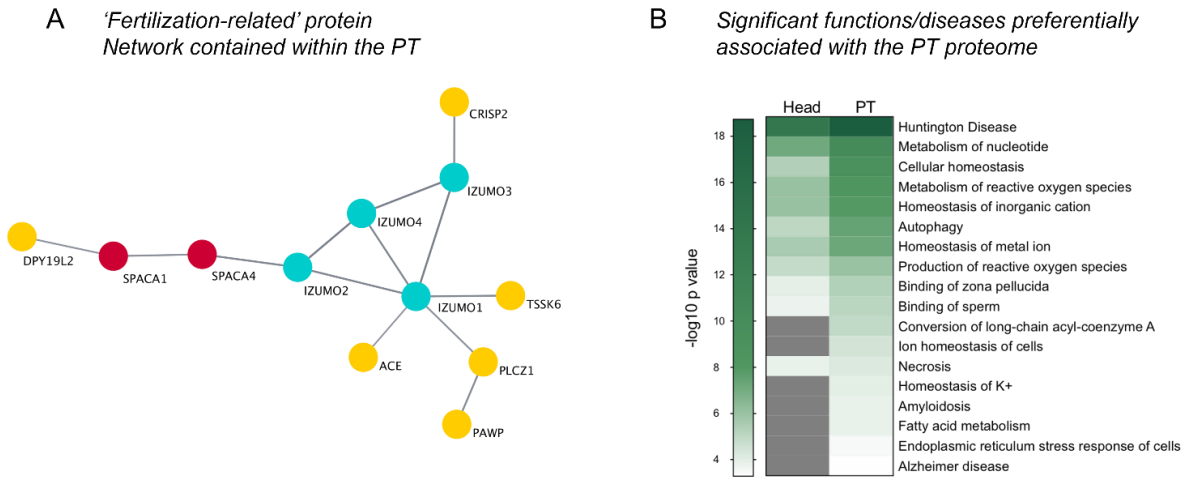

Figure 6. Visualization of fertilization-related proteins and functional pathway analysis. Within the whole PT proteome, a distinct protein cluster comprising key proteins involved in fertilization was detected through String protein network analysis and visualized using Cytoscape (A). (B) Ingenuity

Pathway Analysis software revealed the key diseases and functions enriched within the PT compared to the sperm head (–log10 p-value ≥ 1.3; p-value ≤ 0.05), featuring diseases with a basis in protein misfolding and functions related to the endoplasmic reticulum stress response, cellular homeostasis and fertilization, including 'Binding of sperm' and 'Binding of zona pellucida'. Grey indicates no significant value.

Significantly enriched proteins and pathways in the perinuclear theca compared to the head and tail

While the analyses conducted above yielded intriguing insight into the functions of the PT proteome, many of the proteins contained within the PT were also found to be present within the sperm head proteome and may play roles in both compartments. Thus, to specifically explore the enriched proteins within the PT compared to the sperm head and tail fractions, statistical analyses were employed to calculate fold changes and *p*-values between each permutation. This analysis provided statistical confidence to aid in determining which proteins are most likely to partition into the PT compared to the head or tail, and thus may play crucial roles in the formation and/or function of this structure. Represented by volcano plots, this analysis revealed 37 proteins that were significantly enriched with a fold change ≥ 2 in the PT compared to the head (Figure 7A; Supplementary Table S2). Of the characterized proteins within this list, those with the most substantial fold changes included aminopeptidase (ANPEP), and glutamine rich 2 (QRICH2), the latter of which has been shown to play an important role in sperm cell structural development and fertility [31]. When comparing the PT to the tail, 139 proteins met our significance cut offs indicative of enrichment within the PT compared to the tail (Figure 7C; Supplementary Table S3). As expected, the most substantial compartmentalization was demonstrated by comparing proteins enriched in the head compared to the tail (Figure 7B) where several hundred proteins made the significance cut offs we applied, signifying the distinct proteomic stratification which takes place in these structurally and

functionally diverse cellular compartments. To improve our understanding of the function of the PT within sperm cells, differentially expressed boar sperm proteins were mapped to their human homologs (Supplementary File 1) and pathway analysis was performed using IPA. For this analysis we utilized the Z-score algorithm within IPA to indicate pathways that are likely to be more active in the PT compared to the sperm head or tail (a Z-score cut off ≥ 2 indicates likely active pathways; Z-scores between 1.5 and 2 indicate a trend towards active). The most significant canonical pathway active in the PT compared to the sperm head was related to 'cyclins and cell cycle regulation' (Figure 7D), which is a key pathway associated with spermiogenesis [32]. Several members of this pathway were detected in the PT including: serine/threonine-protein kinase ATR (ATR), glycogen synthase kinase-3 beta (GSK3B) and histone deacetylase 11 (HDAC11). Each of these proteins are also known to play roles in cell death pathways such as apoptosis. Notably, pathway analysis also revealed that apoptosis-associated pathways such as those that occur in response to HIV1, are likely to be active (Figure 7D). Comparison of the head and tail proteomes using IPA revealed the putative activity of several well-characterized signaling pathways including sirtuin signaling and ILK signaling (Figure 7E). Conversely, the tail fractions were enriched in pathways relating to cell metabolism and mitochondrial dynamics including oxidative phosphorylation, the TCA cycle and amino acid degradation (Figure 7F). These are the key pathways involved in ATP production within the mitochondria of mammalian sperm cells [33].

Perinuclear theca protein network enrichment analysis

As the PT is a highly dense structure known to feature extensive protein scaffolding and support high molecular weight protein complex formation [14, 30, 33], we investigated putative protein-protein interactions within the boar sperm PT proteome. Specifically, using the tools String and Cytoscape we constructed a network featuring all PT proteins that were either significantly enriched ($P \leq 0.05$; fold change ≥ 2), or unique to the PT structure compared to the head and

tail. This network analysis revealed the distinct clustering of numerous proteins within the PT (Figure 8) with a majority of proteins putatively linked to at least one partner protein within the network (for singletons that did not form putative interactions see Supplementary Figure S1A).

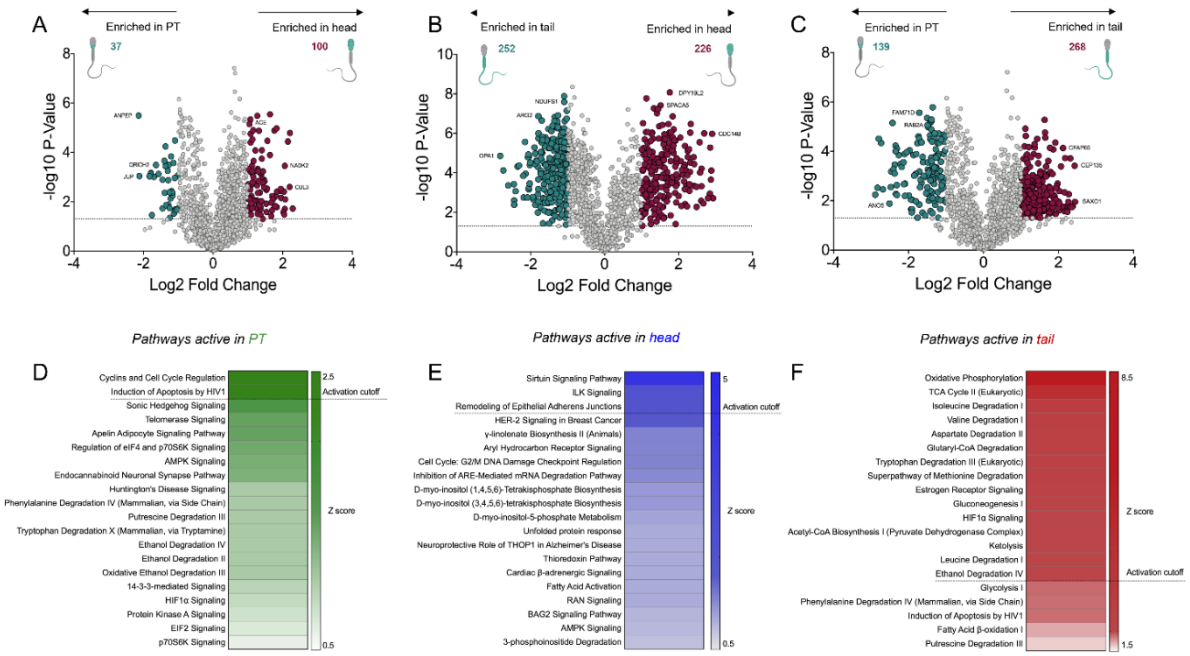

Figure 7. Significantly enriched proteins within the perinuclear theca compared to the sperm head and tail, and functional analyses of the cell compartment proteomes. (A-C) Fold changes and p-values were calculated from abundance values for each protein detected in the perinuclear theca (PT), head and tail. In this analysis a protein was deemed to be significantly enriched in each sample type upon meeting a fold change cut off of ≥ 2 and a p-value of ≤ 0.05 (dotted line). In the volcano plot visualizations these cut offs are equivalent to a log2 fold change of ≥ 1 and a -log10 p-value ≥ 1.3. Proteins that meet these criteria were designated colors (red and green) in panels A-C. (D-F) The Z-score function within Ingenuity Pathway Analysis (IPA) software was used to predict active pathways within each sample type. A Z-score ≥ 2 indicates the likely activity of the pathways listed in panels D-F.

As expected, two distinct clusters within the PT network were formed by the RAB proteins and somatic histone proteins (referred to as 'RAB2B complex' and 'histone-related). However, additional enriched protein clusters were revealed through this analysis with several members of the proteasome forming a large, distinct cluster within the PT network, and several spliceosome-related proteins forming a small cluster (Figure 8). In regard to the proteasome-

related cluster, the specific presence of PSMA8 suggests that this protein cluster best resembles the spermatoproteasome, a structural variant of the proteasome that is formed to promote the degradation of acetylated histones during spermiogenesis [34]. To delineate the role of proteins that were significantly enriched in the sperm head and tail compared to the PT, network analysis was also performed for these cell compartments. For the sperm head, network analysis revealed the presence of a cluster of proteins involved in formation and function of the sperm acrosome, protein transport and the actin cytoskeleton (Figure 9A). Complementing our analysis of the PT, the sperm head also featured some additional proteasome subunits to those detected in the PT, as well as a distinct cluster of proteins with molecular chaperone and protein scaffolding activity. In the sperm tail network, we observed extensive protein clustering of key components involved in the sperm mitochondria/ubiquinone and in cell metabolism and acyl-coA (Figure 9B). In addition to this, the tail network was also enriched in proteins related to cell movement/dyneins, as well as chaperone activity (Figure 9B). For access to the singleton proteins that were enriched in each cell compartment but not featured in the networks see Supplementary Figure S1A-C.

Discussion

The perinuclear theca (PT) is a unique structure within the sperm head that has been reported to house proteins critical for sperm-egg interaction and provide structural support to the nucleus during the long process of sperm transit through the reproductive tracts [1, 3]. Notwithstanding several highly valuable studies of the PT and subsequent in-depth characterization of several PT-associated proteins including; post-acrosomal sheath WW domain-binding protein (PAWP) and glutathione S-transferase omega 2 (GSTO2) [4, 16], the full proteomic content of the PT relative to other sperm components has not been explored using contemporary mass spectrometry approaches. In the current study, we have taken advantage of the latest updates to the *Sus scrofa* proteome and sperm subcellular fractionation strategies established previously

[1] to conduct a comprehensive characterization of the PT proteome. Our study identified and quantified 1,419 proteins in the sperm head, 1,514 proteins in the sperm tail and 813 proteins in the PT. It provides a valuable resource for the field of reproductive science. Moreover, our

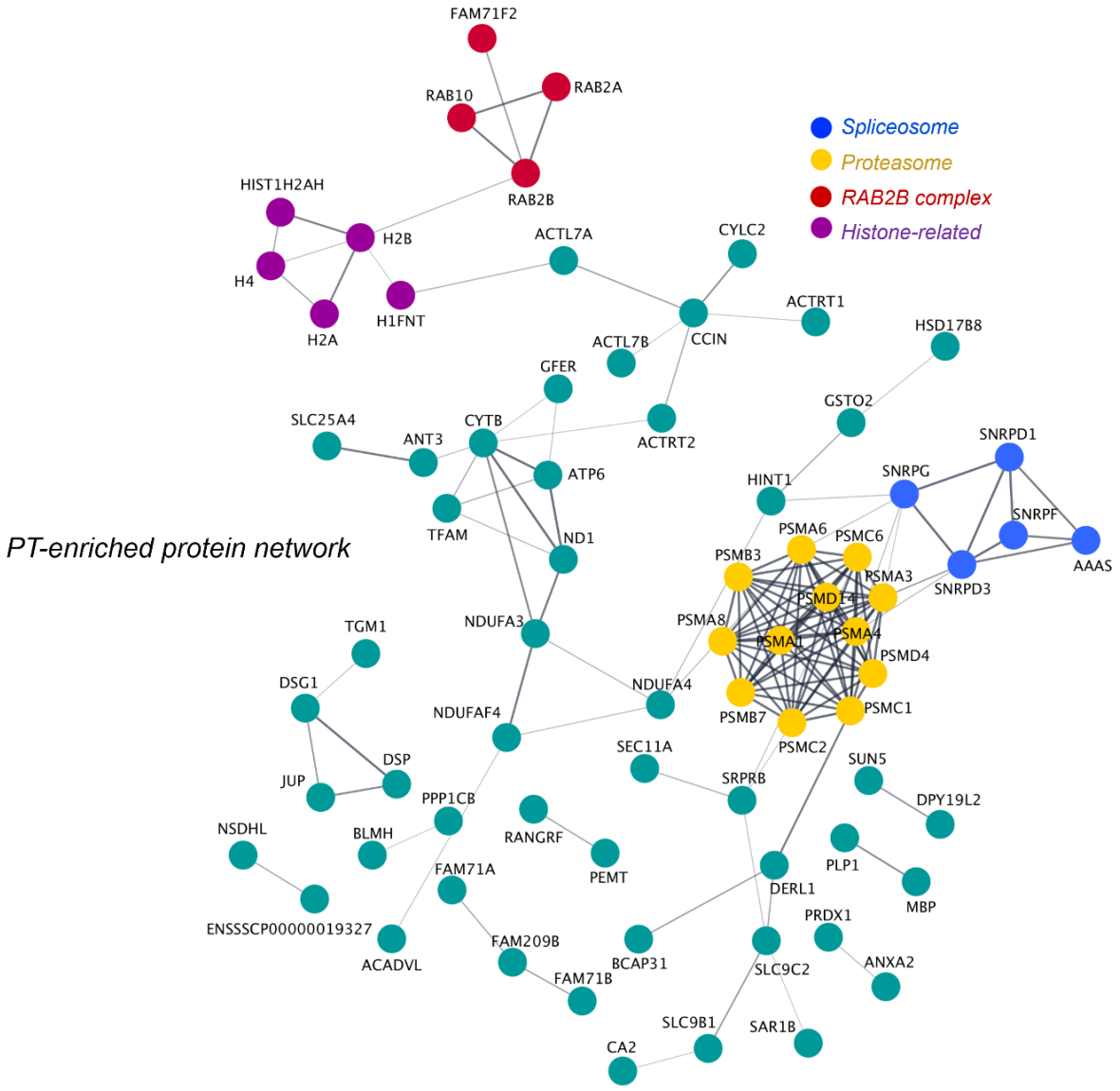

Figure 8. Protein network analysis of the perinuclear theca and identification of key protein clusters. All proteins deemed to be enriched in the perinuclear theca (PT) compared to the sperm head and tail were searched in the online protein interaction database String via their Sus scrofa UniProt protein accessions alongside the 19 proteins that were found to be unique to the PT compared to the head and tail. The protein network formed by the PT proteins was then exported to Cytoscape and protein clusters were manually designated functional annotations based on literature searches conducted on their protein components. This analysis revealed four proteins clusters enriched in proteins related to the 'proteasome' (yellow) and 'spliceosome' (blue), somatic histones (histone-related; purple), RAB

proteins (RAB2B complex; red). Single proteins that did not interact with other PT proteins within the network feature in Supplementary Figure S1A.

analysis revealed that most proteins recently confirmed to play essential roles in sperm-egg fusion is indeed housed within the PT in the mature sperm cell. Herein we consider the individual proteins and protein networks identified in our characterization of the PT and discuss their relationship to be known and less-well-known functions of the PT during mammalian fertilization.

The PT was isolated from the sperm head using a combination of detergents (0.2% Triton X-100, 1 M KCl and 100 mM NaOH) previously established to extract PT proteins from bull [15], rat [35], mouse [29], human and boar spermatozoa [30]. Within this protocol, the final alkaline extraction step is thought to extract all the covalently bound PT proteins. Similarly, some proteins that interact with polar bonds to the PT, such as histones, are detached during the saline extraction step [12, 13]. Somatic histones have been identified as major constituents of the PT of bovine [12] and murid spermatozoa [13], and those somatic histones are extractable using 1 M KCl. However, the extractability of the histones differs in our study whereby somatic histones were still abundantly present in the final alkaline step after high salt treatments. It is unlikely that the histones detected are residual sperm chromatin bound histones as the sperm nucleus has been reported to remain condensed after alkaline treatments. Moreover, Hamilton et al., have recently demonstrated that the core somatic histones detected in the mouse sperm PT are de novo synthesized in round spermatids [13]. These authors were also able to demonstrate a role for such histones post-fertilization using ICSI [13]. While similar experiments would need to be performed in boar sperm to verify that our findings are congruous, the remarkable conservation of somatic histones residing in the PT in eutherian sperm cells points to an important role for the PT in housing these proteins prior to fertilization.

In addition to the identification of histone proteins within the PT, our analysis revealed the presence of numerous RAB family proteins within the PT, some of which were previously reported by Oko [23]. RAB proteins have more than 60 family members in the human genome

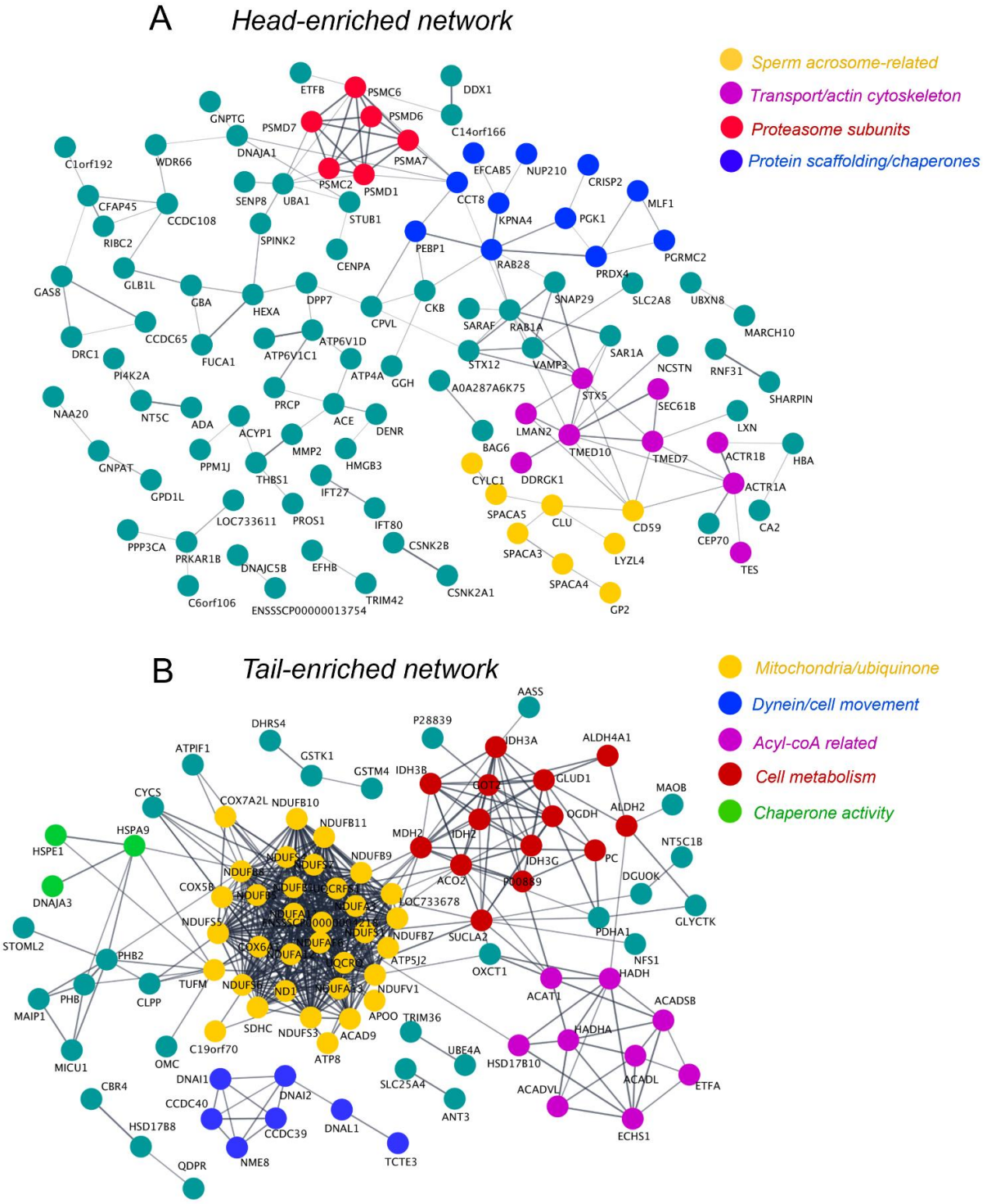

Figure 9. Protein network analysis of head- and tail- enriched proteins within boar spermatozoa and identification of key protein clusters. To form each protein network, proteins significantly enriched in the sperm head (A) or tail (B) compared to the PT were uploaded via their Sus scrofa UniProt accessions to the online protein interaction database String. These protein networks were then exported to Cytoscape and protein clusters were manually designated functional annotations through literature searches of their protein components. Due to the limited annotation of the Sus scrofa proteome, several uncharacterized proteins feature in these networks. In the absence of an assigned gene name, these uncharacterized proteins were labeled with their UniProt accession number where possible. Single proteins that did not interact with other proteins within the head or tail networks can be found in Supplementary Figure S1B-C.

making it the largest branch of the Ras-related family of small-GTPases [36]. There are several well-established functions of RAB proteins including; participation in vesicle trafficking pathways such as membrane tethering; vesicle budding and regulation of vesicle movement; along with cytoskeletal functions [37]. Most RAB proteins have universal expression, with few RAB proteins having biased expression specific to cells or tissues. Related to reproduction, 25 RAB proteins have been reported to play key roles in female meiosis and 12 RAB proteins function in male meiosis [38]. In the present study we have identified 7 RAB proteins (RAB2A, RAB2B, RAB10, RAB14, RAB17, RAB18 and RAB39A) in the PT. Of these proteins, RAB2A and RAB2B are the most well characterized. A previous report in bull spermatozoa has indicated that RAB2A is associated with the membrane of growing proacrosomic and acrosomic secretory vesicles during acrosomal biogenesis. RAB2A subsequently becomes a prominent subacrosomal layer (SAL)-PT protein in mature bull spermatozoa. The authors postulated that RAB2A-mediated vesicular pathways occurring during spermiogenesis may have little in common with those of somatic cells [23]. Given the high sequence similarity (93% based on UniProt alignment) between bovine RAB2A (A0A3Q1MHX8) and porcine RAB2A (A0A480X841) and the fact that RAB2A and RAB2B share 83% identity, it is very likely that RAB2B follows a similar developmental route of deposition during SAL-PT assembly in

developing boar spermatozoa. Notably, our data also revealed that RAB2B, RAB10 and RAB17 were enriched in the PT and that these proteins can potentially form a distinct protein cluster or putative complex within the PT (Figure 8). RAB10 is known to colocalize with its regulator RAB GTPase-activating protein in male germ cells within the manchette structure involved in spermatid head formation [39]. While, germ cell roles are yet to be evaluated for RAB17, this protein is involved in basolateral to apical transcytosis [40, 41], melanosome exocytosis [42] and efferocytosis through the recycling endosome [43, 44]. A recent study has demonstrated that homotypic and heterotypic RAB-RAB protein interactions induce vesicle tethering on two opposing membranes [45], adding strong evidence that RAB proteins can function diversely in membrane tethering. Given these data, it is possible that Golgi-associated RAB2 may be involved in anchoring of the acrosome to the nuclear envelope during sperm head formation through interaction with other RAB proteins and may thus serve as a protein scaffold to tighten the association of the acrosome with the nucleus. Certainly, the positioning of the RAB2 proteins within the PT is indicative that this hypothesis should be explored further in developing germ cells of the boar. Moreover, further experiments should be focused towards understanding the specific mechanisms of vesicle transport mediated by RAB proteins during spermiogenesis.

Within the PT, the ES is commonly considered the first site on the sperm cell that makes contact with the oolemma, subsequently exposing the PAS-PT to the oocyte cytoplasm [3, 46]. In our study, we have uncovered an extensive protein network related to sperm-egg fusion within the PT (Figure 6A). Numerous studies have demonstrated that IZUMO1 is required for sperm-egg fusion [47-49]. It is believed that the appearance of IZUMO1 in the post-acrosomal region of sperm head after the acrosome reaction is indispensable for sperm-egg fusion. Consistent with the network we have described here, testis-specific serine kinase (TSSK6) has been reported to

be involved in the re-localization of IZUMO1 [50]. Intriguingly, two of the best-described potential sperm oocyte-activating factor candidates, phospholipase C zeta (PLCZ) [51] and PAWP [5], were also present in this PT protein network related to fertilization. In terms of validation, our data also revealed that PAWP was indeed localized to the PAS-PT as well the ES, and was alkaline extractable indicating its presence in PT. Additionally, DPY-19-like 2 (DPY19L2), a key causative factor related to human globozoospermia [52] was also found in the PT network. DPY19L2-deficient human spermatozoa have dramatically decreased protein expression, with the modulated proteins including: sperm acrosome associated 1 (SPACA1), IZUMO1, and PLCZ1 [53]. Our findings provide evidence that these proteins are all likely to be present within the PT structure of spermatozoa and thus may be in close proximity to DPY19L2. Aberrations specific to the PT-proteome and PT structure in response to DPY19L2 deficiency will be interesting to explore. Finally, of the proteins within this fertilization-related network we have recently confirmed that cysteine rich secretory protein 2 (CRISP2) is indeed present in the PAS-PT of boar spermatozoa and is involved in protein complex formation and potential protein scaffolding at this site in which the free thiols on cysteine residues play an important role [14]. Taken together, the sperm-egg fusion related network we have documented within the PT is congruous with several previous studies described above and provides a novel basis to understand functional crosstalk between cytosolic molecules within the cytoskeleton.

Intriguingly, pathway analysis of the proteins abundant in the PT compared to the head and tail revealed a surprising enrichment of endoplasmic reticulum (ER) proteins residing in the PT. It is held that during testicular sperm maturation, spermatozoa lose most of their cytoplasmic content and many organelles including the ER. Although there are ER proteins added to the sperm surface during epididymal transit [54], it is unlikely that those ER proteins end up in the PT, since the PT is formed earlier during spermiogenesis. Supporting this, two ER resident

proteins, calreticulin (CALR) and protein disulfide isomerase A3 (PDIA3/ERp57) are known to be present in the developing acrosome of haploid spermatids and are retained in the acrosomes of mature rat spermatozoa [55, 56]. ERp57 interacts with CALR and CANX, the ER chaperones, promoting glycoprotein folding in somatic cells [57] as well as testicular germ cells [58]. Furthermore, ERp57 is associated with the ES of acrosome reacted sperm in rat [59], mice [60] and human [61], indicating a role in sperm-egg fusion. Functioning as a multifunctional thiol-disulfide oxidoreductase, ERp57 has been speculated to trigger conformational changes in the proteins participating sperm-egg fusion [60, 61]. Taken together, the PT enrichment of ERp57, CALR and CANX, amongst other ER proteins, suggests that these proteins may be stored in the PT to ensure their correct position to play a role in initiating the sperm-egg fusion process. This hypothesis requires explicit validation by tracking the localization of ER proteins throughout spermiogenesis and during the process of fertilization.

The PAS-PT is the first sperm head structure that is degraded within the ooplasm after fertilization [3]. Thus, it has been proposed by others that the PT may harbor sperm-borne molecules necessary for zygotic development or degradation processes. Previous investigations of the sperm borne factors present in the PAS-PT have demonstrated their intriguing roles in oocyte activation, pronuclear formation and early embryo development [4-6, 51]. It is likely that, before exerting their functions during gamete fusion and early embryo development, these factors must first become soluble to be able to diffuse through the ooplasm. Thus, the rapid disassociation of PAS-PT after sperm-egg interaction may be indispensable to release the cytosolic molecules from the PT. Importantly, reduction of the disulfide bonds and the activity of glutathione are important for sperm head and nuclear decondensation [62, 63]. GSTO2, an oxidative-reductive enzyme residing in the PAS-PT has been reported to play a role in removal

of the PAS-PT structure, accelerating sperm nuclear decondensation [6]. In line with this role, our data have demonstrated that CRISP2, localized to PAT-PT of the boar sperm head, is capable of forming disulfide bond-sensitive protein complexes at this site [14]. Moreover, our unpublished observations indicate a rapid dispersal of the PT after sperm entry in the oocyte i.e. before the sperm nucleus is decondensing and before mitochondria are degraded. This suggests that the reduction of the protein disulfide bridges may allow solubilization of the PT contents which then can diffuse through the oocyte's cytosol and induce oocyte activation. The dispersal of the PT in the oocyte's cytoplasm also allows the subsequent sperm nuclear chromatin decondensation in order to form the male pronucleus. Oxidation of protamine thiols is crucial for sperm chromatin condensation during sperm maturation and protecting the sperm heads against physical damage and DNA oxidation [64, 65]. A specific sperm nucleus glutathione peroxidase is shown to be responsible for this process [65]. In addition to these putative roles in the initiation of sperm-egg fusion, the PT also acts as a naturally rigid protein layer protecting the sperm nuclear material during the journey of the sperm through the male and female reproductive tracts before encountering the oolemma.

Consistent with the rapid degradation of the PT that has been observed post-fertilization, network analysis of PT proteins revealed an enrichment of proteasome subunits. The proteasome or 'spermatoproteasome' is known to be critical for several steps of mammalian fertilization, including sperm capacitation, acrosomal exocytosis and sperm-zona pellucida penetration [66]. Moreover, the ubiquitin proteasome pathway has been implicated in mammalian spermatogenesis and fertilization [67, 68]. Importantly, it has been demonstrated that both the ubiquitin-proteasome system and autophagy are involved in the degradation of the sperm mitochondria after fertilization in pigs [69]. Given that the PAS-PT and the sperm mitochondrial sheath are assembled using the same machinery [1, 70], a similar degradation

mechanism, analogous to mitophagy, may also apply to the PAS-PT post-fertilization. Strong support for this proposal was garnered through IPA predicting that autophagy is greatly activated in the PT compared to the sperm tail. The knowledge that autophagosomes are present in matured porcine oocytes [71, 72] also raises the possibility that the autophagosomes present in oocytes are recruited to the sperm head after sperm-egg fusion and trigger sperm PT dispersion. Thus, we speculate here that both autophagy and the ubiquitin-proteasome system may aid in PAS-PT degradation post-fertilization in the ooplasm.

In summary, the present study has characterized for the first time the whole PT proteome of boar spermatozoa and evaluated protein abundance relative to the head and tail compartments. This analysis simultaneously confirms decades of in-depth analysis of the individual proteins housed within the PT, while providing an abundance of new information regarding the complexity of the PT structure. Moreover, our analysis of these data has allowed the generation of putative protein networks that exist in the PT and can now be investigated in the context of sperm-egg fusion and sperm cell development. However, there are important limitations to this study and reasons for caution that should also be considered when interpreting the data. This is the first time that a high-resolution proteomics approach has been applied following the PT protein extraction protocol described above. While this extraction protocol has been long established in the field, there are several steps which may yield contamination of proteins from other cell compartments or membranes into the perinuclear theca fraction that may not have been detected in the original studies without mass spectrometry. Namely, the presence of nuclear proteins or nuclear membrane proteins in the PT, while congruous with previous studies, should be interpreted with caution and independently validated. Additionally, the head and tail separation technique, while highly efficient in yielding >99% of head-tail separation, may still yield some contamination that can also be detected through mass spectrometry. An example of this is the presence of translocase of outer mitochondrial membrane 34 (TOMM34)

in the sperm head, while it would be expected to sub-fractionate into the tail fraction. Despite this, TOMM34 has been described to be predominantly present in the cytosol of various cells and is also involved in chaperone systems not only for protein folding and import into the mitochondria but also in the cytosol [73-75]. The fact that this protein is not fully associated to mitochondria may well explain its presence in the sperm head fraction. Comparatively, true marker proteins of the mitochondrial matrix (such as succinate dehydrogenase subunits, see Supplementary File 1) are virtually devoid in the sperm head and PT fractions when compared to the sperm tail fraction. Nonetheless, we suggest that the use of proteins of interest from our PT list should be complemented by orthogonal localization studies to visualize their presence within the PT.

In summary, notwithstanding the caveats outlined above, our data support the notion that during its formation, the condensing PT attracts several proteins that are now identified in this study for their eventual use during and post-fertilization. Furthermore, the PT forms a protective structural layer surrounding the nuclear envelope that may be reinforced through the scaffolding and crosslinking actions of its proteomic constituents such as CRISP2. We speculate that after the disassociation of the PT prior to sperm-egg fusion, the liberated sperm proteins may provide or supplement existing machinery for paternal chromatin decondensation and pronucleus formation. This model fits well with biochemical data provided by the Sutovsky and Oko labs, and others, over the past two decades and contributes to the field by providing the identity of long sought after PT-enriched proteins that may be essential for the efficacy of the sperm-egg interaction.

Conflict of Interest

The authors declare that the research was conducted in the absence of any commercial or financial relationships that could be construed as a potential conflict of interest.

Author contributions

MZ conducted the experiments, wrote the initial draft of the manuscript and contributed to figure preparation, editing and project management. RZC conducted experiments, contributed to study design and analysis of the raw data, and reviewed the manuscript. DASB contributed to data analysis and revised several drafts of the manuscript, TV and JK contributed data to the manuscript and valuable expertise, AJRH contributed to the data collection, resource provision and manuscript preparation, BN contributed to resource provision, data analysis and manuscript editing, JBH contributed to the study design, supervision, provided resources and critical appraisal of the data and reviewed the manuscript. BMG conceived of the study, developed the methods with MZ and contributed to manuscript preparation, revision and editing and supervision. EGB analyzed the data, provided direction for the preparation of the manuscript, wrote the original draft of the manuscript with MZ and coordinated the manuscript revision and submission process.

Funding

MZ is financed by the China Scholarship Council (CSC) (No.201606170117). EGB is recipient of an NHMRC CJ Martin Early Career Fellowship (APP1138701). RZC is supported by the Netherlands Organization for Scientific Research (NWO) funding the Netherlands Proteomics Centre through the X-omics Road Map program (Project 184.034.019) and the EU Horizon 2020 program Epic-XS (Project 823839). The electron microscopy was done in the Cell Microscopy Core of the University Medical Centre Utrecht and partially financed by the National Roadmap for Large-Scale Research Infrastructure of the Dutch Research Council NWO (NEMI; project number 184.034.014 to J.K.).

Acknowledgements

The authors gratefully acknowledge the Center of Cell Imaging in the Faculty of Veterinary Medicine at Utrecht University and the expertise of Dr. R. Wubbolts and Ing. E. van ‘t Veld.

Data availability statement

The data presented in the study are deposited in the ProteomeXchange Consortium via the Proteomics Identification Database (PRIDE) partner repository with the dataset identifier PXD030020.

References

1. Oko R, Sutovsky P. Biogenesis of sperm perinuclear theca and its role in sperm functional competence and fertilization. J Reprod Immunol 2009; 83:2-7.
2. Hamilton LE, Suzuki J, Acteau G, Shi M, Xu W, Meinsohn MC, Sutovsky P, Oko R. WBP2 shares a common location in mouse spermatozoa with WBP2NL/PAWP and like its descendent is a candidate mouse oocyte-activating factor. Biol Reprod 2018; 99:1171-1183.
3. Sutovsky P, Manandhar G, Wu A, Oko R. Interactions of sperm perinuclear theca with the oocyte: implications for oocyte activation, anti-polyspermy defense, and assisted reproduction. Microsc Res Tech 2003; 61:362-378.
4. Wu AT, Sutovsky P, Manandhar G, Xu W, Katayama M, Day BN, Park K-W, Yi Y-J, Xi YW, Prather RSJJoBC. PAWP, a Sperm-specific WW Domain-binding Protein, Promotes Meiotic Resumption and Pronuclear Development during Fertilization. J Biol Chem 2007; 282:12164-12175.
5. Aarabi M, Balakier H, Bashar S, Moskovtsev SI, Sutovsky P, Librach CL, Oko R. Sperm-derived WW domain-binding protein, PAWP, elicits calcium oscillations and oocyte activation in humans and mice. Faseb j 2014; 28:4434-4440.
6. Hamilton LE, Suzuki J, Aguila L, Meinsohn MC, Smith OE, Protopapas N, Xu W, Sutovsky P, Oko R. Sperm-borne glutathione-S-transferase omega 2 accelerates the nuclear decondensation of spermatozoa during fertilization in mice†. Biol Reprod 2019; 101:368-376.
7. Cox LJ, Larman MG, Saunders CM, Hashimoto K, Swann K, Lai FA. Sperm phospholipase Czeta from humans and cynomolgus monkeys triggers Ca2+ oscillations, activation and development of mouse oocytes. Reproduction 2002; 124:611-623.
8. Nakai M, Ito J, Suyama A, Kageyama A, Tobari Y, Kashiwazaki N. Phospholipase Cζ (PLCζ) versus postacrosomal sheath WW domain-binding protein (PAWP): Which molecule will survive as a sperm factor? Anim Sci J 2020; 91:e13345.
9. Zafar MI, Lu S, Li H. Sperm-oocyte interplay: an overview of spermatozoon's role in oocyte activation and current perspectives in diagnosis and fertility treatment. Cell & Bioscience 2021; 11:4.
10. Kimura Y, Yanagimachi R, Kuretake S, Bortkiewicz H, Perry AC, Yanagimachi H. Analysis of mouse oocyte activation suggests the involvement of sperm perinuclear material. Biol Reprod 1998; 58:1407-1415.
11. Ito C, Akutsu H, Yao R, Kyono K, Suzuki-Toyota F, Toyama Y, Maekawa M, Noda T, Toshimori K. Oocyte activation ability correlates with head flatness and presence of perinuclear theca substance in human and mouse sperm. Hum Reprod 2009; 24:2588-2595.
12. Tovich PR, Oko RJ. Somatic histones are components of the perinuclear theca in bovine spermatozoa. J Biol Chem 2003; 278:32431-32438.
13. Hamilton LE, Lion M, Aguila L, Suzuki J, Acteau G, Protopapas N, Xu W, Sutovsky P, Baker M, Oko R. Core Histones Are Constituents of the Perinuclear Theca of Murid

Spermatozoa: An Assessment of Their Synthesis and Assembly during Spermiogenesis and Function after Gametic Fusion. International journal of molecular sciences 2021; 22:8119.
14. Zhang M, Bromfield EG, Veenendaal T, Klumperman J, Helms JB, Gadella BM. Characterization of different oligomeric forms of CRISP2 in the perinuclear theca versus the fibrous tail structures of boar spermatozoa. Biol Reprod 2021.
15. Aul RB, Oko RJ. The major subacrosomal occupant of bull spermatozoa is a novel histone H2B variant associated with the forming acrosome during spermiogenesis. Dev Biol 2002; 242:376-387.
16. Hamilton LE, Acteau G, Xu W, Sutovsky P, Oko R. The developmental origin and compartmentalization of glutathione-s-transferase omega 2 isoforms in the perinuclear theca of eutherian spermatozoa. Biol Reprod 2017; 97:612-621.
17. Kuzmuk KN, Schook LBJTgotp. Pigs as a model for biomedical sciences. 2011; 2:426-444.
18. Zuidema D, Sutovsky P. The domestic pig as a model for the study of mitochondrial inheritance. Cell and Tissue Research 2020; 380:263-271.
19. Oko R, Maravei D. Protein composition of the perinuclear theca of bull spermatozoa. Biol Reprod 1994; 50:1000-1014.
20. Slot JW, Geuze HJJNp. Cryosectioning and immunolabeling. 2007; 2:2480-2491.
21. Leung MR, Zenezini Chiozzi R, Roelofs MC, Hevler JF, Ravi RT, Maitan P, Zhang M, Henning H, Bromfield EG, Howes SC, Gadella BM, Heck AJR, et al. In-cell structures of conserved supramolecular protein arrays at the mitochondria-cytoskeleton interface in mammalian sperm. Proc Natl Acad Sci U S A 2021; 118.
22. Hidalgo-Gutiérrez A, Barriocanal-Casado E, Díaz-Casado ME, González-García P, Zenezini Chiozzi R, Acuña-Castroviejo D, López LC. β-RA Targets Mitochondrial Metabolism and Adipogenesis, Leading to Therapeutic Benefits against CoQ Deficiency and Age-Related Overweight. Biomedicines 2021; 9.
23. Mountjoy JR, Xu W, McLeod D, Hyndman D, Oko R. RAB2A: a major subacrosomal protein of bovine spermatozoa implicated in acrosomal biogenesis. Biol Reprod 2008; 79:223-232.
24. Tyanova S, Temu T, Sinitcyn P, Carlson A, Hein MY, Geiger T, Mann M, Cox J. The Perseus computational platform for comprehensive analysis of (prote)omics data. Nat Methods 2016; 13:731-740.
25. Skerrett-Byrne DA, Anderson AL, Hulse L, Wass C, Dun MD, Bromfield EG, De Iuliis GN, Pyne M, Nicolson V, Johnston SD, Nixon B. Proteomic analysis of koala (phascolarctos cinereus) spermatozoa and prostatic bodies. Proteomics 2021:e2100067.
26. Skerrett-Byrne DA, Trigg NA, Bromfield EG, Dun MD, Bernstein IR, Anderson AL, Stanger SJ, MacDougall LA, Lord T, Aitken RJ, Roman SD, Robertson SA, et al. Proteomic Dissection of the Impact of Environmental Exposures on Mouse Seminal Vesicle Function. Mol Cell Proteomics 2021; 20:100107.
27. Skerrett-Byrne DA, Bromfield EG, Murray HC, Jamaluddin MFB, Jarnicki AG, Fricker M, Essilfie AT, Jones B, Haw TJ, Hampsey D, Anderson AL, Nixon B, et al. Time-resolved proteomic profiling of cigarette smoke-induced experimental chronic obstructive pulmonary disease. Respirology 2021.
28. Szklarczyk D, Gable AL, Nastou KC, Lyon D, Kirsch R, Pyysalo S, Doncheva NT, Legeay M, Fang T, Bork P, Jensen LJ, von Mering C. The STRING database in 2021: customizable protein-protein networks, and functional characterization of user-uploaded gene/measurement sets. Nucleic acids research 2021; 49:D605-D612.

29. Korley R, Pouresmaeili F, Oko R. Analysis of the Protein Composition of the Mouse Sperm Perinuclear Theca and Characterization of its Major Protein Constituent1. Biology of Reproduction 1997; 57:1426-1432.
30. Lécuyer C, Dacheux JL, Hermand E, Mazeman E, Rousseaux J, Rousseaux-Prévost R. Actin-binding properties and colocalization with actin during spermiogenesis of mammalian sperm calicin. Biol Reprod 2000; 63:1801-1810.
31. Shen Y, Zhang F, Li F, Jiang X, Yang Y, Li X, Li W, Wang X, Cheng J, Liu M, Zhang X, Yuan G, et al. Loss-of-function mutations in QRICH2 cause male infertility with multiple morphological abnormalities of the sperm flagella. Nature Communications 2019; 10:433.
32. Wolgemuth DJ, Roberts SS. Regulating mitosis and meiosis in the male germ line: critical functions for cyclins. 2010; 365:1653-1662.
33. Hess H, Heid H, Zimbelmann R, Franke WW. The protein complexity of the cytoskeleton of bovine and human sperm heads: the identification and characterization of cylicin II. Exp Cell Res 1995; 218:174-182.
34. Qian MX, Pang Y, Liu CH, Haratake K, Du BY, Ji DY, Wang GF, Zhu QQ, Song W, Yu Y, Zhang XX, Huang HT, et al. Acetylation-mediated proteasomal degradation of core histones during DNA repair and spermatogenesis. Cell 2013; 153:1012-1024.
35. Oko RJ. Developmental expression and possible role of perinuclear theca proteins in mammalian spermatozoa. Reprod Fertil Dev 1995; 7:777-797.
36. Bock JB, Matern HT, Peden AA, Scheller RH. A genomic perspective on membrane compartment organization. Nature 2001; 409:839-841.
37. Zerial M, McBride H. Rab proteins as membrane organizers. Nature Reviews Molecular Cell Biology 2001; 2:107-117.
38. Shan MM, Sun SC. The multiple roles of RAB GTPases in female and male meiosis. Hum Reprod Update 2021.
39. Lin YH, Ke CC, Wang YY, Chen MF, Chen TM, Ku WC, Chiang HS, Yeh CH. RAB10 Interacts with the Male Germ Cell-Specific GTPase-Activating Protein during Mammalian Spermiogenesis. Int J Mol Sci 2017; 18.
40. Striz AC, Tuma PLJJoBC. The GTP-bound and sumoylated form of the RAB17 small molecular weight GTPase selectively binds syntaxin 2 in polarized hepatic WIF-B cells. 2016; 291:9721-9732.
41. Striz AC, Stephan AP, López-Coral A, Tuma PL. Rab17 regulates apical delivery of hepatic transcytotic vesicles. Mol Biol Cell 2018; 29:2887-2897.
42. Beaumont KA, Hamilton NA, Moores MT, Brown DL, Ohbayashi N, Cairncross O, Cook AL, Smith AG, Misaki R, Fukuda M, Taguchi T, Sturm RA, et al. The recycling endosome protein Rab17 regulates melanocytic filopodia formation and melanosome trafficking. Traffic 2011; 12:627-643.
43. Yin C, Kim Y, Argintaru D, Heit B. Rab17 mediates differential antigen sorting following efferocytosis and phagocytosis. Cell Death & Disease 2016; 7:e2529-e2529.
44. Yin C, Argintaru D, Heit B. Rab17 mediates intermixing of phagocytosed apoptotic cells with recycling endosomes. Small GTPases 2019; 10:218-226.
45. Segawa K, Tamura N, Mima J. Homotypic and heterotypic trans-assembly of human Rab-family small GTPases in reconstituted membrane tethering. J Biol Chem 2019; 294:7722-7739.
46. Vjugina U, Evans JP. New insights into the molecular basis of mammalian sperm-egg membrane interactions. Front Biosci 2008; 13:462-476.
47. Inoue N, Ikawa M, Isotani A, Okabe M. The immunoglobulin superfamily protein Izumo is required for sperm to fuse with eggs. Nature 2005; 434:234-238.
48. Bianchi E, Doe B, Goulding D, Wright GJ. Juno is the egg Izumo receptor and is essential for mammalian fertilization. Nature 2014; 508:483-487.

49. Satouh Y, Inoue N, Ikawa M, Okabe M. Visualization of the moment of mouse sperm-egg fusion and dynamic localization of IZUMO1. J Cell Sci 2012; 125:4985-4990.
50. Sosnik J, Miranda PV, Spiridonov NA, Yoon S-Y, Fissore RA, Johnson GR, Visconti PE. Tssk6 is required for Izumo relocalization and gamete fusion in the mouse. Journal of cell science 2009; 122:2741-2749.
51. Saunders CM, Larman MG, Parrington J, Cox LJ, Royse J, Blayney LM, Swann K, Lai FA. PLC zeta: a sperm-specific trigger of Ca(2+) oscillations in eggs and embryo development. Development 2002; 129:3533-3544.
52. Koscinski I, Elinati E, Fossard C, Redin C, Muller J, Velez de la Calle J, Schmitt F, Ben Khelifa M, Ray PF, Kilani Z, Barratt CL, Viville S. DPY19L2 deletion as a major cause of globozoospermia. Am J Hum Genet 2011; 88:344-350.
53. Guo Y, Jiang J, Zhang H, Wen Y, Zhang H, Cui Y, Tian J, Jiang M, Liu X, Wang G, Li Y, Hu Z, et al. Proteomic Analysis of Dpy19l2-Deficient Human Globozoospermia Reveals Multiple Molecular Defects. Proteomics Clin Appl 2019; 13:e1900007.
54. Guo W, Qu F, Xia L, Guo Q, Ying X, Ding Z. Identification and characterization of ERp29 in rat spermatozoa during epididymal transit. Reproduction 2007; 133:575-584.
55. Ohtani H, Wakui H, Ishino T, Komatsuda A, Miura AB. An isoform of protein disulfide isomerase is expressed in the developing acrosome of spermatids during rat spermiogenesis and is transported into the nucleus of mature spermatids and epididymal spermatozoa. Histochemistry 1993; 100:423-429.
56. Nakamura M, Moriya M, Baba T, Michikawa Y, Yamanobe T, Arai K, Okinaga S, Kobayashi T. An endoplasmic reticulum protein, calreticulin, is transported into the acrosome of rat sperm. Exp Cell Res 1993; 205:101-110.
57. Ellgaard L, Helenius A. Quality control in the endoplasmic reticulum. Nature Reviews Molecular Cell Biology 2003; 4:181-191.
58. Tokuhiro K, Ikawa M, Benham AM, Okabe M. Protein disulfide isomerase homolog PDILT is required for quality control of sperm membrane protein ADAM3 and male fertility [corrected]. Proc Natl Acad Sci U S A 2012; 109:3850-3855.
59. Liu Y, Zhu Y, Wu X, Li Y, Guo Q, Li W, Ding Z. Increased expression of ERp57 in rat oocytes during meiotic maturation is associated with sperm-egg fusion. Mol Reprod Dev 2014; 81:315-325.
60. Ellerman DA, Myles DG, Primakoff P. A role for sperm surface protein disulfide isomerase activity in gamete fusion: evidence for the participation of ERp57. Dev Cell 2006; 10:831-837.
61. Zhang J, Wu J, Huo R, Mao Y, Lu Y, Guo X, Liu J, Zhou Z, Huang X, Sha J. ERp57 is a potential biomarker for human fertilization capability. Molecular Human Reproduction 2007; 13:633-639.
62. Sutovsky P, Schatten G. Depletion of glutathione during bovine oocyte maturation reversibly blocks the decondensation of the male pronucleus and pronuclear apposition during fertilization. Biol Reprod 1997; 56:1503-1512.
63. Perreault SD, Wolff RA, Zirkin BR. The role of disulfide bond reduction during mammalian sperm nuclear decondensation in vivo. Dev Biol 1984; 101:160-167.
64. Seligman J, Kosower NS, Weissenberg R, Shalgi R. Thiol-disulfide status of human sperm proteins. J Reprod Fertil 1994; 101:435-443.
65. Pfeifer H, Conrad M, Roethlein D, Kyriakopoulos A, Brielmeier M, Bornkamm GW, Behne D. Identification of a specific sperm nuclei selenoenzyme necessary for protamine thiol cross-linking during sperm maturation. Faseb j 2001; 15:1236-1238.
66. Zimmerman S, Sutovsky P. The sperm proteasome during sperm capacitation and fertilization. J Reprod Immunol 2009; 83:19-25.

67. Yi YJ, Manandhar G, Sutovsky M, Li R, Jonáková V, Oko R, Park CS, Prather RS, Sutovsky P. Ubiquitin C-terminal hydrolase-activity is involved in sperm acrosomal function and anti-polyspermy defense during porcine fertilization. Biol Reprod 2007; 77:780-793.
68. Sutovsky P. Ubiquitin-dependent proteolysis in mammalian spermatogenesis, fertilization, and sperm quality control: killing three birds with one stone. Microsc Res Tech 2003; 61:88-102.
69. Song W-H, Yi Y-J, Sutovsky M, Meyers S, Sutovsky P. Autophagy and ubiquitin–proteasome system contribute to sperm mitophagy after mammalian fertilization. 2016; 113:E5261-E5270.
70. Kierszenbaum AL. Intramanchette transport (IMT): managing the making of the spermatid head, centrosome, and tail. Mol Reprod Dev 2002; 63:1-4.
71. Lee S, Hiradate Y, Hoshino Y, Tanemura K, Sato E. Quantitative analysis in LC3-II protein in vitro maturation of porcine oocyte. Zygote 2014; 22:404-410.
72. Shen XH, Jin YX, Liang S, Kwon JW, Zhu JW, Lei L, Kim NH. Autophagy is required for proper meiosis of porcine oocytes maturing in vitro. Sci Rep 2018; 8:12581.
73. Durech M, Trcka F, Man P, Blackburn EA, Hernychova L, Dvorakova P, Coufalova D, Kavan D, Vojtesek B, Muller P. Novel Entropically Driven Conformation-specific Interactions with Tomm34 Protein Modulate Hsp70 Protein Folding and ATPase Activities. Mol Cell Proteomics 2016; 15:1710-1727.
74. Chewawiwat N, Yano M, Terada K, Hoogenraad NJ, Mori M. Characterization of the novel mitochondrial protein import component, Tom34, in mammalian cells. J Biochem 1999; 125:721-727.
75. Muller P, Coates PJ, Nenutil R, Trcka F, Hrstka R, Chovanec J, Brychtova V, Vojtesek B. Tomm34 is commonly expressed in epithelial ovarian cancer and associates with tumour type and high FIGO stage. J Ovarian Res 2019; 12:30.

.

Supplementary Material

The Supplementary Material for this article can be found online at:

https://www.frontiersin.org/articles/10.3389/fcell.2022.836208/full#supplementary-material

Chapter 5

Characterization of acrosin and acrosin binding protein as novel CRISP2 interacting proteins in boar spermatozoa

Min Zhang[1], Riccardo Zenezini Chiozzi[2,3,4], Elizabeth G Bromfield[1,5], Albert JR Heck[2,3,4], J Bernd Helms[1], Bart M Gadella[1]*

[1] Department of Biomolecular Health Sciences, Faculty of Veterinary Medicine, Utrecht University, The Netherlands.

[2] Biomolecular Mass Spectrometry and Proteomics, Bijvoet Centre for Biomolecular Research and Utrecht Institute for Pharmaceutical Sciences, Utrecht University, The Netherlands.

[3] Netherlands Proteomics Centre, Utrecht, The Netherlands.

[4] Structural Biochemistry, Bijvoet Centre for Biomolecular Research, Utrecht University, The Netherlands.

[5] Priority Research Centre for Reproductive Science, School of Environmental and Life Sciences, Discipline of Biological Sciences, University of Newcastle, Callaghan, NSW, Australia.

Submitted

Abstract

Previously we reported that cysteine rich secretory protein 2 (CRISP2) is involved in high molecular weight complexes in boar spermatozoa under a native state. In the current study, CRISP2 interacting partners were identified using proteomic technology and their interaction was investigated under non-capacitating conditions, after the induction of *in vitro* sperm capacitation and subsequently during an ionophore A23187 induced acrosome reaction. Blue native gel electrophoresis and native immunoblots revealed that CRISP2 was present within a ~150 kDa protein complex under all three conditions. Interrogation of CRISP2-immunoreactive bands from blue native gels as well as CRISP2 immunoprecipitated products using mass spectrometry consistently revealed that, beyond CRISP2, acrosin and acrosin binding protein (ACRBP) were among the most abundant proteins and present under the three conditions. Co-immunoprecipitation and immunoblotting indicated that CRISP2 interacted with pro-acrosin (~53 kDa) and ACRBP under all three conditions and additionally to acrosin (~35 kDa) after capacitation and the acrosome reaction. The colocalization of these interacting proteins with CRISP2 was assessed via *in situ* proximity ligation assays. The colocalization signal of CRISP2 and acrosin in the acrosome seemed dispersed after capacitation but was consistently present in the sperm tail under all conditions. The fluorescent foci of CRISP2 and ACRBP colocalization appeared to be redistributed within the sperm head from the anterior acrosome to the post acrosomal sheath region upon capacitation. These results suggest that CRISP2 may act as a scaffold for protein complexes formation to ensure the correct positioning of proteins required for the acrosome reaction and zona pellucida penetration.

Keywords: CRISP2; boar spermatozoa; protein complexes; colocalization; capacitation, interacting proteins.

Introduction

To fertilize an egg, spermatozoa must complete their final maturation by residing in the female reproductive tract to undergo a series of physiological and biochemical transformations termed capacitation [1, 2]. Capacitation prepares the sperm to undergo an exocytotic process known as the acrosome reaction and perform vigorous flagellar movements characterized as hyperactivity [3]. At the molecular level, capacitation involves several signaling pathways such as protein kinase A (PKA) activation, protein tyrosine phosphorylation as well as lipid and protein reorganization [4, 5]. Notably, sperm head surface remodeling, a capacitation associated event, has gained attention over the past decades. Specifically, the apical tip of sperm head plasma membrane has been considered as the primary site where capacitated sperm bind to the oocyte zona pellucida (ZP) [6]. Capacitation leads to sperm-ZP recognition by exposing ZP-receptors on the sperm head surface that subsequently can bind to specific carbohydrates of the ZP proteins [7]. Concomitant with transportation of acrosomal proteins, such as acrosin and acrosin binding protein (ACRBP), to the sperm head surface during capacitation has been previously demonstrated in boar sperm. These proteins form high molecular weight complexes with a higher affinity for ZP binding [8]. However, the mechanisms supporting acrosomal protein transportation during capacitation are still unclear. Besides this, it has also been reported that capacitation induces a concentration of lipid rafts at the apical tip of sperm head surface [9]. Sperm lipids rafts are liquid ordered, low density microdomains, serving as platforms for cell adhesion and signaling molecules [8-10]. In capacitating boar sperm the outer acrosomal membrane has been shown to dock with the sperm head plasma membrane by forming trimeric SNARE protein complexes [11, 12]. This closer apposition of the two membranes is required for hybrid vesicle formation occurring during the acrosome reaction [13]. Acrosomal exocytosis is a continuous process involving intermediate steps including progressive disassembly of the acrosomal matrix that is partially driven by proteolysis, for instance acrosin

cleavage [14, 15]. Recently it has been demonstrated that paracrystalline patches of the acrosomal matrix start to fragment during capacitation [16]. Intriguingly, there is evidence that some of the acrosome matrix proteins do interact with acrosomal membrane proteins which are reported to be involved in regulating acrosomal exocytosis [17, 18].

Cysteine Rich Secretory Protein 2 (CRISP2) is a member of the CRISP family that together with Antigen 5 and Pathogenesis related 1 proteins make up the CAP superfamily [19]. Mammalian CRISP2 is exclusively expressed in the male reproductive tract and ultimately becomes an integral component of the sperm head and tail, the acrosome, the post acrosomal region, the fibrous tail structures and the connecting piece [20-23]. CRISP2 possesses an evolutionary conserved CAP domain and a characteristic CRISP domain comprising of a linker region and an ion channel regulatory (ICR) region. *In vitro* studies have shown that mouse CRISP2 can regulate Ca^{2+} flux via ryanodine receptor channels [24]. CRISP2 has also been shown to bind with the cation channel of sperm 1 (CatSper1) subunit of the CatSper ion channel [25]. Consequently, CRISP2 has been implicated in Ca^{2+} related events such as sperm motility, capacitation and the acrosome reaction [26, 27]. Supporting this possibility, Crisp2$^{-/-}$ sperm exhibit altered flagellum waveforms and an impaired ability to undergo a progesterone-evoked acrosome reaction [25]. In terms of mechanism, a yeast two-hybrid screen of the adult mouse testis has been intensively used to identify mouse CRISP2 binding partners. CRISP2 is known to bind to the mitogen-activated protein kinase kinase kinase 11 (MAP3K11) and gametogenetin 1 (GGN1) through its ICR domain [28, 29]. Additionally, CRISP2 also binds to sperm head and tail-associated protein (SHTAP), and this binding is attributed to the CAP domain [30]. The CRISP2-SHTAP complex is redistributed within the sperm head upon capacitation. Given that CRISP2 colocalizes with binding partners in the sperm head and sperm tail, a potential role for CRISP2 interacting complexes in the attainment of sperm function has

been suggested. Nonetheless, those data are mostly derived from the mouse as an animal model. We previously found that boar sperm CRISP2 is present in high molecular weight complexes under a native state in both the perinuclear theca as well as in the outer dense fibers (ODF) and the fibrous sheath (FS) [23]. Therefore, we now sought to identify CRISP2 interacting partners in boar sperm and follow their colocalization *in situ* prior to and during *in vitro* capacitation and the agonist induced acrosome reaction. In the present study we analyzed CRISP2-protein complexes detected under native conditions and CRISP2 targeted antigens by a quantitative, label-free liquid chromatography mass spectrometry (LC-MS/MS) approach.

Materials and methods

Reagents and antibodies

All chemicals were obtained from Sigma (St. Louis, MO, USA) unless otherwise stated. Primary and secondary antibodies used in the present study are listed in Table S1.

Boar spermatozoa preparation

Semen was obtained from highly fertile boars from a commercial breeder (Cooperative Center for Artificial Insemination in Pigs, Veghel, the Netherlands). Semen was diluted to 20 million sperm/ml in a commercial extender, shipped in 80 ml sealed insemination tubes in a cool box (17 °C) and used within 12 h of delivery. Diluted semen from three boars were pooled and washed through discontinuous Percoll (Cat#: 17089101, GE Healthcare, Piscataway, NJ, United States) gradients as previously described [23].

In vitro capacitation and calcium ionophore A23187 induced acrosomal exocytosis

The incubation media used in this study was a modified Tyrode's medium supplemented with bovine serum albumin (BSA), lactate and pyruvate [31]. Capacitating medium consisted of 90 mM NaCl, 10.0 mM HEPES, 3.0 mM KCl, 0.4 mM $MgCl_2$, 2.0 mM $CaCl_2 \cdot 2H_2O$, 0.3 mM Na_2HPO_4, 25 mM $NaHCO_3$, 2.0 mM Na-pyruvate, 5.0 mM D-glucose, 21.6 mM Na lactate, 3.0 mg/mL fatty acid free BSA, 300 ± 10 mOsm/kg, pH 7.4. Medium supplied with neither $CaCl_2$,

$NaHCO_3$ nor BSA was defined as non-capacitating medium and an equimolar amount of NaCl was added to non-capacitating medium to compensate for $NaHCO_3$. Sodium pyruvate and BSA were added into the medium on the same day before use. Complete capacitating medium and non-capacitating medium were equilibrated in the incubator (38.5°C, 5% CO_2) with loose lids or in the water bath (38.5°C) with tight vials for at least 2 h, respectively. Percoll washed sperm were resuspended in capacitating medium (1ml, 20×10^6 sperm/ml) in open tubes and incubated for 2.5 h in the incubator or incubated in non-capacitating medium (1ml, 20×10^6 sperm/ml) in air-tight tubes for 2.5 h at 38.5°C in a pre-warmed water bath.

During the last 30 min of capacitation, sperm cells were exposed to 5 µM calcium ionophore A23187 to induce acrosome exocytosis and incubated under the same conditions as capacitation. All sperm incubations were carried out in 5 ml polystyrene round bottom tubes (Falcon, 352054; Life Sciences, Corning, NY, USA). At least 5 tubes were incubated for each condition. After incubation, sperm cells were spun down and washed twice with phosphate buffered saline (PBS) (137 mM NaCl, 8.0 mM $Na_2HPO_4\cdot2H_2O$, 1.5 mM KH_2PO_4, 2.7 mM KCl, pH 7.4) at 750 x g for 10 min, RT. Sperm cells were either fixed for immunofluorescence or stored at -80°C.

Blue native polyacrylamide gel electrophoresis and native blots

Non-capacitated (NC), capacitated (CAP), and acrosome reacted (AR) sperm cells were lysed in a commercial lysis buffer (Cat#: 88805, Thermo Scientific) with freshly added protease inhibitors: aprotinin, leupeptin, pepstatin and phenylmethanesulfonyl fluoride (PMSF) (Thermo Scientific) for 30 min on ice with mixing, followed by a 15 min centrifugation at 14,000 x g at 4°C. Supernatants were recovered and mixed with 4x native sample buffer (400 mM Tris HCl, pH 8.6, 40% glycerol, 0.04% Brom-phenol-Blue) and 5% G-250 sample additive (Cat#: BN2004, Thermo Scientific) before loading onto 4~20% precast gels (Cat#: 4561094, Bio-Rad). Native running buffer (25 mM Tris-base, 192 mM glycine, pH 8.3) and native

polyacrylamide gel electrophoresis (PAGE) cathode buffer additive (20x) (Cat#: BN2002, Thermo Scientific) were used to make cathode running buffer following the manufacturer's instructions. Electrophoresis was carried out at 150 V, RT for 2~2.5 h. Gels were either stained with Coomassie R-250 or prepared for native blots.

Native immunoblotting was carried out as in conventional western blotting procedures with the exception that the transfer buffer was a tris-glycine buffer (12 mM tris-base, 96 mM glycine, pH 8.3). Proteins were blotted onto 0.45 µm polyvinylidene difluoride (PVDF) membranes (GE Healthcare, Piscataway, NJ, USA) at 25 V, RT for 1 h. After transfer, membranes were fixed in 8% (v/v) acetic acid for 15 min and rinsed with water, then air dried overnight at RT. Dried membranes were rewet in pure methanol to remove excessive bound dye. After rinsing with water, membranes were continued from the blocking step as conventional western blotting immunodetection (see immunoblotting). NativeMark unstained protein standard (LC0725, Thermo Scientific) was used to estimate protein size.

Co-immunoprecipitation

To identify potential CRISP2 interacting proteins, we employed a reciprocal co-immunoprecipitation (Co-IP) assay using a Crosslink Magnetic IP/Co-IP kit (Cat#: 88805, Thermo Scientific). CRISP2 antibody (10 µg per reaction) was cross linked to protein A/G magnetic beads according to the manufacturer's instructions. Sperm lysates were prepared as described above for blue native PAGE. Crosslinked beads and approximately 0.5 mg of sperm lysates were incubated at 4°C overnight with agitation. The beads were collected and washed three time before elution of bound proteins. The supernatants containing targeted antigens were saved for immunoblotting or mass spectrometry (MS) analysis.

Protein identification from blue native PAGE and CRISP2 precipitated antigens

CRISP2-interacting protein complexes were carefully excised from gels (Figure S2A) and CRISP2 targeted antigens from the co-IP eluate were prepared for MS analysis. The efficiency of CRISP2 pull down assays was validated by immunoblotting (Figure S2B). The gel slices were first de-stained then reduced with dithiothreitol (DTT) and alkylated with iodoacetamide (IAA). All gel bands were then digested overnight with Trypsin. Peptides from all samples were analyzed using an Ultimate3000 high-performance liquid chromatography system (Thermo Scientific) coupled online to a Q Exactive HF-x mass spectrometer (Thermo Scientific) as previously described [32]. Buffer A consisted of water acidified with 0.1% formic acid, while buffer B was 80% acetonitrile and 20% water with 0.1% formic acid. The peptides were first trapped for 1 min at 30 µl/min with 100% buffer A on a trap (0.3 mm by 5 mm with PepMap C18, 5 µm, 100 Å; Thermo Scientific); after trapping, the peptides were separated by a 50 cm analytical column packed with C18 beads (Poroshell 120 EC-C18, 2.7 µm; Agilent Technologies). The gradient was 9 to 40% B in 40 min at 400 nl/min. Buffer B was then raised to 55% in 2 min and increased to 99% for the cleaning step. Peptides were ionized using a spray voltage of 1.9 kV and a capillary heated at 275°C. The mass spectrometer was set to acquire full-scan MS spectra (350 to 1400 m/z ratio) for a maximum injection time of 120 ms at a mass resolution of 60,000 and an automated gain control (AGC) target value of 3×10^6. Up to 6 of the most intense precursor ions were selected for MS/MS. HCD fragmentation was performed in the HCD cell, with the readout in the Orbitrap mass analyzer at a resolution of 30,000 (isolation window of 1.4 Th) and an AGC target value of 1×10^5 with a maximum injection time of 54 ms and a normalized collision energy of 27%. The raw files were analyzed with MaxQuant (version 2.0.3) with all the default settings adding deamidation (NQ) and phosphorylation (STY) as dynamic modifications against the Sus scrofa sperm specific proteome (from proteins identified in Zhang et al., 2022 [33]) containing 2,474 entries adding common contaminants. MaxQuant was used with the standard parameters adding only the

"iBAQ Quantification" and "Match between runs" with automatic values. High confidence positive identifications were based on a minimum of two matching peptides.

SDS-PAGE and immunoblotting

Percoll washed sperm cells were sonicated and sperm heads and tails were isolated as described previously [23]. Whole sperm cells, sperm heads and tails were lysed in RIPA buffer (Thermo Scientific) with freshly added protease inhibitors: aprotinin, leupeptin, pepstatin and PMSF (Thermo Scientific) on ice for 30 min followed by a 15 min spin at 14,000 x g, 4°C. Sperm lysates or CRISP2 precipitates were denatured in 4x SDS sample buffer (200 mM Tris-HCl, pH 6.8, 10% β-mercapto-ethanol, 8% SDS, 0.08% bromophenol blue, 40% glycerol) and boiled for 10 min. Samples were loaded on to SDS-PAGE gels (5% stacking gel, 12% resolving gel) and were blotted onto 0.2 µm nitrocellulose membranes (GE Healthcare, Piscataway, NJ, USA) at 100V for 1 h. After blocking for 3 h at RT in 5% (w/v) BSA in PBS with 0.05% (v/v) Tween-20 (PBST), membranes were incubated with primary antibodies (Table S1) overnight at 4°C. After three washes in PBST for 15 min, membranes were incubated with horse radish peroxidase (HRP) conjugated secondary antibodies (Table S1) for 1 h at RT. After rinsing four times in PBST for 20 min, membranes were developed using chemiluminescence (ECL-detection kit; Supersignal West Pico, Pierce, Rockford IL, USA). Migration levels of proteins were visualized using pre-stained protein ladder, 10 to 250 kDa (Thermo Scientific).

Immunolocalization of CRISP2 interacting proteins in boar sperm

Protein colocalization was assessed via *in situ* proximity ligation assays (PLA). For the colocalization of CRISP2 and acrosin, sperm cells were fixed and permeabilized in -20 °C methanol for 5 min, diluted in PBS and deposited on slides. Sperm cells were blocked and incubated with primary antibodies, overnight at 4 °C, followed by appropriate secondary antibodies conjugated with oligonucleotides (Duolink PLA Probe Anti-Rabbit PLUS, Cat#: DUO92002, Anti-Mouse MINUS, Cat#: DUO92004, Sigma). After enzymatic ligation and

amplification, target proteins were colocalized with peanut agglutinin lectin (PNA) via dual labelling with Alexa Flour 488. Colocalization of CRISP2 and ACRBP was performed using Duolink PLA Probemaker kit (Cat#: DUO96020, Sigma) following the manufacturer's instructions. Briefly, sperm cells were fixed in 4% paraformaldehyde (PFA) and permeabilized in cold acetone for 10 min, washed and blocked before incubating with primary antibodies conjugated with oligonucleotides (PLA probes), overnight at 4 °C. After enzymatic ligation and amplification, target proteins residing within a maximum distance of 40 nm were identified by the production of discrete fluorescent foci [34-36]. Additionally, conventional single protein immunostaining was performed following standard protocols [33]. In all cases, fluorescent labeling of sperm cells was visualized with a Leica SPE-II confocal microscope using a 63x objective (NA 1.3, HCX PLANAPO oil). Scale bars were added using Image J software (bundled with 64-bit Java 1.8.0_172, National Institutes of Health, Bethesda, MD, USA).

Results

Identification of CRISP2 interacting proteins in boar spermatozoa

Native blots revealed that anti-CRISP2 recognized a ~150 kDa protein complex in boar sperm, irrespective of whether lysates were extracted from non-capacitated (NC), capacitated (CAP), or acrosome reacted (AR) sperm cells (Figure 1A). Of note, there was an additional lower band (~50 kDa) that likely corresponds to dimeric CRISP2 under non-denaturing conditions (Figure 1A). Western blots from SDS-PAGE gels demonstrated that CRISP2 was present as a ~25 kDa monomer under reducing conditions with no obvious difference in the amount of CRISP2 among the three samples (Figure 1B). Additionally, Coomassie brilliant blue staining of SDS-PAGE gels was conducted to show the total protein loading (Figure S1A). NC, CAP and AR sperm cells were processed, and two methods were used to isolate CRISP2 interacting protein complexes. (i) Protein samples were run through a native gel, immunoblotted with anti-CRISP2 and the 150 kDa band was excised from the gel (Figure S2A) and used in a proteomics workflow.

(ii) CRISP2 interacting protein complexes were immunoprecipitated and the eluate was then used in the proteomics workflow.

As an initial validation, we examined the proteins from native PAGE gel plug samples of the 150 kDa band of NC, CAP and AR sperm samples after detection by mass spectrometry (MS) (Supplementary Table S2). MS analysis of CRISP2-pulldown eluates from NC, CAP and AR sperm samples revealed that CRISP2 was detected amongst the most abundant proteins in the eluate. In addition to CRISP2, we consistently detected the proteins acrosin, and acrosin binding protein (ACRBP) amongst the most abundant proteins within each sample group (Supplementary Table S2). Notably, in the capacitated sample, acrosin, ACRBP and CRISP2 were detected as the top four most abundant proteins in the pulldown, with their collective molecular weight ~150 kDa. Thus, we choose to further characterize these IDs as putative constituents of the 150 kDa complex shown in Figure 1A.

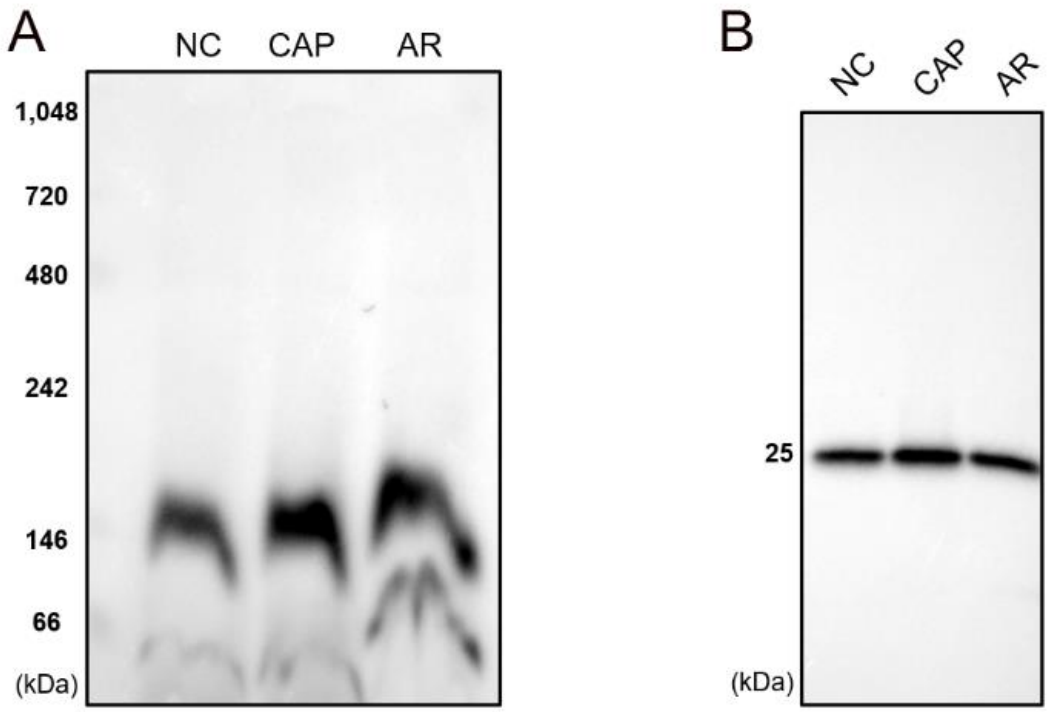

Figure 1. CRISP2 is involved in a ~150 kDa protein complex under native conditions. After incubation and washing, non-capacitated (NC), capacitated (CAP) and acrosome reacted (AR) sperm cells were lysed and prepared for blue native polyacrylamide gel electrophoresis (PAGE) and SDS-

PAGE. (A) Native blots on the lysates from NC, CAP and AR sperm cells probed with anti-CRISP2 antibody. (B) Lysates from NC, CAP and AR sperm cells were mixed with 4x SDS sample buffer, cooked and analyzed by western blots.

We reduced the list of IDs by comparing those obtained through the 150 kDa gel plugs with those obtained through CRISP2 immunoprecipitation. The common proteins that were consistently present using both techniques were ranked by abundance. The list revealed the presence of CRISP2, acrosin, and ACRBP thus providing credence for their further analysis. The top 12 proteins of this common protein list are represented and categorized based on their function in Table 1.

Table 1. Top 12 most abundant CRISP2 interacting partners identified by mass spectrometry in both excised CRISP2 native gel complexes and CRISP2 immunoprecipitation eluates.

Protein IDs	Protein name/**functional category**
	Acrosomal proteins
A0A287AFN9	Acrosin (ACR)
Q29016	Acrosin-binding protein, 60 kDa form (ACRBP)
	Spermadhesins
I7HJH6	AQN-3
Q4R0H8	AWN
	Protease-related
P26461	Sperm-associated acrosin inhibitor (AI)
A0A287BEN1	Serine protease inhibitor kazal-type 2 isoform 1 (SPINK2)
	Histones
A0A287A7G8	Histone H2B
P62802	Histone H4

	Chaperones and proteins with a mitochondrial function
A0A287ATN8	60 kDa chaperonin, 60 kDa heat shock protein, mitochondrial (HSPD1)
F1SMZ6	10 kDa chaperonin, 10 kDa heat shock protein, mitochondrial (HSPE1)
A0A287BPT0	Amine oxidase (IL4I1)
	Ubiquitin
P63053	Ubiquitin A-52 residue ribosomal protein fusion product 1 (UBA52)

Boar sperm acrosin and ACRBP co-immunoprecipitate with CRISP2

Next, the putative interactions between CRISP2 and acrosin/ACRBP were validated using biochemical techniques. Firstly, co-immunoprecipitation using the CRISP2 antibody resulted in detection of acrosin and ACRBP in the lysates of NC, CAP and AR sperm cells (Figure 2A). Immunoblotting analysis of CRISP2 co-immunoprecipitates (eluates) probed with the CRISP2 antibody repeatedly showed that CRISP2 was present in the pull-down products indicating an efficient isolation (Figure 2B, Figure S2B). Probing with the acrosin antibody revealed that proacrosin (~53 kDa) was consistently present in the three conditions, while acrosin (~35 kDa) interaction with CRISP2 was only observed after CAP and AR (Figure 2B). The ACRBP antibody used in our study was against the N-terminal part (aa 205-220) of the human ACRBP allowing it to recognize the ACRBP precursor or the fragments containing the N-terminal part but not the mature form (namely sp32) without the N-terminal half [37]. Application of this antibody confirmed its presence in all the three samples as well as in the CRISP2 pull-down products (Figure 2A and B).

Subcellular localization of acrosin and ACRBP in boar spermatozoa

To gain a better understanding of the biochemical features of acrosin and ACRBP in boar spermatozoa, western blots of the lysates from ejaculated whole sperm, purified sperm heads and sperm tails were isolated and analyzed. In parallel to the western blots of Figure 3

complimentary SDS-PAGE gels were stained with Coomassie brilliant blue to show the total protein loading for whole sperm and the head and tail subfractions (Figure S1B). The results showed that the ~53 kDa proacrosin was the predominant form present in the ejaculated boar spermatozoa (Figure 3A). Two bands corresponding to ~35 kDa and ~28 kDa acrosin were also observed in whole sperm. Immunoblots on the extracts from purified sperm head and tail populations revealed that the ~53 kDa proacrosin and ~35 kDa acrosin were the two major forms associated with sperm heads and tails (Figure 3A). Western blot analysis of ACRBP on the same samples showed that ACRBP was undetectable in the lysates from sperm heads, however, it was abundantly associated with the sperm tail fractions (Figure 3B).

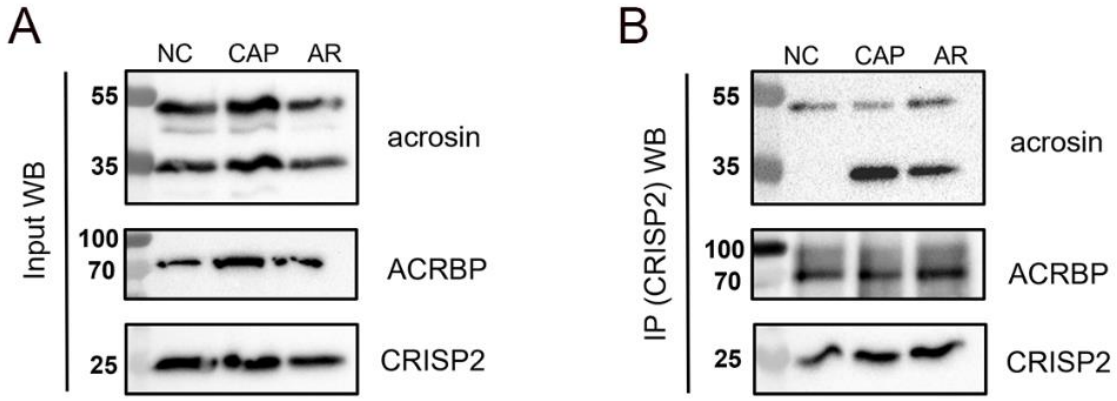

Figure 2. Validation of acrosin and ACRBP as CRISP2 interacting partners by western blots analysis of CRISP2 immunoprecipitation. CRISP2 antibody was cross linked to protein A/G magnetic beads and incubated with lysates from NC, CAP and AR sperm cells overnight at 4°C. After intensive washing, CRISP2 and CRISP2-associated proteins were disassociated from the magnetic beads. (A) Sperm lysates before incubation with the beads were saved and analyzed by western blots. (B) CRISP2 pull down products were analyzed by western blots probed with anti-acrosin, anti-ACRBP and anti-CRISP2 antibodies. Full western blots images were shown in Supplementary Figure S3.

The localization of acrosin and ACRBP in boar spermatozoa was further investigated by immunofluorescence microscopy. It showed that acrosin immunofluorescence was localized in the sperm acrosome (Figure 3C). Additionally, faint fluorescence was observed in the connecting piece and the principal piece of the sperm tail. Immunolocalization of ACRBP

showed that ACRBP fluorescence was present in the plasma membrane and the post-acrosomal region of the sperm head as well as the entire sperm tail (Figure 3D).

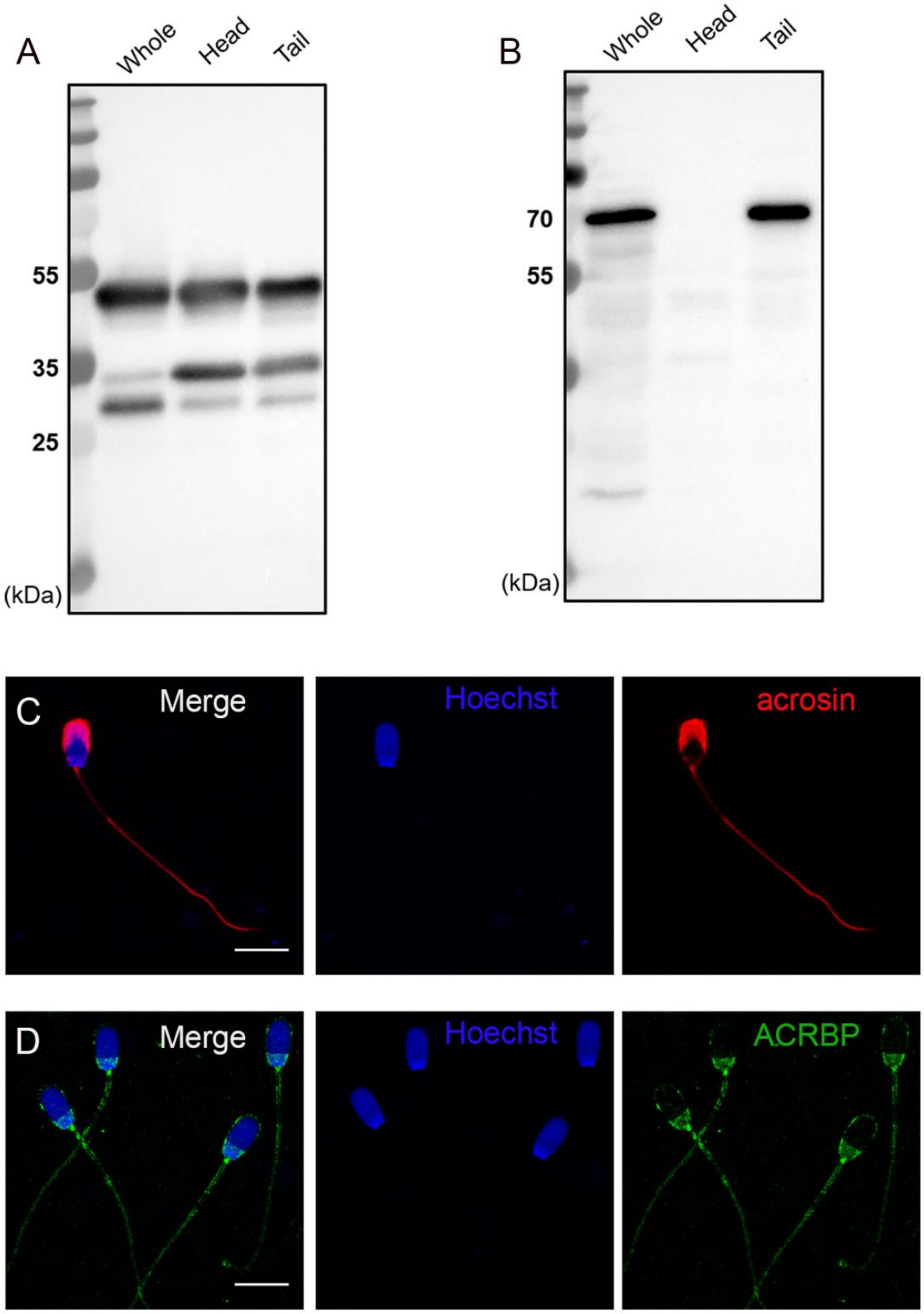

Figure 3. Subcellular localization of acrosin and ACRBP in boar spermatozoa. Western blots of acrosin (A) and ACRBP (B) on the lysates from whole sperm, sperm heads and tails. (C) Percoll washed sperm cells were fixed in -20 °C methanol for 5 min, incubated with anti-acrosin followed by Alexa Flour 568 conjugated secondary antibody (red), counterstained with Hoechst 33342 (blue). (B) Sperm cells were fixed in 4% paraformaldehyde (PFA) and permeabilized in cold acetone for 10 min, incubated with anti-ACRBP followed by Alexa Flour 488 conjugated secondary antibody (green) and counterstained with Hoechst 33342 (blue). Scale bar =10 μm.

CRISP2 colocalizes with acrosin and ACRBP in boar sperm

The conventional immunofluorescence analysis of CRISP2 was performed after 4% paraformaldehyde (PFA) fixation, followed by cold acetone permeabilization or after a fixation/permeabilization in methanol. The former method revealed a consistent staining pattern of CRISP2 in the post-acrosomal region, the connecting piece and the sperm tail in NC, CAP and AR populations (Figure 4A). However, methanol preparation of sperm resulted in additional labelling of the equatorial segment in all the sperm cells and faint fluorescence was also observed on the apical ridge of sperm head in NC and CAP sperm cells (Figure 4B). *In situ* colocalization of CRISP2 and acrosin was investigated by an indirect proximity ligation assay (PLA) in which the PLA probes were connected to the secondary antibodies. Fluorescent PNA was used to assess the acrosome integrity. CRISP2-acrosin interactions were reflected by red PLA signal and were found associated with the post-acrosomal region and the inner acrosome membrane in NC sperm and as discrete foci of colocalization across the acrosome of CAP sperm (Figure 5). PLA foci were also consistently present in the sperm tail (Figure 5). Colocalization of CRISP2 and ACRBP was performed via a direct PLA assay in which the PLA probes were linked to the primary antibodies [36]. Intense green fluorescent foci were observed over the anterior acrosome in NC sperm and these discrete foci of colocalization were translocated to the post acrosomal sheath region after CAP and AR incubation (Figure 6). The pattern of CRISP2 and ACRBP foci redistribution in NC, CAP and AR sperm cells was further

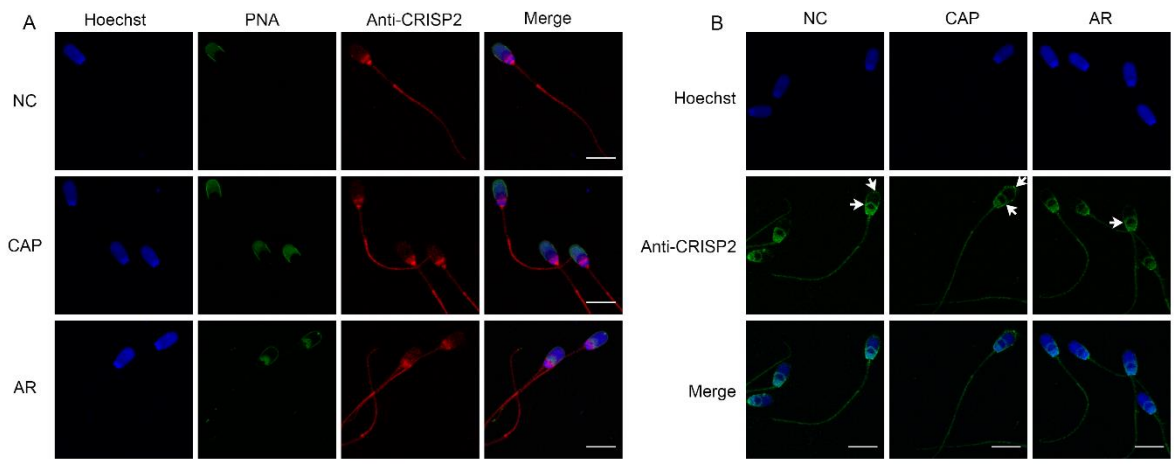

Figure 4. Immunolocalization of CRISP2. (A) NC, CAP and AR sperm cells were fixed in 4% PFA and permeabilized in cold acetone for 10 min, incubated with anti-CRISP2 followed by Alexa Flour 568 conjugated secondary antibody (red), counterstained with PNA (green) and Hoechst 33342 (blue). (B) Immunofluorescent staining of CRISP2 on sperm cells fixed in fixed in -20 °C methanol for 5 min, labelled with Alexa Flour 488 conjugated secondary antibody (green) and counterstained with Hoechst 33342 (blue). Arrows indicated additional CRISP2 signals were observed. Scale bar =10 µm.

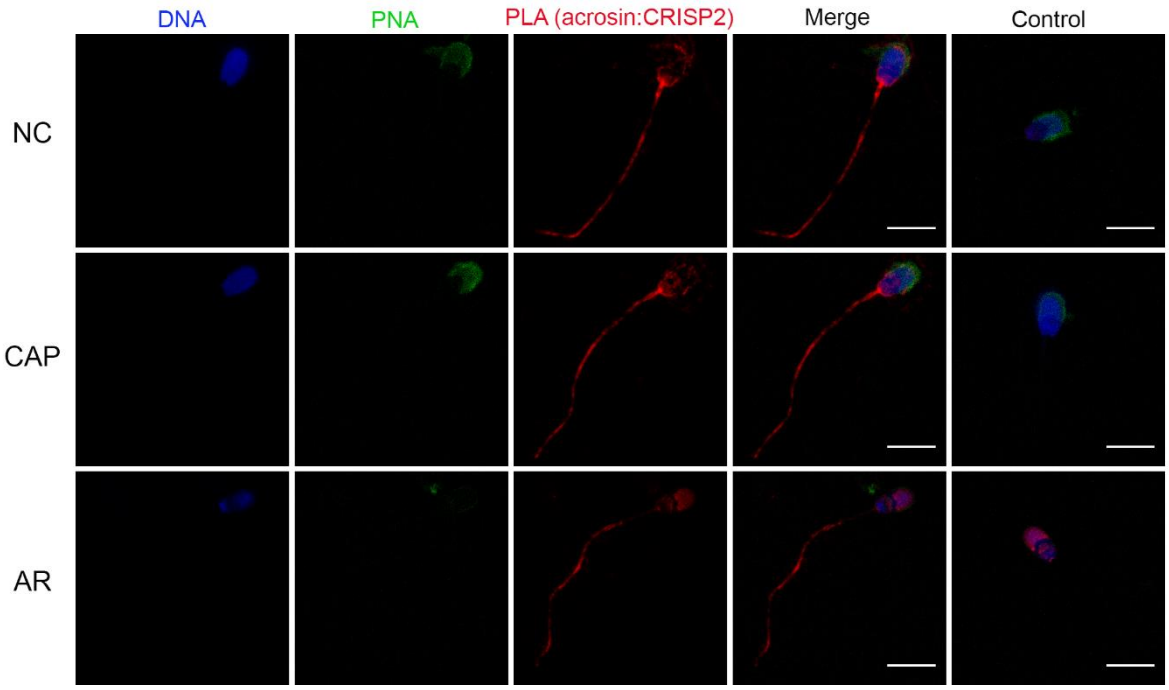

Figure 5. Colocalization of acrosin and CRISP2 via an in situ proximity ligation assay (PLA). NC, CAP and AR sperm cells were permeabilized in -20 °C methanol for 5 min, incubated with anti-acrosin and anti-CRISP2 antibodies, followed by appropriate secondary antibodies conjugated with

oligonucleotides. Sperm cells were counterstained with PNA (green) and Hoechst 33342 (blue). Primary antibodies were omitted in control. Scale bar =10 μm.

quantified (Table 2). Our data revealed that 87.7% of NC sperm have the green foci in the anterior acrosome, whereas 12.3% of the NC sperm have a labelling pattern in the post acrosomal sheath region. The percentage of sperm that have the foci redistribution to the post acrosomal sheath region was increased to 81.4% after capacitation and 85.5% after the acrosome reaction.

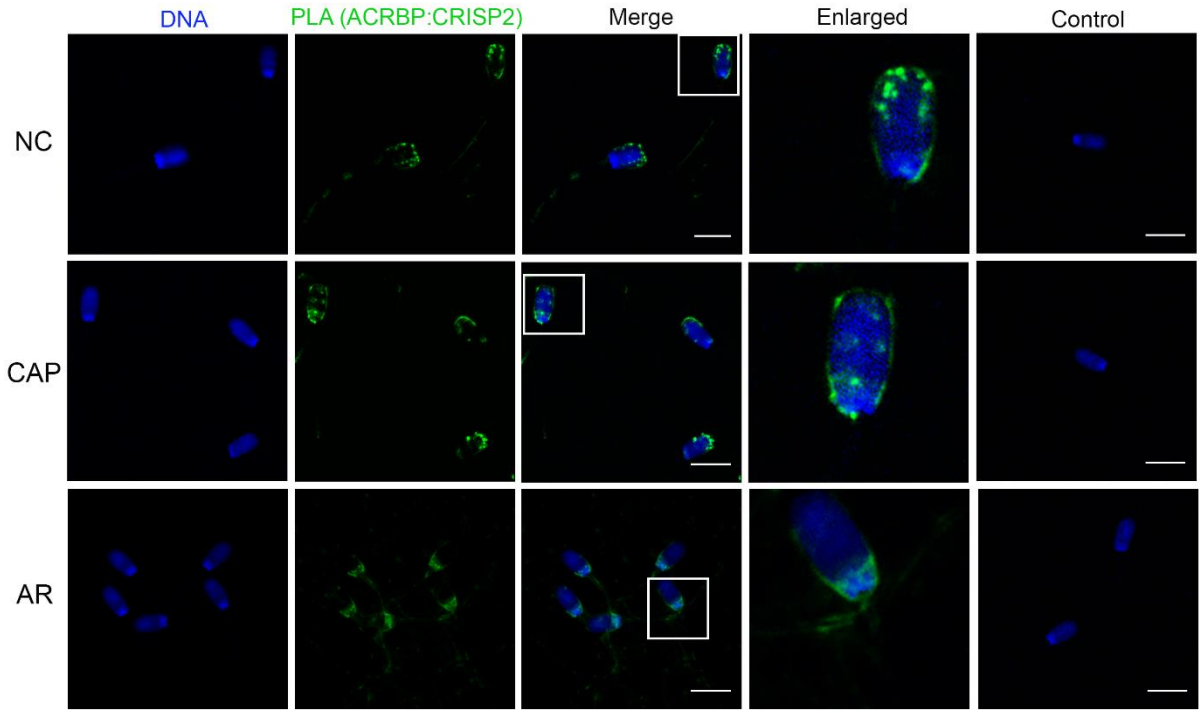

Figure 6. Colocalization of ACRBP and CRISP2 via PLA. Sperm cells were fixed in 4% PFA and permeabilized in cold acetone for 10 min, incubated with primary antibodies conjugated with oligonucleotides, counterstained with Hoechst 33342 (blue). Primary antibodies were omitted in control. Scale bar =10 μm.

Discussion

In this article, we demonstrated that boar sperm CRISP2 was consistently present in a ~150 kDa protein complex under native conditions, irrespective of the sperm functional status (NC, CAP or AR). The ~50 kDa band on native blots was likely a dimeric form of CRISP2. This

Table 2. Analysis of CRISP2-ACRBP foci redistribution within the sperm head from the anterior acrosome (AA) to the post-acrosomal sheath (PAS) region in NC, CAP and AR sperm groups.

Group	No. (%) Sperm show a AA staining pattern	No. (%) Sperm show a PAS staining pattern	No. Sperm examined
NC	265(87.7%)	37(12.3%)	302
CAP	60(18.6%)	263(81.4%)	323
AR	51(14.5%)	300(85.5%)	351

Semen from three different boars were pooled and washed for sperm *in vitro* incubation. This experiment was replicated twice. At least 150 sperm cells were counted for each group from one independent experiment.

property is a feature of other CAP proteins, for instance, Golgi-Associated plant Pathogenesis Related protein 1 (GAPR-1) is present as a dimer in solution [38]. Therefore, our data suggest that CRISP2 may function as a dimer within sperm. The dimerization of CRISP2 is likely to be the result of the conserved CAP domain [39]. We were interested in the isolated CRISP2 complex and sought to identify CRISP2-interacting proteins in boar sperm and investigate the colocalization of target proteins following capacitation and acrosome reaction. Proteomic analysis of the CRISP2 complex under native conditions as well as the eluate of a CRISP2-pull down showed that besides CRISP2, acrosin and acrosin binding protein (ACRBP) were detected as abundant proteins by both techniques and were highly abundant (Supplementary Table S2).

Characterization of acrosin and ACRBP in boar spermatozoa

Acrosin acts as a zona lysin during zona penetration and is not strictly necessary on its own for sperm zona penetration, given that acrosin-deficient mice and rats are fertile [40, 41]. While, sperm from acrosin deficient models exhibited delayed fertilization [41, 42]. However, in other species such as the golden hamster, acrosin-deficient sperm cannot achieve sperm-zona penetration [43]. Therefore, the exact role of acrosin in sperm-zona penetration events is not

yet clear. Other undefined proteases or proteins may compensate for the acrosin$^{-/-}$ phenotype during sperm-zona interaction. Acrosin is localized inactively in the sperm acrosome as a soluble constituent as well as in a particulate fraction forming the acrosomal matrix [16, 44]. Evidence indicates that acrosin is also associated with acrosomal membranes [44, 45]. Biochemically, acrosin is detected as proacrosin (~53-55 kDa), intermediate forms (~45-49 kDa), mature acrosin (~35 kDa) and other forms [46, 47]. In our study, we demonstrated that the ~53 kDa proacrosin form was the predominant form in the extracts of boar spermatozoa. Interestingly, we also observed that a sizeable portion of proacrosin and mature acrosin was associated with the sperm head fractions. A similar phenomenon has been reported for bull sperm acrosin [45]. Surprisingly, proacrosin and acrosin were also found with the sperm tail fractions and it appeared that the ~53 kDa proacrosin was the major form. Immunofluorescent signals of anti-acrosin in the sperm tail supported our immunoblotting results. In fact, previous proteomic analysis of human and pig sperm tails also demonstrates that acrosin contributes to the sperm tail proteome [33, 48]. The detection of acrosin immunofluorescence in the sperm tail was made possible by a rather harsh permeabilization method which led to exposure of the antigen epitope. Immunoblots of extracts from CAP and AR sperm showed no obvious conversion of ~53 kDa proacrosin into ~35 kDa acrosin following CAP and AR treatments. This may be explained by the autocatalytic mechanism of proacrosin which can undergo auto cleavage into other forms of acrosin after solubilization from the sperm cells [49, 50]. Additionally, and in line with our results, a previous study in rabbit sperm revealed that the bulk of proacrosin remained unprocessed during capacitation and the calcium ionophore A23187 induced acrosome reaction [51].

Porcine ACRBP is synthesized as a precursor and processed into a mature form (sp32) by removal of the N-terminal half of the ACRBP [52]. sp32 has been intensively investigated

because it is a major protein which is phosphorylated during capacitation [53] and involved in sperm-zona interaction [54]. Moreover, sp32 phosphorylation levels correlate with the conversation of proacrosin into mature acrosin [55]. However, the fate of sperm ACRBP after ejaculation is barely studied. The present study has focused on the biochemical features of boar sperm ACRBP after ejaculation using an antibody against the central part of N-terminal sequence. Our results demonstrate that the precursor ACRBP was still present in ejaculated boar spermatozoa and associated with the sperm tail fractions after sonication. Immunostaining of ACRBP indicated the localization of ACRBP in the plasma membrane as well as the post-acrosomal region of the sperm head. This indicates that the absence of ACRBP on the immunoblots of sperm head fractions was likely caused by sonication. Consistent with our study, Zigo et al., report the localization of boar ACRBP in the post-acrosomal region and the midpiece of the sperm [56]. Specifically, in addition to the wild type Acrbp mRNA expressed in pig, human and guinea pig, there exists another intron 5-retaining variant Acrbp mRNA termed ACRBP-V5 in mice [37]. ACRBP-V5 is essential for packaging of proacrosin into acrosomal granules for normal acrosome formation during early spermiogenesis and ACRBP retains proacrosin inactively in the acrosome until acrosomal exocytosis [57]. It is still unclear how ACRBP is processed into sp32 due to the fact that ACRBP itself doesn’t have a strong consensus site for convertase cleavage and ACRBP does not undergo proteolytic processing in proprotein convertase 4 (PCSK4) null mice [58]. ACRBP processing into sp32 may be regulated by other yet unknown proteases. Thus, we propose that a population of ACRBP is likely not processed into sp32 during epididymal maturation. Instead, this ACRBP population is probably stabilized by interacting with other proteins or by other post-translational modifications, for example phosphorylation, as occurred to the sp32 during capacitation [53].

Colocalization of CRISP2 target proteins in boar sperm

Immunoprecipitation blots showed that the ~53 kDa proacrosin was consistently present in CRISP2 pull-down products from the lysates of NC, CAP and AR sperm cells. Interestingly, the absence of ~35 kDa acrosin in CRISP2 precipitates from the lysates of NC sperm cells and emerging in CRISP2 precipitates from the lysates of CAP and AR sperm cells indicates that the interaction between CRISP2 and the ~35 kDa acrosin is an event associated with capacitation. The fact that ~35 kDa acrosin was present in total lysates of NC sperm cells excludes the possibility that CRISP2 interacted with the ~35 kDa acrosin produced by autocatalytic reaction of the ~53 kDa proacrosin. On the contrary, it suggests that there was indeed an efficient conversion of ~53 kDa proacrosin into ~35 kDa acrosin during capacitation and the acrosome reaction. Limited by the imaging technology, we could not define the precise subcellular localization of the CRISP2-acrosin complex *in situ*. However, the CRISP2-acrosin signal was dispersed in the acrosome during capacitation. It is possible that the CRISP2-acrosin complex is involved in the paracrystalline patches that are present in the acrosomal matrix [16]. The consistent localization of CRISP2-acrosin complexes in the sperm tail corresponded to the presence of ~53 kDa proacrosin in the immunoblots of CRISP2 precipitates. In line with this, the ~53 kDa proacrosin was the predominant form associated with sperm tail fractions. CRISP2 might function in retaining the ~53 kDa proacrosin inactively in the sperm tail thereby providing an explanation for the stiffness of the midpiece in Crisp2$^{-/-}$ sperm [25].

Our findings that acrosomal proteins interact with CRISP2 may suggest that perinuclear theca proteins (the site of CRISP2) can interact with acrosomal proteins in spermatozoa. Consistent with this hypothesis, a robust study on another perinuclear theca protein, calicin, demonstrated an interaction with inner acrosomal membrane and nuclear envelope proteins [59]. Likewise, the identification that mitochondrial functional proteins can interact with CRISP2 may indicate that the ODF proteins are also interacting with mitochondrial proteins. The interaction of the

ODF with the mitochondria in the midpiece has been recently reported for sperm from pigs and other mammalian species [60]. Notably, in the list of the most abundant proteins identified in the CRISP2 eluate and native gel plugs, two molecular chaperones were also identified which have been shown associated with human sperm during capacitation and may be involved in sperm-ZP interaction [61].

In addition to the proteomic identification of proteins that were present in the CRISP2 positive protein complexes, it is important to realize that due to the condensed nature of protein structures in mature sperm cells, numerous additional minor proteins were detected. Both the excised 150 kDa band as well as CRISP2 co-immuno precipitates may contain proteins that are not directly interacting with CRISP2 and are detected due to the high sensitivity of mass spectrometry and low accuracy of gel band extraction. The fact that two independent CRISP2 complex isolation techniques led to the identification of a similar CRISP2 interactome is validating, however, all interacting proteins of interest require extensive biochemical validation as we have performed here for acrosin and ACRBP.

In summary, this study has identified ACRBP and acrosin as novel CRISP2 interacting partners in boar sperm. We have shown that the interaction between the target proteins was dynamic following capacitation suggesting that CRISP2 complexes play roles during capacitation. Our prior study implies that CRISP2 forms distinct protein complexes dependent on cysteine oxidation and oligomerization of the CAP domain regulated by Zn^{2+} [23]. CRISP2 uses both pathways scaffolding itself as well as other proteins contributing to the condensed structures of mammalian spermatozoa. In the future, the role of CRISP2 as a scaffolding protein in the formation of protein complexes important for fertilization should be further explored. Altogether these discoveries enhance and expand the roles of CRISP2 as a protein that is

involved in protein complex formation and dissociation, thus in sperm function and in the fertilization process.

Data Availability Statement

The mass spectrometry proteomics data in the study have been deposited to the ProteomeXchange Consortium via the PRIDE partner repository with the dataset identifier PXD037181.

Acknowledgements

The authors gratefully thank the Center of Cell Imaging in the Faculty of Veterinary Medicine at Utrecht University and the expertise of Dr. R. Wubbolts and Ing. E. van ‘t Veld.

Funding

MZ is financed by the China Scholarship Council (CSC) (No. 201606170117). EB is recipient of an NHMRC CJ Martin Early Career Fellowship (APP1138701). The proteomics analysis was done by RC at the Netherlands Proteomics Centre and partially financed by the National Roadmap for Large-Scale Research Infrastructure of the Dutch Research Council NWO through the X-omics Road Map program (Project 184.034.019 to AH) and the EU Horizon 2020 program Epic-XS (Project 823839 to RC and AH).

Conflict of interest

The authors have no conflict of interests to disclose.

Author contributions

MZ performed the experiments, wrote the draft of the manuscript and contributed to figure preparation and manuscript editing. RC conducted experiments, contributed to analysis of the raw data and reviewed the manuscript. EB analyzed the data, contributed to figure preparation and manuscript revision. AH contributed to the data collection, resource provision and manuscript revision. JH contributed to supervision, provided resources and reviewed the

manuscript. BG conceived of the study, contributed to manuscript preparation, revision and editing and supervision.

References

1. Chang MC. Fertilizing capacity of spermatozoa deposited into the fallopian tubes. Nature 1951; 168:697-698.
2. Austin CR. The capacitation of the mammalian sperm. Nature 1952; 170:326.
3. Stival C, Puga Molina Ldel C, Paudel B, Buffone MG, Visconti PE, Krapf D. Sperm Capacitation and Acrosome Reaction in Mammalian Sperm. Adv Anat Embryol Cell Biol 2016; 220:93-106.
4. Visconti PE, Krapf D, de la Vega-Beltrán JL, Acevedo JJ, Darszon A. Ion channels, phosphorylation and mammalian sperm capacitation. Asian J Androl 2011; 13:395-405.
5. Gadella BM, Tsai PS, Boerke A, Brewis IA. Sperm head membrane reorganisation during capacitation. Int J Dev Biol 2008; 52:473-480.
6. Boerke A, Tsai PS, Garcia-Gil N, Brewis IA, Gadella BM. Capacitation-dependent reorganization of microdomains in the apical sperm head plasma membrane: functional relationship with zona binding and the zona-induced acrosome reaction. Theriogenology 2008; 70:1188-1196.
7. Tumova L, Zigo M, Sutovsky P, Sedmikova M, Postlerova P. Ligands and Receptors Involved in the Sperm-Zona Pellucida Interactions in Mammals. Cells 2021; 10.
8. Kongmanas K, Kruevaisayawan H, Saewu A, Sugeng C, Fernandes J, Souda P, Angel JB, Faull KF, Aitken RJ, Whitelegge J, Hardy D, Berger T, et al. Proteomic Characterization of Pig Sperm Anterior Head Plasma Membrane Reveals Roles of Acrosomal Proteins in ZP3 Binding. J Cell Physiol 2015; 230:449-463.
9. van Gestel RA, Brewis IA, Ashton PR, Helms JB, Brouwers JF, Gadella BM. Capacitation-dependent concentration of lipid rafts in the apical ridge head area of porcine sperm cells. Mol Hum Reprod 2005; 11:583-590.
10. Bou Khalil M, Chakrabandhu K, Xu H, Weerachatyanukul W, Buhr M, Berger T, Carmona E, Vuong N, Kumarathasan P, Wong PT, Carrier D, Tanphaichitr N. Sperm capacitation induces an increase in lipid rafts having zona pellucida binding ability and containing sulfogalactosylglycerolipid. Dev Biol 2006; 290:220-235.
11. Tsai PS, Garcia-Gil N, van Haeften T, Gadella BM. How pig sperm prepares to fertilize: stable acrosome docking to the plasma membrane. PLoS One 2010; 5:e11204.
12. Tsai PS, Brewis IA, van Maaren J, Gadella BM. Involvement of complexin 2 in docking, locking and unlocking of different SNARE complexes during sperm capacitation and induced acrosomal exocytosis. PLoS One 2012; 7:e32603.
13. Zanetti N, Mayorga LS. Acrosomal swelling and membrane docking are required for hybrid vesicle formation during the human sperm acrosome reaction. Biol Reprod 2009; 81:396-405.
14. Foster JA, Gerton GL. The Acrosomal Matrix. Adv Anat Embryol Cell Biol 2016; 220:15-33.
15. Buffone MG, Foster JA, Gerton GL. The role of the acrosomal matrix in fertilization. Int J Dev Biol 2008; 52:511-522.
16. Leung MR, Ravi RT, Gadella BM, Zeev-Ben-Mordehai T. Membrane Remodeling and Matrix Dispersal Intermediates During Mammalian Acrosomal Exocytosis. Front Cell Dev Biol 2021; 9:765673.

17. Bi M, Hickox JR, Winfrey VP, Olson GE, Hardy DM. Processing, localization and binding activity of zonadhesin suggest a function in sperm adhesion to the zona pellucida during exocytosis of the acrosome. Biochem J 2003; 375:477-488.
18. Inoue N, Ikawa M, Nakanishi T, Matsumoto M, Nomura M, Seya T, Okabe M. Disruption of mouse CD46 causes an accelerated spontaneous acrosome reaction in sperm. Mol Cell Biol 2003; 23:2614-2622.
19. Gibbs GM, Roelants K, O'Bryan MK. The CAP superfamily: cysteine-rich secretory proteins, antigen 5, and pathogenesis-related 1 proteins--roles in reproduction, cancer, and immune defense. Endocr Rev 2008; 29:865-897.
20. Foster JA, Gerton GL. Autoantigen 1 of the guinea pig sperm acrosome is the homologue of mouse Tpx-1 and human TPX1 and is a member of the cysteine-rich secretory protein (CRISP) family. Mol Reprod Dev 1996; 44:221-229.
21. Busso D, Cohen DJ, Hayashi M, Kasahara M, Cuasnicú PS. Human testicular protein TPX1/CRISP-2: localization in spermatozoa, fate after capacitation and relevance for gamete interaction. Mol Hum Reprod 2005; 11:299-305.
22. O'Bryan MK, Sebire K, Meinhardt A, Edgar K, Keah HH, Hearn MT, De Kretser DM. Tpx-1 is a component of the outer dense fibers and acrosome of rat spermatozoa. Mol Reprod Dev 2001; 58:116-125.
23. Zhang M, Bromfield EG, Veenendaal T, Klumperman J, Helms JB, Gadella BM. Characterization of different oligomeric forms of CRISP2 in the perinuclear theca versus the fibrous tail structures of boar spermatozoa†. Biol Reprod 2021; 105:1160-1170.
24. Gibbs GM, Scanlon MJ, Swarbrick J, Curtis S, Gallant E, Dulhunty AF, O'Bryan MK. The cysteine-rich secretory protein domain of Tpx-1 is related to ion channel toxins and regulates ryanodine receptor Ca2+ signaling. J Biol Chem 2006; 281:4156-4163.
25. Lim S, Kierzek M, O’Connor AE, Brenker C, Merriner DJ, Okuda H, Volpert M, Gaikwad A, Bianco D, Potter D, Prabhakar R, Strünker T, et al. CRISP2 Is a Regulator of Multiple Aspects of Sperm Function and Male Fertility. Endocrinology 2019; 160:915-924.
26. Jimenez-Gonzalez C, Michelangeli F, Harper CV, Barratt CL, Publicover SJ. Calcium signalling in human spermatozoa: a specialized 'toolkit' of channels, transporters and stores. Hum Reprod Update 2006; 12:253-267.
27. Publicover S, Harper CV, Barratt C. [Ca2+]i signalling in sperm--making the most of what you've got. Nat Cell Biol 2007; 9:235-242.
28. Gibbs GM, Bianco DM, Jamsai D, Herlihy A, Ristevski S, Aitken RJ, Kretser DM, O'Bryan MK. Cysteine-rich secretory protein 2 binds to mitogen-activated protein kinase kinase kinase 11 in mouse sperm. Biol Reprod 2007; 77:108-114.
29. Jamsai D, Bianco DM, Smith SJ, Merriner DJ, Ly-Huynh JD, Herlihy A, Niranjan B, Gibbs GM, O'Bryan MK. Characterization of gametogenetin 1 (GGN1) and its potential role in male fertility through the interaction with the ion channel regulator, cysteine-rich secretory protein 2 (CRISP2) in the sperm tail. Reproduction 2008; 135:751-759.
30. Jamsai D, Rijal S, Bianco DM, O'Connor AE, Merriner DJ, Smith SJ, Gibbs GM, O'Bryan MK. A novel protein, sperm head and tail associated protein (SHTAP), interacts with cysteine-rich secretory protein 2 (CRISP2) during spermatogenesis in the mouse. Biol Cell 2009; 102:93-106.
31. Bernecic NC, Zhang M, Gadella BM, Brouwers J, Jansen JWA, Arkesteijn GJA, de Graaf SP, Leahy T. BODIPY-cholesterol can be reliably used to monitor cholesterol efflux from capacitating mammalian spermatozoa. Sci Rep 2019; 9:9804.
32. Krstic J, Reinisch I, Schindlmaier K, Galhuber M, Riahi Z, Berger N, Kupper N, Moyschewitz E, Auer M, Michenthaler H, Nössing C, Depaoli MR, et al. Fasting improves therapeutic response in hepatocellular carcinoma through p53-dependent metabolic synergism. Sci Adv 2022; 8:eabh2635.

33. Zhang M, Chiozzi RZ, Skerrett-Byrne DA, Veenendaal T, Klumperman J, Heck AJR, Nixon B, Helms JB, Gadella BM, Bromfield EG. High Resolution Proteomic Analysis of Subcellular Fractionated Boar Spermatozoa Provides Comprehensive Insights Into Perinuclear Theca-Residing Proteins. Front Cell Dev Biol 2022; 10:836208.
34. Faron-Górecka A, Szlachta M, Kolasa M, Solich J, Górecki A, Kuśmider M, Żurawek D, Dziedzicka-Wasylewska M. Understanding GPCR dimerization. Methods Cell Biol 2019; 149:155-178.
35. Hegazy M, Cohen-Barak E, Koetsier JL, Najor NA, Arvanitis C, Sprecher E, Green KJ, Godsel LM. Proximity Ligation Assay for Detecting Protein-Protein Interactions and Protein Modifications in Cells and Tissues in Situ. Curr Protoc Cell Biol 2020; 89:e115.
36. Söderberg O, Gullberg M, Jarvius M, Ridderstråle K, Leuchowius KJ, Jarvius J, Wester K, Hydbring P, Bahram F, Larsson LG, Landegren U. Direct observation of individual endogenous protein complexes in situ by proximity ligation. Nat Methods 2006; 3:995-1000.
37. Kanemori Y, Ryu JH, Sudo M, Niida-Araida Y, Kodaira K, Takenaka M, Kohno N, Sugiura S, Kashiwabara S, Baba T. Two functional forms of ACRBP/sp32 are produced by pre-mRNA alternative splicing in the mouse. Biol Reprod 2013; 88:105.
38. Serrano RL, Kuhn A, Hendricks A, Helms JB, Sinning I, Groves MR. Structural analysis of the human Golgi-associated plant pathogenesis related protein GAPR-1 implicates dimerization as a regulatory mechanism. J Mol Biol 2004; 339:173-183.
39. Sheng J, Olrichs NK, Gadella BM, Kaloyanova DV, Helms JB. Regulation of Functional Protein Aggregation by Multiple Factors: Implications for the Amyloidogenic Behavior of the CAP Superfamily Proteins. Int J Mol Sci 2020; 21.
40. Baba T, Azuma S, Kashiwabara S, Toyoda Y. Sperm from mice carrying a targeted mutation of the acrosin gene can penetrate the oocyte zona pellucida and effect fertilization. J Biol Chem 1994; 269:31845-31849.
41. Isotani A, Matsumura T, Ogawa M, Tanaka T, Yamagata K, Ikawa M, Okabe M. A delayed sperm penetration of cumulus layers by disruption of acrosin gene in rats. Biol Reprod 2017; 97:61-68.
42. Adham IM, Nayernia K, Engel W. Spermatozoa lacking acrosin protein show delayed fertilization. Mol Reprod Dev 1997; 46:370-376.
43. Hirose M, Honda A, Fulka H, Tamura-Nakano M, Matoba S, Tomishima T, Mochida K, Hasegawa A, Nagashima K, Inoue K, Ohtsuka M, Baba T, et al. Acrosin is essential for sperm penetration through the zona pellucida in hamsters. Proc Natl Acad Sci U S A 2020; 117:2513-2518.
44. Bozzola JJ, Polakoski K, Haas N, Russell LD, Campbell P, Peterson RN. Localization of boar sperm proacrosin during spermatogenesis and during sperm maturation in the epididymis. Am J Anat 1991; 192:129-141.
45. Ferrer M, Rodriguez H, Zara L, Yu Y, Xu W, Oko R. MMP2 and acrosin are major proteinases associated with the inner acrosomal membrane and may cooperate in sperm penetration of the zona pellucida during fertilization. Cell Tissue Res 2012; 349:881-895.
46. Peknicová J, Moos J. Monoclonal antibodies against boar acrosomal antigens labelling undamaged acrosomes of spermatozoa in immunofluorescence test. Andrologia 1990; 22:427-435.
47. Polakoski KL, Parrish RF. Boar proacrosin. Purification and preliminary activation studies of proacrosin isolated from ejaculated boar sperm. J Biol Chem 1977; 252:1888-1894.
48. Amaral A, Castillo J, Estanyol JM, Ballescà JL, Ramalho-Santos J, Oliva R. Human sperm tail proteome suggests new endogenous metabolic pathways. Mol Cell Proteomics 2013; 12:330-342.
49. Zahler WL, Polakoski KL. Benzamidine as an inhibitor of proacrosin activation in bull sperm. Biochim Biophys Acta 1977; 480:461-468.

50. Zahn A, Furlong LI, Biancotti JC, Ghiringhelli PD, Marijn-Briggiler CI, Vazquez-Levin MH. Evaluation of the proacrosin/acrosin system and its mechanism of activation in human sperm extracts. J Reprod Immunol 2002; 54:43-63.
51. Sillerico T, Valdivia M, de Ioannes A, Barros C. Proacrosin and acrosin determination during capacitation and acrosome reaction in rabbit spermatozoa. Biocell : official journal of the Sociedades Latinoamericanas de Microscopia Electronica ... et. al 1996; 20:133-142.
52. Baba T, Niida Y, Michikawa Y, Kashiwabara S, Kodaira K, Takenaka M, Kohno N, Gerton GL, Arai Y. An acrosomal protein, sp32, in mammalian sperm is a binding protein specific for two proacrosins and an acrosin intermediate. J Biol Chem 1994; 269:10133-10140.
53. Dubé C, Leclerc P, Baba T, Reyes-Moreno C, Bailey JL. The proacrosin binding protein, sp32, is tyrosine phosphorylated during capacitation of pig sperm. J Androl 2005; 26:519-528.
54. Kato Y, Kumar S, Lessard C, Bailey JL. ACRBP (Sp32) is involved in priming sperm for the acrosome reaction and the binding of sperm to the zona pellucida in a porcine model. PloS one 2021; 16:e0251973.
55. Sun PL, Yang LX, Cui JJ, Tian Y, Liu Y, Jin Y. Activation of proacrosin accompanies upregulation of sp32 protein tyrosine phosphorylation in pig sperm. Genet Mol Res 2013; 12:6579-6587.
56. Zigo M, Manaskova-Postlerova P, Jonakova V, Kerns K, Sutovsky P. Compartmentalization of the proteasome-interacting proteins during sperm capacitation. Sci Rep 2019; 9:12583.
57. Kanemori Y, Koga Y, Sudo M, Kang W, Kashiwabara S, Ikawa M, Hasuwa H, Nagashima K, Ishikawa Y, Ogonuki N, Ogura A, Baba T. Biogenesis of sperm acrosome is regulated by pre-mRNA alternative splicing of Acrbp in the mouse. Proc Natl Acad Sci U S A 2016; 113:E3696-3705.
58. Tardif S, Guyonnet B, Cormier N, Cornwall GA. Alteration in the processing of the ACRBP/sp32 protein and sperm head/acrosome malformations in proprotein convertase 4 (PCSK4) null mice. Mol Hum Reprod 2012; 18:298-307.
59. Zhang X-Z, Wei L-L, Jin H-J, Zhang X-H, Chen S-R. The perinuclear theca protein Calicin helps shape the sperm head and maintain the nuclear structure in mice. Cell Reports 2022; 40:111049.
60. Leung MR, Zenezini Chiozzi R, Roelofs MC, Hevler JF, Ravi RT, Maitan P, Zhang M, Henning H, Bromfield EG, Howes SC, Gadella BM, Heck AJR, et al. In-cell structures of conserved supramolecular protein arrays at the mitochondria-cytoskeleton interface in mammalian sperm. Proc Natl Acad Sci U S A 2021; 118.
61. Mitchell LA, Nixon B, Aitken RJ. Analysis of chaperone proteins associated with human spermatozoa during capacitation. Mol Hum Reprod 2007; 13:605-613.

Supplementary materials

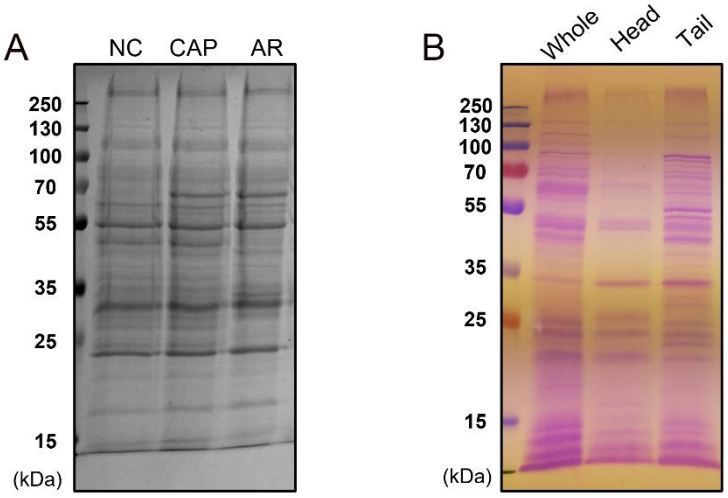

Supplementary figure S1. Same amount sperm cells were lysed in the same volume buffer and the same amount lysates were loaded on SDS-PAGE gels. (A) Lysates from NC, CAP and AR sperm cells were analyzed by SDS-PAGE and coomassie blue staining. (B) Lysates from whole sperm cells/head/tail fractions were analyzed by SDS-PAGE and Coomassie blue staining.

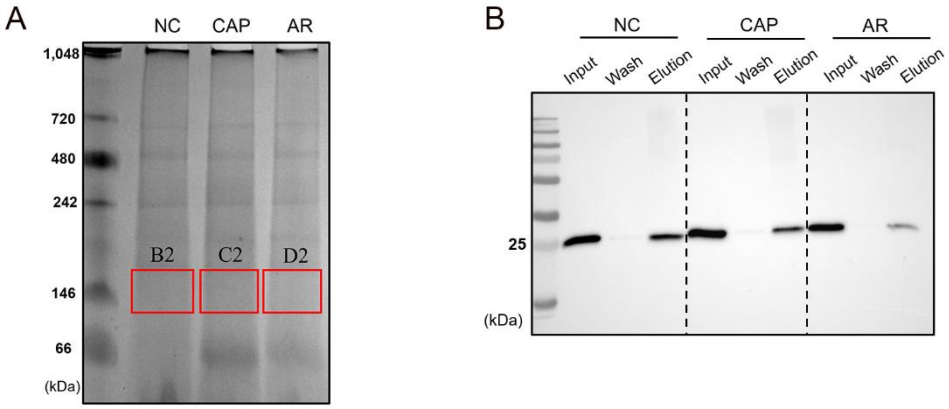

Supplementary figure S2. (A) Blue native PAGE analysis on the lysates from NC, CAP and AR sperm cells. Gels in red tangle box (~150 kDa) were carefully sliced and prepared for MS analysis. (B) Validation of CRISP2 by western blots analysis on CRISP2 precipitates before MS analysis.

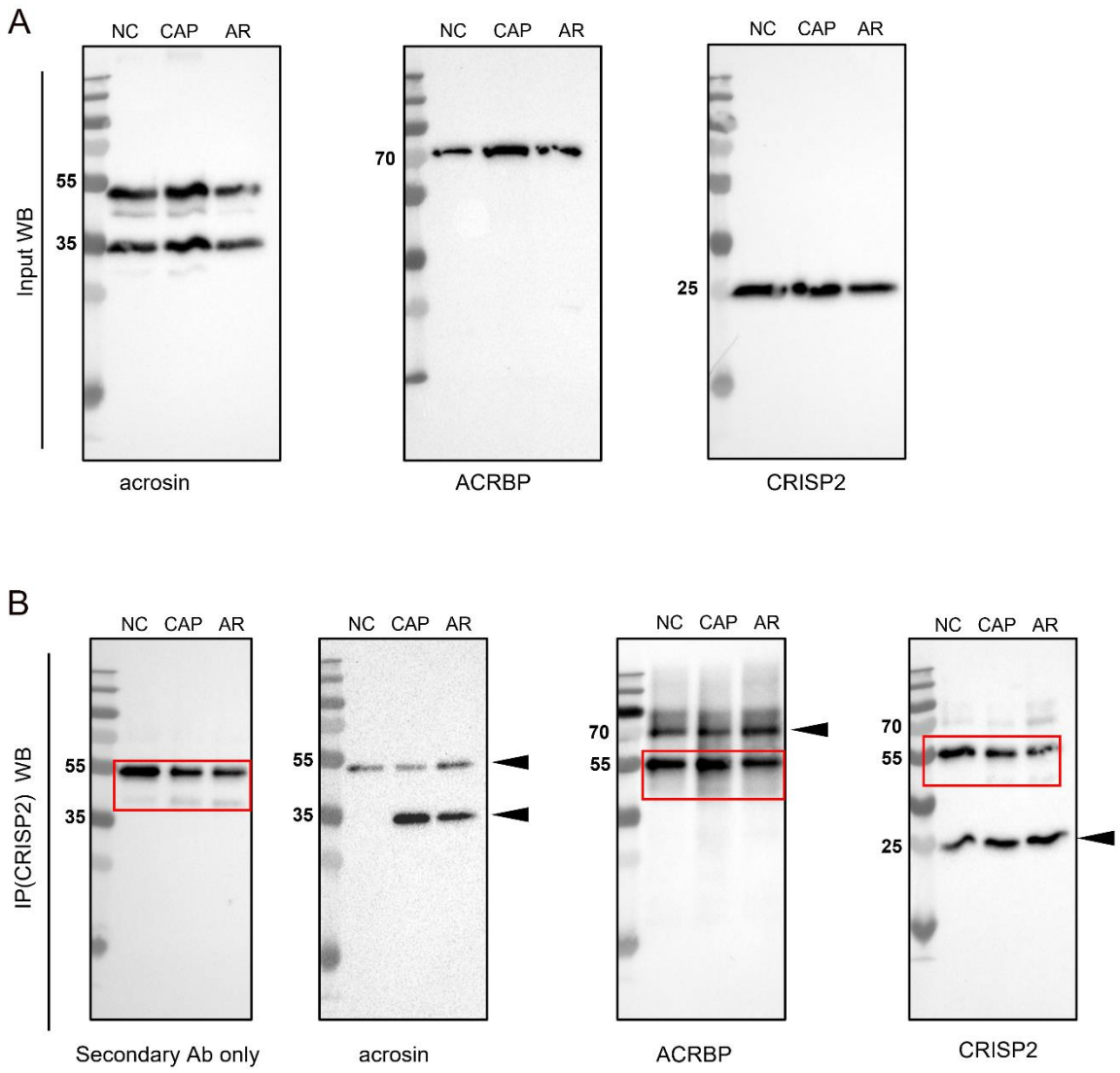

Supplementary figure S3. Full western blots images corresponding to Figure 2. In Figure S3B, blots were incubated with secondary antibody only and bands in red tangle box indicated small contamination from primary antibody. Black arrows indicated the expected protein bands corresponding to input western blots.

Supplementary Table S1. List of primary and secondary antibodies used in experiments. WB indicates western blot; IF indicates Immunofluorescence; IIF indicates Indirect Immunofluorescence.

Primary antibodies	Supplier	Species	Type	Dilution		Reference
				WB	IIF	
CRISP2	Proteintech	rabbit	polyclonal	1:1000	1:100	19066–1-A
acrosin (ACR-2)	Thermo Scientific	mouse	monoclonal	1:1000	1:100	MA1-19180
ACRBP	antibodies-online	rabbit	polyclonal	1:500	1:50	ABIN5618703
PNA Alexa Fluor 488	Thermo Scientific	peanut		5 μg/ml (IF)		L21409

Secondary antibodies	**Supplier**	**Dilution**
Goat anti rabbit HRP	Jackson	1:5000
Goat anti mouse HRP	Jackson	1:5000
Goat anti rabbit Alexa Fluor 488	Thermo Scientific	1:100
Goat anti rabbit Alexa Fluor 568	Thermo Scientific	1:100
Goat anti mouse Alexa Fluor 568	Thermo Scientific	1:100

Supplementary Table S2 is available via the following link:
file://UU069626/Users/Zhang067/OneDrive%20-%20Universiteit%20Utrecht/Min/Min%20Zhang/Supplementary%20Table%20S2.xlsx

Chapter 6

Summarizing discussion

Introduction to mammalian CRISPs

Over the past 30 years, mammalian cysteine rich secretory proteins (CRISPs) have been investigated due to their biased expression in the male reproductive system. With the introduction of new gene editing technologies, single, double and multiple Crisp gene knockout mice models have recently been generated and studied [1-9]. These studies demonstrated that CRISPs are indispensable for male fertility. Each CRISP protein participates in multiple steps during fertilization process and contributes different roles to reach optimal male fertility. Most mammals have three types of CRISPs named CRISP1, CRISP2 and CRISP3, respectively. Some rodents express an additional member, CRISP4, which is derived from the same gene as CRISP1 [10]. CRISPs are synthesized during spermiogenesis, secreted during epididymal maturation and upon ejaculation. The first type, CRISP1/CRISP4, is secreted by the epididymal epithelium into the lumen of the epididymal duct and adhere there to the sperm surface during epididymal maturation. The second type, CRISP2, is the sole CRISP form that is exclusively expressed in spermatids, is only expressed in the testis, and remains intracellularly present in elongating spermatids and spermatozoa. The third type, CRISP3, is secreted from the seminal vesicles or the prostate glands into the seminal plasma. Although general functional overlap between different types of the CRISPs and a compensatory mechanism has been proposed [3, 8], CRISP2 (testis) and CRISP3 (accessory secretory male sex glands) hold specialized functions that can not be compensated by epididymal CRISP1/CRISP4. Moreover, CRISP2 is the only type of CRISP that is located inside sperm and is not secreted into extracellular fluids while the other three types, CRISP1/3/4, are secreted either from the epithelia of the epididymal duct or from the seminal vesicles and/or prostate glands into seminal fluids. Thus, CRISP2 is not only unique in originating from the testis, but also in that it has an intracellular localization. On the other hand, the three other types of CRISP, CRISP1/3/4, may become adhered to the sperm surface during epididymal maturation and/or ejaculation. A Crisp2 mutation results in a

stiffness of the flagellum [2, 3, 7] with adverse effects on the development of hyper activate motility and proper migration through the female tract [3]. Nonetheless, the molecular mechanisms underlying the resulting fertility defects are still elusive. By studying CRISP2 in a porcine model, our goal is to gain more knowledge about the functional roles of mammalian CRISP2 in the fertilization process. CRISP2, like the other types of CRISP, are known to interact with proteins to form protein complexes. Two domains in CRISP2 can contribute to protein oligomerization: (i) The cysteine rich domain containing 10 cysteine residues can under oxidation of free sulfhydryl groups form intra- and inter- molecular disulfide bridges [10]; (ii) The CAP domain can form protein oligomers in a Zn^{2+} dependent manner [11, 12]. Both domains of CRISP2 can be involved in protein complex formation that are apparent in the dense protein structures typically present in the sperm cells (see **chapter 1**) and thus are involved in proper sperm function.

Forming the condensed structures of mammalian spermatozoa

Mammalian sperm carry a variety of highly condensed insoluble protein structures in the nucleus, the acrosome, the perinuclear theca (PT) and in the accessory structures of the sperm tail (see **chapter 1**). These condensed protein structures provide allow progressive sperm movements, to prepare the sperm cell to find, bind and fertilize an egg. Late testicular spermatids are transcriptionally silenced and thus spermatozoa have seized *de novo* protein synthesis. Therefore, protein post-translational modifications (PTMs) and surface exchange of proteins drive functional changes of the sperm during its voyage towards the to be fertilized oocyte. Both cysteine oxidation/disulfide bond formation as well as the interaction with Zn^{2+} are important for affecting enzyme activity, protein complexes formation ,and protein solubility [13].

Cysteine oxidation and Zn^{2+} dependent protein oligomerization

Cysteine oxidation has been reported to occur for sperm chromatin compaction as well as for the generation of progressive sperm motility during epididymal transit [14]. CRISPs are rich in cysteine residues with 10 cysteines clustered in the CRISP domain and 6 in the CAP domain [12, 15]. All these cysteine residues can be involved in disulfide bond formation. In **chapter 2**, we characterized the different oligomeric forms of CRISP2 in the fibrous tail structures versus the PT of sperm head. Immunogold labelling on ultra-sections of boar spermatozoa revealed that CRISP2 was localized in the post-acrosomal sheath (PAS)-PT and was present in reduction-sensitive complexes in the sperm head fractions. CRISP2 was also present in multimers that were resistant to SDS and β-mercapto-ethanol treatment. The SDS stable and β-mercapto-ethanol insensitive properties were reported in a non-mammalian CRISP protein which lacks the ion channel regulatory (ICR) domain [16]. Further ultrastructural localization showed that CRISP2 was present in the outer dense fibers (ODFs) and the fiber sheath (FS) of the sperm tail. The location of CRISP2 to the fibrous tail structures is conserved among human [17], rat [18], mouse [19]. The insoluble characteristics of these condensed structures as a scaffold may resemble restricting the disassociation of identical proteins. This is in line with fiber structures that are still present after prolonged treatments with reducing agents [20]. In addition, the amyloidogenic propensity of the CAP domain as other CAP proteins [10-12] may contribute to the insolubility of CRISP2 as has been observed for both CRISP2 and other CAP family members [11, 21]. Metal ions are well-known inducers of protein oligomerization and the CAP domain is capable of binding divalent cations [22-24]. In support of this, prior studies have shown that Zn^{2+} induces the oligomerization of mouse CRISP2 and human CRISP1 *in vitro* [11, 12]. Notably, Zn^{2+} is an important metal cation for a normal functioning male reproduction system. Zn^{2+} deficiency results in severe testis damage and inhibits spermatogenesis [25-27]. Extracellular Zn^{2+} concentrations are progressively increasing within the male reproductive tract and there is an overall uptake of Zn^{2+} from germ cells to

spermatozoa [28]. Zn^{2+} concentrations in epididymal spermatozoa are higher than in testicular spermatozoa. However, these concentrations are still much lower than in ejaculated spermatozoa. High Zn^{2+} concentrations are also found in seminal fluids [29-31] and epididymal spermatozoa can load extracellular Zn^{2+} rapidly under *in vitro* experimental conditions [28]. In line with this, many Zn^{2+} transporter proteins (ZIPs) are expressed from spermatogonia to spermatozoa and show different compartmental distributions [28, 32, 33]. Thus, the intracellular Zn^{2+} patterns are changing at the different stages of sperm cell maturation [28]. The local concentration of Zn^{2+} is high enough in the ODFs of testicular spermatozoa for a -SH-Zn-SH complex formation. This complex may be functional to prevent pre-oxidation during spermiogenesis [34]. However, during epidydimal maturation there is an obvious lower Zn^{2+} content in the flagellum which allows oxidation of sulfhydryl groups and stiffening the ODFs to develop potential progressive motility [34, 35]. The progressive motility subsequently develops into a hyper-activated movement during capacitation at the site of fertilization and is a driving force for sperm migration in the female tract and penetration the egg coats [36, 37]. The fact that both ejaculated and epidydimal spermatozoa from Crisp2$^{-/-}$ mice, exhibit a stiff flagellum [3, 7] suggests that flagellar Zn^{2+} levels might be altered due to dysregulation of Zn^{2+} uptake or elimination. As a consequence, the ODFs are incapable of developing the progressive motility during epidydimal transit.

Fate of sperm structures before and after fertilization

Zn^{2+} also acts as a functional reversible regulator in sperm chromatin condensation and decondensation. It is believed that -SH-Zn-SH bridges are formed between protamine thiols of cysteine during epididymal transit [38], which are important for compaction of adjacent chromatin fibers and for protection of DNA from potential damages during the journey to fertilize the egg. Reversibly, Zn^{2+} removal form those -SH-Zn-SH bridges is necessary for sperm chromatin decondensation soon after fertilization to form a male pronucleus. *In vitro*

studies showed that Zn^{2+} chelation by ethylene diamine tetra acetate (EDTA) induced rapid decondensation of chromatin of ejaculated spermatozoa [39-41]. It has been questioned why Zn^{2+} removal did not result in oxidation of thiols into disulfide bonds as occurred in tail structures. The removal of Zn^{2+} in the oocyte's cytosol has been proposed to be relevant for decondensation of sperm chromatin [38].

Intrigued by our findings in chapter 2 that CRISP2 was localized in the PAS-PT of the sperm head as β-mercapto-ethanol sensitive protein complexes and the emerging functional roles of PAS-PT post fertilization, in **chapter 3**, we investigated the fate of CRISP2 from the PT before and after fertilization. The PAS-PT houses functional molecules necessary for oocyte activation. Two well characterized candidates for oocyte activation are phospholipase C zeta 1 (PLCz1/PLCζ) and post-acrosomal WW domain-binding protein (PAWP). Both proteins are present in the PT and have been demonstrated to induce Ca^{2+} oscillations within the oocyte [42-44]. The essential role of PLCζ was confirmed in Plcz1 deficient mice [45] as well as in human patients with fertility failure due to a mutation in PLCζ [46, 47]. The PAS-PT is the first internal sperm structure to be solubilized in the ooplasm [48, 49]. The observation that only spermatozoa displaying dispersal of the PT are capable of activating the oocyte after microinjection [48, 50], indicates that solubilization/disassociation of the PAS-PT is an initial step. Our finding, that CRISP2 was dispersed rapidly from the PAS-PT prior to any signs of sperm nucleus decondensation raises the possibility that reduction of disulfide bridges of cysteines in the cysteine rich domain and/or removal of Zn^{2+} in the CAP domain of CRISP2 is the way to initiate protein dissociation from the PAS-PT (Figure 1). Glutathion-transferase omega 2 (GSTO2) was also found in the PAS-PT of mammalian spermatozoa [51]. GSTO2 is a member of the omega class of glutathione-S-transferase (GST) enzymes, GSTO2 possesses basic glutathione (GSH) reductase activity. However, GSTO2 has been reported to have higher dehydroascorbate (DHA)

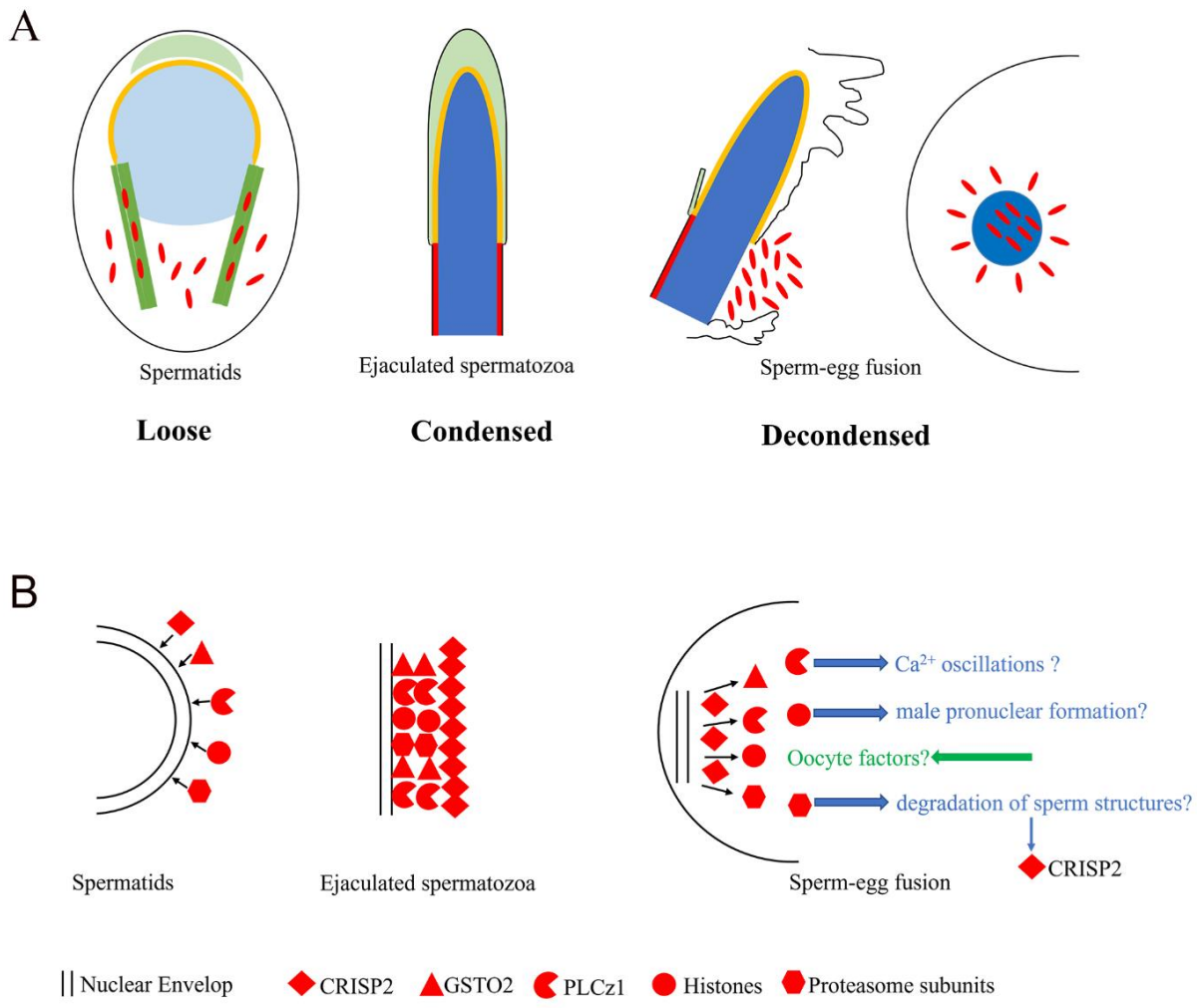

Figure 1. Hypothetical model for the fate of PAS-PT from spermatids via sperm into the oocyte. (A) During spermatogenesis, PAS proteins (red ovals) are condensing to the manchette (green rectangle) at the periphery of the nuclear envelope into the PAS region. Ejaculated spermatozoa have condensed PAS-PT structures. The condensed PAS proteins are liberated rapidly after fertilization, when sperm structures are introduced in the cytosol of the oocyte. Some of the liberated PAS proteins are involved in male pronucleus formation and oocyte activation. (B) Identified PAS proteins such as CRISP2 [52], GSTO2 [53], PLCz1 [43], core histones [54], proteasome subunits [55] are attracted to the spermatid's nuclear envelop during spermatogenesis. These PAS proteins form a packed protein matrix in ejaculated spermatozoa. Soon after sperm-egg fusion, the reductive power of the oocyte's cytosol reduces the disulfide bridges between cysteine residues so that CRISP2 and other PAS proteins dissociate from the PAS structure. In addition to the CRISP domain of CRISP2 which contains 10 cysteine residues can under oxidation of free sulfhydryl groups form disulfide bridges, the CAP domain of CRISP2 has a conserved Zn^{2+} binding domain which is involved in additional protein oligomerization [11]. Post-fertilization changes in Zn^{2+} [56] may thus provide additional changes in the condensation of PAS structure. Some of the liberated PAS proteins may be involved in activating the oocyte Ca^{2+} oscillation

(PLCz1), male pronuclear formation (core histones), and degradation of sperm structures (proteasome subunits).

reductase activity than GSH itself [57-59]. Therefore, ascorbic acid (AA) levels are crucial for GSTO2 to exert its role as a protective antioxidant [58]. The GSH pathway is not active when sperm GSTO2 is packed in an insoluble protein layer, so the availability of local GSH in the PAS-PT is highly limited. The recruitment of GSH from the oocytes seems plausible, since GSH is actively present in the ooplasm and participates also in the male pronucleus formation [60, 61]. Our study in **chapter 3** also indicates that CRISP2 of the PAS-PT is eliminated before a male pronucleus is formed. This finding implies that the dispersal and degradation of the PAS-PT is essential for the subsequent sperm nuclear chromatin decondensation in order to form the male pronucleus (Figure 1). In fact, failure in sperm DNA decondensation and male pronucleus formation coincides with the retainment of a condensed intact PT in a sperm cells after its introduction into an oocyte via intracytoplasmic sperm injection (ICSI) [49]. Therefore, persistence of PT structure would cause a delay in sperm DNA decondensation to form a male pronucleus.

In **chapter 4** we identified the composition of PT from boar spermatozoa using a quantitative, label-free liquid chromatography mass spectrometry (LC-MS/MS) approach. We identified 813 proteins within the PT and confirmed the presence of previously characterized PT proteins by others including the two favored oocyte activation factors, PLCζ [45, 62] and PAWP [63], GSTO2 [53] as well as Calicin [64], Cylicin2 [65], Ras-related protein Rab-2A (RAB2A) [66], Actin-related proteins (ARPT1&T2) [67] and the core histones subunits (H2A, H2B, H3 and H4) [54, 68]. Surprisingly, by using Ingenuity Pathway Analysis (IPA) software (Qiagen), we identified a fertilization related and CRISP2 involving protein network which was enriched in the PT proteome as compared to the sperm head proteome. Additionally, the PT proteome also

supported several functions related to “metabolism and production of reactive oxygen species”, “autophagy”, “amyloidosis”, “homeostasis of metal ions”, “endoplasmic reticulum (ER) stress response in cells” and several functions associated with neurodegenerative diseases including “Huntington disease” and “Alzheimer disease”. Common dominators for these functions and relations to diseases are “protein aggregation” and “cellular stress”. A proteomic study on the identification Zn^{2+} interacting proteins from in vitro capacitated boar sperm showed that Zn^{2+} interacting proteins were mostly associated with Huntington’s and Parkinson’s diseases [69]. Recently, a review proposed that spermatozoa can serve as a non-traditional model for studying Huntington disease [70]. Moreover, we identified an enriched cluster of spliceosome-related proteins within the PT as compared to the sperm head and tail proteome. Numerous neurological diseases have been linked to splicing defects [71, 72]. In fact, the human brain and testis share the highest numbers of common shared expressed proteins comparing to other body tissues [73]. Several classical neuronal signaling pathways are associated with sperm functionality [74]. For example, human neurons and sperm share characteristics of the exocytosis process [73]. Our proteome study on the sperm PT also provides references of common proteins and functional protein association networks that are shared with neurons. Additionally, our study in **chapter 4** describes the enrichment of proteasome subunits clustered within PT proteome. Proteasomes have been shown to be present in mammalian spermatozoa and the ubiquitin proteasome system (UPS) is involved in sperm capacitation [75], acrosome reaction, and sperm-zona interaction processes [76, 77]. Importantly, the UPS and autophagy were shown to participate in degradation of the sperm mitochondria after *in vitro* porcine fertilization [78]. Based on the enriched proteasome subunits in the PT, we speculate that the UPS is responsible for PT structure degradation after fertilization. Further experiments on the validation of the formation of functional proteasomes out of the PT proteasome subunits as well as their subsequent role in degradation of PT structures are required.

Given the protein composition of the PT described in **chapter 4**, we aimed to identify proteins that were interacting with CRISP2, as is described in **chapter 5** of this thesis. This identification was done by examination of CRISP2-immunoreactive bands from blue native gels and detecting proteins that co-immunoprecipitated with CRISP2 using mass spectrometry. Previous studies have identified several CRISP2 binding proteins by screening the adult mouse testis. These include cation channel of sperm 1 (CatSper1) [79], mitogen-activated protein kinase kinase kinase 11 (MAP3K11) [80], gametogenetin 1 (GGN1) [81] and sperm head and tail-associated protein (SHTAP) [19]. We identified acrosin and acrosin binding protein (ACRBP) as novel CRISP2 interacting proteins. We also investigated their interaction upon capacitation and ionophore A23187 induced acrosome reaction via *in situ* proximity ligation assays. The fluorescent colocalization foci of CRISP2 and ACRBP colocalization were redistributed from the anterior acrosome to the post acrosomal sheath region during capacitation. The interaction of CRISP2 and ACRBP appears to be associated with the capacitation process since interaction foci remained present in the post-acrosomal region after acrosome reaction. The CRISP2-acrosin interaction signal was dispersed in the acrosome during capacitation and could only be observed after very harsh permeabilization method, showing the presence of acrosin in the acrosomal matrix [82]. It is likely that the CRISP2-acrosin complex is involved in the structure of paracrystalline patches that are present in the acrosomal matrix [83]. Additionally, our data also revealed a list of potentially interacting candidates that are functionally categorized into spermadhesins, protease inhibitors, core histones, chaperons, proteins with a mitochondrial function and ubiquitin. Biochemical validation of these interacting protein candidates is required. Nonetheless, our data suggest that CRISP2 might play multiple roles in sperm function and the fertilization process.

Future perspectives

This thesis investigates the dynamics of (i) the formation of dense protein structures during spermiogenesis and epididymal sperm maturation (**chapter 1**); (ii) The presence of CRISP2 in these dense protein structures (**chapter 2**); (iii) The rapid dispersal of CRISP2, thus of the PT post fertilization (**chapter 3**); (iv) The composition of PT including CRISP2 (**chapter 4**); and (v) the functional proteins interacting with CRISP2 (**chapter 5**). It is clear that the ejaculated sperm are showing most robust and condensed state of the dense protein structures. This is ergonomically important for creating a minimal volume of well protected chromatin in the sperm head, a concentrated enzyme matrix for sperm-zona penetration in the acrosome. Condensed structures are also present in the sperm flagellum which has unique flexibility and metabolic properties. These properties can be adjusted to proper sperm motility characteristics during sperm maturation in the epididymis as well as during capacitation in the oviduct (or during IVF treatment). Both the formation of the dense protein structures in the testis and in the epididymal environments as well as the decondensation of these dense protein structures during post-fertilization events deserve further attention with special emphasis on the role of CRISP2 in (de)condensation dynamics (for a model of the function of CRISP2 in this context see Figure 1).

The oocyte shows her capacity to transform gametes into an embryo when ICSI is applied for human infertility treatments, especially caused by severe male factors. The oocyte is able to degrade sperm structures and recycling genomic substances to form pronucleus. Remarkably, the oocyte can even repair fragmented paternal DNA after fertilization [84]. It has been demonstrated that ooplasmic ubiquitin-like autophagy receptor sequestosome 1 (SQSTM1) is recruited for sperm mitophagy [78]. A cell free system, in which de-membraned spermatozoa were incubated with oocyte extracts, confirmed ooplasmic SQSTM1 binding to sperm mitochondria [85]. The decondensation of the PT by the ooplasm (**chapter 3**) is highlighted at

the end of this thesis because the PT proteins detected in **chapter 4** are likely to be co-liberated from this structure and to function in the oocyte locally at the site where sperm structures must be processed. The sperm cell may bring factors into the oocyte that are involved in proteolysis (all functional proteasome subunits are detected in the PT) or even help the oocyte in proper processing of the highly condensed protamine sperm DNA toroids to form the male pronucleus [54]. In order to study this process into further detail, we suggest to use a cell free system [85] that can be modified to screen for diverse purposes: (i) for oocyte markers that can be potentially used to predict the oocyte capacity of coping with sperm structures post fertilization; and (ii) how liberated sperm proteins from the PT may aid mitophagy, proteolysis and sperm DNA processes that occur rapidly and locally at the site of fertilization within the oocyte. Such knowledge is instrumental to understand the molecular bases of mammalian fertilization and the role of CRISP2 in the biological relevant processes.

References

1. Brukman NG, Miyata H, Torres P, Lombardo D, Caramelo JJ, Ikawa M, Da Ros VG, Cuasnicú PS. Fertilization defects in sperm from Cysteine-rich secretory protein 2 (Crisp2) knockout mice: implications for fertility disorders. Mol Hum Reprod 2016; 22:240-251.
2. Lim S, Kierzek M, O'Connor AE, Brenker C, Merriner DJ, Okuda H, Volpert M, Gaikwad A, Bianco D, Potter D. CRISP2 is a regulator of multiple aspects of sperm function and male fertility. Endocrinology 2019; 160:915-924.
3. Curci L, Brukman NG, Weigel Muñoz M, Rojo D, Carvajal G, Sulzyk V, Gonzalez SN, Rubinstein M, Da Ros VG, Cuasnicu PS. Functional redundancy and compensation: Deletion of multiple murine Crisp genes reveals their essential role for male fertility. The FASEB Journal 2020; 34:15718-15733.
4. Hu J, Merriner DJ, O'Connor AE, Houston BJ, Furic L, Hedger MP, O'Bryan MK. Epididymal cysteine-rich secretory proteins are required for epididymal sperm maturation and optimal sperm function. Mol Hum Reprod 2018; 24:111-122.
5. Da Ros VG, Maldera JA, Willis WD, Cohen DJ, Goulding EH, Gelman DM, Rubinstein M, Eddy EM, Cuasnicu PS. Impaired sperm fertilizing ability in mice lacking Cysteine-RIch Secretory Protein 1 (CRISP1). Dev Biol 2008; 320:12-18.
6. Volpert M, Furic L, Hu J, O'Connor AE, Rebello RJ, Keerthikumar S, Evans J, Merriner DJ, Pedersen J, Risbridger GP, McIntyre P, O'Bryan MK. CRISP3 expression drives prostate cancer invasion and progression. Endocr Relat Cancer 2020; 27:415-430.
7. Gaikwad AS, Nandagiri A, Potter DL, Nosrati R, O'Connor AE, Jadhav S, Soria J, Prabhakar R, O'Bryan MK. CRISPs Function to Boost Sperm Power Output and Motility. Front Cell Dev Biol 2021; 9:693258.
8. Carvajal G, Brukman NG, Weigel Muñoz M, Battistone MA, Guazzone VA, Ikawa M, Haruhiko M, Lustig L, Breton S, Cuasnicu PS. Impaired male fertility and abnormal epididymal epithelium differentiation in mice lacking CRISP1 and CRISP4. Sci Rep 2018; 8:17531.
9. Turunen HT, Sipilä P, Krutskikh A, Toivanen J, Mankonen H, Hämäläinen V, Björkgren I, Huhtaniemi I, Poutanen M. Loss of cysteine-rich secretory protein 4 (Crisp4) leads to deficiency in sperm-zona pellucida interaction in mice. Biol Reprod 2012; 86:1-8.
10. Gaikwad AS, Hu J, Chapple DG, O'Bryan MK. The functions of CAP superfamily proteins in mammalian fertility and disease. Hum Reprod Update 2020; 26:689-723.
11. Sheng J, Olrichs NK, Geerts WJ, Li X, Rehman AU, Gadella BM, Kaloyanova DV, Helms JB. Zinc binding regulates amyloid-like aggregation of GAPR-1. Biosci Rep 2019; 39.
12. Sheng J, Gadella BM, Olrichs NK, Kaloyanova DV, Helms JB. The less conserved metal-binding site in human CRISP1 remains sensitive to zinc ions to permit protein oligomerization. Sci Rep 2021; 11:5498.
13. Lehti MS, Sironen A. Formation and function of sperm tail structures in association with sperm motility defects. Biol Reprod 2017; 97:522-536.
14. O'Flaherty C, Matsushita-Fournier D. Reactive oxygen species and protein modifications in spermatozoa. Biol Reprod 2017; 97:577-585.
15. Gibbs GM, Roelants K, O'bryan MK. The CAP superfamily: cysteine-rich secretory proteins, antigen 5, and pathogenesis-related 1 proteins—roles in reproduction, cancer, and immune defense. Endocrine reviews 2008; 29:865-897.
16. Sugiyama H, Burnett L, Xiang X, Olson J, Willis S, Miao A, Akema T, Bieber AL, Chandler DE. Purification and multimer formation of allurin, a sperm chemoattractant from Xenopus laevis egg jelly. Mol Reprod Dev 2009; 76:527-536.

17. Busso D, Cohen DJ, Hayashi M, Kasahara M, Cuasnicú PS. Human testicular protein TPX1/CRISP-2: localization in spermatozoa, fate after capacitation and relevance for gamete interaction. Mol Hum Reprod 2005; 11:299-305.
18. O'Bryan MK, Sebire K, Meinhardt A, Edgar K, Keah HH, Hearn MT, De Kretser DM. Tpx-1 is a component of the outer dense fibers and acrosome of rat spermatozoa. Mol Reprod Dev 2001; 58:116-125.
19. Jamsai D, Rijal S, Bianco DM, O'Connor AE, Merriner DJ, Smith SJ, Gibbs GM, O'Bryan MK. A novel protein, sperm head and tail associated protein (SHTAP), interacts with cysteine-rich secretory protein 2 (CRISP2) during spermatogenesis in the mouse. Biol Cell 2009; 102:93-106.
20. Henkel R, Stalf T, Miska W. Isolation and partial characterization of the outer dense fiber proteins from human spermatozoa. Biol Chem Hoppe Seyler 1992; 373:685-689.
21. Sheng J, Olrichs NK, Gadella BM, Kaloyanova DV, Helms JB. Regulation of Functional Protein Aggregation by Multiple Factors: Implications for the Amyloidogenic Behavior of the CAP Superfamily Proteins. Int J Mol Sci 2020; 21.
22. Darwiche R, Kelleher A, Hudspeth EM, Schneiter R, Asojo OA. Structural and functional characterization of the CAP domain of pathogen-related yeast 1 (Pry1) protein. Sci Rep 2016; 6:28838.
23. Assumpção TCF, Ma D, Schwarz A, Reiter K, Santana JM, Andersen JF, Ribeiro JMC, Nardone G, Yu LL, Francischetti IMB. Salivary antigen-5/CAP family members are Cu2+-dependent antioxidant enzymes that scavenge O_2–. and inhibit collagen-induced platelet aggregation and neutrophil oxidative burst. J Biol Chem 2013; 288:14341-14361.
24. Maldera JA, Vasen G, Ernesto JI, Weigel-Muñoz M, Cohen DJ, Cuasnicu PS. Evidence for the involvement of zinc in the association of CRISP1 with rat sperm during epididymal maturation. Biol Reprod 2011; 85:503-510.
25. Merker HJ, Günther T. Testis damage induced by zinc deficiency in rats. J Trace Elem Med Biol 1997; 11:19-22.
26. Mason KE, Burns WA, Smith JC, Jr. Testicular damage associated with zinc deficiency in pre- and postpubertal rats: response to zinc repletion. J Nutr 1982; 112:1019-1028.
27. Yamaguchi S, Miura C, Kikuchi K, Celino FT, Agusa T, Tanabe S, Miura T. Zinc is an essential trace element for spermatogenesis. Proc Natl Acad Sci U S A 2009; 106:10859-10864.
28. Foresta C, Garolla A, Cosci I, Menegazzo M, Ferigo M, Gandin V, De Toni L. Role of zinc trafficking in male fertility: from germ to sperm. Hum Reprod 2014; 29:1134-1145.
29. Colagar AH, Marzony ET, Chaichi MJ. Zinc levels in seminal plasma are associated with sperm quality in fertile and infertile men. Nutr Res 2009; 29:82-88.
30. Srivastava A, Chowdhury AR, Setty BS. Testicular regulation and sub-cellular distribution of zinc in the epididymis and vas deferens of rhesus monkey (Macaca mulatta). Acta Endocrinol (Copenh) 1986; 113:440-449.
31. Saito S, Zeitz L, Bush IM, Lee R, Whitmore WF, Jr. Zinc content of spermatozoa from various levels of canine and rat reproductive tracts. Am J Physiol 1967; 213:749-752.
32. Zhu X, Yu C, Wu W, Shi L, Jiang C, Wang L, Ding Z, Liu Y. Zinc transporter ZIP12 maintains zinc homeostasis and protects spermatogonia from oxidative stress during spermatogenesis. Reprod Biol Endocrinol 2022; 20:17.
33. Protic I, Golic I, Vidakovic S, Korac B, Korac A. Heterogeneous Immunolocalisation of Zinc Transporters ZIP6, ZIP10 and ZIP14 in Human Normo- and Asthenozoospermic Spermatozoa. Current Issues in Molecular Biology 2022; 44:3444-3454.
34. Henkel R, Baldauf C, Bittner J, Weidner W, Miska W. Elimination of zinc from the flagella of spermatozoa during epididymal transit is important for motility. Reproductive Technology 2001; 10:280-285.

35. Henkel R, Bittner J, Weber R, Hüther F, Miska W. Relevance of zinc in human sperm flagella and its relation to motility. Fertil Steril 1999; 71:1138-1143.
36. Harayama H. Flagellar hyperactivation of bull and boar spermatozoa. Reprod Med Biol 2018; 17:442-448.
37. Suarez SS, Dai XB, DeMott RP, Redfern K, Mirando MA. Movement characteristics of boar sperm obtained from the oviduct or hyperactivated in vitro. J Androl 1992; 13:75-80.
38. Björndahl L, Kvist U. Human sperm chromatin stabilization: a proposed model including zinc bridges. Mol Hum Reprod 2010; 16:23-29.
39. Rodriguez H, Ohanian C, Bustos-Obregon E. Nuclear chromatin decondensation of spermatozoa in vitro: a method for evaluating the fertilizing ability of ovine semen. Int J Androl 1985; 8:147-158.
40. Gopalkrishnan K, Hinduja IN, Kumar TC. In vitro decondensation of nuclear chromatin of human spermatozoa: assessing fertilizing potential. Arch Androl 1991; 27:43-50.
41. Kvist U, Afzelius BA, Nilsson L. THE INTRINSIC MECHANISM OF CHROMATIN DECONDENSATION AND ITS ACTIVATION IN HUMAN SPERMATOZOA*. Development, Growth & Differentiation 1980; 22:543-554.
42. Aarabi M, Balakier H, Bashar S, Moskovtsev SI, Sutovsky P, Librach CL, Oko R. Sperm-derived WW domain-binding protein, PAWP, elicits calcium oscillations and oocyte activation in humans and mice. Faseb j 2014; 28:4434-4440.
43. Saunders CM, Larman MG, Parrington J, Cox LJ, Royse J, Blayney LM, Swann K, Lai FA. PLC zeta: a sperm-specific trigger of Ca(2+) oscillations in eggs and embryo development. Development 2002; 129:3533-3544.
44. Mejía-Flores I, Chiquete-Félix N, Palma-Lara I, Uribe-Carvajal S, de Lourdes Juárez-Mosqueda M. During capacitation in bull spermatozoa, actin and PLC-ζ undergo dynamic interactions. Zygote 2017; 25:558-566.
45. Hachem A, Godwin J, Ruas M, Lee HC, Ferrer Buitrago M, Ardestani G, Bassett A, Fox S, Navarrete F, de Sutter P, Heindryckx B, Fissore R, et al. PLCζ is the physiological trigger of the Ca(2+) oscillations that induce embryogenesis in mammals but conception can occur in its absence. Development 2017; 144:2914-2924.
46. Kashir J, Jones C, Lee HC, Rietdorf K, Nikiforaki D, Durrans C, Ruas M, Tee ST, Heindryckx B, Galione A, De Sutter P, Fissore RA, et al. Loss of activity mutations in phospholipase C zeta (PLCζ) abolishes calcium oscillatory ability of human recombinant protein in mouse oocytes. Human Reproduction 2011; 26:3372-3387.
47. Mu J, Zhang Z, Wu L, Fu J, Chen B, Yan Z, Li B, Zhou Z, Wang W, Zhao L, Dong J, Kuang Y, et al. The identification of novel mutations in PLCZ1 responsible for human fertilization failure and a therapeutic intervention by artificial oocyte activation. Mol Hum Reprod 2020; 26:80-87.
48. Sutovsky P, Manandhar G, Wu A, Oko R. Interactions of sperm perinuclear theca with the oocyte: implications for oocyte activation, anti-polyspermy defense, and assisted reproduction. Microsc Res Tech 2003; 61:362-378.
49. Ramalho-Santos J, Sutovsky P, Simerly C, Oko R, Wessel GM, Hewitson L, Schatten G. ICSI choreography: fate of sperm structures after monospermic rhesus ICSI and first cell cycle implications. Hum Reprod 2000; 15:2610-2620.
50. Kimura Y, Yanagimachi R, Kuretake S, Bortkiewicz H, Perry AC, Yanagimachi H. Analysis of mouse oocyte activation suggests the involvement of sperm perinuclear material. Biol Reprod 1998; 58:1407-1415.
51. Hamilton LE, Zigo M, Mao J, Xu W, Sutovsky P, O'Flaherty C, Oko R. GSTO2 Isoforms Participate in the Oxidative Regulation of the Plasmalemma in Eutherian Spermatozoa during Capacitation. Antioxidants (Basel) 2019; 8.

52. Zhang M, Bromfield EG, Veenendaal T, Klumperman J, Helms JB, Gadella BM. Characterization of different oligomeric forms of CRISP2 in the perinuclear theca versus the fibrous tail structures of boar spermatozoa†. Biol Reprod 2021; 105:1160-1170.
53. Hamilton LE, Acteau G, Xu W, Sutovsky P, Oko R. The developmental origin and compartmentalization of glutathione-s-transferase omega 2 isoforms in the perinuclear theca of eutherian spermatozoa. Biol Reprod 2017; 97:612-621.
54. Hamilton LE, Lion M, Aguila L, Suzuki J, Acteau G, Protopapas N, Xu W, Sutovsky P, Baker M, Oko R. Core Histones Are Constituents of the Perinuclear Theca of Murid Spermatozoa: An Assessment of Their Synthesis and Assembly during Spermiogenesis and Function after Gametic Fusion. Int J Mol Sci 2021; 22.
55. Zhang M, Chiozzi RZ, Skerrett-Byrne DA, Veenendaal T, Klumperman J, Heck AJR, Nixon B, Helms JB, Gadella BM, Bromfield EG. High Resolution Proteomic Analysis of Subcellular Fractionated Boar Spermatozoa Provides Comprehensive Insights Into Perinuclear Theca-Residing Proteins. Front Cell Dev Biol 2022; 10:836208.
56. Ebisch IM, Thomas CM, Peters WH, Braat DD, Steegers-Theunissen RP. The importance of folate, zinc and antioxidants in the pathogenesis and prevention of subfertility. Hum Reprod Update 2007; 13:163-174.
57. Schmuck EM, Board PG, Whitbread AK, Tetlow N, Cavanaugh JA, Blackburn AC, Masoumi A. Characterization of the monomethylarsonate reductase and dehydroascorbate reductase activities of Omega class glutathione transferase variants: implications for arsenic metabolism and the age-at-onset of Alzheimer's and Parkinson's diseases. Pharmacogenet Genomics 2005; 15:493-501.
58. Kim Y, Cha SJ, Choi HJ, Kim K. Omega Class Glutathione S-Transferase: Antioxidant Enzyme in Pathogenesis of Neurodegenerative Diseases. Oxid Med Cell Longev 2017; 2017:5049532.
59. Zhou H, Brock J, Liu D, Board PG, Oakley AJ. Structural insights into the dehydroascorbate reductase activity of human omega-class glutathione transferases. J Mol Biol 2012; 420:190-203.
60. Maedomari N, Kikuchi K, Ozawa M, Noguchi J, Kaneko H, Ohnuma K, Nakai M, Shino M, Nagai T, Kashiwazaki N. Cytoplasmic glutathione regulated by cumulus cells during porcine oocyte maturation affects fertilization and embryonic development in vitro. Theriogenology 2007; 67:983-993.
61. Sutovsky P, Schatten G. Depletion of glutathione during bovine oocyte maturation reversibly blocks the decondensation of the male pronucleus and pronuclear apposition during fertilization. Biol Reprod 1997; 56:1503-1512.
62. Escoffier J, Yassine S, Lee HC, Martinez G, Delaroche J, Coutton C, Karaouzène T, Zouari R, Metzler-Guillemain C, Pernet-Gallay K, Hennebicq S, Ray PF, et al. Subcellular localization of phospholipase Cζ in human sperm and its absence in DPY19L2-deficient sperm are consistent with its role in oocyte activation. Mol Hum Reprod 2015; 21:157-168.
63. Wu AT, Sutovsky P, Manandhar G, Xu W, Katayama M, Day BN, Park KW, Yi YJ, Xi YW, Prather RS, Oko R. PAWP, a sperm-specific WW domain-binding protein, promotes meiotic resumption and pronuclear development during fertilization. J Biol Chem 2007; 282:12164-12175.
64. Zhang XZ, Wei LL, Jin HJ, Zhang XH, Chen SR. The perinuclear theca protein Calicin helps shape the sperm head and maintain the nuclear structure in mice. Cell Rep 2022; 40:111049.
65. Hess H, Heid H, Zimbelmann R, Franke WW. The protein complexity of the cytoskeleton of bovine and human sperm heads: the identification and characterization of cylicin II. Exp Cell Res 1995; 218:174-182.

66. Mountjoy JR, Xu W, McLeod D, Hyndman D, Oko R. RAB2A: a major subacrosomal protein of bovine spermatozoa implicated in acrosomal biogenesis. Biol Reprod 2008; 79:223-232.
67. Heid H, Figge U, Winter S, Kuhn C, Zimbelmann R, Franke W. Novel actin-related proteins Arp-T1 and Arp-T2 as components of the cytoskeletal calyx of the mammalian sperm head. Exp Cell Res 2002; 279:177-187.
68. Tovich PR, Oko RJ. Somatic histones are components of the perinuclear theca in bovine spermatozoa. J Biol Chem 2003; 278:32431-32438.
69. Zigo M, Kerns K, Sen S, Essien C, Oko R, Xu D, Sutovsky P. Zinc is a master-regulator of sperm function associated with binding, motility, and metabolic modulation during porcine sperm capacitation. Commun Biol 2022; 5:538.
70. Lawlor M, Zigo M, Kerns K, Cho IK, Easley Iv CA, Sutovsky P. Spermatozoan Metabolism as a Non-Traditional Model for the Study of Huntington's Disease. Int J Mol Sci 2022; 23.
71. Tsuiji H, Iguchi Y, Furuya A, Kataoka A, Hatsuta H, Atsuta N, Tanaka F, Hashizume Y, Akatsu H, Murayama S, Sobue G, Yamanaka K. Spliceosome integrity is defective in the motor neuron diseases ALS and SMA. EMBO Mol Med 2013; 5:221-234.
72. Nik S, Bowman TV. Splicing and neurodegeneration: Insights and mechanisms. WIREs RNA 2019; 10:e1532.
73. Matos B, Publicover SJ, Castro LFC, Esteves PJ, Fardilha M. Brain and testis: more alike than previously thought? Open Biol 2021; 11:200322.
74. Ramírez-Reveco A, Villarroel-Espíndola F, Rodríguez-Gil JE, Concha, II. Neuronal signaling repertoire in the mammalian sperm functionality. Biol Reprod 2017; 96:505-524.
75. Kerns K, Morales P, Sutovsky P. Regulation of Sperm Capacitation by the 26S Proteasome: An Emerging New Paradigm in Spermatology. Biol Reprod 2016; 94:117.
76. Sutovsky P, Manandhar G, McCauley TC, Caamaño JN, Sutovsky M, Thompson WE, Day BN. Proteasomal Interference Prevents Zona Pellucida Penetration and Fertilization in Mammals1. Biology of Reproduction 2004; 71:1625-1637.
77. Zimmerman SW, Manandhar G, Yi YJ, Gupta SK, Sutovsky M, Odhiambo JF, Powell MD, Miller DJ, Sutovsky P. Sperm proteasomes degrade sperm receptor on the egg zona pellucida during mammalian fertilization. PLoS One 2011; 6:e17256.
78. Song WH, Yi YJ, Sutovsky M, Meyers S, Sutovsky P. Autophagy and ubiquitin-proteasome system contribute to sperm mitophagy after mammalian fertilization. Proc Natl Acad Sci U S A 2016; 113:E5261-5270.
79. Lim S, Kierzek M, O'Connor AE, Brenker C, Merriner DJ, Okuda H, Volpert M, Gaikwad A, Bianco D, Potter D, Prabhakar R, Strünker T, et al. CRISP2 Is a Regulator of Multiple Aspects of Sperm Function and Male Fertility. Endocrinology 2019; 160:915-924.
80. Gibbs GM, Bianco DM, Jamsai D, Herlihy A, Ristevski S, Aitken RJ, Kretser DM, O'Bryan MK. Cysteine-rich secretory protein 2 binds to mitogen-activated protein kinase kinase kinase 11 in mouse sperm. Biol Reprod 2007; 77:108-114.
81. Jamsai D, Bianco DM, Smith SJ, Merriner DJ, Ly-Huynh JD, Herlihy A, Niranjan B, Gibbs GM, O'Bryan MK. Characterization of gametogenetin 1 (GGN1) and its potential role in male fertility through the interaction with the ion channel regulator, cysteine-rich secretory protein 2 (CRISP2) in the sperm tail. Reproduction 2008; 135:751-759.
82. Foster JA, Gerton GL. The Acrosomal Matrix. Adv Anat Embryol Cell Biol 2016; 220:15-33.
83. Leung MR, Ravi RT, Gadella BM, Zeev-Ben-Mordehai T. Membrane Remodeling and Matrix Dispersal Intermediates During Mammalian Acrosomal Exocytosis. Front Cell Dev Biol 2021; 9:765673.

84. Ješeta M, Myšková M, Žáková J, Crha I, Crha K, Chmelikova E, Kistanova E, Ventruba P. Can oocytes repair fragmented DNA of spermatozoa? Medical Journal of Cell Biology 2020; 8:73-77.
85. Song WH, Zuidema D, Yi YJ, Zigo M, Zhang Z, Sutovsky M, Sutovsky P. Mammalian Cell-Free System Recapitulates the Early Events of Post-Fertilization Sperm Mitophagy. Cells 2021; 10.

Nederlandse samenvatting

De aanwezigheid van CRISP eiwitten in zoogdieren

In dit proefschrift wordt de aanwezigheid en organisatie van het cysteïne-rijke intrinsieke secretie-eiwit (CRISP2) in zoogdieren beschreven. De afgelopen 30 jaar zijn CRISP eiwitten intensief onderzocht omdat ze tot expressie komen in het mannelijke voorplantingssysteem en een rol spelen in de mannelijke fertiliteit. Nieuwe genetische technologieën hebben het mogelijk gemaakt om de gevolgen van enkele en/of meervoudige uitschakeling van de transcriptie van Crisp genen in muismodellen te bestuderen. Uit deze studies bleek duidelijk dat CRISP eiwitten een rol spelen in het bevruchtingsproces. Elk CRISP eiwit blijkt betrokken te zijn bij één of meerdere stappen van het bevruchtingsproces en draagt bij aan een optimale mannelijke vruchtbaarheid. In de meeste zoogdiersoorten zijn drie familie-leden van CRISP aanwezig, te weten CRISP1, CRISP3, en het in dit proefschrift bestudeerde CRISP2. Bij knaagdieren is naast deze drie CRISP eiwitten ook het CRISP4 aanwezig. CRISP4 is een expressieproduct van het Crisp4 gen, dat ontstond door een verdubbeling van het Crisp 1 gen en tijdens de evolutie muteerde tot het huidige Crisp4 gen.

CRISPs zijn aanwezig in spermatiden/spermacellen gedurende spermiogenese, epididymale rijping en tijdens de ejaculatie. CRISPs worden als extracellulair geassocieerde eiwitten aan deze cellen gevonden. CRISP1/CRISP4 eiwitten worden door epitheelcellen van de epididymis gesecreteerd in de ductus epididymis en worden vervolgens verankerd aan het oppervlak van spermacellen. CRISP3 wordt door de seminale klier en de prostaat klier gesecreteerd in het seminale plasma. Het in dit proefschrift bestudeerde CRISP2 komt exclusief tot expressie in de testis tijdens de elongatie van spermatiden. CRISP2 blijft, in tegenstelling tot zijn naamgeving, intracellulair aanwezig in het cytosol van de spermacellen. CRISP2 is ten opzichte van CRISP1,3 en 4, om twee redenen uniek: i) CRISP2 heeft een testis-specifieke oorsprong; en ii)

CRISP2 is alleen intracellulair in de spermacellen aanwezig. Een mutatie in het Crisp2 gen resulteert in een stijfheid van de sperma-flagellum, waardoor de spermacellen in het vrouwelijk geslachtsapparaat geen hypermotiliteit kunnen ontwikkelen. Het moleculaire mechanisme achter deze fertiliteits-afwijking is echter nog onbekend. Het doel van dit proefschrift was om meer kennis te verkrijgen omtrent de rol en de functie van CRISP2 in het bevruchtingsproces. CRISP eiwitten staan erom bekend dat ze met andere eiwitten interacties kunnen aangaan om zodoende oligomere eiwitcomplexen te vormen. Twee domeinen in het CRISP2 kunnen aan deze eiwit-oligomerisatie bijdragen, te weten: (i) Het cysteïne-rijke domein dat 10 cysteïnes bevat. De vrije sulfhydryl groepen van deze cysteïnes kunnen geoxideerd worden en aldus intra- en inter-molecular disulfide bruggen vormen; (ii) Het CAP domein, dat eiwit-oligomeren kan vormen op een Zn^{2+}-afhankelijke manier. Beide domeinen van het CRISP2 kunnen daarmee een bijdrage leveren aan de vorming van eiwit-complexen, die in hoge mate aanwezig zijn in gecondenseerde eiwitstructuren in spermacellen (zie **hoofdstuk 1**) en daarmee een bijdrage leveren aan een goed functionerende spermacel.

De vorming van gecondenseerde eiwit structuren in spermacellen van zoogdieren

In spermacellen van zoogdieren worden sterk gecondenseerde en niet-oplosbare eiwitstructuren gevonden in o.a. de kern, het acrosoom, de perinucleaire theca (PT) en in de perifere structuren van de spermastaart (zie **hoofdstuk 1**). Deze gecondenseerde eiwitstructuren geven de spermacel haar progressieve motiliteit en bereiden ze de spermacel voor om de eicel te vinden, te binden en uiteindelijk te bevruchten. Late spermatiden in de testis vertonen echter geen transcriptie en translatie meer. Alleen via post-translationele modificaties (PTMs) en oppervlakte-uitwisseling van eiwitten kunnen functionele veranderingen van spermacellen teweegbrengen, die optreden gedurende de reis naar de te bevruchten eicel. Voor de CRISP eiwitten zijn zowel de cysteïne oxidatie/disulfide brug vorming als de interactie met Zn^{2+} van

belang voor het veranderen van enzym activiteit, eiwit-complex formatie en de oplosbaarheid van eiwitten.

Cysteïne oxidatie en Zn^{2+} afhankelijke eiwit-oligomerisatie

Cysteïne oxidatie treedt op bij chromatine condensatie in spermacellen en tijdens de ontwikkeling van progressieve motiliteit van spermacellen gedurende het transport door de epididymis. CRISP eiwitten zijn verrijkt in cysteïne residuen met 10 cysteïnes in het CRISP domein en 6 cysteïnes in het CAP domein. Al deze cysteïne residuen kunnen betrokken zijn bij de vorming van disulfide bindingen. In **hoofdstuk 2** zijn verschillende oligomere vormen van CRISP2 bestudeerd die voorkomen in het vezelachtige gedeelte van de spermastaart versus die van de PT in de sperma-kop. Immuno-goud-labelling van spermacellen onthulde dat CRISP2 aanwezig is in de PT. CRISP2 bleek tevens voor te komen in eiwitcomplexen in de sperma-staart. Deze CRISP2 complexen bleken onder reducerende condities uit elkaar te vallen. De multimere vorm van CRISP2 bleek resistent te zijn tegen SDS en β-mercapto-ethanol behandeling, hetgeen voorheen al gerapporteerd was voor niet-zoogdier CRISP eiwitten. Verdere ultrastructurele localisatie liet zien dat CRISP2 in de spermastaart aanwezig is in de ‘outer dense fibers’ (ODFs) en in de ‘fibrous sheath’ (FS). De aanwezigheid van CRISP2 in deze spermastaart structuren blijkt geconserveerd te zijn in de mens, muis en rat. De onoplosbare eigenschappen van deze gecondenseerde structuren kan de dissociatie van eiwitten verhinderen. Dit zou vergelijkbaar kunnen zijn met de resistentie van vezelachtige eiwit structuren tegen na langdurige behandeling met reducerende agentia. Bovendien kunnen de amyloïdogene eigenschappen van het CAP domain van CRISP2 (net als bij andere CAP eiwitten) bijdragen aan de onoplosbaarheid CRISP2. Dit fenomeen is beschreven voor een aantal CRISP en CAP eiwitten waaronder het CRISP2 eiwit. Divalente metaal-ionen kunnen eiwit-oligomerisatie induceren en het CAP domein is in staat om divalente kationen te binden. Dat blijkt uit eerdere *in vitro* studies waarin werd aangetoond dat Zn^{2+} de oligomerisatie van

muizen CRISP2 en humaan CRISP1 induceert. Hierbij dient opgemerkt te worden dat Zn^{2+} belangrijk is voor het normaal functioneren van het mannelijke voorplantingssysteem. Zn^{2+} deficiëntie resulteert in zware beschadigingen van de testis en remt de spermatogenese. Extracellulaire Zn^{2+} concentraties nemen progressief toe in de mannelijke reproductieve tractus en er is een opname van Zn^{2+} vanaf het spermatide-stadium tot aan de vorming van rijpe spermatiden. Zn^{2+} concentraties in geëjaculeerde spermacellen zijn dan ook hoger dan die in testiculaire spermacellen. Hoge Zn^{2+} gehaltes zijn ook gevonden in de seminale vloeistof, terwijl epididymale spermacellen het extracellulaire Zn^{2+} snel kunnen opnemen *in vitro*. In overstemming met deze observaties zijn de aanwezigheid van meerdere Zn^{2+} transporteiwitten (ZIPs) vanaf het spermatogonium stadium tot en met de spermacel vorming. De ZIPs vertonen verschillende compartimentale verdelingen in deze celtypes, waardoor de intracellulaire Zn^{2+} patronen veranderen tijdens de verschillende stadia van de spermacel-vorming, -maturatie en -capacitatie. De lokale Zn^{2+} gehaltes zijn hoog genoeg in de ODFs van testiculaire spermacellen om SH-Zn-SH complexen te vormen. Dit complex kan functioneel zijn doordat het oxidatie voorkomt van deze structuren tijdens de spermiogenese. Echter, tijdens de epididymale spermarijping is er een lager gehalte aan Zn^{2+} aanwezig in de flagellum. Deze verlaging veroorzaakt de oxidatie van vrije sulfhydrylgroepen en daarmee het stijver worden van de ODFs waardoor de spermacellen de voorwaartse motiliteit verkrijgen. Deze voorwaartse motiliteit ontwikkelt zich verder tot een hyper-geactiveerde motiliteit tijdens de capacitatie van de spermacel in de omgeving van de eicel. Deze hyper-geactiveerde motiliteit is de drijvende kracht van de spermacel om de eicel en haar omringende structuren te kunnen penetreren en uiteindelijk te kunnen bevruchten. Het feit dat zowel geëjaculeerde als epididymale spermacellen afkomstig van Crisp2$^{-/-}$ muizen een stijvere flagellum hebben dan wildtype muizen suggereert dat CRISP2 betrokken is bij het flexibeler worden van deze structuur. Het

gevolg daarvan is dat de ODFs niet meer in staat zijn om een juiste bijdrage te leveren aan de motiliteitsveranderingen die optreden tijdens het epidydimale transport.

Spermastructuren voor en na de bevruchting

Zn^{2+} speelt ook een rol als een reversibele regulator van sperma chromatine-condensatie en -decondensatie. Men denkt dat tijdens het epididymale spermatransport er SH-Zn-SH bruggen gevormd worden tussen cysteïne-groepen van protamines. Deze bruggen zijn belangrijk voor de zeer sterkte condensatie van het chromatine en daarmee ook voor de bescherming van het DNA tegen potentiële beschadiging voorafgaand en tijdens de bevruchting. De verwijdering van Zn^{2+} uit deze SH-Zn-SH bruggen is noodzakelijk voor de decondensatie van het sperma-chromatine, wat optreedt direct na de bevruchting en zal leiden tot de vorming van een mannelijke pronucleus. *In vitro* studies hebben laten zien dat Zn^{2+} chelatie met behulp van ethylene-diamine-tetra-acetaat (EDTA) een snelle decondensatie van het chromatine in geëjaculeerde spermacellen induceert. Het is niet bekend waarom deze Zn^{2+} verwijdering niet resulteert in de oxidatie van thiolgroepen tot disulfide bindingen, zoals dat wel gebeurt in staart structuren. De verwijdering van Zn^{2+} in het cytosol van de eicel wordt verondersteld van belang te zijn bij de decondensatie van het spermachromatine.

De aanwezigheid van CRISP2 in de PT van de spermakop in de vorm van β-mercapto-ethanol -gevoelige eiwitcomplexen, alsmede de functionele rol die de PT heeft na de bevruchting, bracht ons er toe om in **hoofdstuk 3** onderzoek te verrichten naar het lot van CRISP2 en de PT voor en na de bevruchting. De PT bevat een aantal eiwitten die noodzakelijk zijn bij de activering van de bevruchte eicel. Twee goed gekarakteriseerde kandidaten voor eicel activering zijn het fosfolipase C zeta 1 (PLCz1/PLCζ) en het post-acrosomale WW domein-bindende eiwit (PAWP). Beide eiwitten zijn aanwezig in de PT en induceren Ca^{2+} oscillaties in de eicel. Een essentiële rol voor PLCζ is vastgesteld in een Plcz1-deficiënt muizenmodel en in

mannen met een fertiliteitsstoornis die veroorzaakt wordt door een mutatie in PLCζ . De PT is de eerste interne structuur van een spermacel die wordt opgelost in het cytosol van de eicel. De waarneming dat alleen spermacellen met een dispersie van de PT in staat zijn eicellen te activeren na een micro-injectie toont aan dat de dissociatie van de PT een essentiële stap is in eicel activatie. In **hoofdstuk 3** laten we zien dat CRISP2 snel dissocieert van de PT, nog voor de decondensatie van de spermacel nucleus. Het is daarom mogelijk dat de reductie van disulfide-bruggen tussen twee cysteïne-residuen in het cysteïne-rijke domein, en/of de verwijdering van Zn^{2+} in het CAP domein van CRISP2, een manier is om eiwit-dissociatie van de PT te initiëren (zie voor een schematische voorstelling Figuur 1 van **hoofdstuk 6**). In dit verband is Glutathion-transferase Ω 2 (GSTO2) een interessant eiwit dat tevens in de PT van spermacellen van zoogdieren voorkomt. GSTO2 behoort tot de Ω klasse van glutathione-S-transferase (GST) enzymen. GSTO2 bezit basische glutathion (GSH) reductase activiteit. Het GSH pad is inactief zolang GSTO2 ingepakt blijft in de onoplosbare eiwitlaag van de PT. Echter, na de bevruchting komt GSTO2 vrij uit de PT in het cytosol van de eicel. GSH is daarmee actief aanwezig in de eicel en is direct betrokken bij de mannelijke pronucleus formatie. Onze studies in **hoofdstuk 3** laten zien dat het CRISP2 dat loskomt uit de PT ook afgebroken wordt, nog voorafgaand aan de mannelijke pronucleus formatie. Deze bevindingen laten zien dat de dispersie en mogelijk ook de degradatie van PT eiwitten zoals CRISP2 essentieel zijn voor de decondensatie van het spermachromatine. In de literatuur is beschreven dat gebreken in de sperma DNA condensatie samengaan met het onvolledige oplossen van de PT. Dit fenomeen is waargenomen nadat spermacellen werden geïntroduceerd in eicel middels een intra-cytoplasmatische sperma injectie (ICSI). Hieruit bleek dat indien de PT structuur nog deels intact bleef, er een vertraging of verhindering is van sperma DNA decondensatie werd waargenomen, waardoor de mannelijke pronucleus niet of te traag werd gevormd.

In **hoofdstuk 4** hebben we de eiwit samenstelling van de PT in spermacellen van de beer geïdentificeerd door gebruik te maken van kwantitatieve, label- vrije vloeistof chromatografische massa spectrometrie (LC-MS/MS). Er zijn 813 eiwitten gedetecteerd in de PT, waaronder eerder geïdentificeerde PT eiwitten zoals eiwitten die betrokken zijn bij de eicel activering, PLCζ en PAWP, GSTO2, calicin, cylicin2, ras-gerelateerd eiwit rab-2A (RAB2A)[66], actine-gerelateerde eiwitten (ARPT1&T2), en diverse subunits van histonen (H2A, H2B, H3 and H4). Door het gebruik van 'Ingenuity Pathway Analysis' (IPA, Qiagen) konden we een fertilisatie-gerelateerd eiwitnetwerk identificeren waarin CRISP2 een rol speelt. Dit PT eiwitnetwerk bleek verrijkt te zijn met verschillende eiwitten die betrokken zijn bij "metabolisme en productie van reactieve zuurstof radicalen", "autofagie", "amyloïdose", "homeostase van metaal ionen", "endoplasmic reticulum (ER) stress response in cellen" maar ook bij neurodegeneratieve ziektes zoals "de ziektes van Huntington, Parkinson en Alzheimer". Een algemene overeenkomst van deze eiwitten is dat ze een relatie hebben met ziektes waarin "eiwit aggregatie" en "cellulaire stress" betrokken zijn. Een *in vitro* proteoomstudie naar de identificatie van Zn^{2+} interacterende eiwitten in gecapaciteerde spermacellen van de beer liet ook zien dat Zn^{2+} interacterende eiwitten het meest geassocieerd werden met de ziekte van Huntington en Parkinson. In een recent verschenen overzichtsverhaal wordt daarom verondersteld dat spermacellen kunnen dienen als een niet-traditioneel model om de ziekte van Huntington te bestuderen.

Naast deze eiwitten identificeerden we ook een cluster van spliceosoom-gerelateerde eiwitten in de PT. Verschillende neurologische ziekten worden gelinkt aan splicing afwijkingen. Het is bovendien bekend dat het humane brein en de testis de hoogste graad van vergelijkbare eiwitexpressie vertonen ten opzichte van andere weefsels in het lichaam. Verschillende klassieke neuronale signaalroutes zijn ook betrokken bij het functioneren van spermacellen. Zo

hebben humane neuronen en spermacellen veel overeenkomsten in eiwitten die betrokken zijn bij de exocytose. Onze proteoomstudie van de spermacel PT ontcijferde een aantal eiwitten en functionele eiwit netwerken die ook actief zijn in neuronen. Onze studie in **hoofdstuk 4** beschrijft de verrijking van proteasoom-eitwitten in het PT-proteoom. De PT blijkt alle structurele en regulerende eiwitonderdelen van een proteasoom te bevatten. Proteasomen zijn al eerder beschreven in spermacellen van zoogdieren. Het ubiquitine proteasoom systeem (UPS) blijkt betrokken te zijn bij spermacapacitatie, de acrosoom reactie, en bij de sperma-zona interactie. De UPS and autofagie zijn betrokken bij de degradatie van de mitochondriën uit de spermacel na *in vitro* fertilisatie (IVF) bij het varken. Omdat alle proteasoom-eiwitonderdelen verrijkt zijn in de PT, speculeren we dat het UPS (verantwoordelijk is voor de afbraak van de PT structuur) deels afkomstig kan zijn uit de PT en geactiveerd wordt door dissociatie na de bevruchting. Toekomstige experimenten moeten aantonen of functionele proteasomen kunnen worden geassembleerd uit de gedissocieerde PT eiwitten, die vervolgens in het cytosol van de eicel de ongewenste sperma-eiwitten kunnen degraderen.

Op basis van de eiwit-samenstelling van de PT zoals beschreven in **hoofdstuk 4** is er in **hoofdstuk 5** onderzoek gedaan naar eiwitten die een directe interactie aangaan met CRISP2. Interacties met CRISP2 werden bestudeerd door CRISP2-immunoreactieve banden uit natieve gelen te snijden en de geassocieerde eiwitten vervolgens met LC-MS/MS te identificeren. Eerdere studies hebben verschillende CRISP2-bindende eiwitten aangetoond in de testis van volwassen muizen. Daaronder behoorde het kationen-kanaal van sperma 1 (CatSper1), mitogeen-geactiveerde eiwitkinase-kinase-kinase 11 (MAP3K11), gametogenetine 1 (GGN1) en het spermakop en -staart geassocieerde eiwit (SHTAP). Wij identificeerden acrosine en het acrosine-bindend eiwit (ACRBP) als nieuwe CRISP2-interacterende eiwitten. De interacties van deze eiwitten met CRISP2 is ook onderzocht onder *in vitro* geïnduceerde sperma-

capacitatie en na ionofoor A23187-geïnduceerde acrosoom reactie met behulp van een *in situ* 'proximity ligation assay'. De fluorescente signalen voor eiwit interacties waren als foci te zien voor CRISP2 en ACRBP en verschoven van de apicale kant naar het post-acrosomale gedeelte van de spermakop gedurende de capacitatie van sperma. De veranderde CRISP2 interactie met ACRBP lijkt geassocieerd te zijn met het capacitatie-proces omdat de interactie-foci aanwezig bleven in het post-acrosomale deel van de spermakop. De CRISP2-acrosin interactie daarentegen was aanwezig voor de geïnduceerde sperma-capacitatie, maar verdween na de sperma-capacitatie en kon na intensieve permeabilisatie terug gevonden worden in de acrosomale matrix. Dit toont aan dat acrosine in het acrosoom zit. CRISP2-acrosin complexen kunnen mogelijk betrokken zijn bij de vorming van para-kristallijne structuren die aanwezig zijn in de acrosoommatrix. Onze data leverde tevens een lijst op van potentiële CRISP2-interacterende kandidaten die functioneel kunnen worden ingedeeld als spermadhesines, protease remmers, histon subunits, chaperonen, eiwitten met een mitochondriële functie en ubiquitine. Biochemische validatie van deze interacterende eiwit kandidaten is echter noodzakelijk. Desalniettemin suggereren onze data dat CRISP2 een veelzijdige rol kan spelen in het functioneren van spermacellen rondom het bevruchtingsproces.

Toekomst aspecten

In dit proefschrift worden de dynamische aspecten onderzocht van: (i) De vorming van gecondenseerde eiwitstructuren gedurende de spermiogenese in de testis en de spermacel maturatie in de epididymis (**hoofdstuk 1**); (ii) De aanwezigheid van CRISP2 in deze gecondenseerde eiwitstructuren (**hoofdstuk 2**); (iii) De snelle dissociatie van CRISP2 uit de PT direct na de bevruchting en de daaropvolgende afbraak van het vrijgekomen CRISP2 (**hoofdstuk 3**); (iv) De eiwitsamenstelling van de PT (**hoofdstuk 4**); en (v) De eiwitten die een interactie aangaan met CRISP2 (**hoofdstuk 5**). Een geëjaculeerde spermacel moet de hoogste staat van robuustheid bezitten en een minimaal volume hebben. Enerzijds om ergonomisch in

staat te zijn de eicel te kunnen bevruchten en anderzijds om inert te zijn voor een niet-altijd vriendelijke omgeving in de mannelijke en vrouwelijke tractus waar de spermacel doorheen moet om uiteindelijk de eicel te kunnen bereiken. De compactheid en de robuustheid van de spermacel worden bereikt door condensatie van eiwitten in specifieke structuren en het verwijderen van zowel celorganellen als het cytosol. Op deze manier vormen zich ook super-gecondenseerde protamines in de spermacelkern waardoor er een bijna kristallijne toroïde structuur van het DNA ontstaat. De spermacel heeft daarmee een kern met een minimaal volume die is omgeven door een kernenvelop vrijwel zonder poriën. Deze biedt samen met een sterk gecondenseerde eiwitstructuur -de PT- bescherming tegen radicalen en mutagentia. Het acrosoom bevat een geconcentreerde, deels kristallijne, enzymmatrix die langzaam uiteenvalt gedurende de zona penetratie. Ook in de spermastaart zijn gecondenseerde eiwitstructuren aanwezig die de flagellum unieke flexibele en metabole eigenschappen geven. Deze eigenschappen kunnen aangepast worden zodat er een juiste spermamotiliteit wordt verkregen, bijvoorbeeld tijdens sperma-maturatie in de epididymis waar voorwaartse bewegelijkheid wordt gegenereerd, en tijdens sperma-capacitatie in de eileider (of tijdens een IVF behandeling) waar hyper-geactiveerde motiliteit wordt gegenereerd. Zowel de vorming van de gecondenseerde eiwitstructuren in de testis en de epididymis als de decondensatie ervan na de bevruchting in de eicel behoeven verder onderzoek. Voor een model dat we postuleren, met speciale aandacht voor de rol van het eiwit CRISP2 in deze dynamische processen, verwijzen we naar Figuur 1 van **hoofdstuk 6**.

De eicel heeft het vermogen om te versmelten met een spermacel en daarbij op een juiste manier om te gaan met de componenten die via de spermacel binnenkomen. De eicel is bijvoorbeeld in staat om spermastructuren af te breken en componenten daaruit te recyclen zodat een mannelijke pronucleus kan worden gevormd. De eicel is ook tot op zekere hoogte in staat om

na de bevruchting beschadigd paternaal DNA te repareren. In het ooplasma is een ubiquitine-achtige autofagie receptor sequestosoom 1 (SQSTM1) aanwezig om de mitochondriën van de spermacel via mitofagie af te breken. In een celvrij systeem waarin membraanloze spermacellen zijn geïncubeerd met cytosol extracten van de eicel, bleek dat het ooplasma SQSTM1 specifiek bindt aan de sperma mitochondriën. Daarbij is het van belang dat direct na de bevruchting van de eicel en voorafgaand aan al deze door het ooplasma ingezette acties, er eerst een decondensatie van de PT optreedt (**hoofdstuk 3**). Dit wordt benadrukt in **hoofdstuk 6**, omdat de eiwitten die in de PT aanwezig zijn (**hoofdstuk 4**) waarschijnlijk net zoals CRIP2 vrijkomen in het ooplasma. Lokaal, dat wil zeggen rondom de spermacel structuren in het ooplasma, kunnen deze vrijgekomen PT eiwitten een functie hebben in het verwerken van spermastructuren. Zo kunnen er vanuit de PT eiwitten vrijkomen die betrokken zijn bij proteoloyse (alle functionele subunits van proteasomen zijn gedetecteerd in de PT), of die betrokken zijn in het op een juiste manier verwerken van de super-gecondenseerde promatine-DNA toroïden van de spermacel. Daarnaast zijn er in de PT eiwitten aanwezig die na het loskomen in het ooplasma betrokken kunnen zijn bij epigenetische markering van chromatine (histonen subunits), gen editing (spliceosoom eiwitten) en bij de activering van de eicel (o.a. een specifieke fosfolipase C). Dit proces kan in detail bestudeerd worden in een celvrij system, dat kan gemanipuleerd worden om de volgende processen in kaart te kunnen brengen: (i) Eicelmarkers die gebruikt kunnen worden om te voorspellen of een eicel de potentie heeft om na de bevruchting sperma-structuren op een juiste manier te verwerken; en (ii) hoe de vrijgekomen sperma eiwitten van de PT betrokken zijn in processen zoals mitofagie, proteolyse, eicel activering en sperma-chromatine verwerking. Deze kennis is noodzakelijk om de moleculaire basisprincipes van de bevruchting van de eicel in zoogdieren te begrijpen en de rol van CRISP2 in deze processen op te helderen.

Acknowledgements

Time flies! After six years exploring at the department of B&C, I draw a perfect ending to my PhD life. Looking back on the past, I have got so many support, help and care from my supervisors, colleagues, friends and families that encouraged me going through all the difficult times!

My deep thanks to my supervisors, Prof. Dr. J.B. Helms and Dr. B.M. Gadella. **Bernd**, thanks for your critical comments and suggestions which improved my research a lot, more important, you have learned me how to think about scientific questions in a critical way. **Bart**, how lucky I am to have you as my supervisor! You are a great supervisor not only for research but also for life. You are always optimistic and have plan B for me. Whenever I was depressed with my experiments, you always told me there were no bad results, and discussed all the possibilities so that I knew how to further and what to do to solve the problems. Thanks for giving me much support and advises on how to balance life and work. I love science and enjoy my life!

Liz, I really appreciated that I have had you as my second supervisor. You are a talented scientist! Without your smart ideas, hard work and suggestions, I could not have made this thesis possible. I am very grateful that you are always there for me.

Nafiseh, I can't believe we have been working together for six years! Pipetting together in the lab will be my memorable moments in my PhD life. Thanks very much for listening to me as a friend and warm hugs when I was in a bad mood. I am so happy that you become a mother! I wish you and your family a happy and wonderful life!

Petra, you are the mother of B&C! I still remember that the first day I arrived in Netherlands, you picked me up in the airport. Thanks so much for all the help! I wish you a happy retirement!

Maya, Thanks for organizing all the parties and lab activities! You make my PhD life more colorful! You are really a creative person!

Thanks to **Dora** for all the comments and suggestions on my FMM presentations. **Nick, Ruud, Martijn** and **Aike**, thanks for all the jokes and it is fun to chat with you. Thank **Chris** for your kind help with solving computer problems. Thanks to **Jeroen** and **Iris** for all the orderings. Thanks to **all the colleagues from B&C group**, I wish you all the best!

I would like to thank **Tineke** and **Judith** for their help in the immuno-gold labelling, **Riccardo** and **Albert** for their help in the proteomic experiments, **Richard** and **Esther** for introducing me in confocal microscopy. Thanks to **Naomi** for learning me experimental technics, and it was a pleasure to work with you! I wish you all the best! Thanks to **Leni** for the pig IVF introduction at the JDV, and thanks to all **other people from F&R group**.

I would also like to thank my chinese friends I met in Netherlands: **Jie**, **Xiaogang**, **Bo**, **Qingkang**, **Wenjuan**, **Fangrui**, **Boning**, **Mingxi, Ziying** and **Xinyi**, we share chinese food and celebrate our traditional festivals together! Having you around makes me less homesick! Mother committee club: **Yvonne**, **Qianqian**, **Yuanjie**, we share parenting experience and have endless topics to chat! Our many outgoing days were fun!

Finally, my hearted thanks to my parents, grandparents, my sister and all family members for your love and care! My dear daughter, **Juli**, I have been your mother for six years! And I am so

proud of being your mother. Your smiles heal me and give me power and make me brave! My beloved husband, **Wenhui**, thanks for your accompanying and support from my journey of bachelor to PhD. Thanks for your patience and care, I love you!

Min Zhang

16/11/2022

About the author

Min Zhang was born on 16th, May, 1990 in Tai'erzhuang, Shandong province, China. She attended her primary school, middle school and high school in Tai'erzhuang. In September 2009, she started her undergraduate study at the College of Animal Medicine, Qingdao Agricultural University, China. She obtained her bachelor's degree in July 2013. The same year in September, she started her master research at the College of Veterinary Medicine, Jilin University, China, under the supervision of Prof. dr. Xiaobing Li and Prof. dr. Xinwei Li. Her research project was to study the mechanism of SREBP-1c/Cidea pathway in the hepatic lipidosis of dairy cows with negative energy balance. She obtained her master's degree in July 2016. The same year, she applied and obtained a 4-year PhD scholarship from the China Scholarship Council. In October 2016, she started her PhD project under the supervision of Dr. B.M. (Bart) Gadella and Prof. dr. J.B. (Bernd) Helms at the department of Biomolecular Health Sciences, Faculty of Veterinary Medicine, Utrecht University, The Netherlands.

List of publications

This thesis

Zhang M, Bromfield EG, Veenendaal T, Klumperman J, Helms JB, Gadella BM. Characterization of different oligomeric forms of CRISP2 in the perinuclear theca versus the fibrous tail structures of boar spermatozoa†. Biol Reprod. 2021 Nov 15;105(5):1160-1170.

Zhang M, Chiozzi RZ, Skerrett-Byrne DA, Veenendaal T, Klumperman J, Heck AJR, Nixon B, Helms JB, Gadella BM, Bromfield EG. High Resolution Proteomic Analysis of Subcellular Fractionated Boar Spermatozoa Provides Comprehensive Insights Into Perinuclear Theca-Residing Proteins. Front Cell Dev Biol. 2022 Feb 18;10:836208.

Zhang M, Bromfield EG, Helms JB, Gadella BM. The fate of porcine sperm CRISP2 from the perinuclear theca before and after in vitro fertilization. Biol Reprod. 2022 Nov 14;107(5):1242-1253.

Zhang M, Chiozzi RZ, Bromfield EG, Heck AJR, Helms JB, Gadella BM. Characterization of acrosin and acrosin binding protein as novel CRISP2 interacting proteins in boar spermatozoa. *Submitted.*

Other publications

Bernecic NC, **Zhang M**, Gadella BM, Brouwers JFHM, Jansen JWA, Arkesteijn GJA, de Graaf SP, Leahy T. BODIPY-cholesterol can be reliably used to monitor cholesterol efflux from capacitating mammalian spermatozoa. Sci Rep. 2019 Jul 8;9(1):9804.

Leung MR, Zenezini Chiozzi R, Roelofs MC, Hevler JF, Ravi RT, Maitan P, **Zhang M**, Henning H, Bromfield EG, Howes SC, Gadella BM, Heck AJR, Zeev-Ben-Mordehai T. In-cell structures of conserved supramolecular protein arrays at the mitochondria-cytoskeleton interface in mammalian sperm. Proc Natl Acad Sci U S A. 2021 Nov 9;118(45):e2110996118.

Leung MR, Roelofs MC, Ravi RT, Maitan P, Henning H, **Zhang M**, Bromfield EG, Howes SC, Gadella BM, Bloomfield-Gadêlha H, Zeev-Ben-Mordehai T. The multi-scale architecture of mammalian sperm flagella and implications for ciliary motility. EMBO J. 2021 Apr 1;40(7):e107410.

Conference abstract

Zhang M, Zenezini Chiozzi R, Kaloyanova DV, Helms JB, Gadella BM. Characterization of CRISP2 in ejaculated boar sperm and its involvement in oligomerization protein complex formation. Animal Reproduction Science 2020; 220:106416.

Oral presentations

Zhang M, Bromfield EG, Helms JB, Gadella BM. CRISP2 plays a role in the decondensation of the perinuclear theca prior to male pronucleus formation in fertilized pig oocytes. Veterinary Science Day 2021-2022, Utrecht, The Netherlands.

Zhang M, Bromfield EG, Helms JB, Gadella BM. The fate of porcine sperm CRISP2 from the perinuclear theca before and after in vitro fertilization. **Best oral presentation winner** of the 38th Association of Embryo Technology in Europe (AETE) conference 2022, Utrecht, The Netherlands.